RESEARCH & REVIEWS IN ENGINEERING – Summer, 2019

Kitap Adı	:	**Research & Reviews in Engineering – Summer, 2019**
İmtiyaz Sahibi	:	Gece Kitaplığı
Genel Yayın Yönetmeni	:	Doç. Dr. Atilla ATİK
Kapak&İç Tasarım	:	Sevda KIRDAR
Sosyal Medya	:	Arzu ÇUHACIOĞLU
Yayına Hazırlama	:	Gece Akademi Dizgi Birimi
Yayıncı Sertifika No	:	15476
Matbaa Sertifika No	:	34559
ISBN	:	978-605-7852-97-7

Editor

Dr. Mahmut TURHAN

(Medel Mühendislik ve Elektronik San.Tic.A.Ş.)

Gece Publishing

ABD Adres/ USA Address: 387 Park Avenue South, 5th Floor, New York, 10016, USA

Telefon/Phone: +1 347 355 10 70

Gece Akademi

Türkiye Adres/Turkey Address: Kocatepe Mah. Mithatpaşa Cad. 44/C Çankaya, Ankara, TR

Telefon/Phone: +90 312 431 34 84 - +90 555 888 24 26

web: www.gecekitapligi.com —www.gecekitap.com

e-mail: geceakademi@gmail.com

CONTENTS

SEGMENTATION OF CHOROIDAL REGION ON RETINAL IMAGES

Onur ÇAKAR [1] , Hasan Erdinç KOÇER [2] , Zeynep DADACI [3]

[1] Bursa Provincial Directorate of National Education, Software Developer in Energy Efficiency Unit, Bursa- Turkey.
[2] Selçuk University, Technology Faculty, Department of Electrical & Electronic Engineering, Konya-Turkey.
[3] Konya Medicana Hospital, Ophthalmology Specialist, Konya-Turkey.

1. INTRODUCTION

The retina is the only place where the blood vessels can be directly visualized without external interference. On the back of the retina, the yellow-pigmented oval-shaped area through which the visual axis passes is called the macula, and the pit in the middle is called the fovea. The point where the optic nerve passes through a perforated region at the back of the hard layer is called the optical disc. The optic disc, in which more than one million nerve fibers are collected, is where the optic nerves are attached to the retina. It includes sclera, choroid and retina layers.

Optical coherence tomography (OCT) is an imaging technique that is capable of providing cross sectional images of the retina. This method uses optical reflective properties of the tissues to provide detailed information about the internal retinal structures by using Near-Infrared imaging technique. Cross sectional OCT scans are color coded according to reflective properties of the retinal structures.

Looking at previous studies based on image processing for the measurement of choroidal thickness, we see that these are mostly studies for macular degeneration. Tuncer et al. (2014) evaluated the subfoveal choroid thickness in normal eyes with optical coherence tomography. Vedran Kajić et al. (2011) proposed an automatic segmentation algorithm for the detection of retinal pigment epithelium on normal and pathological eye pictures. In this study, the authors tried to obtain the boundary lines of the choroid using the improved Dijkstra algorithm and the Canny edge finder filter. In their study, David Alonso-Caneiro et al. (2013) attempted to determine the borderline of the inner and outer choroidal layer using edge-finding, linear-weight mapping, gradient-based method and graph theory. Dara Koozekanani (2001) tried to determine the thickness of the retinal border lines and choroidal layer in the images taken with OCT. In this study, one-dimensional edge detection technique and Markov model were used to determine the retinal boundaries. Varsha Manjunath et al. (2010), in their study, they tried to determine the choroidal thickness by using a statistical approach on OCT images from patients with healthy eyes. Preeti Gupta et al. (2015) developed a software for automatic measurement of choroid thickness. In the study performed by Zsuzsanna Géhl et al., (2014), choroidal thickness measurements were evaluated statistically. Magdy Moussa et al. (2016) performed measurements of choroidal thickness on 129 OCT images and evaluated the measurement results according to age and sex characteristics.

2. MATERIAL AND METHOD

In this section, the data used in the study (OCT images) and the application stages of the study are given. In this study, 30 retinal cross-sectional images taken from the right and left eyes of the 15 patients with OCT device (Carl Zeiss Meditec - Primus 200) were used. The cross-sectional images obtained from the OCT device are color and gray level images and are in the dimension of 1745 * 900 pixels and in jpeg format. Figure 1 shows the

color and gray level sample cross-sectional retinal images obtained by OCT technique.

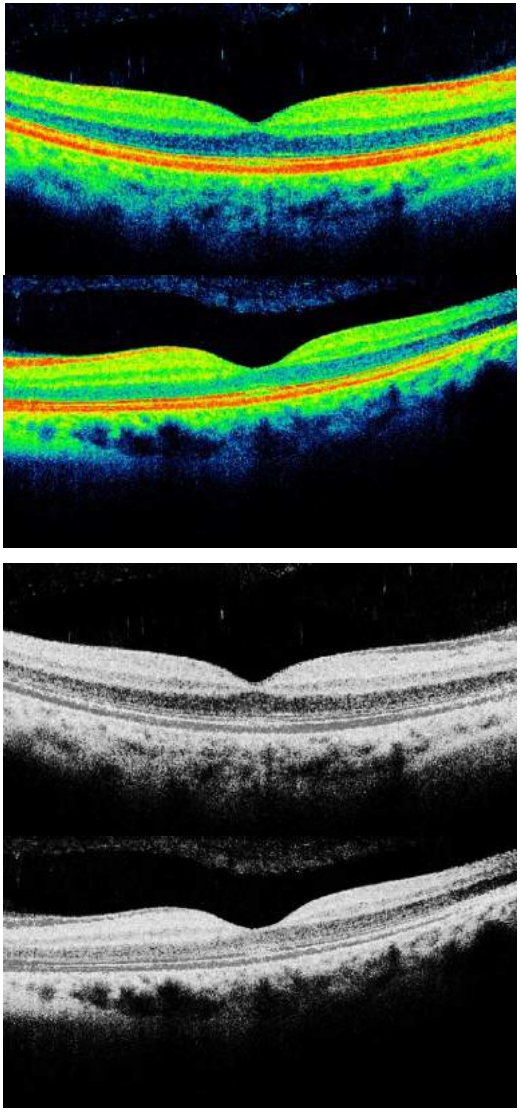

Figure 1. Sample retinal section images taken by OCT technique (RGB and Gray Level)

Firstly, OCT section images were examined. The retinal pigment epithelial layer was red in color, unlike the other layers. Considering that this situation would facilitate the determination of the upper limit of measurement during the segmentation phase, work continued on colored (RGB) picture.

The study for measurement of image-based choroidal thickness consists of five basic steps. These are respectively; taking the image (i), pre-processing and filtering (ii), segmentation of the choroid layer (iii), feature extraction (iv) and measurement (v). The block diagram showing the process steps is given in Figure 2.

Figure 2. Process steps of the study

In the pre-processing stage, noise reduction and image enhancement studies were performed on the raw images taken from the OCT device. At this stage, the mean filter, used for noise removal, was applied to the images, which allowed for better segmentation and better quality retinal images.

At the segmentation stage, reference regions (nebula-like layer with epithelium tissue layer and capillaries) and sub-choroidal dots were determined to measure choroidal thickness. At this stage, the section called pigment epithelium in the OCT image was further clarified in terms of red color and the lower border boundary line was tried to be obtained more easily. During this process, a standard filter was not used, and the color values of the epithelial tissue pixel values were marked in full red (255.0.0).

In the feature extraction process, the line is drawn down from the fovea point determined in the previous stage to the point where the choroid layer ends. The lengths were then measured by drawing lines at the predetermined range and distance to the right and left of the center line. Experimental studies were performed on a computer with 3 GHz, intel i7 processor and 8 gb memory. Segmentation and feature extraction operations are coded in Visual Studio C # programming language platform.

3. SEGMENTATION PROCESS

The segmentation process includes processes for detecting regions of the interest in an image. In this study, the following procedures were performed in the segmentation stage in order to measure the choroidal thickness from OCT images:

i. Elimination of noises (filtering and morphological processes),
ii. Determination of the lowest point (fovea),

iii. Clarification of pigment epithelial tissue layer,
iv. Drawing the lower boundary line of pigment epithelium tissue,
v. Determination of lower bound points of the choroid layer.

Figure 3 shows an OCT image containing the parameters (fovea, retinal pigment epithelium layer, choroid layer upper boundary line, choroid layer lower border line and vertical lines used for measurement) used for the measurement of choroidal thickness.

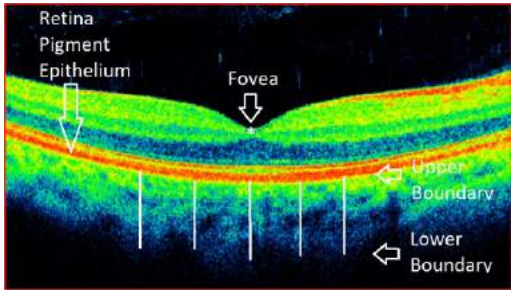

Figure 3. OCT image containing parameters to be used for segmentation

When taking images with the OCT device, all the tissue layers in the eye are included in the imaging and there are unwanted noises at the top and bottom of the picture. Morphological processes were applied to eliminate these noise. These morphological processes are operations called dilation and erosion. In the dilation process, two variables are used: the input image and the structural component. When the center of the structural component matches on the image, all pixels are marked. As in the dilation process, two variables are used in erosion, namely the input image and the structural component. The structural component is moved over the image and only the center pixel is marked at the time of matching. Figure 4 shows a sample OCT image that the noises eliminated using morphological processes.

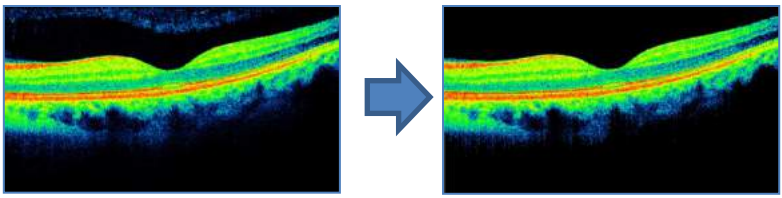

Figure 4. Elimination of noise using morphological process

When the OCT images were examined, it was seen that the pixels determining in the process of marking the choroid region, the lower border of the nebulae area formed as sharp lines. To resolve this, it is necessary to soften the image. It has been ensured that the brightness difference between pixels is closed by applying the mean filter which is frequently preferred in the literature.

The mean filter is used to soften the image and is based on the closure of the brightness difference between pixels and neighbors. It is generally known in the literature as a low-pass filter (Figure 5).

A	B	C
D	E	F
G	H	I

$$E' = 1/9\ (A+B+C+D+E+F+G+H+I)$$

Figure 5. Mean filter usage in a 3x3 image

The mean filter has the ability to reduce the local variance, thus reducing the signal to noise ratio (SNR). Therefore, it is generally recommended to use several filters at the same time (Narayanan and Wahidabanu, 2009). Figure 6 shows the mean-filtered image of the noise-free OCT image.

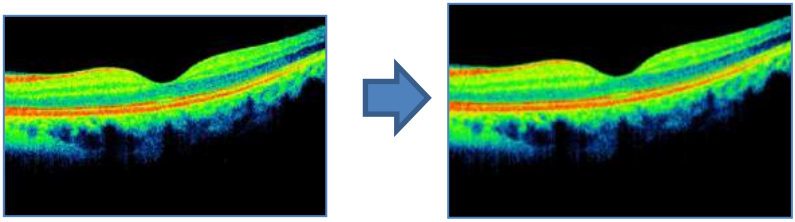

Figure 6. Mean filter application result

In the next step, red color clarification was applied to determine the lower boundary line of the epithelial tissue layer. In this process, pixels close to the red color using the nested loop are converted to a full red color. Thus, the image becomes available to the segmentation process to determine the lower boundary line of the epithelial tissue region. Figure 7 shows an image of the red clarification process for the epithelial region.

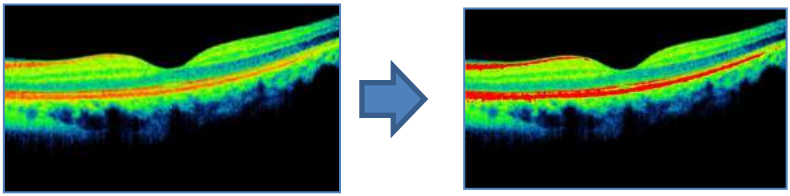

Figure 7. Red color highlighting process

Following the red clarification, the lower boundary line of the epithelial tissue layer, the upper boundary line of the sclera, and the lower boundary points of the nebulae network layer have been determined. In this process, the RGB pixel values are scanned starting from the top left corner of the image. Red color is used to find the lower boundary line of epithelial tissue, the upper boundary line of sclera and black border is used to determine the lower boundary points of the nebula region. Figure 8 shows the result of determining the upper and lower boundary lines.

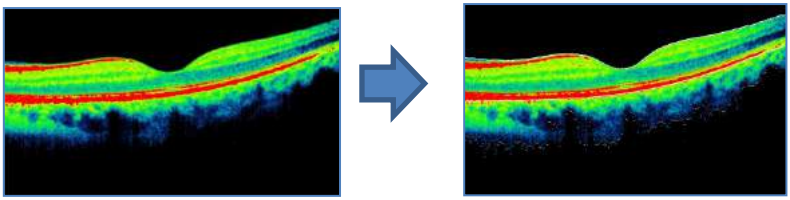

Figure 8. Determination of boundary lines

Following the determination of the boundary lines, the process of finding the fovea point was started. Fovea point is located by tracing the upper boundary line from left to right. Figure 9 shows a fovea point marked image.

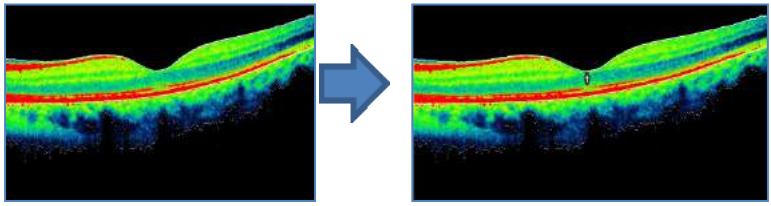

Figure 9. Determination of Fovea Point

In the measurement of choroidal thickness, a vertical line is drawn from the lower boundary line of the epithelial tissue layer to the bottom of the nebula layer in the downward direction from the fovea. The choroidal thickness is determined by taking the average of the length of the other lines drawn to the right and left of this upright. In the software developed under the study, the number of these lines and the distances between them can be determined parametrically (Figure 10-a). The measured values of the drawn lines in micrometers are shown to the user in the developed software (Figure 10-b).

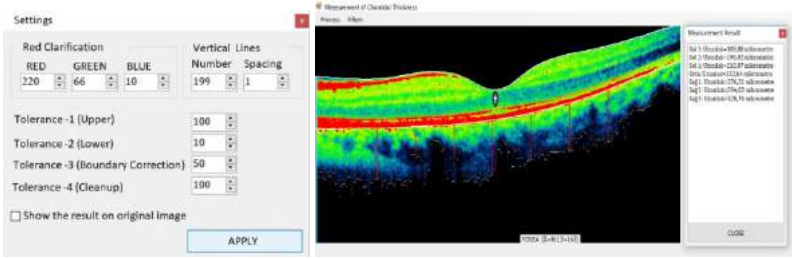

(a) (b)

Figure 10. (a) Parameter setting window, (b) choroid thickness measurement values (micrometer) window

4. RESULTS AND DISCUSSION

In this section, the results obtained by the software are compared with the results obtained by the ophthalmology specialist. The ophthalmologist specialist marked five lengths for the measurement of choroidal thickness over 30 eyes of 15 subjects. The software settled in the OCT device indicates the marked lengths in micrometers according to the calibrated values at their display resolution. Sample measurement are given in Figure 11.

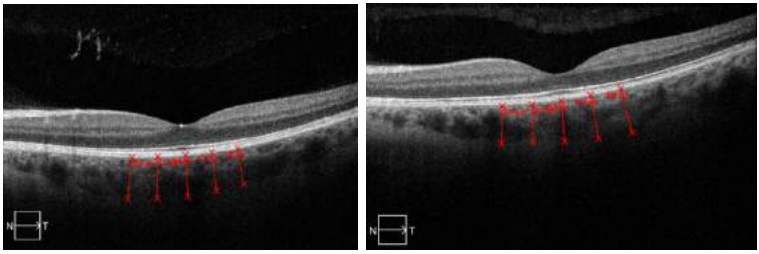

Figure 11. Expert measurement sample images (micrometer)

In Table 1, the measurement results of the ophthalmologist specialist and the measurement that the software found are given in micrometers. Column number 3, shown in the table, is the length of the middle line descending based on the fovea. Others (1,2,4,5) are the lengths of the lines determined by drawing horizontal lines in a similar range to the left and right of this midline. These boundary lines are the lines drawn between the lower boundary line of the epithelial tissue and the point where the nebula vein layer ends. The "Avg." columns in the table show the calculated average length of the 5 vertical lines drawn. In the left-most column of the table, the name and surname (The surname is hidden because it is a private information) of the patient and the information that belonged to the eye (L=left and R=right).

Table 1. Comparison of choroidal thickness measurement results (in micrometers)

	The measurement results of the ophthalmologist						The measurement results of the software					
Surname* Name Right(R)/Left (L)	1	2	3	4	5	**Avg.**	1	2	3	4	5	**Avg.**
B* Saygı R	290	287	280	279	279	**283**	225,7	246,5	314,8	216,8	172,2	**235,2**
B* Saygı L	458	462	465	434	411	**446**	222,7	261,3	288,0	264,3	273,2	**261,9**
B* Gamze R	286	270	257	221	182	**243,2**	225,7	228,6	294,0	285,1	270,2	**260,7**
B* Gamze L	239	263	276	290	343	**282,2**	282,1	181,1	210,8	258,3	201,9	**226,8**
C* Melike R	277	283	328	372	382	**328,4**	282,1	243,5	207,9	282,1	228,6	**248,8**
C* Melike L	490	493	502	507	502	**498,8**	255,4	187,1	258,3	213,8	332,6	**249,4**
D* Zeynep R	401	405	393	384	375	**391,6**	311,8	231,6	445,5	193,0	317,7	**299,9**
D* Zeynep L	322	339	346	359	367	**346,6**	368,2	308,8	255,4	427,6	193,0	**310,6**
G* Serap R	364	369	371	358	352	**362,8**	258,3	279,1	270,2	288,0	240,5	**267,2**
G* Serap L	347	363	423	458	467	**411,6**	522,7	207,9	481,1	273,2	317,7	**360,5**
G* Mustafa R	419	419	420	393	345	**399,2**	184,1	395,4	418,1	385,9	377,3	**352,1**
G* Mustafa L	321	331	337	338	330	**331,4**	335,6	344,5	237,6	380,1	252,4	**310,0**
G* Merve R	432	406	402	382	382	**400,8**	353,4	400,9	329,6	261,3	368,2	**342,6**
G* Merve L	435	444	454	438	418	**437,8**	276,2	386,1	338,5	311,8	439,5	**350,4**
K* Sagbatullah R	234	212	226	210	198	**216**	219,7	136,6	258,3	246,5	314,8	**235,1**
K* Sagbatullah L	253	288	301	287	288	**283,4**	109,8	264,3	273,2	249,4	314,8	**242,3**
K* M.Tahsin R	332	349	337	323	298	**327,8**	377,1	445,5	371,2	389,0	362,3	**389,0**
K* M.Tahsin L	314	304	301	297	262	**295,6**	302,9	308,8	317,7	350,4	368,2	**329,6**
K* Aysegül R	292	313	319	302	254	**296**	356,4	258,3	196,0	184,1	169,2	**232,8**
K* Aysegül L	272	277	274	280	275	**275,6**	335,6	258,3	130,6	243,5	329,6	**259,5**
O* Mehmet R	400	414	429	430	415	**417,6**	362,3	380,1	326,7	291,0	277,3	**327,4**
O* Mehmet L	456	487	500	490	488	**484,2**	231,6	299,9	323,7	371,2	288,0	**302,8**
K*Süleyman R	337	360	324	302	298	**324,2**	320,7	297	228,6	255,4	169,2	**254,1**
K* Süleyman L	298	292	323	364	385	**332,4**	299,9	392,0	335,6	279,1	297	**320,7**
T* Merve R	400	393	409	380	341	**384,6**	335,6	350,4	181,1	225,7	181,1	**254,7**
T* Merve L	338	337	336	321	306	**327,6**	315,2	301,4	271,3	285,1	211,9	**276,9**
T* Erkun R	311	292	299	278	237	**283,4**	362,3	400,9	362,3	311,8	365,3	**360,5**
T* Erkun L	225	270	239	214	224	**234,4**	169,2	323,7	106,9	344,5	187,1	**226,2**
Y* Dilara R	306	304	290	246	228	**274,8**	308,8	184,1	190,0	279,1	294,0	**251,2**
Y* Dilara L	265	262	284	328	338	**295,4**	329,6	240,5	169,2	323,7	276,2	**267,8**

** The surname is hidden because it is a private information*

When we examine Table 1, we see that there are differences between the average measurement values. We can find the difference between the results of the expert measurement and the results that the software automatically measures as the percentage ratio with the following equation:

$$Difference = \frac{1}{n} \sum_{1}^{n} abs(mean_n^1 - mean_n^2) \quad (1)$$

The percentage difference for all measurement results is 18,23%. Therefore, the choroidal thickness is measured automatically with computer-aided software successfully.

An ophthalmologist draws a vertical lines starting from the lower part of the epithelial tissue to the bottom border line of the choroid while measuring the choroidal thickness on OCT images. This is done manually by the ophthalmologist for each eye and takes a long time.

The results obtained in the study are very satisfactory. When the results were analyzed, it was seen that the measurement differences were mostly

caused by the bottom of the nebula structure. This is because the lower boundary line is in a recessed structure. It is suggested that studies should be carried out to draw the lower boundary line of this region which has a mostly protruding shape.

5. CONCLUSION

In this study, an image processing software was developed to perform this process automatically. OCT images in RGB format are used for ease of detection of epithelial tissue. First of all, morphological processes called dilation and erosion were applied and the noise in the upper and lower spaces of OCT images were removed. Noise removal is necessary for the determination of fovea and choroidal lower boundary points. Mean filter is important in the process of clarifying the red color of epithelial tissue. The lower boundary line of the epithelial tissue and the lower boundary points of the nebula region were found from the pixel neighborhoods. The thickness of the choroid region between these two boundary lines was measured by pixel to metric transformation.

In this study, it is seen that the choroidal thickness can be measured automatically by using computer aided image processing software. We believe that this study will make an important contribution to future studies in this area.

6. ACKNOWLEDGEMENTS

This paper contains the results obtained within the scope of Onur Çakar's master thesis. Ethics committee report was received from Selçuk University Medical Faculty for the use of OCT images. We would like to thank Selçuk University Scientific Research Projects Coordinator for supporting the work with the project number 19704014.

REFERENCES

1. D. Alonso-Caneiro, S.A. Read and M.J. Collins, "Automatic segmentation of choroidal thickness in optical coherence tomography," *Biomedical Optics Express*, 4(12): 2795-2812, 2013.
2. D. Koozekanani, "Retinal Thickness Measurements From Optical Coherence Tomography Using a Markov Boundary Model," *IEEE Transactions on Medical Imaging*, 20(9): 901-916, 2001.
3. İ. Tuncer, E. Karahan, M.Ö. Zengin, "Normal gözlerde subfoveal koroid kalınlığının optik koherens tomografi ile ölçülmesi," *Retina-Vitreus*; 22:137-139, 2014.
4. M. Moussa, D. Sabry and W. Soliman, "Macular choroidal thickness in normal Egyptians measured by swept source optical coherence tomography," *BMC Ophthalmology*, 16:138, 2016.
5. S.K. Narayanan and R.S.D. Wahidabanu, "A View on Despeckling in Ultrasound Imaging," *International Journal of Signal Processing, Image Processing and Pattern Recognition*, 2(3): 85-98, 2009.
6. P. Gupta., T. Jing, P. Marziliano, C.Y. Cheung, M. Baskaran, E.L. Lamoureux, T.Y. Wong, C.M.G. Cheung and C-Y. Cheng, "Distribution and Determinants of Choroidal Thickness and Volume Using Automated Segmentation Software in a Population-Based Study," *Am J Ophthalmology*, 159(2): 293-301, 2015.
7. V. Kajić, M. Esmaeelpour, B. Považay, D. Marshall, P.L. Rosin and W. Drexler, "Automated choroidal segmentation of 1060 nm OCT in healthy and pathologic eyes using a statistical model," *Biomedical Optics Express*, 3(1):86-103, 2011.
8. V. Manjunath, M. Taha, J.G. Fujimoto and J.S. Duker, "Choroidal Thickness in Normal Eyes Measured Using Cirrus-HD Optical Coherence Tomography," *Am J Ophthalmology*, 150(3): 325–329, 2010.
9. Z. Géhl, K. Kulcsar, H.JM. Kiss, J. Nemeth, O.A. Maneschg and M.D. Resch, "Retinal and choroidal thickness measurements using spectral domain optical coherence tomography in anterior and intermediate uveitis," *BMC Ophthalmology*, 14:103, 2014.

THE USE OF LEATHER MATERIALS IN SHAMANIC CLOTHES AND CONTEMPORARY INTERPRETATIONS

Deniz GÜRLER KARAMAN[1] ,
Selime MENTEŞ ÇOLAK[2]

[1] Uşak University Leather Application and Research Center, Uşak, Turkey.
[2] Ege University Engineering Faculty Leather Engineering Department, İzmir, Turkey.

INTRODUCTION

Shamanism is one of the oldest religious practices and beliefs. Those who are believed to be capable of contacting good and evil spirits, get respect from their communities and communicate with their ancestors during the rituals are called as “Shamans” and healers [1].

Shamans wear special costumes for religious rituals or healing ceremonies. These costumes which are made using various decorations and accessories chosen in accordance with their status and ability remain popular today, as ethnic clothing. Shamanic costumes produced with modern techniques for the people who maintain the practice or interested in the traditions are on the market around the world.

The belief that makes these costumes important and valuable is that it has a sacredness which symbolizes the spirit helpers, leads to the connection between the spirit and sky gods apart from their spiritual abilities. Shamanic costumes which have been decorated with different symbols and objects are exhibited in various museums. There are various examples of these costumes within the catalogues of Stuttgart's Linden Museum, Tampere’s Tampere Museum and St. Petersburg's Museum of Ethnography [2].

Leather has always been an important material for human beings and it was commonly used after stones and woods during the ancient times. The clothes and accessories of shamans have great importance in their rituals and ceremonies. It has been observed that leather was also used for making shamanic costumes and objects. This study aims to present information on shamanic costumes that carry specific objects which represent the whole universe and appear as an authentic style of clothing through the variables as time, place and concept within its use.

RITUAL COSTUMES

Shamanic costumes are special garments that provide a spiritual connection between the universe and people and symbolize this sacredness with a religious and creative approach. They are regarded as one of the materials that helps shamans gather strength and descriptions and motifs on these costumes are chosen to depict the powers through which shamans communicate with other world [3].

The form of these costumes represents the meaning while their design determines the details of the form. Consequently, they have various motifs that symbolize the animal spirits of the Earth and the sky. The structure of the design has been assigned a functional and esoteric meaning and changed through different cultural traditions [4].

The most original practices of Shamanism, which has continued its existence around the world, are mostly maintained in Asia and Siberian region. For this reason, the dresses and costumes of the shamans of the Turkish tribes living in Asia and Siberian region which adopted the shamanic belief are significant materials [2].

There are common characteristics of these costumes which are based on the foundations of the belief system despite differences in the origin and culture of the people to whom it belongs. The materials used for creating and decorating the costumes are the basic elements that provide them with an opportunity to gain meaning apart from the form. It has been observed that leather is a commonly used material in Asia and Siberian region and the design, sewing method and surface decoration differ depending on the animal skin. Shaman costumes made of bovine leather have less pieces and stitches as it has a larger surface. More pieces and detailed stitches are used for other animal skins as sheep and goat etc. Leather strips or fringes are usually used for the hemline (Figure 1) [5].

Figure 1: Leather Shaman Ritual Costume [5].

These leather strips or fringes represent the spirit of a shaman rising to the sky like a bird. Leather is used with natural color or dyed and embroidery, beading, motifs and applique symbolize the power and status of s shaman (Figure 2) [6].

Figure 2: Mongolian Shamanic Dress [6].

It is seen that there are leather drums or frame drums besides the costumes exhibited in several museums. These are the important tools for shamans believed to help spiritually rising into the sky (Figure 3) [7]. Donkey skin is commonly used for the drums according to the researches and historical archives. Frayed leather is replaced to be hang on a tree in the woods. The tree is considered to be a significant icon in Shamanism and the world is defined as the "World Tree" as idealized with trees [8].

There are various images and symbols on the drums. The purpose of these objects whose front face is covered with leather and the other one is surrounded by leather ropes to enable holding is believed to remove negative energy and repel evil spirits through the sound. It is common to use various rattles, bells etc. due to similar beliefs.

In certain cultures, the skins and claws of helping spirits as squirrels, rabbits etc. are also hang on the costumes [9].

Figure 3: Shaman Costume and Timpano [7]

Other complementary elements of a shamanic costume are headdress and mask used together. It is also remarkable that they are usually made from

leather and decorated with horns and feathers. The bird is the most commonly used figure in these costumes and it is identified with the rise of the spirit. The eagle owl is especially one of the most powerful motifs and its feathers are used for the decoration of the headdresses besides the leather fringes depicting birds (Figure 4) [10, 11].

Skins of the birds as eagle owl etc. are used to make leather headdresses and their wings remain as an ornament. Some tribes used sable, wolf and bear skin for their costumes and headdresses apart from processing their fur for other garments.

Figure 4: Shamanic Headdresses [10, 11].

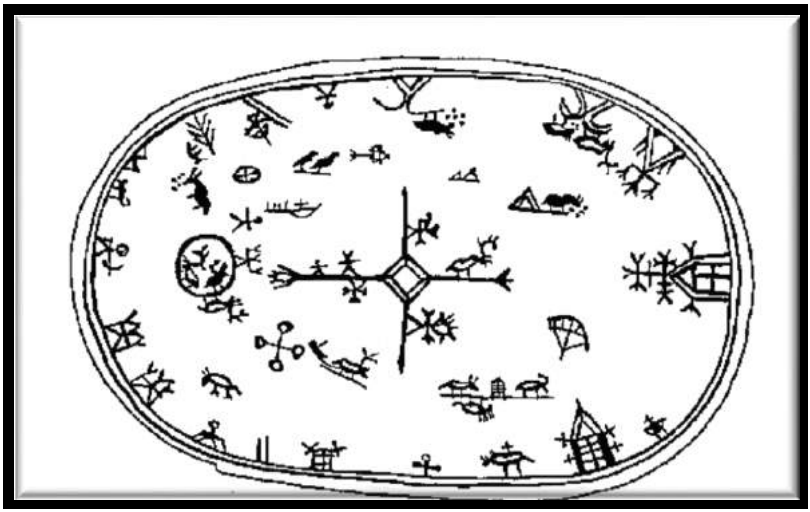

Figure 5: Shaman Drum Patterns [11].

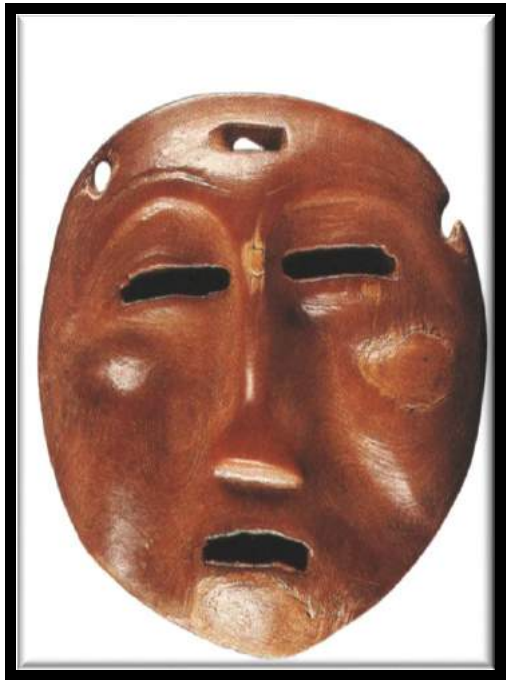

Figure 6: Mask of Shaman [12]

Figure 7: Shaman Costume, Head, Mask and Drum [12]

Masks have been used within communities from the different parts of the world. The main purpose is that the person who performs the ritual or ceremony hiding their face from the gods. The belief that masks symbolize the protective spirits of ancestors and respect for a spiritual journey between the different dimensions are the main reasons continuing this tradition. Various figures and symbols are drawn on the masks which are made using wood, leather and metals besides animal skin. Hides of the strong animals as bear, wolf etc. are both designed as masks and headdresses [13, 14].

Figure 8: The Bear Pelt and Mask of Shaman [14].

Another material that completes the costumes is a whip (bardag) which is also regarded as sacred. It is believed that these whips which made from leather belts repel the evil spirits from the patient's body [15]. Whips and drums are accepted as a horse for riding to the other world in different cultures. It has been observed that drum-sticks attached with leather belts are prepared both as a stick and whip and head of the stick is decorated using feathers, bells and rattles.

Shamans consider it important to preserve the costumes except for ceremonial use and they store it in a special place within their tent. Altai people preserve the costumes in leather bags [16].

Leather has always been one of the main materials used for making, protecting and decorating the costumes besides being a status symbol. The skin of the hunted animals could be used both for clothing and making these

sacred dresses. However, as mentioned above, the animals used for this purpose are chosen according to their meaning and symbols in Shamanism.

SHAMANISM AND COSTUMES TODAY

Shamanism is one of the mystical beliefs which has survived until today. Modern people who especially focusing on having a healthy and peaceful life has started to take interest in healing methods of the nature as complementary and alternative medicine. This interest brings lots of people and communities with those who continues their shamanic traditions together. Modern day shamans who attempt to share experiences of shamanic healing through conferences and events, also introduce Shamanism and rituals through their personal web sites [17, 18, 19, 20].

This continuing interest increases the demand for shamanic clothes and objects. Thus, various costumes which are designed using materials similar to the originals have a specific sales volume and market share in the clothing industry. These costumes which are priced higher and considered as sacred represent an important field for "modern shamans" of the 21th century and consumers who interested in shamanic practices and discipline.

Figure 9: Genuine Native American Navajo Indian Shaman Headdress [21].

Figure 10: The Modern Shaman [22].

Figure 11: Modern Shaman Drum [23].

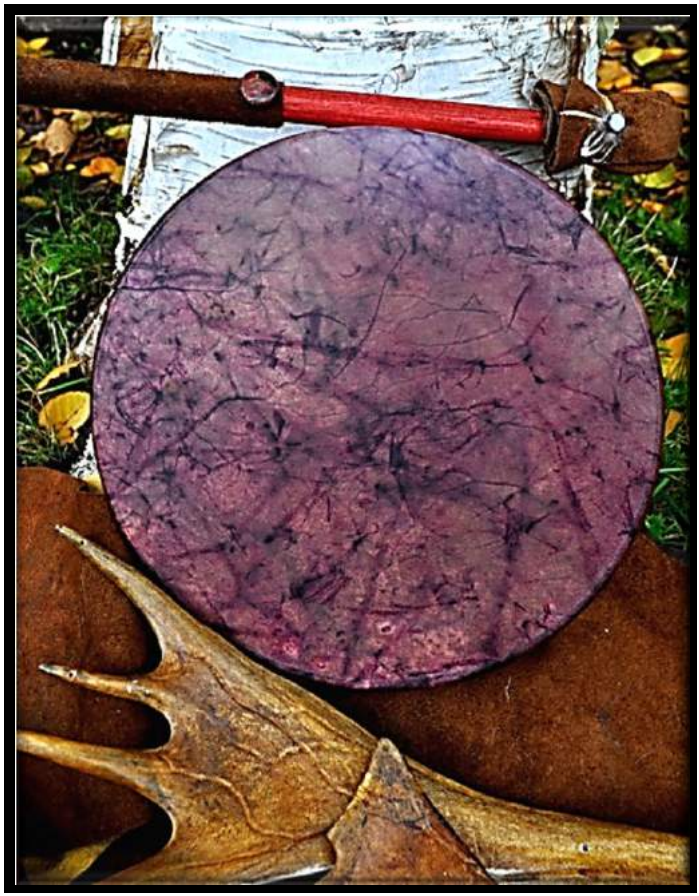

Figure 12: Custom Medicine Drum [24]

Figure 13: Drum Making Kits [24]

Wolf skin, bear hide and reindeer skins are the most commonly used leather types for this purpose. Their bones are also used with various healing stones for designing shamanic accessories (Figure 14).

Figure 14: Modern Shaman Accessories Decorated with Deer Skin, Onyx Stone, Gems and Bones [24]

Shamanism and interest for shamanic costumes have attracted fashion designers' attention and they display their contemporary costume designs within fashion weeks and other events. Shaman's parkas of Inuit people, interpreted by KTZ, one of the design brands in UK have been discussed in various researches for generations and accepted as "the most unique garment from Canada". The men's collection during the events in fall 2015, has been inspired from the designs and motifs of Inuit clothing including a sweater which has nearly the same patterns and motifs of a caribou skin parka from 1900s. The history of the collection have inspired interest for the origin of the parkas and meaning begind the symbolic design (Figure 15) [25].

Figure 15: "U.K. design label, KTZ, 'copied' the design from an Inuit shaman's parka considered by experts as the 'most unique garment known to have been created in the Canadian Arctic.' (Kieran Oudshoorn/CBC (from book Northern Voices) /Tristan Fewings/Getty Images)" [25].

It has been discussed that animistic beliefs, spiritual beings and shamanic practices have influence on designers and fashion industry. In addition, an interesting metaphor of Hugo Boss for designers is mentioned in the article by Kasper Tang Vangkilde, "Possessed by the Zeitgeist: Inspiration and Prophecy in the Business of Fashion". Boss has assigned an adjective to designers for having a foresight as shamans and underlined one of the characteristics of shamanic people as saying: *"In a way, it's just to follow the wave, because, from my point of view, a designer is a kind of shaman. It is a person who has a possibility of catching something which is not really visible; something which is in the air, which everybody can breathe, but which only some people have the possibility, or the faculty, of translating into reality, into real and concrete things" [26].*

Shamanism which has affected people's inner world, daily life and style, also influences modern leather clothing and accessories through historical materials and designing objects. It may be recommended for the designers interested in this mystical experience and heritage to follow "Shaman Journal of the International Society for Academic Research on Shamanism" which examines Shamanism with a scientific approach and contributes to academic field through publishing various articles apart from accessible online resources. The journal has been published by Molnár and Kelemen Oriental Publishers since 1993 and it is an official publication of International Society for Academic Research on Shamanism [27].

The effects of both Shamanism and shamanic clothes have maintained until today. It is remarkable that leather is commonly used in these costumes and other accessories. The findings on tanning process in that period have not been found according to the studies. The pieces are exhibited in the museums and they are not accessible to take samples. However, there are certain predictions about use of plants, oils and smoke for tanning in a belief and healing system which communicates with the nature.

Using the methods of modern technology which will provide lightweight processed leather particularly for shamanic costumes with regards to wearing-comfort, application of shamanic symbols on leather surfaces using the techniques of printing, embroidery etc. and revival of this unique and mystic clothing through modern designing details represent a point of view for designers to create significant collections.

REFERENCES

1. https://samanizm.net/ acess date 21.02.2019
2. YARDIMCI,G., Kezban., Türk Töresinin Hazineleri Kutsal Şaman Elbiseleri İkonografisi, International Journal of Cultural and Social Studies (IntJCSS),: Volume 3 (Special Issue) e-ISSN : 2458-9381ISSN, December 2017
3. http://www.ergenekun.net/uygur-turkleri-arasinda-samanlar-ve-tedavi-yontemleri.html/2 acess date 21.02.2019
4. KILIÇ,Selim., Semantıc Approach to The Turkısh Shamanıc Costumes, Zeitschrift für die Welt der Türken Journal of World of Turks ZfWT Vol. 2, No. 1 ,2010
5. Leather Shaman Rituel Costume, Russian Museum Etnografy https://artsandculture.google.com/asset/evenk-shaman-ritual-costume, acess date 21.09.2019
6. Mongolian Shamanism dress; http://www.ipernity.com/doc/wolfgang-pfriemer/6031255acess date 21.09.2019
7. Shaman costume from the Zanabazar Museum of Fine Arts, http://crushevil.co.uk/ acess date 21.02.2019
8. İZGİ, C. Mustafa ., An Overview of Shamans and Shamanism Lokman Hekim Journal,; 2 (1): 31-38,2012
9. SARI, İbrahim., Şaman Türkleri,noktaekitap,08 Ocak 2017
10. GORBATCHEVA,V., FEDEROVA,M., Art of Sbiria ,Parkstone International, 9 Mar 2016
11. Russian Museum of Ethnography (St. Petersburg), acess date 21.02.2019
12. http://masterpieces.asemus.museum/masterpiece acess date 21.02.2019
13. BAĞCI, Atilla, Şamanizm İnancında Ritüel Maskeları ve Gömü Maskeleri, Türk Dünyası / Turkısh World Dil ve Edebiyat Dergisi / Journal of Language and Literature Sayı/Issue: 46) - ISSSN: 1301-0077 Ankara, Turkey DOI Numarası/DOI Number: 10.24155/tdk.2018.79,2018
14. WİLLİAM A. Fox, WİNNİPEG J. Eldon Molto, The Shaman Of Long Poınt, https://www.ontarioarchaeology.on.ca/Resources/Publications/oa57-2-fox.pd, , Folklore (Estonia) 4 DOI: 10.7592/FEJF1997.04, acess date 22.02.2019
15. BAYAT, Fuzili, Ana Hatlarıyla Türk Şamanlığı, Otüken Neşriyat, YAYIN NU: 648 KÜLTÜR SERİSİ: 307, ISBN 975-437-571-2,İstanbul 2006.
16. http://www.sharedwisdom.com/article/modern-shaman , acess date 10.02.2019
17. https://www.takingcharge.csh.umn.edu/shamanism acess date 10.02.2019
18. http://www.simonnebutler.co.nz/9-signs-your-calling-is-as-a-modern-day-shaman/ acess date 10.02.2019
19. http://www.medicinewoman.com/ acess date 10.02.2019
20. https://picclick.com/Genuine-Native-American-Navajo-Indian-Headdress-Full-Coyote ,acess date 22.02.2019.
21. BONAİR; Dwight, The Modern Shaman, 06.10.2012 , http://beforeitsnews.com ,acess date 10.01.2019
22. http://shamantrommer.dk/shaman-drums/ ,acess date 10.01.2019
23. https://www.ancestral-pathways.com acess date 22.02.2019
24. ZEREHİ Sima Sahar, Inuit shaman parka 'copied' by KTZ design well-studied by anthropologists, https://www.cbc.ca/news/canada/north/inuit-shaman-parka-design-history-, CBC News · Posted: Dec 02, 2015 4:00 AM CT | Last Updated: December 2, 2015; acess date 12.02.2019

25. VANGKİLDE, Kasper Tang, Possessed by the Zeitgeist: Inspiration and Prophecy in the Business of Fashion, Journal of Business Antropology, Page 1 of 23 JBA 4(2): 178-200 Fall 2015
26. SHAMAN Journal of the International Society for Academic Research on Shamanism, https://www.isars.org/shaman/ ,acess date 10.01.2019.

HYDROGEN PRODUCTION FROM RENEWABLE ENERGY SOURCES AND ITS STORAGE

İbrahim GÜNEŞ [1]

[1] Associate Profesor, Istanbul University-Cerrahpasa, Faculty of Engineering, Department of Electrical and Electronics Engineering, Avcilar, Istanbul, Turkey.

Introduction

Hydrogen is not present in the form of compounds in the nature, but in pure form. Hydrogen is mostly in water, in various hydrocarbon forms and in other chemical compounds. It is necessary to pass through a number of transformation processes so that hydrogen can be used for energy purposes [1-4].

The ordinary power eaten up by a human body still is 0.1 kW and generally 0.4 kW for a committed body, passing on about 0.1 kW of work. The usage of plants did not change the earth in light of the way that the carbon dioxide, which was liberated by the general population and animals, was reabsorbed by the plants in the photosynthesis strategy. [5-7].

Toward the day's end, the essentialness substance of 0.33 kg of hydrogen identifies with the imperativeness substance of 1 kg of oil. The imperativeness substance of a fuel is normally called the warming worth. The refinement between the upper and the lower warming characteristics is the enthalpy of vaporization of water according to the state of the water as a result of the consuming. For hydrogen, the lower warming quality is 33.3 kWh kg-1, and the upper warming worth is 39.4 kWh kg-1. Hydrogen is the most rich of all parts in the world, and it is felt that the considerable segments were, and still are, being worked from hydrogen and helium. It has been evaluated that hydrogen makes up over 90% of the extensive number of particles or 75% of the mass of the universe. [8-10].

The vitality from the daylight is changed over into power by methods for photovoltaic cells. The power is utilized to separate water into hydrogen and oxygen. The last is discharged in the climate and hydrogen is put away, transported and conveyed. At last, hydrogen together with the oxygen is combusted and the vitality is discharged as work and warmth leaving water or steam into the climate. Therewith, the hydrogen cycle is shut. Hydrogen cycle is given in Fig. 1 [11]. Power from a manageable power source, for instance wind control, photovoltaic, hydropower and geothermal power can be used for the electrolysis of water. Electrolysis at incorporating temperature and encompassing weight requires a base voltage of 1.481V and in this manner a base imperativeness of 39.7 kWh kg-1 hydrogen. Today electrolysis structures eat up about 47 kWh kg-1 hydrogen, for instance the viability is around 85%.[10]

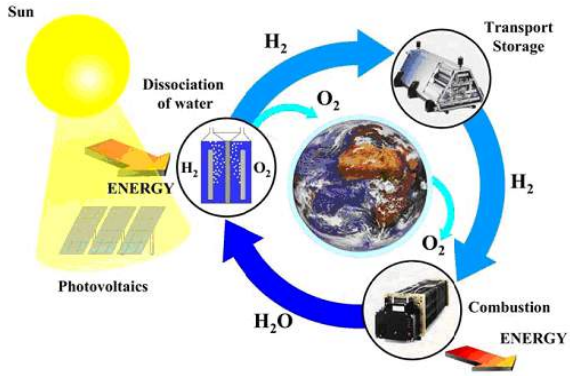

Fig. 1. The hydrogen cycle [11].

The process of separating water into hydrogen and oxygen using direct current is called electrolysis. It is known as the simplest method for the production of hydrogen. Within the electrolysis cell are two electrodes, usually planar metal or carbon plates, and a conductive liquid called electrolyte, immersed in them. When the direct current source is connected to these electrodes, it flows directly in the conductive liquid, from the positive electrode to the negative electrode. As a result, water in the electrolyte, hydrogen released from the cathode and the oxygen from the anode will separate. Here, in contrast to the separation of water only, a substance such as potassium hydroxide is usually added to the electrolyte as a conductivity enhancer, since the water is not a good conductor [12 , 13].

For water electrolysis, at normal pressure and temperature, ideally 1.23 volts is sufficient. Reaction is slow and for some reasons higher voltage is used in electrolysis process. When the hydrogen production rate is proportional to the actual current intensity, high current densities are preferred for economic reasons. Therefore, in practice, the voltage applied per cell is usually about 2 volts. Theoretically, 2.8 kW-hour electric energy is sufficient for every cubic meter of oxygen, while the amount of electricity used in practice for the reasons summarized above is 3.9-4.6 kW-hour. Accordingly, the yield of electrolysis is about 70%. But, in the recent years, 90% efficiency has been achieved thanks to the work done in this field and advanced technology [14-16].

Nickel-plated steel electrodes are used in practice in electrolysis cells. Electrolysis seems to be the only method that can be developed in the fossil fuel cycle for the production of abundant hydrogen. Hydrogen production from water electrolysis is 50 years. It is a system with a simple infrastructure, high efficiency and no moving parts [17-20]. Separating the hydrogen and oxygen are called electrolysis, it is using direct current for electrolysis of water to the process. It is using for the production of hydrogen is applied as the simplest method. In principle, in electrolysis cell, usually a plane metal or

carbon plates, and the two electrodes immersed in them, referred to as conductive electrolyte is a liquid [20].

In this study, hydrogen energy production by electrolysis method and storage of the produced energy was discussed for Turkey.

Hydrogen Storage Methods

Hydrogen storing essentially proposes the decline of the gigantic volume of the hydrogen gas. 1 kg of hydrogen at encompassing temperature and natural weight takes a volume of 11 m3. In order to manufacture the hydrogen thickness in a limit structure work ought to either be associated with pack hydrogen, or the temperature must be lessened underneath the essential temperature or finally, the stun must be diminished by the cooperation of hydrogen with another material. The second crucial worldview of a hydrogen amassing system is the reversibility of the hydrogen take-up and release. This model precludes all covalent hydrogen carbon blends as hydrogen accumulating materials in light of the way that the hydrogen is perhaps released from carbon hydrogen blends if they are warmed to temperatures above 800°C or if the carbon is oxidized [21–23].

The most widely recognized capacity frameworks are high weight gas chambers with a greatest weight of 20 MPa. New light weight composite chambers have been produced which can withstand a weight up to 80 MPa thus the hydrogen can achieve a volumetric thickness of 36 kg m-3, roughly half as much as in its fluid structure at the typical breaking point. The gravimetric hydrogen thickness diminishes with expanding weight because of the expanding thickness of the dividers of the weight barrel. [23]

The security of pressurized chambers is an issue of concern particularly in exceptionally populated locales. Future weight vessels are visualized to comprise of three layers: an internal polymer liner, overwrapped with a carbon-fiber composite (which is the pressure bearing part) and an external layer of an aramid-material fit for withstanding mechanical and consumption harm. The objective that the business has set for itself is a 70 MPa barrel with a mass of 110 kg bringing about a gravimetric stockpiling thickness of 6% mass and a volumetric stockpiling thickness of 30 kg m-3. Hydrogen can be packed utilizing standard cylinder type mechanical blowers. Slight alterations of the seals are at times essential so as to make up for the higher diffusivity of hydrogen. [23]

Storage as Pressurized Gas; This method is the most economical solution and the hydrogen energy density is quite high depending on the size of the vessel and the size of the pressure vessels. The amount of hydrogen stored because of necessity is inadequate. Moreover, due to the safety of the pressure vessels used, the cabin is empty and the weight is high. Deposition and transportation can be done at ambient temperature. Because of high pressure, there is no energy loss in the part that becomes liquid in the tank [24].

Liquid Storage of Hydrogen; Liquid hydrogen is used as fuels in rockets, supersonic and hypersonic space vehicles. Hydrogen is liquid at about 200K and 2 bar. Liquid hydrogen is stored in super-insulated double-walled cryogenic vessels that minimize heat transfer and boiling. The fuel required for vehicles is delivered to the motor when both liquid and gas are taken from the phase. Liquid hydrogen (LH2) tanks for hydrogen vehicles are used successfully [25, 26].

Liquid hydrogen is secured in cryogenic tanks at 21.2 K at encompassing weight. In view of the low fundamental temperature of hydrogen (33K), liquid hydrogen must be secured in open structures in light of the fact that there is no liquid stage existent over the essential temperature. The load in a shut amassing system at room temperature could augmentation to around 104 bar. The volumetric thickness of liquid hydrogen is 70.8 kg m-3 and barely higher than that of solid hydrogen (70.6 kg m-3). The challenges of liquid hydrogen storing are the imperativeness capable liquefaction process and the warm security of the cryogenic amassing vessel in order to decrease the rise off of hydrogen. The hydrogen molecule is made out of two protons and two electrons. The blend of the two electron turns conceivably prompts a coupling state if the electron turns are threatening to parallel. The wave limit of the molecule must be antagonistic to symmetric in context on the exchanging of the space headings of two fermions (turn = 1/2). Thusly, two social affairs of hydrogen particles exist as demonstrated by the full scale nuclear turn (I = 0, antiparallel nuclear turn and I = 1, parallel nuclear turn). The essential social occasion with I = 0 is called para-hydrogen and the second assembling with I = 1 is called ortho-hydrogen. Run of the mill hydrogen at room temperature contains 25% of the para structure and 75% of the ortho structure. The ortho structure can't be set up in the unadulterated state. Since the two structures differentiate in essentialness, the physical properties furthermore shift. The conditioning and limits of para hydrogen are around 0,1 K lower than those of average hydrogen. [26].

At the point when hydrogen is cooled from room temperature (RT) to the typical breaking point (nbp =21.2K) the ortho hydrogen changes over from a harmony convergence of 75% at RT to half at 77K and 0.2% at nbp. The self-change rate is an initiated procedure and moderate, the half-life time of the transformation is more noteworthy than one year at 77K [26].

Advantages and Disadvantages of Liquid Hydrogen Storage

Relatively Lightweight Storage; Hydrogen fuel can be sprayed directly with the aid of high-pressure liquid hydrogen pump. If there is an air conditioner unit in the container, liquid hydrogen can be used for cooling purposes. Uncontrolled combustion can be prevented and reduction of NOx emissions is achieved. The energy required for liquefaction is great. Hydrogen gas is used for liquefaction [27].

When the gas is in liquid from, some of it evaporates, so the phase change must take place rapidly. Liquid evaporation losses occur during storage and use of hydrogen in tanks. The fuel tank to be used has a very good thermal

insulation. The heat transfer caused by the fact that the storage insulation is done literally causes the storage pressure to increase. To prevent the pressure from increasing, vaporized hydrogen must be thrown into the atmosphere [27-29].

Hydrogen will be put away in different courses relying upon the application, for example versatile or stationary. Today we think around a few proficient and safe approaches to store hydrogen, anyway there are numerous other new potential materials and strategies conceivable to build the hydrogen thickness altogether. The material science challenge is to all the more likely comprehend the electronic conduct of the collaboration of hydrogen with different components and particularly metals. Complex mixes like Al(BH4)3 must be explored and new mixes from the light weight metals and hydrogen will be found. In view of today best innovation, a vehicle fueled with an interior ignition motor expends 2.4 kg (3 liter) of gas per 100 km. Enthusiastically this compares to 0.8 kg of hydrogen per 100 km. So as to drive the vehicle for 500 km before refilling the hydrogen stockpiling framework, the vehicle needs 4 kg of hydrogen ready. The tank with 4 kg hydrogen put away in a metal hydride is around 300 kg and has a volume of roughly 60 liter. Since such a capacity vessel is primarily a steel compartment loaded up with a metallic powder, it very well may be utilized as a valuable component of the vehicle. For this situation not the majority of the heaviness of the capacity framework is extra load to the vehicle [29].

Hydrogen Storage Underground

Underground storage of hydrogen is another form of storage in compressed gas. It is the least costly storage method for large amounts of hydrogen. Hydrogen can be stored both underground and underground mines. Underground gas storage requires minimum investment cost. However, the disadvantage of this method is the 5% loss of stored hydrogen. One of the cost-enhancing reasons for underground storage is the storage system disposal cycle [29].

Hydrogen can be stored underground in the various conditions. These are the large salt cavemen, empty mineral beds, empty oil wells, and natural caves.

A porous layer in the water permeable structure below the surface is generally sand or sandstone, particularly suitable dome-shaped geological structure. Before the hydrogen gas is introduced into the underground storage, cavities are formed in the layers and the surface is covered with cement or similar chemicals[29].

Discussion and Conclusion

In this study, for the case that the water electrolysis process underground water, a solution was produced to the problem of hydrogen energy storage, which is one of the biggest problems. Underground water in suitable geological structures, facilities electrodes, with drilling the creation of

underground electrolysis system by tapping into above ground in the alternative energy sources with electrolysis system of nutrition as a result of solar panels and derived from wind turbine energy battery system instead of electrolysis feed used and hydrogen conversion to energy is provided. The storage of hydrogen is costly and requires a high pressure tube, underground storage of compressed gaseous hydrogen storage another form of it.

Underground storage of hydrogen is low cost for the hydrogen in large quantities at low cost the storage method. Hydrogen can be stored underground, natural and subsequently in the cave. Underground gas storage tanks require minimal investment costs. However, this method has the disadvantage that the stored compressed hydrogen causing loss of 5%. One of the reasons the cost of building the underground gas storage is formed when the end of the discharge cycle storage system[29].

Disposal of this gas requires an additional cost. Hydrogen can be stored in a variety of underground space. Hydrogen produced from sea, lake, surface water sources such as streams, is sent to underground geological repository with pipelines, it is possible. Be more cost-effective storage operations of extracting oxygen from the electrolysis of underground waters in subterranean cavity may be achieved by keeping the hydrogen underground cavity. Block diagram of hydrogen production and underground storage suggested by our study is given in Fig. 2.

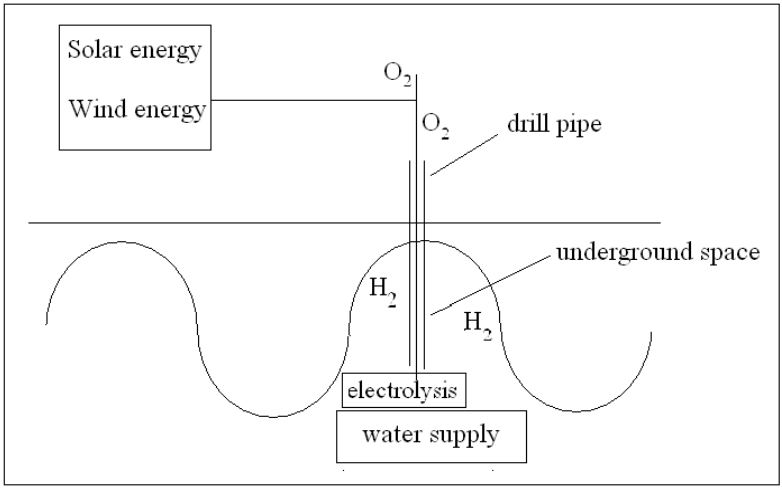

Fig. 2. Block diagram of hydrogen production and storage underground [30].

Hydrogen is likely to be the synthetic fuel for the future because of the large heating value and the possibility to use hydrogen produced from renewable energy in a closed cycle. The conversion of the energy stored in

hydrogen into work is theoretically more efficient using a fuel cell than an internal combustion engine. Therefore the mobile energy consumption could be reduced by approximately 35% with the introduction of fuel cells but the introduction of hydrogen as a synthetic fuel is independent of the fuel cells. However, just like the fossil fuels have started the industrial age, hydrogen will start an economic and technical revolution. Once the investments for the production of renewable energy are carried out human beings will profit from a hydrogen based environmentally clean energy economy[29-30].

Possible sources for hydrogen fuel production in Turkey; Hydraulic energy, solar energy, wind energy, Sea-wave energy, geothermal energy and nuclear energy. In terms of the development process like Turkey and the countries in the technological transition stage, Long-term photovoltaic solar-hydrogen system seems appropriate.

In this method of producing hydrogen from electrolysis of water by electric energy obtained from photovoltaic channels, 108.7 kg of hydrogen can be obtained from 1 m^3 of water, equivalent to 422 liters of gasoline. Hydrogen production in Turkey is the presence of hydrogen stored chemically in the bottom of the Black Sea, a long coastal line. 90% of the Black Sea's water is anaerobic and contains H_2S.

The hydrogen upheaval following the mechanical age has recently begun. Hydrogen creation, stockpiling and change has achieved an innovative dimension albeit a lot of upgrades and new disclosures are as yet conceivable. The hydrogen stockpiling is regularly considered as the bottleneck of the sustainable power source economy dependent on the engineered fuel hydrogen. Six distinctive hydrogen stockpiling strategies have been depicted. Among the settled high weight barrels for research center applications and the fluid hydrogen for air and space applications, metal hydrides and complex hydrides offer a sheltered and productive approach to store hydrogen. Further logical research and specialized improvements will prompt new materials with a higher volumetric and gravimetric hydrogen thickness. The best materials today demonstrate a volumetric stockpiling thickness of 150 kg•m-3 which can be enhanced by roughly half as indicated by hypothetical estimations.

Acknowledgments

This work was supported by the Research Fund of the University of Istanbul. Project number BEK-2016-22593

REFERENCES

1. Choudhuri A (2000) An experimental and numerical investigation on hydrogen–hydrocarbon composite fuel combustion. Ph.D. dissertation, School of Aerospace and Mechanical Engineering, University of Oklahoma, Norman
2. Choudhuri A, Gollahalli SR (2000) Combustion characteristics of hydrogen–hydrocarbon hybrid fuel. Int J Hydrogen Energy 25: 451–62
3. Choudhuri A, Gollahalli SR (2000) Laser induced Fluorescence measurements of radical concentrations in hydrogen–hydrocarbon blended gas fuel flames. Int J Hydrogen Energy 25: 1119–1127
4. Peters N (1993) Flame calculations with reduced mechanism-an outline. Reduced kinetics mechanism for application in combustion systems. Lecture Notes in Physics. New York, Springer 3–14
5. Alnıak MO, Palacı Y, Güneş İ (2007) New Materials for High Pressurized Hydrogen Storage, II. International Hydrogen Energy Congress & Exhibition, Turkey, 13-15 Jul 2007, 481-486
6. Alnıak MO, Güneş İ, Toktamış MM, Türksoy ME (2008) Hydrogen Usage and Storage, 12. International Research Conference, Trends in the Development of Machinery and Associated Technology, TMT İstanbul, Turkey, 1-4 Aug 2008, 756-764
7. Alnıak MO, Garip M, Güneş İ, Karaçam E, Bolcan C (2007) Adding Hydrogen into the CNG Tank to Increase Efficiency. II. International Hydrogen Energy Congress & Exhibition, Turkey, 13-15 Jul 2007, 645-651
8. Bockris JOM (2002) The Origin of Ideas on a Hydrogen Economy and Its Solution to the Decay of the Environment. Int J Hydrogen Energy 27: 31-74
9. Kiyobayashi T, Srinivasan SS, Sun DL, Jensen CM (2003) Kinetic Study and Determination of the Enthalpies of Activation of the Dehydrogenation of Titanium- and Zirconium-Doped $NaAlH_4$ and Na_3AlH_6. J Phys Chem A 107: 7671-7674
10. Momirlan M, Veziroğlu TN (2002) Current Status of Hydrogen Energy. Renew. Sust. Energ Rev 6: 141-179
11. Züttel A., (2004) Hydrogen storage methods, Die Naturwissenschaften 91: 157-172
12. Chen P, Xiong ZT, Luo JZ, Lin JY, Tan KL (2002) Interaction of hydrogen with metal nitrides and imides. Nature 420(6913): 3024-3036
13. Fakioglu E, Yurum Y, Veziroglu TN (2004) A review of hydrogen storage systems based on boron and its compounds. Int J Hydrogen Energy 29 (13): 1371-1376
14. Griessen R, and Riesterer T (1988) Heat of Formation Models in Hydrogen in Intermetallic Compounds I Electronic, Thermodynamic, and Crystallographic Properties, Preparation, Springer Series Topics in Applied Physics 63: 219-284.
15. Takeichi N, Senoh H, Yokota T, Tsuruta H, Hamada K, Takeshita HT, Tanaka H, Kiyobayashi T, Takano T, Kuriyama N (2003) Hybrid hydrogen storage. Int J Hydrogen Energy 28: 1121-1134
16. Bulletin, Magazin der Eidgenössischen Technischen Hochschule Zürich 276 (2000)
17. Climate Change 2001, Synthesis Report, Robert T. Watson (ed.), Published for the Intergovernmental Panel on Climate Change IPCC (2001) Cambridge University Press, Cambridge, UK
18. International Energy Agency (IEA, AIE) (2002), Key World Energy Statistics Edition.
19. Handbook of Chemistry and Physics, Weast R. C., ed. 57 (1976), CRC Press

20. Steinfeld A, Palumbo R (2001) Solar Thermochemical Process Technology. Encyclopedia of Physical Science and Technology. R. A. Meyers Ed., Academic Press 15, 237-256
21. Product specification from GTec SA, rte de Clos-Donroux 1, CH-1870 Monthey, Switzerland.
22. Huston EL (1984) A Liquid Solid Storage of Hydrogen.In: Proceedings of the 5th World Hydrogen Energy Conference. 3, 15–20 July 1984, Toronto, Canada
23. Flynn TM (1992) A Liquification of Gases. McGraw-Hill Encyclopedia of Science &Technology. 7th edition. 10, New York: McGraw-Hill, 106-109
24. Gary C, Anghaie S (2017) based on NASA/NIST databases. http://www.inspi.ufl.edu/ data/h_prop_package.html. Accessed 25 Dec 2017
25. Ardenne M, Musiol G, Reball S (1990) Effekte der Physik. Verlag Harry Deutsch, 712-715
26. London F, Physik Z (1930) Z. Physik. Chem 11: 222-231
27. Brunauer S, Emmett PH, Teller E (1938) J. Amer. Chem. Soc. 60: 309
28. Dillon AC, Jones KM, Bekkedahl TA, Kiang CH, Bethune DS, Heben MJ (1997) Storage of hydrogen in single-walled carbon nanotubes. Nature 386: 377-379
29. Dillon AC (2000) In: Proceedings of the 2000 DOE/NREL hydrogen program review, 8–10 May 2010
30. Güneş İ, (2016) Hydrogen production and storage underground, 3rd International Conference on Recycling and Reuse, İSTANBUL, TÜRKIYE, 28-30 Eylül 2016, pp.15-16

RECENT TRENDS AND ADDITION OF NANOPARTICLES IN FRICTION STIR WELDING TECHNIQUE

Anıl ŞİMŞEK[1],

Mikail ASLAN[2]

[1] Metallurgical Material Science Engineering, GaziantepUniversity, Gaziantep, Turkey.
[2] Metallurgical Material Science Engineering, GaziantepUniversity, Gaziantep, Turkey.

I. INTRODUCTION

In 1991 for aluminum alloy applications, the friction stir welding (FSW) was introduced firstly as a solid state bonding technique by the United States Institute of Welding (TWI) [1],[2]. As a basic, in this technique, a rotating non-consumable tool in which consisting of pin and shoulders is located on adjacent edges of the sheets to be joined and passed through the joint line. Heat energy coming from the friction produced by shoulder leads base metals to be welded to each other. Due to the environmentally, versatile and energy saving properties of this technique, in the applications of metal joing and nanomaterials, the FSW technique has been shown significant improvement over the last decades. Especially, this technique is very suitable for welding aluminum alloys having high strength properties and some metal alloys which are challenging to be joined by traditional fusion welding. The FSW technique is now can be used for not only aluminum alloys but also various materials including even steels and polymers. Thus, for the development of this technique, the heat transportation, plastic flow, defect formation, tool design and usage of nanomaterials need to be investigated by engineers.

On the other hand, this technique has some disadvantages. For instance, during joing process, some defects, such as tunnel, void and wormhole may have seen in the joints[3]. This affects the microstructure, quality and properties of the joint. For this reason, many parameters such as rotational and transverse speeds can be improved. Especially, as an external factor, addition of nanoparticles or nanopowders severely has impact on the microstructure quality and mechanical properties of joint materials after welding process. Recently, engineers and scientists have been investigated the effect of nanoparticles on the welded joint in terms of microstructure and mechanical properties. Bahrami et al.[4] examined the microstructural appearance and the mechanical behavior of AA7075-O-nano-SiC metal matrix composites (MMCs). Sahraeinejad et al.[5] were able to combine some nanopowders (Al_2O_3, SiC, B_4C) in a AA5059 sheet. Khodabakhshi et al.[6] studied on the inclusions that occur after FSP of AA5052 with TiO2 nanoparticles.

II. RECENT DEVELOPMENTS OF FRICTION WELDING

The development of the FSW technique is still considered to play an important role in the joining of materials over the past 20 years. One of these developments is related to the pin design. Thomas et al.[7] studied types of pin designs. The pins were design as a shape of frustum which requires less material consumption than that of a cylindrical tool with similar root size. Typically, whorl decreases the displacement volume by approximately 60%, while MX-Triflute (MXT) decreases this volume by approximately 70%. The design of Whorl and MXT types leads to reduce (a) welding force, (b) the pin and plasticized material (c) facilitate more easy to flow of the softened material, (d) simplify the downward magnifying effect and thereby increasing heat generation. Using these two tools, it was confirmed that aluminum plates having a diameter of up to 50 mm can be joined by seamless

fusion in one turn. The 75-mm-thick 6082Al-T6 was welded in two passes (each penetrating approximately 38 mm) by FSW having a Whorl instrument. Thomas et al. [7] pointed out that the main factor examined the supremacy of the whorl pins on traditional cylindrical pins is swept away the volume along the rotation volume of the pin itself.

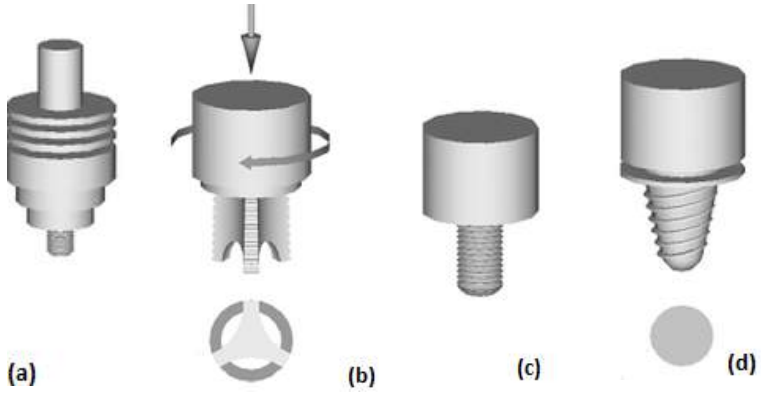

Fig.1. Various friction stirrer welding pins: (a) a cylindrical needle used at the source of thin plates, (b) a conical shape pin at the source of the thick plates, and (c) TriangleTM Improved type pin overlap welding for friction. Adapted from [8] © 2003 WILEY-VCH Verlag GmbH & Co. KGaA, Weinheim.

Thomas et al.[9] recommended that both a-skew pins and Flared-Trifute (FT) are convenient for T joints type where the welding interface is perpendicular to the machine axis. On the other hand, different types of shoulder design are used in TWI for dissimilar materials. These types enhance the connection between the shoulder and the work pieces by retaining the plastic material inside of the private and re-entry features. In particular, it can be used to weld metallic alloys which are very difficult to weld with aluminum alloys used for high strength aerospace and conventional fusion welding techniques [10]-[18].

Another development is related to tool design. A different tool design in FSW technique on the microstructural alteration based on FSW's fundamental principles which is shown in Fig. 2 and 3 has been recently developed by Mishra et al. [19, 20].

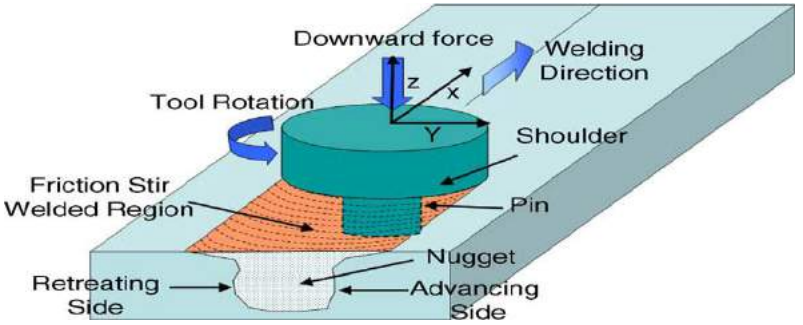

Fig. 2 Representation of Friction Stir Welding Process. Adapted from [21] ©2005 Elsevier B.V

In this process, a pin and shoulder swiveling device are disposed on a single piece of material for local microstructure modification, in particular for property development. For instance, in the trading 7075Al alloy by the FSW method, a fine-grained microstructure was obtained for high tensile super elasticity[19, 22]. In addition, the FSW technique was used in the production of a surface composite material on the Al fundament[23] and homogenization of Al alloys, MMCs and cast aluminum alloys in powder metallurgy (PM)[24], [25].

The tool design effects the heat production, the plastic stream, the required power and the smoothness of the welded joint. Table 2 represents some new tool designed in TWI. MXT and Whorl tool designs have lesser pin volumes than cars with cylindrical pins. The conic threads in the overall design trigger a component of the vertical speed which simplifies plastic stream. The groove in the MXT increases the interface area between the tool and the workpiece, resulting in increased heat generation speeds, softening and material flow. As a result, more intense mixing for tool movement reduces both the forward travel force and the welding torque[8], [26]. Although the Triflute, cylindrical and Whorl tool designs are convenient for forehead welding, they are not handy for the source of lap welds, where extreme refining of the top plate may occur with the retention of the adhering oxide between the overlapping surfaces. A-skew and Flared-Triflute (FT) tools have been improved to provide a breakdown of the interfacial oxide sheet and a larger source than the normal for the forehead welding[27].

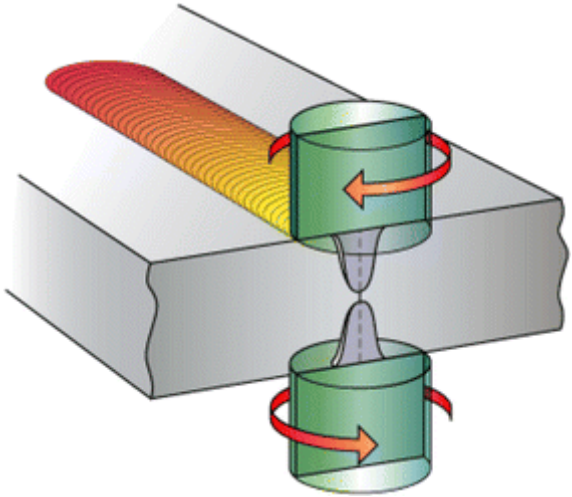

Fig.3. Schematic drawing of a double-sided friction mixer applied to thick plates. Adapted from [28], [29] © ASM International 2014

While the FT design is similar to an expanded grooved MXT, A-skew TM tool is a conic tool with an sloping inclination of the axis of the machine shaft. These devices show increment on the swept volume relative to the pin, thereby extending the mixing zone and resulting in a more extensive weld and accomplished shoe joints. Zhao et al.[30] investigated the importance of tool pin design on mechanical properties and weldability of FSW processed Al sheets. Cylindrical and conic tool pins did not provide a vertical influential mixing that led to wormholes at the bottom of the TMAZ. In addition, error-free sources were obtained when using conic tools with teeth. Other studies have supported that tools with screw threads produce more heat and improve the flow of softer material by applying smoother strength. Since the material flows mostly towards the retracted side, insufficient plasticity and material flow result in a wormhole on the advancing side[31], [32]. This result comes to be more pronounced at low temperatures due to stagnant material flow. The choice of pin angle, the angle between the cone surface and the axis of the pin, is other important factor affecting the FSW process; increasing the angle causes a more homogeneous temperature release in the vertical direction, which helps in reducing distortion[33]. Based on a quantitative understanding of material flow, the design of these tools is just beginning. Colegrove et al.[34] used a FLUENT-based thermal model to design a vehicle to minimize cross force during the FSW of the aluminum alloy. They have studied a variety of tool geometries, including Trivex, which

have a similar shape motion force and downward forces as a triangular shape with gibbous surfaces, and are significantly lower at lower shear stresses, especially in the case of notable shear stresses, and lower for Trifex tools than for Triflute. They recomended that Trivex which has convex surfaces prevents the adhesion of the tool-metal interface to the material which decreases the shear force and consequently reduces the movement of the force. Triflute, however, has flow inhibiting properties and the tool adheres to the material moreover at low shear stresses.

Table 1. A selection of tools designed at United States Institute of Welding. Adopted from [8], [21] © ASM International 2014

Tool	Schematics	Rotary reversal	Total pin shape	Ratio of pin volume to cylindrical pin volume	Swept volume to pin volume ratio	Applications
MX Triflute		No	Threaded, tapered with three flutes	0.3	2.6	Butt welding with further lower welding torque
A-Skew		No	Inclined cylindrical with threads	1	Depends on pin angle	Lap welding with lower thinning of upper plate
Re-stir	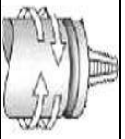	Yes	Tapered with threads	0.4	1.8	When minimum asymmetry in weld property is desired
Flared Triflute	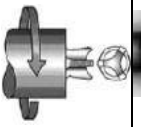	No	Tri-flute with flute ends flared out	0.3	2.6	Lap welding with lower thinning of upper plate
Whorl		No	Tapered with threads	0.4	1.8	Butt welding with lower welding torque
Cylindrical	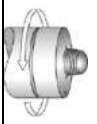	No	Cylindrical with threads	1	1.1	Butt welding; fails in lap welding

III. NANOPARTICLES IN FSW

The good mechanical performance of light aluminum alloys has gave a pioneer to increased use in shipbuilding, maritime, aerospace and transportation industries. On the other hand, one of the disadvantages of these alloys is that they can be welded low by conventional methods[35], [36]. Another disadvantage following the use of Al parts is the vigorous adhesive wear on their surface when in contact with hard materials. One possible solution to this problem is the addition of hard nanoparticles to Al matrices. Many of the developments[37], [38] to fabricate MMCs require the metal to melt and cure again, and there are drawbacks to these phenomena due to the busebact.

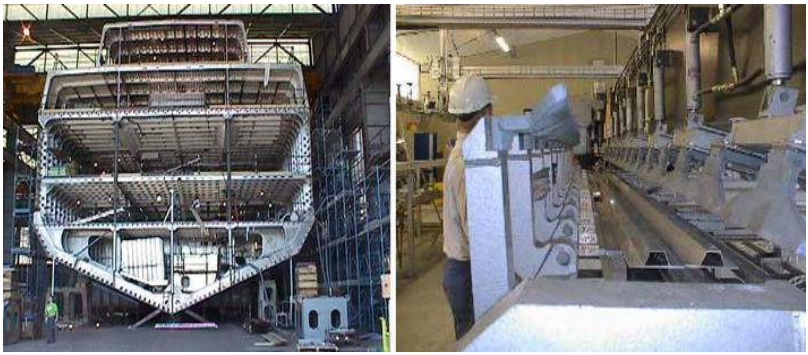

Fig. 4 Combining Al-extrusion panels used in ship building with friction mixture[39]-[41].

MMCs produced by strengthening aluminum matrices with nanoparticles exhibit improved properties (eg high strength, hardness, increased creep and fatigue strength and tribological features) compared to non-reinforced Al alloys[42], [43]. In recent studies, Sarkari Khorrami combined the iron particles through the multi-part FSP to produce naive Aluminum (Al)-Iron (Fe) MMC[44]. In similar principle, Golmohammadi et al.[45] used FSP technique to combine Ni particles in a cast Al A413 matrix.

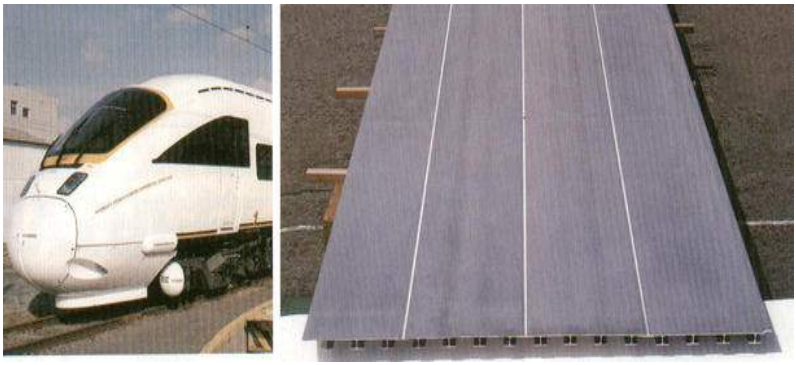

Fig. 5 Stirling of the participation of Al-panels in the production of high-speed trains in Japan Stirling[39].

Bahrami et al.[4] examined microstructural aspects and mechanical behavior of nano-Silicon Carbide(SiC) MMCs. Sahraeinejad et al.[5] studied some nanopowders (Al2O3, SiC, B_4C) were added to an AA5059 substrate; compared and produced AA1100 supported with distinct microprocessors due to the wear of carbon fibers ,glass and polymer[46]. Khodabakhshi et al[6] investigated the ruins after friction mixing with TiO2 nanoparticles of AA5052. Dragatogiannis et al.[47] used the FSW technique for dissimilar 5083 and 6082 Al alloys materials reinforced with TiC nanoparticles. They synthesized TiC nanoparticles by chemical vapour deposition technique. It can be seen in Fig. 6 that the TiC nanoparticles are spheres having a radius approximately of 150–200 nm. In this study, the microhardness of the studied materials was enhanced (~18%) by the addition of the TiC nanoparticles.

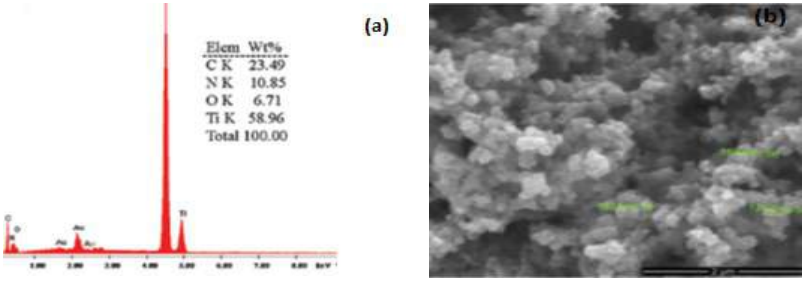

Fig. 6. (a) EDS analysis of TiC nanoparticles and (b) SEM image. Adapted from [47] © 2018 Informa UK Limited.

In addition to this study, In Fig. 8, regions of the mixing area of TiC nanoparticles are controlled by optical microscopy. In Fig. 8(a) and (b), the

top zone of a portion of the flow arm and the mixing area were observed. In this region, it appears that the reinforcement particles seem to be regulated in metal matrix bands. Fig. 8 (c) shows the mixing area (SZ) and the thermomechanically affected zone (TMAZ) towards the retarder aspect of the sample. The mixing region seems to be rich in titanium carbide nanoparticles. In addition, AA6082 can be observed mechanically with AA5083 to the metal matrix. In Fig. 8 (d), the inferior center of the mixing region was controlled. The particle disintegration seems much better with regions with very few color contrast in this region.

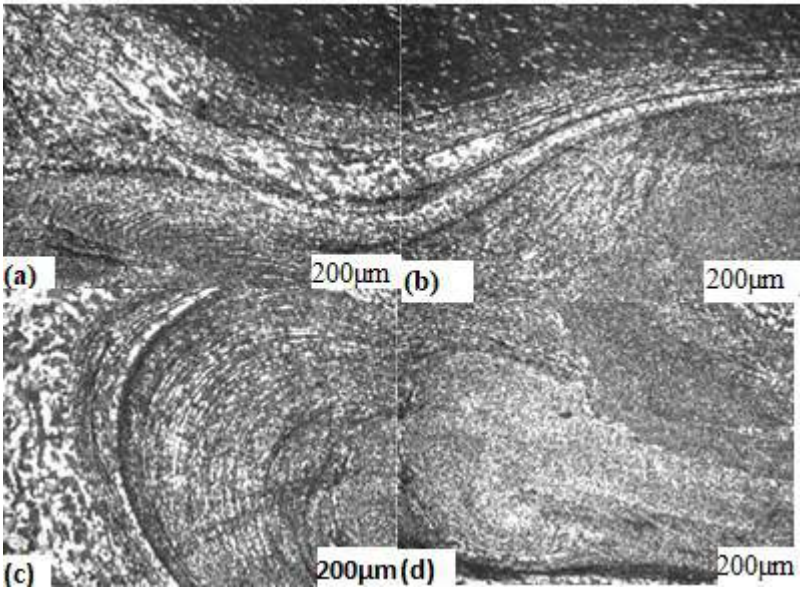

Fig. 8. Optical micrographs of several regions of the mixer region of TiC nanoparticles at 100 x magnification. (a) the upper area of the Stirring Zon(b) the part of the flow arm (c) Stirring Zone towards RS and the lower center of the TMAZ (d) SZ. Adapted from [47] © 2018 Informa UK Limited.

Bahrami et al.[48],[49] investigated the influences of silicon carbide (SiC) nanoparticles on the friction mix welded 7075 Al alloy joints and reported that the weld resistance and size of the particles significantly affected the welding structure. Paidar et al.[50] have demonstrated that SiC nanoparticles are added to the superior X wear resistance and strength of the friction stir spot welding (FSSW) of 2024-T3 aluminum alloy.

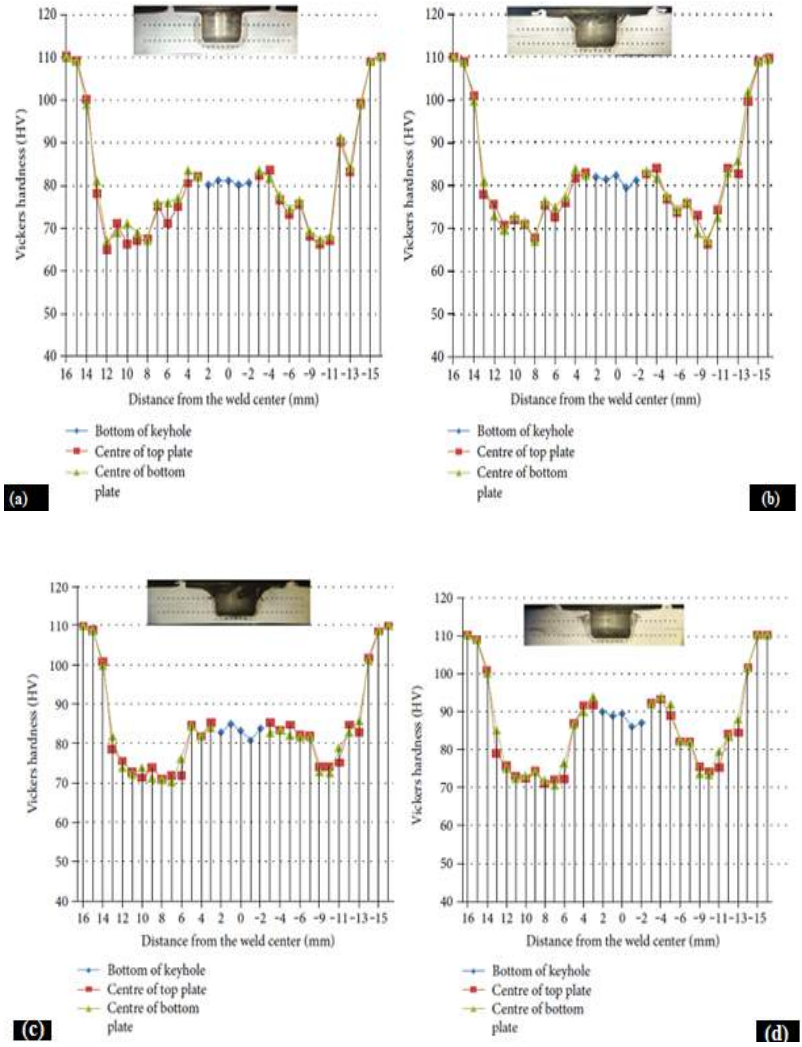

Fig. 12 Hardness profile of the weld joints along the bottom and top layers (a) Silicon-Carbide (SiC) free, (b) volume fraction of 14% SiC, (c) volume fraction of 22% SiC and (d) SiC Volume fraction of 29%.Adapted from [51] Copyright © 2018 S. Suresh et al

Dehghani et al.[52] used silicon carbide (SiC) particles in the friction stir spot welding (FSSW) of non-crack steels to investigate their tensile strength and microhardness. It is clearly understood that the inclusion of nano fillers significantly develops the mechanical features of the basic matrix[53, 54].

Barmouz et al.[55], [56] examined the SiC /Cu composite produced FSW and reported that inclusion of silicon carbide (SiC) nanosized particles increased the hardness and abrasion resistance of the composite. Suresh et al.[51] conducted a study of the microstructural characterization of 6061-T6 aluminum alloy reinforced with SiC nanoparticles using FSSW. Their microhardness values of studied each sample is shown in Fig. 12. The average hardness in the SZ of the specimen without silicon carbide was 81.25 HV. The average hardness values in SZ are 85.92 HV, 93.27 HV and 82.62 HV, in turn, with 22%, 29% and 14% SiC filling. The hardness of SZ increases with the increase in the volume fraction of the SiC nanoparticles. In addition to this, a significant hardness change was not observed between 0% and 14% volume fraction. This may be due to inadequate silicon carbide nanoparticles in the joint. The peak worth in the SZ was 93 HZ hardness, with a volume ratio of 29%. Thus, It is found that the additions of SiC nanoparticles considerably affects the grain size and hence the weld properties.

On the other hand, in the aluminum matrix, the silicon carbide nanoparticles differ in a harsh area, affecting grain size, different thermal shrinkage and refining grains of filler material [21], [57], [58]. You et al.[57]studied Aluminum matrix composites reinforced Al_2O_3 nanoparticles produced from Al\SiO_2 powder mixtures by FSP technique. In this study, the microstructure of the specimen after FSW process was characterized using a TEM (transmission electron microscope). The ordinary microstructure of the friction stir processed specimen exposed by transmission electron microscope (TEM) BFI (bright field image) is shown in Fig. 13. The nanoparticles are well-dispersed in the Al matrix, either in the interior of the grain or grain boundary. nano-sized Al_2O_3 particles mostly indicated irregular shapes (see Fig. 3a). In samples processed with higher tool rotation speed, the aggregation of the nanoparticles is clearly seen in Fig. 2b. This indicates the amount of Al_2O_3nanoparticles increases significantly. In the FSP, the SiO2 nanoparticles were disintegrated and dispensed in an Al matrix by stirring tool. Due to the reaction between Al and SiO_2, Si and Al_2O_3 are synthesized as shown in Fig.13c. SiO_2 is dispersed into Al and is surrounded by Al_2O_3 nanoparticles. The grain size of the Aluminum matrix was specified using the transmission electron microscope (TEM) dark field image (DFI). An ordinary aluminum matrix grain found by TEM DFI is seen in Fig. 13d. Hence, the produced composite indicates good mechanical properties (see for further details in [57]).

Boron Nitride (BN) nanoparticles can be used in FSW technique for the improvement of the microstructural and wear behavior of joint materials. Palanivel et al. [59] investigated AA6082/TiB_2 hybrid aluminum composites in terms of wear and microstructural properties.

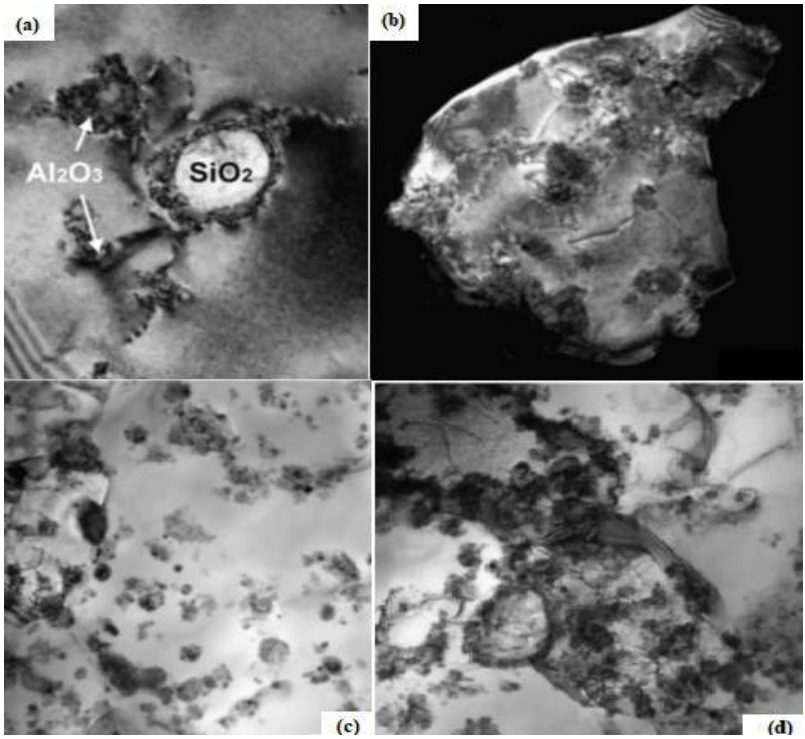

Fig. 13 (a) TEM/ BFI showing a SiO2 particle surrounded by Al2O3 particles; (d) TEM / BFI of the specimen fabricated by friction stir process 1400-15-4. Adapted from [57] © 2013 Elsevier Inc.

In this study, Electron Back Scattered Diagram (EBCD) images of the studied aluminum alloy and the hybrid composites are given in Fig. 6 with their associated grain sizes. In this image, the aluminum alloy exhibits elongated grains owing to the rolling process while all Aluminum Metal Composites exhibit fine and equiaxed grains. Hence, their study showed that the reinforcement of TiB_2 + BN nanoparticles changed the morphology of the wear debris while the reinforcement of BN nanoparticles reduced the presence of the larger flake. Furthermore, the reinforcement of TiB_2 + BN particles increased the sliding wear resistance of the Aluminum Metal Composites.

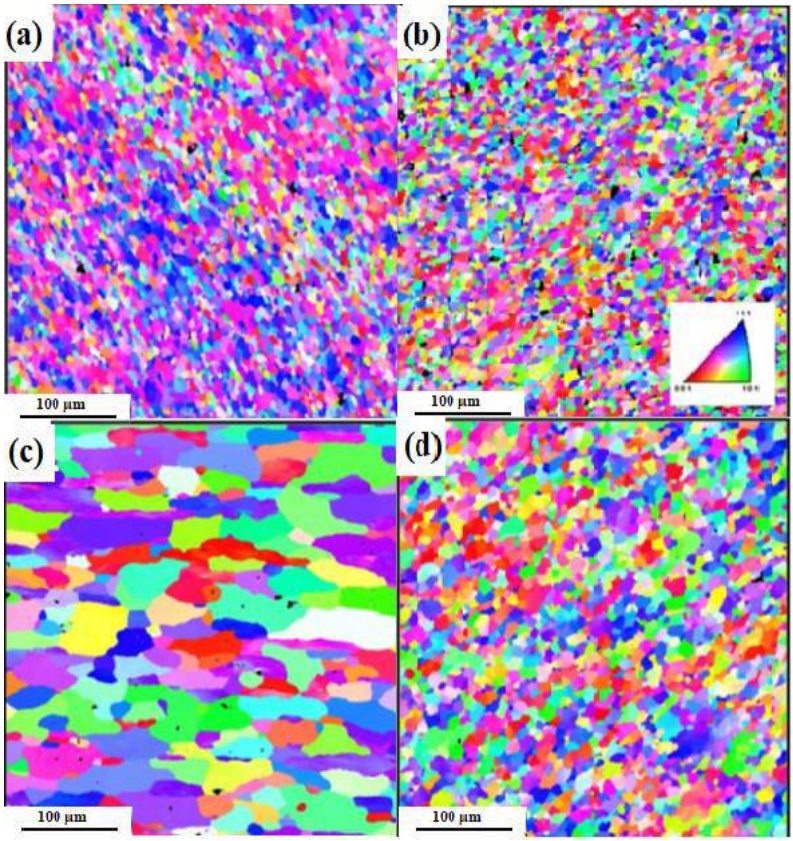

Fig. 14 Electron Back Scattered Diagram (map of AA6082 Aluminum Metal Composites containing (a) TiB2 + BN, (b) BN particles and (d) TiB2 and (c) AA6082 aluminum alloy. Adapted from [59] © 2014 Elsevier B.V

IV. CONCLUSION

Despite the considerable interest in FSW technology over the last decade, the basic physical comprehension of this process is still missing. This needs to understand some important issues, such as tool geometry design, nanoparticles effects on mechanical properties in FSW technique, microstructural stability, welding resistance tools and welding of different metals and alloys. Hence, In order to speed up the FSW development process, to increase its potential and its use in production, it is important to control the process parameters, equipment with adaptive systems and also a center for friction welding with basic equipment including inspection tools. This will allow researchers to concentrate on their work in the advancement of equipment and technologies using their experiences.

References

1. W. Thomas, and C. Dawes, "TWI bulletin 6 November," December, 1995.
2. W. Thomas, E. Nicholas, J. Needham et al., "GB Patent Application No. 9125978.8, December, 1991," TWI Bull, vol. 124, 1995.
3. A. Esmaeili, M. B. Givi, and H. Z. Rajani, "A metallurgical and mechanical study on dissimilar Friction Stir welding of aluminum 1050 to brass (CuZn30)," Materials Science and Engineering: A, vol. 528, no. 22-23, pp. 7093-7102, 2011.
4. M. Bahrami, M. F. Nikoo, and M. K. B. Givi, "Microstructural and mechanical behaviors of nano-SiC-reinforced AA7075-O FSW joints prepared through two passes," Materials Science and Engineering: A, vol. 626, pp. 220-228, 2015.
5. S. Sahraeinejad, H. Izadi, M. Haghshenas et al., "Fabrication of metal matrix composites by friction stir processing with different particles and processing parameters," Materials Science and Engineering: A, vol. 626, pp. 505-513, 2015.
6. F. Khodabakhshi, A. Simchi, A. Kokabi et al., "Effects of nanometric inclusions on the microstructural characteristics and strengthening of a friction-stir processed aluminum–magnesium alloy," Materials Science and Engineering: A, vol. 642, pp. 215-229, 2015.
7. W. Thomas, E. Nicholas, S. Smith et al., "Aluminum 2001-Proceedings of the TMS 2001 Aluminum Automotive and Joining Sessions," TMS, vol. 213, 2001.
8. W. M. Thomas, K. I. Johnson, and C. S. Wiesner, "Friction stir welding–recent developments in tool and process technologies," Advanced Engineering Materials, vol. 5, no. 7, pp. 485-490, 2003.
9. W. Thomas, R. Dolby, S. In David et al., "Proceedings of the Sixth International Conference on Trends in Welding Research," Pine Mountain, GA, ASM International, pp. 203-211, 2003.
10. C. Chen, and R. Kovacevic, "Joining of Al 6061 alloy to AISI 1018 steel by combined effects of fusion and solid state welding," International Journal of Machine Tools and Manufacture, vol. 44, no. 11, pp. 1205-1214, 2004.
11. K. Kimapong, and T. Watanabe, "Friction stir welding of aluminum alloy to steel," Welding journal, vol. 83, no. 10, pp. 277, 2004.
12. L. Ceschini, I. Boromei, G. Minak et al., "Effect of friction stir welding on microstructure, tensile and fatigue properties of the AA7005/10 vol.% Al2O3p composite," Composites science and technology, vol. 67, no. 3-4, pp. 605-615, 2007.
13. R. Prado, L. Murr, D. Shindo et al., "Tool wear in the friction-stir welding of aluminum alloy 6061+ 20 Al 2 O 3: a preliminary study," Scripta materialia, vol. 1, no. 45, pp. 75-80, 2001.
14. J. Esparza, W. Davis, and L. Murr, "Microstructure-property studies in friction-stir welded, Thixomolded magnesium alloy AM60," Journal of Materials Science, vol. 38, no. 5, pp. 941-952, 2003.
15. W. Lee, Y. Yeon, and S. Jung, "Joint properties of friction stir welded AZ31B–H24 magnesium alloy," Materials Science and Technology, vol. 19, no. 6, pp. 785-790, 2003.
16. G. Bussu, and P. Irving, "The role of residual stress and heat affected zone properties on fatigue crack propagation in friction stir welded 2024-T351 aluminium joints," International Journal of Fatigue, vol. 25, no. 1, pp. 77-88, 2003.
17. J.-Q. Su, T. Nelson, R. Mishra et al., "Microstructural investigation of friction stir welded 7050-T651 aluminium," Acta materialia, vol. 51, no. 3, pp. 713-729, 2003.

18. M. Mahoney, C. Rhodes, J. Flintoff et al., “Properties of friction-stir-welded 7075 T651 aluminum,” Metallurgical and materials transactions A, vol. 29, no. 7, pp. 1955-1964, 1998.
19. R. S. Mishra, and M. W. Mahoney, "Friction stir processing: a new grain refinement technique to achieve high strain rate superplasticity in commercial alloys." pp. 507-514.
20. R. S. Mishra, S. McFadden, N. Mara et al., “High strain rate superplasticity in a friction stir processed 7075 Al alloy,” 1999.
21. R. S. Mishra, and Z. Ma, “Friction stir welding and processing,” Materials science and engineering: R: reports, vol. 50, no. 1-2, pp. 1-78, 2005.
22. Z. Ma, R. S. Mishra, and M. W. Mahoney, “Superplastic deformation behaviour of friction stir processed 7075Al alloy,” Acta materialia, vol. 50, no. 17, pp. 4419-4430, 2002.
23. R. S. Mishra, Z. Ma, and I. Charit, “Friction stir processing: a novel technique for fabrication of surface composite,” Materials Science and Engineering: A, vol. 341, no. 1-2, pp. 307-310, 2003.
24. Z. Ma, S. R. Sharma, R. S. Mishra et al., "Microstructural modification of cast aluminum alloys via friction stir processing." pp. 2891-2896.
25. P. B. Berbon, W. H. Bingel, R. S. Mishra et al., “Friction stir processing: a tool to homogenize nanocomposite aluminum alloys,” 2001.
26. W. Thomas, "Friction stir welding-recent developments." pp. 229-236.
27. W. Thomas, D. Staines, K. Johnson et al., “Com-stir–compound motion for friction stir welding and machining,” Adv Eng Mater, vol. 5, pp. 273-4, 2003.
28. G. Çam, “Friction stir welded structural materials: beyond Al-alloys,” International Materials Reviews, vol. 56, no. 1, pp. 1-48, 2011.
29. W. Thomas, E. Nicholas, E. Watts et al., "Friction based welding technology for aluminium." pp. 1543-1548.
30. Y.-H. Zhao, S.-B. Lin, F.-X. Qu et al., “Influence of pin geometry on material flow in friction stir welding process,” Materials science and technology, vol. 22, no. 1, pp. 45-50, 2006.
31. M. Guerra, C. Schmidt, J. C. McClure et al., “Flow patterns during friction stir welding,” Materials characterization, vol. 49, no. 2, pp. 95-101, 2002.
32. H. Schmidt, and J. Hattel, “A local model for the thermomechanical conditions in friction stir welding,” Modelling and simulation in materials science and engineering, vol. 13, no. 1, pp. 77, 2004.
33. G. Buffa, J. Hua, R. Shivpuri et al., “Design of the friction stir welding tool using the continuum based FEM model,” Materials Science and Engineering: A, vol. 419, no. 1-2, pp. 381-388, 2006.
34. P. Colegrove, and H. Shercliff, “Development of Trivex friction stir welding tool Part 2–three-dimensional flow modelling,” Science and Technology of Welding and Joining, vol. 9, no. 4, pp. 352-361, 2004.
35. A. Steuwer, M. Peel, and P. Withers, “Dissimilar friction stir welds in AA5083–AA6082: the effect of process parameters on residual stress,” Materials Science and Engineering: A, vol. 441, no. 1-2, pp. 187-196, 2006.
36. M. Peel, A. Steuwer, P. Withers et al., “Dissimilar friction stir welds in AA5083-AA6082. Part I: process parameter effects on thermal history and weld properties,” Metallurgical and Materials Transactions A, vol. 37, no. 7, pp. 2183-2193, 2006.
37. D. Pantelis, A. Tissandier, P. Manolatos et al., “Formation of wear resistant Al–SiC surface composite by laser melt–particle injection process,” Materials science and technology, vol. 11, no. 3, pp. 299-303, 1995.
38. J. Hashim, L. Looney, and M. Hashmi, “Metal matrix composites: production by the stir casting method,” Journal of materials processing technology, vol. 92, pp. 1-7, 1999.

39. S. Kallee, "Railway manufacturers implement friction stir welding," Weld. J., vol. 81, no. 10, pp. 47-50, 2002.
40. C. Dawes, "Friction Stir Prosess Welds Aluminium Alloys," Welding Jounal, vol. 36, 1995.
41. W. Thomas, and E. Nicholas, "Friction stir welding for the transportation industries," Materials & design, vol. 18, no. 4-6, pp. 269-273, 1997.
42. D. Aruri, K. Adepu, K. Adepu et al., "Wear and mechanical properties of 6061-T6 aluminum alloy surface hybrid composites [(SiC+ Gr) and (SiC+ Al2O3)] fabricated by friction stir processing," Journal of Materials Research and Technology, vol. 2, no. 4, pp. 362-369, 2013.
43. I. Lee, C. Hsu, C. Chen et al., "Particle-reinforced aluminum matrix composites produced from powder mixtures via friction stir processing," Composites Science and Technology, vol. 71, no. 5, pp. 693-698, 2011.
44. M. S. Khorrami, S. Samadi, Z. Janghorban et al., "In-situ aluminum matrix composite produced by friction stir processing using FE particles," Materials Science and Engineering: A, vol. 641, pp. 380-390, 2015.
45. M. Golmohammadi, M. Atapour, and A. Ashrafi, "Fabrication and wear characterization of an A413/Ni surface metal matrix composite fabricated via friction stir processing," Materials & Design, vol. 85, pp. 471-482, 2015.
46. S. M. Arab, S. Karimi, S. A. J. Jahromi et al., "Fabrication of novel fiber reinforced aluminum composites by friction stir processing," Materials Science and Engineering: A, vol. 632, pp. 50-57, 2015.
47. D. Dragatogiannis, E. Koumoulos, I. Kartsonakis et al., "Dissimilar friction stir welding between 5083 and 6082 Al alloys reinforced with TiC nanoparticles," Materials and Manufacturing Processes, vol. 31, no. 16, pp. 2101-2114, 2016.
48. M. Bahrami, N. Helmi, K. Dehghani et al., "Exploring the effects of SiC reinforcement incorporation on mechanical properties of friction stir welded 7075 aluminum alloy: fatigue life, impact energy, tensile strength," Materials Science and Engineering: A, vol. 595, pp. 173-178, 2014.
49. M. Bahrami, K. Dehghani, and M. K. B. Givi, "A novel approach to develop aluminum matrix nano-composite employing friction stir welding technique," Materials & Design, vol. 53, pp. 217-225, 2014.
50. M. Paidar, and M. L. Sarab, "Friction stir spot welding of 2024-T3 aluminum alloy with SiC nanoparticles," Journal of Mechanical Science and Technology, vol. 30, no. 1, pp. 365-370, 2016.
51. S. Suresh, K. Venkatesan, and E. Natarajan, "Influence of SiC Nanoparticle Reinforcement on FSS Welded 6061-T6 Aluminum Alloy," Journal of Nanomaterials, vol. 2018, 2018.
52. S. Tebyani, and K. Dehghani, "Effects of SiC nanopowders on the mechanical properties and microstructure of interstitial free steel joined via friction stir spot welding," Materials & Design, vol. 90, pp. 660-668, 2016.
53. N. Elango, N. S. Gupta, Y. Lih Jiun et al., "The effect of high loaded multiwall carbon nanotubes in natural rubber and their nonlinear material constants," Journal of Nanomaterials, vol. 2017, 2017.
54. N. Elango, and A. Faudzi, "A review article: investigations on soft materials for soft robot manipulations," The International Journal of Advanced Manufacturing Technology, vol. 80, no. 5-8, pp. 1027-1037, 2015.
55. M. Barmouz, M. K. B. Givi, and J. Seyfi, "On the role of processing parameters in producing Cu/SiC metal matrix composites via friction stir processing: Investigating microstructure, microhardness, wear and tensile behavior," Materials characterization, vol. 62, no. 1, pp. 108-117, 2011.

56. M. Barmouz, P. Asadi, M. B. Givi et al., "Investigation of mechanical properties of Cu/SiC composite fabricated by FSP: Effect of SiC particles' size and volume fraction," Materials Science and Engineering: A, vol. 528, no. 3, pp. 1740-1749, 2011.
57. G. You, N. Ho, and P. Kao, "In-situ formation of Al2O3 nanoparticles during friction stir processing of AlSiO2 composite," Materials Characterization, vol. 80, pp. 1-8, 2013.
58. Y. Sun, and H. Fujii, "The effect of SiC particles on the microstructure and mechanical properties of friction stir welded pure copper joints," Materials Science and Engineering: A, vol. 528, no. 16-17, pp. 5470-5475, 2011.
59. R. Palanivel, I. Dinaharan, R. F. Laubscher et al., "Influence of boron nitride nanoparticles on microstructure and wear behavior of AA6082/TiB2 hybrid aluminum composites synthesized by friction stir processing," Materials & Design, vol. 106, pp. 195-204, 2016/09/15/, 2016.

INVESTIGATION OF AIR QUALITY OF BANDIRMA DISTRICT/TURKEY

Kazım Onur DEMİRARSLAN [1] , Serden BASAK [2]

[1] Asst. Prof. Artvin Coruh University, Faculty of Engineering, Department of Environmental Engineering, Artvin, Turkey.
[2] Asst. Prof. Artvin Coruh University, Faculty of Health Sciences, Department of Occupational Health and Safety, Artvin, Turkey.

1. INTRODUCTION

Environmental problems are among the major problems of the second half of the 20th century and the current century. Behind the environmental problems, there are many variables such as deterioration of the quality of life, health concerns, deterioration of the ecological balance (Orhan 2012). Among these problems, air pollution is also an important one. There are many definitions about air pollution in the literature. Air pollution is the deterioration of the atmosphere which is a mixture of colorless and odorless gases, as a result of human activities. According to another definition, air pollution is the elevation of pollutant factors such as dust, gas, water vapor, smoke and odor in atmosphere for various reasons, thus becoming harmful to people, other living things and non-living assets. Air pollution is one of the most important issues because of its direct relevance to human health, among urban problems. A healthy person breathes 16 kg of air a day, and pollutants diminish air quality by reducing oxygen in the air (Kopar & Zengin 2009; Sumer 2014). Although the concept of air pollution has been on the agenda for many years, it has moved to the highest level among the environmental problems that have been experienced with industrialization. Air is polluted as a result of Natural Resources and human activities. Natural air pollutants can be listed as forest fires, volcanic eruptions, and dust storms. The significant sources of air pollutants as a result of human activities are transportation, industry, and heating (İmal et al 2013). Air pollution due to fossil fuel consumption, especially in crowded cities around the world, reduces the quality of life and brings many diseases. Today, a number of measures are being taken by local and national governments to address this problem. Studies are being carried out to increase the use of clean energy sources that do not pollute the environment (Şahin et al 2016). Air pollutants can be examined in two parts as gases and particles. These pollutants are seen as gas (SO_2, NOx, HC, CO, CO_2) and dust (smoke, metallic smoke, fly ash, mist, aerosols) (İmal et al 2013; Demirarslan & Akıncı 2018).

The main factors effective in the formation of air pollution in Turkey are considered as domestic heating, meteorological factors, industry, topography, and traffic. However, the most important problems encountered in the elimination of air pollution are expressed as lack of consciousness in society, financial insufficiencies, inadequate supervision and difficulties in providing quality fuel. The most taken measure for preventing air pollution problem is the use of high-quality fuel which is followed by supervisions, emissions permits for industrial enterprises and exhaust gas measurements of motor vehicles (Aydoğdu, 2014).

In this study, the air quality of Bandırma District, which is in the first 10 settlements of the Marmara region and the second largest port city of southern Marmara, was investigated. PM10, SO_2, and NO_2 measurements taken between 2013 and 2017 at Bandırma station were used in air quality assessment. In addition, in the study, the average of winter data from 1 October to 31 March of each study year was taken. The results were compared with the limit values of Air Quality Assessment and Management

Regulation (AQAMR) dated as 06.06.2008 and numbered as 26898. In this way, it is aimed to eliminate the lack of knowledge in the literature about the air quality of Bandırma region in Turkey.

2. MATERIAL and METHOD

2.1. Description of the study site

Bandırma, which is located in the Gulf of Bandırma known as its town name, is a port district in Balıkesir in the south of the Marmara Sea in Turkey. There are Gönen in the west, Karacabey in the East, Kapıdağ and Erdek in the North, Manyas and Kuşgölü in the South. Bandırma, which has a surface area of 690 km^2, is between 1 and 764 meters altitude from the sea. Bandırma, which is the most developed District of Balıkesir province, is located in the middle of the Triangle of Istanbul, Bursa, and Izmir, which are important trade centers. It has the potential to become an important logistics center in all transportation networks with an advanced industrial structure in the Marmara region. The companies, in the area of fertilizer (BAGFAŞ), flour, feed, cotton gin, rice, vegetable oil, stock chicks, meat chicken, eggs, tomato paste, frozen seafood products, marble and stone processing and Eti mining boron and acid plants, are realizing their production in Bandırma (Aydın et al. 2015; Örücü et al 2008). In addition, Bandırma district is a center of attraction with its continuous development potential and easy accessibility to big cities such as Istanbul and Bursa. Bandırma has become a cosmopolitan settlement where various cultures meet as an area of migration (Saçılık et al 2018). According to the results of the address based Population Registration System of Bandırma province, its population between 2013-2017 is given in Figure 1 which shows that the population of the study area has increased steadily since 2013. The study area can be seen in Figure 2.

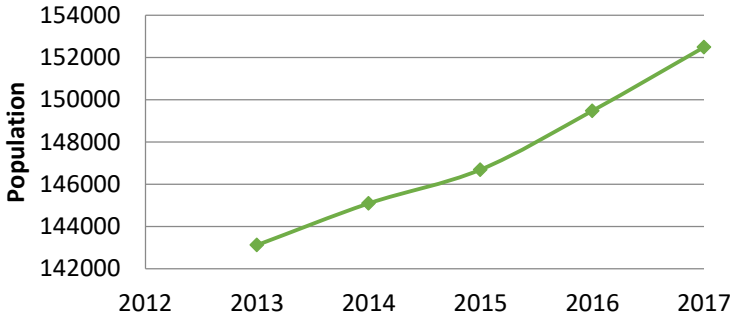

Figure 1. Population of Bandırma province between 2013-2017 according to the results of the address based Population Registration System.

Figure 2. Study area.

The air quality of the study area was measured using PM10, SO_2, and NO_2 pollutants. There is an air quality measurement station operating since March 1, 2013 (IÇDR, 2016). The coordinates of this station are 40°20'52" N, 27°58'29" E. In the station, PM10, SO_2, NO_2, NO_x pollutants and meteorological parameters such as air temperature, wind direction, wind speed, relative humidity, air pressure are also measured. The pollution data for the period between March 1, 2013 and December 31, 2017 was taken from the Ministry of Environment and Urbanization's Air Monitoring Stations website.

The wind data of the study area were obtained from the General Directorate of Meteorology and covered the dates between January 1, 2015 and December 31, 2016. These data were converted into the wind rose by WRLPLOT view 5.5.63 software. The wind rose obtained is given in Figure 3.

Figure 3. Wind rose of the study area.

3. RESULTS

The PM10, SO_2, and NO_2 parameters of the air quality measurement of the Ministry of Environment and Urbanization in Bandırma district taken between March 1, 2013 and December 31, 2017, were interpreted.

3.1. PM10 parameter.

Particulate substances have an important place in air pollutants. The term particle substance indicates solids and liquids that are suspended in the air. The effect of these pollutants varies according to the age and health conditions of the people (Demirarslan & Kaya 2017).

The highest value of PM10 in Bandırma is 818 $\mu g/m^3$, which was measured on February 1, 2015 at 7:00 pm. The average of the PM10 values measured annually is shown in Figure 4, and the average of the winter data covering October 1 and March 31 values of 2013-2017 is given in Figure 5. The distribution of the average PM10 values measured annually is shown in Figure 6.

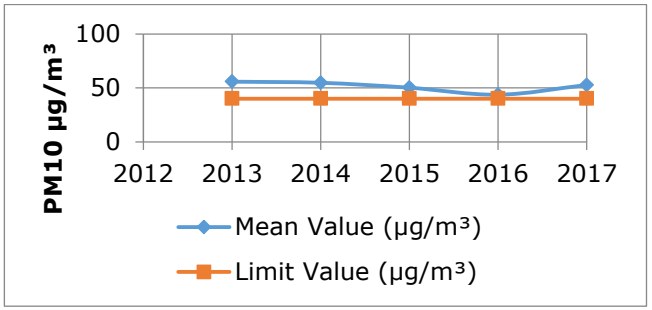

Figure 4. Average PM10 values measured on an annual basis.

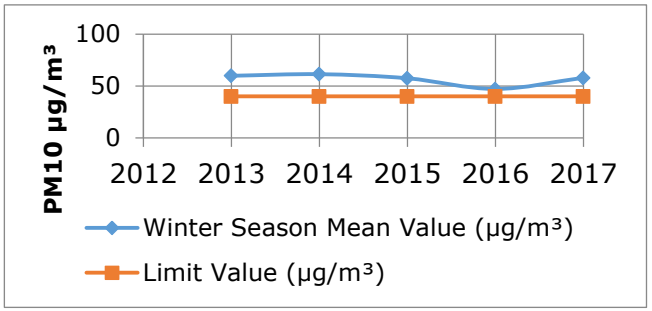

Figure 5. Average PM10 data of the winter month between 1 October 1 and March 31.

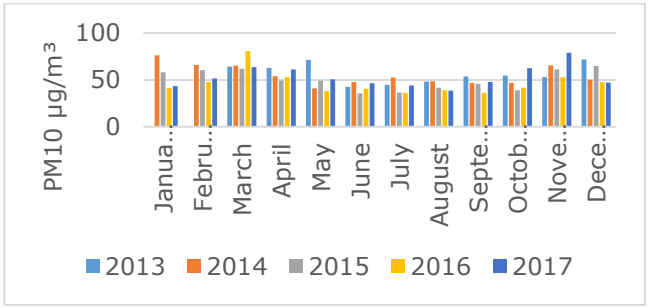

Figure 6. Distribution of average PM10 values measured annually by months.

The measured values were compared with the AQAMR limit values. It is observed that the annual average value and the average values of winter months exceed the limit values.

According to the distribution of the concentration of PM10 by months, it is observed that density falls in the summer months compared to the other months. Therefore, it is understood that the concentration of PM10 is mostly caused by heating in winter. It can be said that the concentration in summer months is due to traffic and industry.

3.2 SO_2 parameter

SO_2 is a colorless, non-flammable and non-glowing gas. Approximately 60% of the sulfur oxides released each year are formed by burning coal. In particular, thermal power plants where lignite coal is used as fuel are the biggest sources of SO_2 emissions (Erdem & Mayda 2017).

The highest SO_2 value is 426 µg/m³, recorded at 07:00 am on December 23, 2014. Figure 7 shows the average SO_2 values, which are measured annually, and Figure 8 shows the average of winter months data, which covers 2013-2017 from October 1, to March 31. The distribution of the average SO_2 values measured annually by months is also shown in Figure 9.

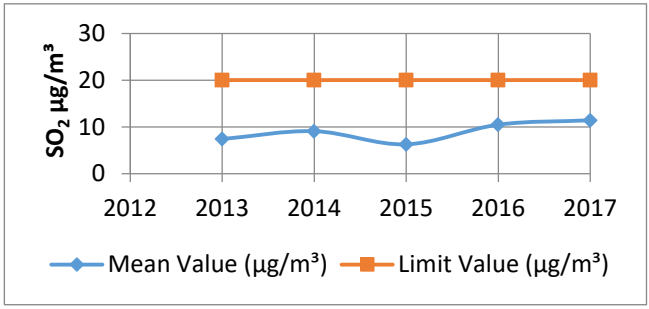

Figure 7. Average SO_2 values measured on an annual basis.

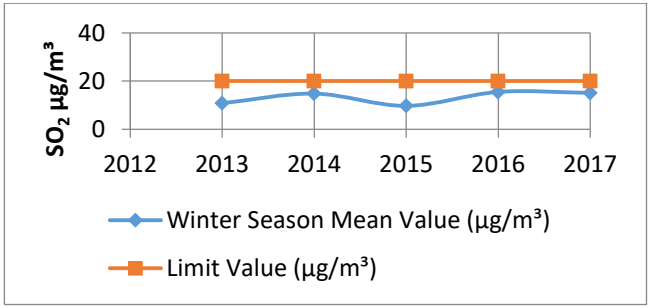

Figure 8. Average of SO_2 data for the winter months covering from October 1 to March 31.

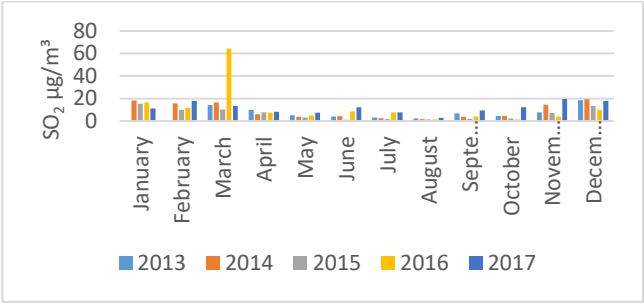

Figure 9. Distribution of average SO_2 values measured annually by months.

When the measured values are compared with the AQAMR limit values, it is understood that the annual average value and average values of winter months are below the limit values. SO_2 concentrations exceeded the hourly limit value of 350 µg/m³ once in the study area. A Natural Gas Company with EMRA (Republic of Turkey Energy Market Regulatory Authority) license dated March 23, 2004 operating in the district can be shown as a factor for this result (URL-2).

When the distribution of the SO_2 pollutant by months is examined, it can be seen that the concentrations due to heating rise in the winter months. Especially in March 2016, this rise was quite high. The reason for the concentration observed in the summer months can be said to be industrial.

3.3 NO_2 parameter

The NO_2 is usually released from vehicles, power plants, industrial emissions, and the agricultural industry. In addition, NO_2 emissions can occur by burning all fossil fuels (URL-1).

The highest measured NO_2 value was 230 µg/m³, recorded at 4:00 pm on 08.03.2017. The average number of NO_2 values measured annually is shown in Figure 10 and the average of the winter data between October 1 to March 31, 2013-2017, is also given in Figure 11.

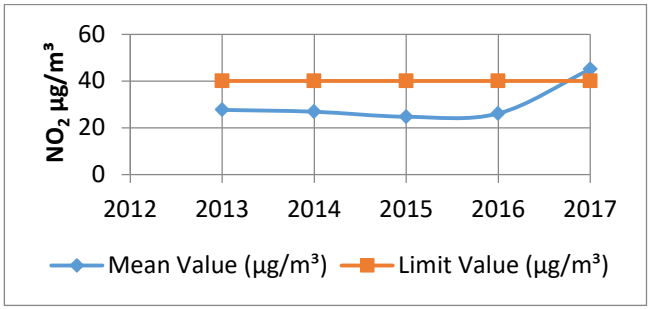

Figure 10. Average NO_2 values measured annually.

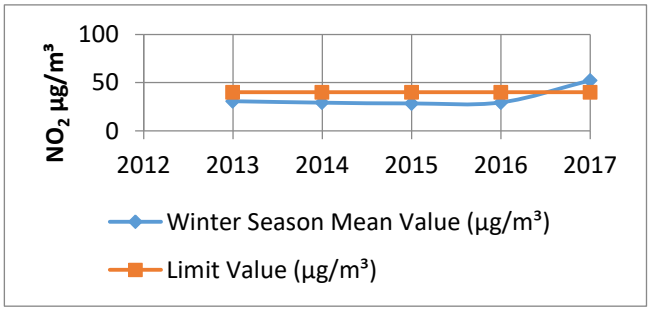

Figure 11. Average of winter NO_2 data between October 1 and March 31.

When the measured values are compared with the AQAMR limit values, it is observed that the average annual value between 2013-2016 and the average winter months are below the limit values. However, in 2017, it is observed that the limit values were exceeded in both cases. Compared to the hourly limit value of 200 µg/m³, measured NO_2 concentrations were exceeded 18 times total.

NO_2 distributions belonging to 2013-2017 were examined (Figure 12), the distribution difference between summer and winter months was not excess, showing that the pollution is mostly sourced from traffic and industry. However, in January, February, March, April, and May of 2017, the level is quite high.

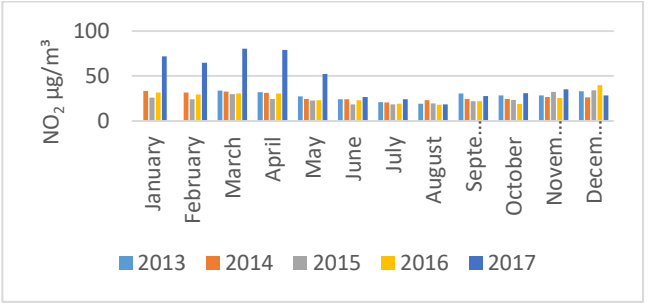

Figure 12. Distribution of the average NO_2 values measured annually by months.

4. Conclusions

Bandırma district has become a very attractive settlement especially because it is on the shores of the Marmara Sea and therefore has the harbors within it, as well as being close to industrial-trade centers such as Istanbul, Bursa, and Kocaeli. In addition to all these, the beach and the shores also give a touristic aspect. However, all these advantages bring with them various environmental problems. Air pollution is an important one of these environmental problems.

In this study, air quality of the study area was investigated by measuring PM10, SO_2, and NO_2 concentrations. The PM10 concentration was compared with the AQAMR limit values. According to the results, the average annual value and the average values in winter months exceed the limit values. According to the distribution of the PM10 concentration recorded between 2013-2017 by months, it is observed that there are lower concentrations in summer than in winter months. Therefore, it is understood that the concentration of PM10 is mostly caused by heating in winter. It can be said that the concentration in summer is due to traffic and industry. According to the SO_2 concentration results, it is understood that the average annual value and the average values in winter months are below the limit values. In the study, it was determined that the SO_2 concentration exceeded the hourly limit value of 350 µg/m³ once between 2013-2017. When the distribution of the SO_2 pollutant by months is examined, it can be seen that the concentrations due to heating rise in the winter months. When NO_2 concentrations are examined, it is observed that the average annual value between 2013-2016 and the average values in winter months are below the limit values; but in 2017, the limit values are exceeded in both cases. Compared to the hourly limit value of 200 µg/m³, the measured NO_2 concentrations were exceeded 18 times total. When NO_2 distributions between 2013-2017 were examined, it was determined that the distribution difference between summer and winter months was not much. This situation shows that pollution is mostly sourced from traffic and industry in summer.

According to the wind rose of the study area, the prevailing wind direction is coming to the city center by the Marmara Sea from the North East. It is seen that this wind could not be enough to disperse the air pollution occurring in the town center that is gaining altitude from the seaside coastline.

References

1. Aydın, A., Özel, H., Ergün, S., Aydoğan, T. 2015, Bandırma İktisadi ve İdari Bilimler Fakültesi'nin Bandırma Ekonomisine Katkılarının Hesaplanması: 2014 Yılı Örneği, https://www.researchgate.net/publication/315575870_Bandirma_Iktisadi_ve_Idari_Bilimler_Fakultesi'nin_Bandirma_Ekonomisine_Katkilarinin_Hesaplanmasi_2014_Yili_Ornegi [accessed Jul 08 2018]
2. Aydoğdu, İ. 2014 Yerel ve bölgesel düzeyde çevre kirliliği sorunları: Elazığ İli örneği, Harput Araştırmaları Dergisi, 1 (1): 133-148.
3. Demirarslan, K.O., Kaya, A. 2017 Kömür madenciliği kaynaklı hava kirliliği: Partikül madde ve metan emisyonları üzerine literatür araştırması. Bilimsel Madencilik Dergisi, 56 (1):23-31.
4. Demirarslan, K.O., Akıncı, H. 2018 CBS ve Hava Kalitesi Verileri Kullanılarak Marmara Bölgesinin Kış Sezonunda Hava Kalitesinin Değerlendirilmesi. Doğal Afetler ve Çevre Dergisi, 4 (1): 11-27.
5. Erdem, S, Mayda, A. 2017 Düzce Hava Kalitesi İzleme İstasyonu 1 Nisan 2015-31 Mart 2017 Tarihleri Arasındaki Verilerinin İncelenmesi. Sakarya Tıp Dergisi, 7 (4): 176-183.
6. İÇDR, 2016, Balıkesir İli 2016 Yılı Çevre Durum Raporu 2016, T.C. Balıkesir Valiliği Çevre Ve Şehircilik İl Müdürlüğü
7. İmal, M, Karapınar, Ç, Doğan, O. 2013 Hava Kalitesine Doğalgazın Etkisi: Kahramanmaraş Örnek Çalışması, Kahramanmaraş Sütçü İmam Üniversitesi Mühendislik Bilimleri Dergisi, 16 (2): 22-28.
8. Kopar, İ, Zengin, M. 2009 Coğrafi Faktörlere Bağlı Olarak Erzurum Kentinde Hava Kalitesinin Zamansal ve Mekânsal Değişiminin Belirlenmesi, Türk Coğrafya Dergisi, 0 (53): 51-69.
9. Orhan, G. 2012 Hava kirliliği ve asit yağmurları: uzun menzilli sınırlar ötesi hava kirliliği sözleşmesi ve protokolleri karşısında Türkiye'nin konumu. Marmara Üniversitesi Avrupa Topluluğu Enstitüsü Avrupa Araştırmaları Dergisi, 20 (1): 123-150.
10. Örücü , E., Aydın, G., Kızılgöl, Ö., Hasgül, Ö. 2008 Bandırma Limanının Etkinliğinin Arttırılması Ve Bandırmanın Lojistik Merkez Haline Getirilmesine Yönelik Saha Çalışması, Bandırma İktisadi Araştırmalar Enstitüsü Yayın No: 2, http://www.bandirmaticaretodasi.org/ media / lojistik_limanrapor.pdf.
11. Saçılık, M. Y., Çevik, S., Toptaş, A. 2018 Geçmişin Mutfağından Gelecekteki Sofralara: Bandırma-Erdek Yöresinin Gastronomik Mirası, Journal of Tourism and Gastronomy Studies, 6(1): 300-319.
12. Şahin, K, Bağcı, H, Sarı, E. 2016 Havza'da (Samsun) hava kirliliği algısı. Studies of The Ottoman Domain (Osmanlı Hakimiyet Sahası Çalışmaları), 6 (11):29-42.
13. Sümer, G. 2014 Hava Kirliği Kontrolü: Türkiye'de Hava Kirliliğini Önlemeye Yönelik Yasal Düzenlemelerin ve Örgütlenmelerin İncelenmesi. Uluslararası İktisadi ve İdari İncelemeler Dergisi, 0 (13): 37-56.
14. URL-1, https://www3.epa.gov/airnow/no2.pdf. Accessed: July, 2018.
15. URL-2, https://www.aksadogalgaz.com.tr/Dogal-Gaz-Dagitim-Bolgelerimiz/Aksa-Dogalgaz-Bandirma. Accessed: July, 2018.

ARTIFICIAL NEURAL NETWORKS FOR HYDRAULIC SYSTEMS

Begüm Y. DAĞLI [1] , Yesim TUSKAN [2] , Dilay UNCU[3]

[1] Vocational School of Technical Sciences, Manisa Celal Bayar University, Manisa, Turkey.
[2] Civil Engineering Department, Manisa Celal Bayar University, Manisa, Turkey.
[3] Civil Engineering Department, Manisa Celal Bayar University, Manisa, Turkey.

1. INTRODUCTION

The main beneficial forms of water are drinking-use (domestic, industrial), irrigation, energy production, recreation, fishing and river transport. For these purposes, water resources can be divided into relatively old (traditional) resources such as groundwater, rivers and lakes and relatively new sources such as seas, rainwater and used water.

Acquisition of the water demand includes demand management, resource management and development of new resources. The purpose of demand management is to provide the same service level with less water. Resource management consists of the control of leaks, the use of recycled water, groundwater and artificial sustain of rivers. In case of insufficient demand and resource management, new water resources need to be developed to meet the water needs. The widespread use of computers in the second half of the 20th century increased the use of Artificial Intelligence methods in hydrological, hydrostatic and hydrodynamic studies. The society makes almost all of its operations on these innovative technologies and they are enables to found new methods. So the Artificial Neural Networks as a sub-topic formed under the concept of Artificial Intelligence has become the focus of the researchers interested in this subject.

1.1. METHOD OF ARTIFICIAL NEURAL NETWORKS (ANN)

In areas especially such as water resources engineering, coastal-port engineering and, hydrology, the preferred artificial neural network method has emerged as a result of the artificially similar of the biological nervous system. As a result, the non-linear system models are considered as a closed box with the support of this method called ANN

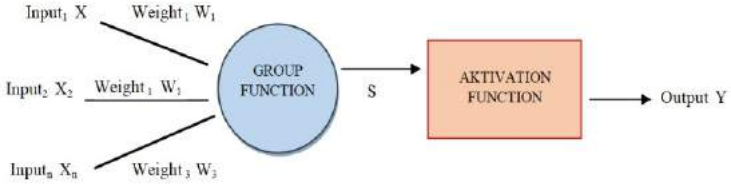

Figure 1. A Typical Neural Network Cell (Fausett, 1994)

The artificial neural network used in the method, which provides an alternative solution to complex problems, consists of artificial nerves. As shown in the Figure 1, the neural network system is consists of five sections as the inputs (X1, X2, X3, Σ Xn), weights (W1, W2, W3, W Wn), group function (Σ), activation function (f) and outputs.

The connection of the inputs to the artificial cells takes place with the support of the weights that express the importance and effect of the system information. The effect is also growing with weights. The zero weight means that the input is ineffective (Fausett, 1994).

Group function calculates the weighted net input. The most common weighted total function is used in this case.

$$S = W_1 x_1 + W_2 x_2 + \ldots\ldots\ldots + W_n x_n = \sum_{i=1}^{n} W_i x_i \quad (1)$$

The activation function evaluates the net input obtained with the group function and determines the appropriate output. The most widely used function is the sigmoid function because of its continuous and derivative behavior among the non-linearity of the activation functions. (Öztemel, 2003).

The value obtained by the activation function is the output of the artificial cell. The inputs and outputs for the linear activation function are equal. Logarithmic Sigmoid function produces values between 0 to 1 for all output values. The difference of the tangent hyperbolic function is that the outputs take values between -1 and 1. The selected activation function determines the output value of the cell.

1.1.1. ANN'S NETWORK STRUCTURES

The structures used in the ANN were determined by considering the differences between the cells. These differences affect the performance and characteristics of the method. The structural diversity is defined in 3 groups as recurrent-feed, feed-forward and cascade connection. Feed-forward and recurrent-feed network structure is given in Figure 2.

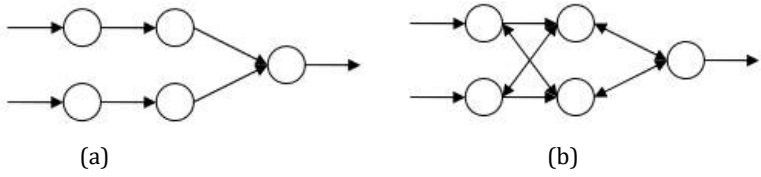

Figure 2. (a) feed-forward structure, (b) recurrent-feed structure

In feed-forward networks, as seen in Figure 2(a), the input and output proceed in one direction in the form of regular layers. In this network structure, there is usually no loop between connections, so the output is quickly accessed.

As given in Figure 2(b), the cells in the recurrent network can give input to the cells before. This network structure contains loops and is particularly preferred for prediction applications. In the cascade-linked network structure, the artificial nerve cell can only input from the cells in the previous layers.

1.1.2. ANN LEARNING ALGORITHMS

Obtaining the appropriate outputs for the inputs given in the ANN depends on the determination of the weight values of the connections, i.e. the training of the network. Repeated cycles and periods are related to the learning algorithms used to train the network until the desired output value is reached. Numerous algorithms are available for training neural network models. Commonly applied learning algorithms are divided into three as advisory, non-consultant and reinforced learning. (Elmas, 2011; Cigizoglu & Kişi, 2005).

The process of minimizing carried out under the supervision of the consultant is maintained until the correct output values are obtained. In the non-consultant learning algorithm, only inputs are defined to the network and no target outputs are given. Especially in the method used in classification problems, the relationship between the parameters is expected to be self-taught by the network without consultation. Reinforced learning is similar to advisory learning, but this algorithm does not provide target outputs to the ANN.

1.1.3. ANN LEARNING RULES

The characteristics required for ANN are carried out according to some rules, regardless of which algorithm is used. The learning rules are used to determine how weights are set to the defined sample. (Şen, 2004).

The Hebb learning rule forms the basis of learning rules. According to the Hebb rule, the weight value of the connection between the active cells must be increased.

In the Hopfield learning rule, the strengthening or attenuation of the weight values of the connections is carried out with the fixed learning coefficient assigned between 0 and 1. According to the Kohonen learning rule, cells compete to learn and the connection weight values of the winner cells are updated.

1.1.4. DETERMINATION OF ANN NETWORK MODEL AND LEARNING ALGORITHM

The topology of ANN is based on collection and activation functions, learning algorithms and learning rules. It is very important to determine the application network model of the problem. To overestimate the complication, the processor elements is not preferred. Simplification of the number of

processor elements is also realized by changing the network model. Table 2.1 gives the purpose of use and successful network models.

The learning algorithm is very important in determining the ANN structure. The architecture related to the learning algorithm is also mandatory. The learning algorithm determines the success of the application. There are many algorithms developed according to the study area.

In addition to the network model and learning algorithm, the number of network layers in the design process is also important. Analysis of the number of network layers to produce the best results is aimed (Tayfur, 2011).

ANNs are utilized to model the processes that are uncertain or too complex. Hydraulic systems are one of the most suitable fields of civil engineering for ANN use. In the next section, the studies on the ANN analysis are divided into categories for the purpose of use of hydraulic systems.

2. MODELING OF HYDRAULIC SYSTEMS WITH ANN

Many hydraulic structures are used for various purposes in water resources systems. A classification based on the function performed by the structure is given in Table 2.1 (Gupta, 2016).

Table 2.1. The Classification of Hydraulic Systems

Type	Purpose	Structure
Flow measurement structures	To determine discharge	Weirs, orifices, flumes
Storage structures	To store water	Dams, tanks
Flow control structures	To regulate the quantity and pass excess flow	Spillways, outlets, gates, valves
Diversion structures	To divert the main course of water	Coffer dams, weirs, canal head works, intake works
Conveyance structures	To guide flow from one location to another	Open channels, pressure conduits, pipes, canals, sewers
Collection structures	To collect water for disposal	Drain inlets, infiltration galleries, wells
Energy dissipation structures	To prevent erosion and structural damage	Stilling basins, surge tanks, check dams
Shore protection structures	To protect the banks	Dikes, groins, jetties, revetments, breakwaters
River training and waterway stabilization structures	To maintain a river channel and water transportation	Levees, cutoffs, locks, piers
Sediments and quality control structures	To control or remove sediments and other pollutants	Racks screens, traps, sedimentation tanks, filters, sluiceways
Offshore structures	Exploratory drilling, production, storage, export	Oil and gas platforms, piers, wharfs, pipelines
Hydraulic machines	To convert energy from one form to other	

2.1. FLOW MEASUREMENT STRUCTURES

The ANN method has been accurately utilized in the hydrological systems such as hydrology and water resources (Cigizoglu & Kisi, 2005; Hu et al., 2005; Jayawardena et al., 2006; Kisi, 2007).

An ANN-based rainfall- runoff model was used by Hu et al. (2005) to generate the feasibility of the new measures. The results of seven watersheds were taken to the account and were successfully implemented.

The compiled data from the Global Runoff Data Centre was utilized to model the discharge data sets by Jayawardena et al (2006). Radial basis functions were used to predict the evaluation of the time series. The results were indicated that the low dimensional deterministic components were caused the alteration of the river's flow.

An analogy of different ANNs algorithms for short term daily stream flow prediction was studied by Kisi (2007). Four different training ANN algorithms: backpropagation (BP), conjugate gradient (CG), cascade correlation (CC), and Levenberg-Marquardt (LM) were evaluated by using streamflow data of the North Platte River in the United States. The daily statistical parameters; mean standard deviation S_x, variation coefficient C_V, skewness coefficient C_{sx}, minimum x_{min}, maximum x_{max} are introduced in Table 2.2. The model performances were controlled by utilizing untrained data.

Table 2.2. Statistical Parameters of ANNs Models (Kisi,2007).

Streamflow data (m^3/s)	1 day ahead forecast					
	Mean	S_x	C_{sx}	C_V	x_{min}	x_{max}
Observed	2.61	2.11	3.23	0.81	0.42	14.9
BP forecast	2.57	2.02	3.12	0.79	0.49	14.9
CG forecast	2.58	2.07	3.12	0.80	0.62	14.8
CC forecast	2.62	2.05	3.11	0.78	0.32	15.9
LM forecast	2.62	2.14	3.25	0.82	0.47	15.0

ANN models were widely utilized to optimize the sewage flow and water standard by Proano et al. 1998; Price et al. 1998; Morshed & Kaluarachchi 1998). Khorchani and Blanpain (2005) used to develop a non-linear side weir overflow system. The primer aim of the paper was to design a side weir overflow system that is easy to implement and fast using ANNs. The model developed seems to be more closely grouped according to the De Marchi model given in Figure 2.1.

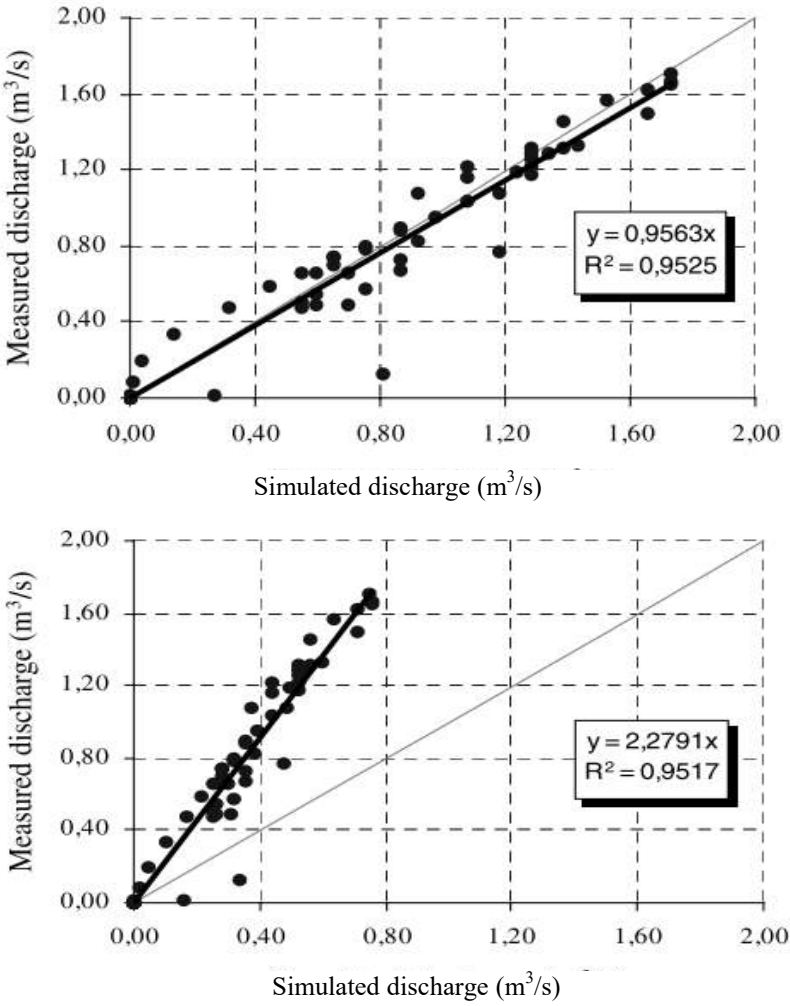

Figure 2.1. Comparison between predicted and measured results of the discharge model (Khorchani and Blanpain 2005)

The outputs of laboratory model of triangular labyrinth side weirs were observed and analyzed using ANN by Kisi et al. (2012). The prediction performance of the models was compared with multi linear regression (MLR) and multi nonlinear regression (MNLR) models for the 2000 experimental data. The higher accuracy was obtained for ANN model compared to the MLR model than MNLR model as depicted in Figure 2.2.

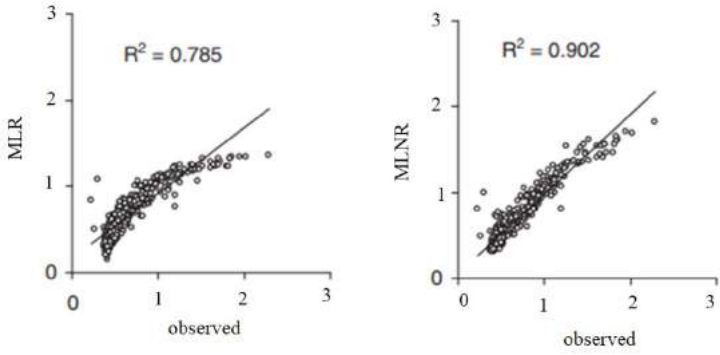

Figure 2.2. The prediction capacity of the MNLR and MLR models (Kisi et al. 2012)

Separated ANN models to generate the discharge coefficient for a weir of different geometrical and flow variables were observed by Al-Suhili et al. (2014). Different apertures dimensions were evaluated and the height of apertures determined from the bed level. The effect of width of apertures on Cd coefficient was compared with the effect of height. The results showed that the width was the major parameter

2.2. STORAGE structures

The seepage discharge in dams was analyzed by Baghalian (2012) by utilizing ANN model. ANN model was created with the Back Error Propagation (BEP) method. This study indicated that the proposed ANN model has a good approximation to identify the piezometric head in selected points under the dam.

Ahmadi-Nedushan et al. (2003) studied a multi-layer perception ANN model to predict the displacements of plumb-lines located in a concrete gravity dam.

A MLR and MLP-ANN models for the estimation of horizontal displacements in an arch-gravity dam were compared by Mata (2011). Consequently, the developed ANN model had a good approximation to model the behavior of concrete dam and estimate the seepage discharge.

Miao et al. (2012) used a MLP-ANN to determine the seepage flow. The proposed MLP-ANN model was optimized by a genetic algorithm.

Santillán et al. (2013) utilized a statistical seepage flow rate model to estimate the response of La Baells Dam foundation. The values of RMSE were compared by considering predicted and measured data of flow discharges.

Consequently, it is observed that ANNs were powerful tools to estimate the seepage phenomenon.

The multipurpose dam with small drainage area was investigated by Hasebe and Nagayama (2002). A reservoir operation was modeled by the fuzzy and ANN models by using examples of floods during flood and non-flood seasons.

Kim and Kim (2008) studied an ANN model to model the settlement of the crest on dams. The Clements theory was depicted in Figure 2.3. for the comparison with the ANN model by using 9 data sets.

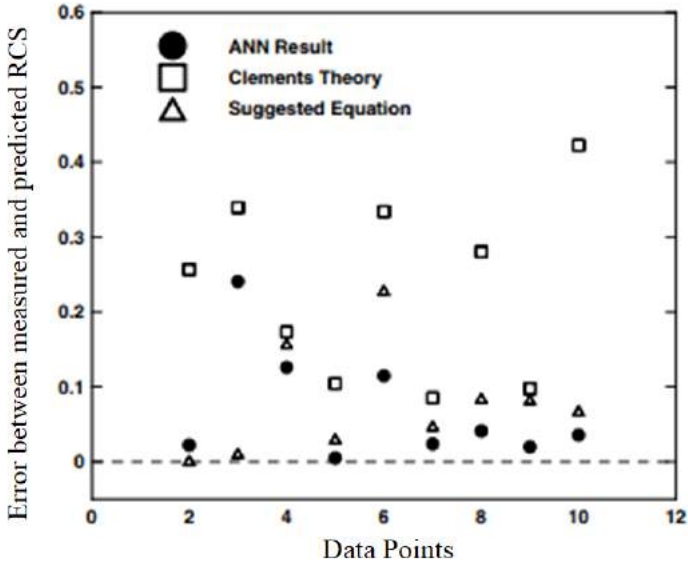

Figure 2.3. the predicted and measured estimation of the proposed model (Kim and Kim, 2008)

The predicted RCS using ANN model developed versus measured values were compared with the Clements theory, and the suggested equation as depicted in Figure 2.4.

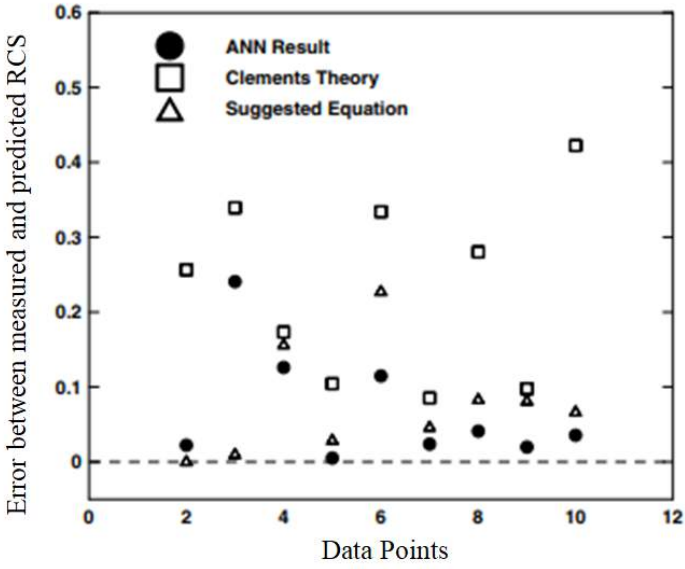

Figure 2.4. The measured and predicted RCS for estimation approach. (Kim and Kim, 2008)

2.2. FLOW CONTROL STRUCTURES

An ANN model of the system was investigated by Darsono, & Labadie, (2007). Consequently, the estimation of the proposed ANN model was in good agreement with measured data as shown in Figure 2.5.

Some investigations were attempted to predict the scour holes using numerical methods such as FEM in recent years. Azamathulla et al. (2008) utilized in-situ measurements to train the networks. The outcomes of the system depicted that the ANN model has a high accuracy to model the scour system.

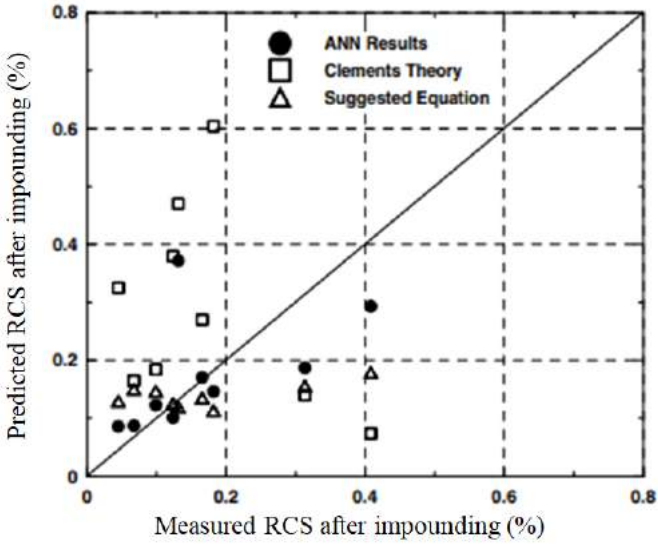

Figure 2.5. The OPTCON and ANN prediction of the model (Darsono, & Labadie, 2007).

Roushangar et al. (2014) studied the energy dissipation system by using ANN model with 12 configurations. Genetic expression programming has also tried to define the problem. The graphs showing the relationship between the two methods (ANN and GEP) indicated that the ANN method yields more appropriate results.

2.3. DIVERSION STRUCTURES

By considering the effect of the separation wall in full - bodied couplings, Baylar et al (1999) determined the rate of swelling to be directed to the lateral water intake structure by the back - spread artificial neural network method.

Khalil et al. (2005) was observed the water demand in diverse canal and reservoirs by compiled database. The ANN model was successfully modeled the system with accurate forecasts. Figure 2.6. provides a scatter plot of ±20 percent error bounds of the proposed problem.

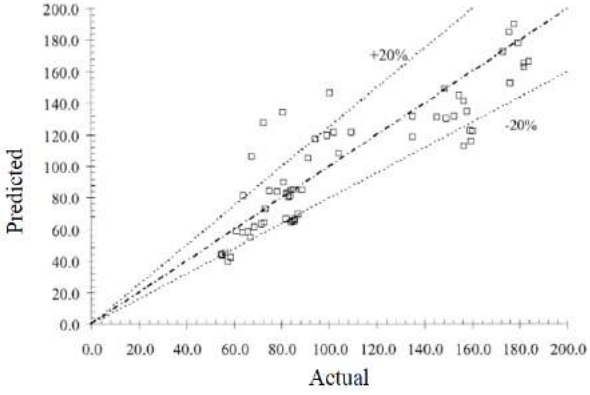

Figure 2.6. Scatter plot of Model Predictions Versus Actual Flows (Khalil et al. 2005).

Sattari, et al. (2007) estimated the amount of water that evaporated from the reservoir in its studies using multilayer back propagation artificial neural network model. They investigated the reservoir parameters by dissolving the continuity equation for the reservoir with both measured and simulated currents. As a result, they observed that they were generally matched.

An ANN was determined by Emiroglu et al. (2011), to model the discharge coefficient of triangular labyrinth side-weirs as depicted in Figure 2.7.

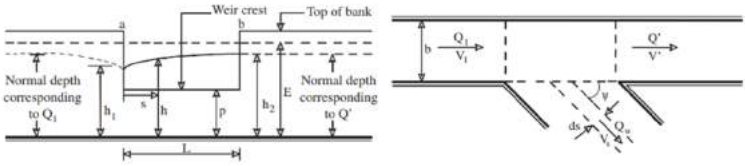

Figure 2.7. Definition sketch of subcritical flow over a rectangular side-weir (Emiroglu et al. 2011).

The ANN model proposed by Emiroglu et al. (2010) was compared with multiple nonlinear and linear regression models. It can be concluded that the proposed system has a better capacity to model this problem.

2.4. CONVEYANCE STRUCTURES

The feedback algorithm is described by Karunanithi et al. (1994) to model river flow estimation. The BP algorithm was utilized by Liu and James (2000) to predict the discharge capacity in two-staged channels.

Dawson and Wilby (2001) developed models by using the precipitation-flow values with the ANN method in order to predict the flow of Thames and Mole Rivers. They showed that the models developed with ANN method gave better results instead of complex estimation methods.

Aci (2006) discussed the estimation of the flows in a river compiled from the precipitation and previous flow observations in the basin of that stream. For this purpose, it has chosen the artificial neural network method which is frequently used in similar estimation applications in recent years. He chose the Akarçay Basin, a closed basin in Central Anatolia for its application. 4 types of models have been designed depending on the parameters such as the placement of the rainfall observation stations in the basin and the observation interval. It has been formed by training and testing phase in accordance with ANN methodology. He presented these comparisons as tables and graphs. ANN method can be applied successfully to rainfall observations, flow estimation problems and can be produced a safe estimation.

An ANN model was utilized by Jafar et al. (2010) to estimate the appropriate duration of the pipes in an urban water distribution system. The model was trained by evaluated a 14-year data set obtained from the north of France. This article showed that the ANN method has high accuracy for urban water systems.

2.5. COLLECTION STRUCTURES

Guo (2001) studied a semi-virtual basin model with a drainage area of less than 150 acres, which helps in the preparation of network training and time-dependent weights matrix according to precipitation and flow vectors.

Radfar (2015) searched to develop more efficient Permeable Interlocking Concrete Pavements (PICP) design guidelines utilizing an ANN model that scrutinize site-specific design variables to predict system performance of the (Time Domain Reflectometers-TDR). The capacity indices were given in Table 2.3.

Table 2.3. Performance statistics of models (Radfar 2015).

Model	Correlation Coefficient R	Root Mean Squared Error RMSE	Mean Absolute Error MAE	Number of hidden layer neurons
TDR01	0.90	0.003	0.003	13
TDR05	0.824	0.012	0.005	10
TDR09	0.844	0.021	0.008	17
TDR13	0.807	0.024	0.008	16
TDR25	0.863	0.016	0.006	14

As shown in Table 2.3 The model could be used in estimating the runoff discharge by evaluated different environmental conditions.

Shetty and Chellam (2003) studied on membrane fouling problem in nanofiltration process by using ANN model. The results were showed that the developed model can be predicted the term fouling of NF membranes.

Mjalli et al. (2007) applied ANN models based black box approach and on current historical data, to model the wastewater treatment plants in Qatar. A diagram of the plant is depicted in Figure 2.8.

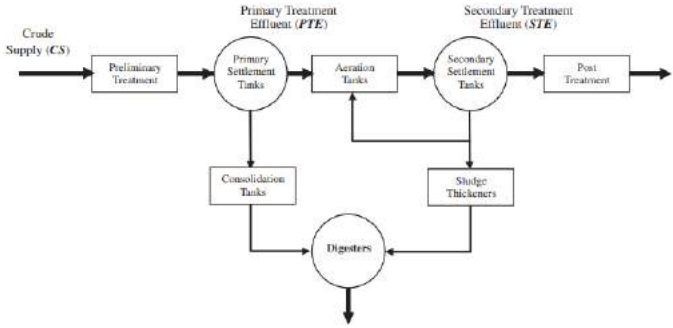

Figure 2.8 The diagram of the model

Sahooa et al. (2005) applied an ANN and an ANFIS model to estimate the pesticide occurrence by using 124 samples from 124 wells. It was observed that the shallow depths of the groundwater tables are more accurate to pesticide contamination.

2.6. ENERGY DISSIPATION STRUCTURES

Singh et al. (2009) utilized ANN and support vector machine (SVM) to correlate the removal capacity of the basins. When compared to performance indices, it was observed that ANN gave better results.

It has been publicized that sediment loss because of stream channel erosion in various 12 locations is increasing (Trimble 1997). The habitat loss and water quality were investigated for two watersheds with the same agriculture land coverage in Atlanta, Georgia. Higher water quality and greater species variety has been observed in watersheds with more permeable surfaces (Gillies, et al. 2003). Hence, proper stormwater management was required to limit channel erosion and improve quality of water resources.

Chanson (2015) designed the safety waters to run above, below, around or around the dam. IN this model, additional storage capacity and maximum reservoir input were used.

Haesloop and Holt (1990) focused on the ANN model to the development of dynamic models of surge tank systems to construct the process.

The ANN models were used by Güven et al. (2006) to estimate the mean pressure fluctuations beneath a hydraulic jump occurring on sloping stilling basins.

The minimum jump length and minimum stagnation data were combined and analyzed by Negm (2002). An ANN model is developed for both length of jump ratio and sequent depth ratio and its results was compared to the generated design equations.

2.8. SHORE PROTECTION STRUCTURES

As the ANN is a multifaceted technique, the rubble-mound provides good results in the calculation of the breakwater stability (Iglesias et al. 2008) or the beach planforms in the highland (Iglesias et al. 2009a, 2009b, 2010).

Two ANN models were generated by López, & Iglesias (2013) with the short wave parameters to predict the significant infra gravity wave height inside a harbour. The structure of the model is depicted in Figure 2.9.

ANN was trained using a set of data to generate a model to predict a problem assessment (Mase et al. 1995; Yagci et al. 2005). The Particle Swarm Optimization (PSO) and a PSO-ANN model were utilized by Kuntoji et al. (2018) to predict the evaluation of the wave transmission.

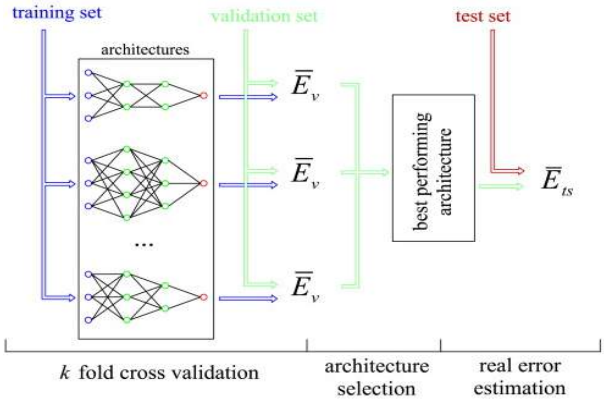

Figure 2.9 Schematic of the procedure for architecture selection and estimation of the real error (López & Iglesias 2013).

2.9. RIVER training and waterway stabilization structures

The equilibrium scour depth (Figure 2.10) was modeled by Bateni et al. (2007) as a function of five variables; flow depth, mean velocity, critical flow velocity, mean grain diameter and pier diameter.

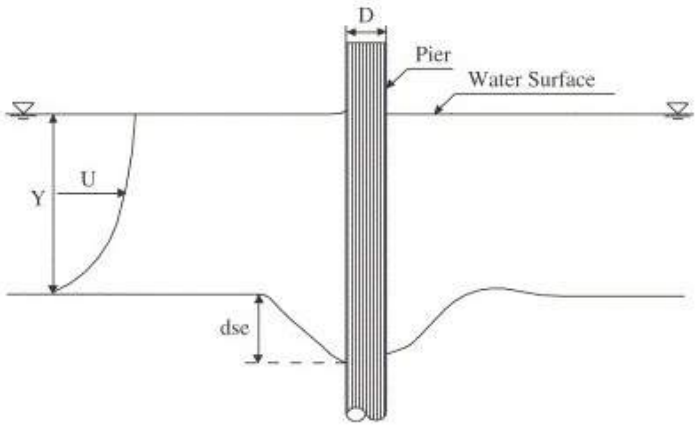

Figure 2.10 Flow and local scour around a circular pier (Bateni et al. 2007)

A typical configuration for a multi-layer perceptron (MLP) and radial basis function (RBF) were compared. To predict the balance scour depth, a hidden layered MLP network was chosen as the most suitable network. This

network with 13 hidden nodes has been examined as the best model to estimate the temporal diversity of the scour depth

An ANN model to observe the local scour at bridge pier was designed by Kaya (2009). A back-propagation algorithm was developed to model for the proposed problem.

A test area of 230 km length along the lower Mississippi River was studied by Aanstoos et al. (2012). The outcomes of the problem depicted that with the multi-polarization synthetic opening radar (SAR) data has a high accuracy rates to obtain for the detection of slump slides in the levees.

A BPN model to estimate the scour depth around bridge piers was determined by Lee et al. (2007). The prediction capacity of the BPN model was compared with conventional studies. The outcomes of the proposed model showed that the scour depth around bridge piers can be efficiently estimated by utilizing the BPN model.

2.10. Sediments and quality control structures

Capodaglio et al. (1991) used the forward-feed, back-propagation ANN model for analysis of the volume conditions at the waste water treatment center. The sediment volume index (SVI) was used to represent the conditions of bulk change due to blistering, and the data was introduced in the artificial neural network using the time series input scheme.

Su et al. (1992) conducted studies on the biological treatment with biological C, N and P inhibitors. The three feed-back feed-in network was used to generate the anaerobic pre-treatment unit, aeration tanks and a deposition reservoir.

Tyagi ve Du (1992) used the technique of artificial neural network to reveal the kinetic model structure due to heavy metal reduction in the sludge in the activation process. The task of the artificial neural network model was applied to estimate the maximum specific growth rate according to the different combinations of heavy metals in waste water.

Pu and Hang (1994) presented an ANN model by using biological determinants and active sediment process to predict medium-scale local wastewater treatment plant performance.

A study to produce nonlinear ANN estimation models as described in a waste water treatment plant was carried out by Ahmed Gamal El-Din et al. (2004). Nonlinear ANN models were compared based on a case study regarding wastewater treatment performance. The advantages and shortcomings of the ANN method are outlined.

Fırat ve Güngör (2004) studied to determine the amount of suspension carried by streams by feed forward neural networks. They used the suspension measures made by EIE (Electrical Works Survey Administration) in the training and test set of the problem. In this study, considering the river

flow rate and the amount of suspending agent by considering only the flow rate of artificial neural networks and used a very good difference between the data groups used although they have determined that a good result. While making a solution with artificial neural networks, the data groups were normalized according to the type of activation function used and the education phase was reached, and the architecture, learning degree and momentum coefficient were found by trial and error until the best result was obtained during the training.

An ANN model to determine the sediment removal efficiency was developed by Ansari and Athar (2013) with a good accuracy.

2.11. OFFSHORE structures

The analysis of coastal hydraulics generally involves heuristics and empirical experience and it is effected through some simplifications and modeling techniques.

Deo and Naidu (1999) applied ANNs method for wave forecasting. More and Deo (2003) used ANNs in wind forecasting.

Deo et al. (1997) used artificial neural networks with remote sensing systems and satellite values for interpolation of ocean wave heights from small intervals (the average average wave height per week).

Guarize et al., (2007) developed a very efficient hybrid Artificial Neural Network (ANN)–Finite Element Method (FEM) procedure to perform a nonlinear mapping of the current for the random dynamic analysis of mooring lines and risers.

An ANN study on the study of the critical stress range was conducted by Quéau et al. (2014). Here, the fatigue life was controlled by the maximum stress range. Compared to the results of OrcaFlex, the relative errors reached ± 13% and 99% of cases with extreme values.

An ANN model to predict the floating production systems (FPS) was designed by Pina et al. (2016) by using the water depth, characteristics of the platform hull, and the riser layout.

A case study for a scientific drill ship was examined by Mahfouz (2007). In this study ANN model was designed to predict the wind speed under dynamic positioning. Wind, wave drift and current loads were the main components that affect the ship and create momentum.

Dagli et al., (2019) investigated the fluid-structure interaction problem by solidity ratio approach. Hydrodynamic wave forces were represented by the Stoke's Second Order wave theory. Morison equation was employed to obtain lateral wave forces. The results of computational fluid dynamics were evaluated ANN with the Levenberg-Marquardt optimization algorithm. The performance of the model indicated that, hydrodynamic forces can be obtained successfully by implementing the solidity ratio.

2.12. HYDRAULIC machines

López, and Iglesias, (2014) were utilized ANN to predict the pneumatic efficiency of an oscillating water column wave energy converter with a given geometry under different wave conditions In the study, ANN structure was selected with a comparative situation with 18 options. In the ANN study, the physical model for turbines performed under different wave conditions, tidal levels and the values of the damping coefficient were investigated. A perfect accordance was achieved by ANN method.

Amundarain et al. (2011) presented well turbines to model wave energy implemented by rotational speed of the system. Many structures of ANNs utilizing three and four layers were generated. Predicted and measured outcomes comparing in the uncontrolled and controlled cases were presented to achieve the model accuracy of the ANN.

Valério et al. (2008) developed ANN model for Archimedes Wave Swing (AWS) which is a fully-submerged Wave Energy Converter. Levenberg–Marquardt algorithm was chose to model the dynamic behaviour of a system. Figure 2.11. shows 40s of the data on wave excitation force and floater's velocity of internal model control developed by using ANN.

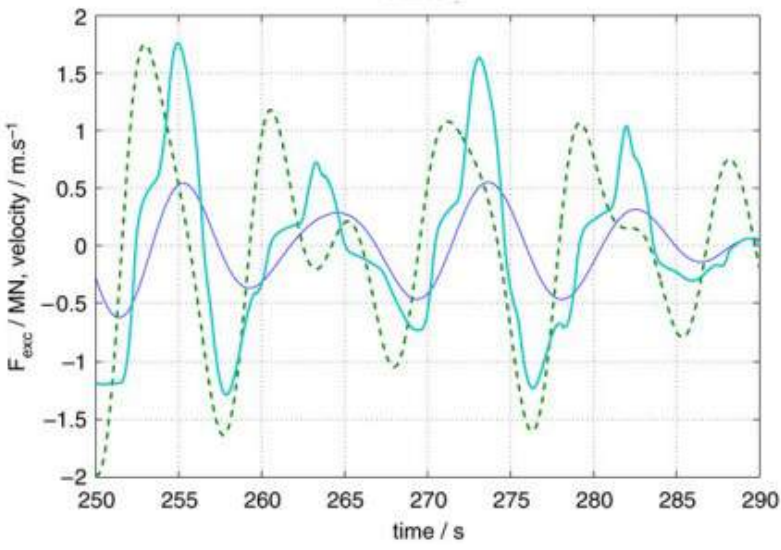

Figure 2.11 Wave excitation force and floater's vertical velocity (Valério et al. 2008)

It can be seen that, when no control strategy is used, the velocity is not in phase with the wave excitation force.

3. CONCLUSIONS

The Artificial Neural Network (ANN), which is widely used in civil engineering applications, has been an important source for the simulation and estimation of different physical events in the last decade. Artificial neural networks offer an alternative way to tackle complex and ill-defined problems. ANN has been applied in various areas of hydraulics and water resources engineering This paper reviews the applications of Artificial Intelligent method on hydraulic systems. The use of ANN technique to model and predict the impact of changing water structures' locations on the hydraulic performance of: flow measurement structures, storage structures, flow control structures, diversion structures, conveyance structures, collection structures, energy dissipation structures, shore protection structures, river training and waterway stabilization structures, sediments and quality control structures, offshore structures, hydraulic machines are considered in the current paper. The results of implementing the ANN technique showed that ANN models may be used as alternative methods in Hydraulic Engineering analyses and predictions.

REFERENCES

1. Fausett, L. Fundamentals of Neural Networks Architectures, Algorithms and Applications. Prentice-Hall, New Jersey, 1994, 48-49.
2. Öztemel, E. Yapay Sinir Agları. Papatya Yayıncılık, Ġstanbul, 2003, 44s.
3. Elmas, Ç. Yapay Zeka Uygulamaları, Seçkin Kitabevi, Ankara, 2011, 424s.
4. Cigizoglu, H. K., & Kisi, O. (2005). Flow prediction by three back propagation techniques using k-fold partitioning of neural network training data. Hydrology Research, 36(1), 49-64.
5. Şen, Z. (2004). Yapay sinir ağları ilkeleri. Su Vakfı.
6. Tayfur, G. Soft Computing in Water Resources Engineering, WIT Press, Southampton, 2012, 288s.
7. Gupta, R. S. (2016). Hydrology and hydraulic systems. Waveland Press.
8. Hu, T. S., Lam, K. C., & Ng, S. T. (2005). A Modified Neural Network for Improving River Flow Prediction/Un Réseau de Neurones Modifié pour Améliorer la Prévision de L'Écoulement Fluvial. Hydrological sciences journal, 50(2).
9. Jayawardena, A. W., Xu, P. C., Tsang, F. L., & Li, W. K. (2006). Determining the structure of a radial basis function network for prediction of nonlinear hydrological time series. Hydrological sciences journal, 51(1), 21-44.
10. Kişi, Ö. (2007). Streamflow forecasting using different artificial neural network algorithms. Journal of Hydrologic Engineering, 12(5), 532-539.
11. Proano, C. O., Minns, A. W., Verwey, A. & Boogaard, H. F. P. 1998 Emulation of sewerage system computational model for the statistical processing of large numbers of simulations. In: Proc. of 3rd International Conference on Hydroinformatics, 24–26 August, 1998, Copenhagen, Denmark, Balkema Rotterdam, pp. 813–818
12. Price, R. K., Samedov, J. N. & Solomatine D. P. 1998 An artificial neural network model of a generalized channel network. In: Proc. of 3rd International Conference on Hydroinformatics, 24–26 August, 1998, Copenhagen, Denmark, Balkema, Rotterdam, pp. 1145–1152.
13. Morshed, J. & Kaluarachchi, J. J. 1998 Application of artificial neural network and genetic algorithm in flow and transport
14. Khorchani, M., & Blanpain, O. (2005). Development of a discharge equation for side weirs using artificial neural networks. Journal of Hydroinformatics, 7(1), 31-39.
15. Kisi, O., Emiroglu, M. E., Bilhan, O., & Guven, A. (2012). Prediction of lateral outflow over triangular labyrinth side weirs under subcritical conditions using soft computing approaches. Expert systems with Applications, 39(3), 3454-3460.
16. Al-Suhaili, R. H., Al-Baidhani, J. H., & Al-Mansori, N. (2014). Hydraulic characteristics of a rectangular weir combined with equal and unequal size three rectangular bottom openings. Int J Comput Eng Res (IJCER), 4(1), 13-29.
17. Baghalian, S., Bonakdari, H., Nazari, F., & Fazli, M. (2012). Closed-form solution for flow field in curved channels in comparison with experimental and numerical analyses and artificial neural network. Engineering Applications of Computational Fluid Mechanics, 6(4), 514-526.
18. Nedushan, B. A., & Chouinard, L. E. (2003). Use of artificial neural networks for real time analysis of dam monitoring data. In Annual Conference of the Canadian Society for Civil Engineering (pp. 4-7).
19. Mata, J. (2011). Interpretation of concrete dam behaviour with artificial neural network and multiple linear regression models. Engineering Structures, 33(3), 903-910.

20. Miao, X. Y., Chu, J. K., Qiao, J., & Zhang, L. H. (2012). Predicting seepage of earth dams using neural network and genetic algorithm. In Advanced Materials Research (Vol. 403, pp. 3081-3085). Trans Tech Publications.
21. Santillán, D., Fraile-Ardanuy, J., & Toledo, M. Á. (2013, August). Dam seepage analysis based on artificial neural networks: The hysteresis phenomenon. In The 2013 International Joint Conference on Neural Networks (IJCNN) (pp. 1-8). IEEE.
22. Hasebe, M., & Nagayama, Y. (2002). Reservoir operation using the neural network and fuzzy systems for dam control and operation support. Advances in Engineering Software, 33(5), 245-260.
23. Kim, Y. S., & Kim, B. T. (2008). Prediction of relative crest settlement of concrete-faced rockfill dams analyzed using an artificial neural network model. Computers and Geotechnics, 35(3), 313-322.
24. Darsono, S., & Labadie, J. W. (2007). Neural-optimal control algorithm for real-time regulation of in-line storage in combined sewer systems. Environmental Modelling & Software, 22(9), 1349-1361.
25. Azamathulla, H. M., Deo, M. C., & Deolalikar, P. B. (2008). Alternative neural networks to estimate the scour below spillways. Advances in Engineering Software, 39(8), 689-698.
26. Roushangar, K., Akhgar, S., Salmasi, F., & Shiri, J. (2014). Modeling energy dissipation over stepped spillways using machine learning approaches. Journal of Hydrology, 508, 254-265.
27. Baylar, A., Emiroğlu, M. E., & Arslan, A. (1999). Geriye yayılma yapay sinir ağı kullanılarak yanal su alma yapısına yönelecek olan süruntü maddesi oranının bulunması. DEÜ Mühendislik Fakültesi Fen ve Mühendislik Dergisi, 1(2), 1-11.
28. Khalil, A. F., McKee, M., Kemblowski, M., & Asefa, T. (2005). BASIN SCALE WATER MANAGEMENT AND FORECASTING USING ARTIFICIAL NEURAL NETWORKS 1. JAWRA Journal of the American Water Resources Association, 41(1), 195-208.
29. Sattari, M. T., Fard, A. F., Docherkhesaz, M., & Öztürk, F. (2007). Yapay sinir ağları yöntemi ile savalan sulama rezervuarının simülasyonu. Ankara Üniversitesi Ziraat Fakültesi Tarım Bilimleri Dergisi, 13(4), 337-345.
30. Emiroglu, M. E., Bilhan, O., & Kisi, O. (2011). Neural networks for estimation of discharge capacity of triangular labyrinth side-weir located on a straight channel. Expert Systems with Applications, 38(1), 867-874.
31. Emiroglu, M. E., Kisi, O., & Bilhan, O. (2010). Predicting discharge capacity of triangular labyrinth side weir located on a straight channel by using an adaptive neuro-fuzzy technique. Advances in Engineering Software, 41(2), 154-160.
32. Karunanithi, N., Grenney, W. J., Whitley, D., & Bovee, K. (1994). Neural networks for river flow prediction. Journal of computing in civil engineering, 8(2), 201-220.
33. Liu, W., & James, C. S. (2000). Estimation of discharge capacity in meandering compound channels using artificial neural networks. Canadian Journal of Civil Engineering, 27(2), 297-308.
34. Dawson, C. W., & Wilby, R. L. (2001). Hydrological modelling using artificial neural networks. Progress in physical Geography, 25(1), 80-108.
35. Aci, M. 2006. Yapay Sinir Ağları İle Hidrolojik Modelleme, Yüksek Lisans Tezi, Celal Bayar Üniversitesi, 85 s., Manisa.
36. Jafar, R., Shahrour, I., & Juran, I. (2010). Application of Artificial Neural Networks (ANN) to model the failure of urban water mains. Mathematical and Computer Modelling, 51(9-10), 1170-1180.
37. Guo, J. C., Urbonas, B., & Stewart, K. (2001). Rain catch under wind and vegetal cover effects. Journal of Hydrologic Engineering, 6(1), 29-33.

38. Radfar, A. (2015). Artifical neural network models for the analysis of permeable pavement performance.
39. Shetty, G. R., Malki, H., & Chellam, S. (2003). Predicting contaminant removal during municipal drinking water nanofiltration using artificial neural networks. Journal of Membrane Science, 212(1-2), 99-112.
40. Mjalli, F. S., Al-Asheh, S., & Alfadala, H. E. (2007). Use of artificial neural network black-box modeling for the prediction of wastewater treatment plants performance. Journal of Environmental Management, 83(3), 329-338.
41. Sahoo, G. B., Ray, C., & Wade, H. F. (2005). Pesticide prediction in ground water in North Carolina domestic wells using artificial neural networks. Ecological Modelling, 183(1), 29-46.
42. Singh, K. P., Basant, A., Malik, A., & Jain, G. (2009). Artificial neural network modeling of the river water quality—a case study. Ecological Modelling, 220(6), 888-895.
43. Trimble, S. W. (1997). Contribution of stream channel erosion to sediment yield from an urbanizing watershed. Science, 278(5342), 1442-1444.
44. Gillies, R. R., Box, J. B., Symanzik, J., & Rodemaker, E. J. (2003). Effects of urbanization on the aquatic fauna of the Line Creek watershed, Atlanta—a satellite perspective. Remote sensing of environment, 86(3), 411-422.
45. Chanson, H. (Ed.). (2015). Energy dissipation in hydraulic structures. CRC Press.
46. Haesloop, D., & Holt, B. R. (1990, May). A neural network structure for system identification. In 1990 American Control Conference (pp. 2460-2465). IEEE.
47. Güven, A., Günal, M., & Cevik, A. (2006). Prediction of pressure fluctuations on sloping stilling basins. Canadian Journal of Civil Engineering, 33(11), 1379-1388.
48. Negm, A. M. (2002, September). Optimal roughened length of prismatic stilling basins. In Proceedings of the 5th International Conference on Hydro-Science and Engineering, Poland.
49. Iglesias, G., Lo´pez, I., Carballo, R., Castro, A. (2009a). Headland-bay beach planform and tidal range: A neural network model. Geomorphology 112(1 – 2), 135–143.
50. Iglesias, G., Lo´pez, I., Castro, A., Carballo, R. (2009b). Neural network modelling of planform geometry of headland-bay beaches. Geomorphology 103(4), 577–587.
51. Iglesias, G., Diz-Lois, G., Taveira Pinto, F. (2010). Artificial intelligence and headland-bay beaches. Coastal Eng. 57(2), 176–183.
52. López, M., & Iglesias, G. (2013). Artificial intelligence for estimating infragravity energy in a harbour. Ocean Engineering, 57, 56-63.
53. Mase, H., Sakamoto, M., and Sakai, T. (1995). "Neural network for stability analysis of rubble-mound breakwaters." J. Waterway Port Coastal Ocean Eng., 121(6), 294–299. doi:10.1061/(ASCE)0733-950X(1995)121:6(294).
54. Yagci, O., Mercan, D.E., Cigizoglu, H.K., and Kabdasli, M.S. (2005). "Artificial intelligence methods in breakwater damage ratio estimation." J. Ocean Eng., 32(17–18), 2088–2106. doi:10.1016/j.oceaneng.2005.03.004
55. Kuntoji, G., Rao, M., & Rao, S. (2018). Prediction of wave transmission over submerged reef of tandem breakwater using PSO-SVM and PSO-ANN techniques. ISH Journal of Hydraulic Engineering, 1-8.
56. Bateni, S. M., Borghei, S. M., & Jeng, D. S. (2007). Neural network and neuro-fuzzy assessments for scour depth around bridge piers. Engineering Applications of Artificial Intelligence, 20(3), 401-414.
57. Kaya, A. (2010). Artificial neural network study of observed pattern of scour depth around bridge piers. Computers and Geotechnics, 37(3), 413-418.

58. Aanstoos, J. V., Hasan, K., O'Hara, C. G., Dabbiru, L., Mahrooghy, M., Nobrega, R., & Lee, M. A. (2012, October). Detection of slump slides on earthen levees using polarimetric SAR imagery. In 2012 IEEE Applied Imagery Pattern Recognition Workshop (AIPR) (pp. 1-7). IEEE.
59. Lee, T. L., Jeng, D. S., Zhang, G. H., & Hong, J. H. (2007). Neural network modeling for estimation of scour depth around bridge piers. Journal of hydrodynamics, 19(3), 378-386.
60. Capodaglio, A. G., Jones, H. V., Novotny, V., & Feng, X. (1991). Sludge bulking analysis and forecasting: application of system identification and artificial neural computing technologies. Water Research, 25(10), 1217-1224.
61. Su, H. T., McAvoy, T. J., & Werbos, P. (1992). Long-term predictions of chemical processes using recurrent neural networks: A parallel training approach. Industrial & engineering chemistry research, 31(5), 1338-1352.
62. Tyagi, R. D., & Du, Y. G. (1992). Operational determination of the activated sludge process using neural networks. Water Science and Technology, 26(9-11), 2461-2464.
63. El-Din, A. G., Smith, D. W., & El-Din, M. G. (2004). Application of artificial neural networks in wastewater treatment. Journal of Environmental Engineering and Science, 3(S1), S81-S95.
64. Firat, M., & Güngör, M. (2004). Askı madde konsantrasyonu ve miktarının yapay sinir ağları ile belirlenmesi. Teknik Dergi, 15(73).
65. Ansari, M. A., & Athar, M. (2013). Artificial neural networks approach for estimation of sediment removal efficiency of vortex settling basins. ISH Journal of Hydraulic Engineering, 19(1), 38-48.
66. Deo, M. C., & Naidu, C. S. (1998). Real time wave forecasting using neural networks. Ocean engineering, 26(3), 191-203.
67. More, A., & Deo, M. C. (2003). Forecasting wind with neural networks. Marine structures, 16(1), 35-49.
68. Deo, M. C., & Rao, V. V. (1997). Neural networks for wave height interpolation. Computer-Aided Civil and Infrastructure Engineering, 12(3), 217-225.
69. Guarize, R., Matos, N. A. F., Sagrilo, L. V. S., & Lima, E. C. P. (2007). Neural networks in the dynamic response analysis of slender marine structures. Applied Ocean Research, 29(4), 191-198.
70. Quéau, L. M., Kimiaei, M., & Randolph, M. F. (2014). Artificial neural network development for stress analysis of steel catenary risers: sensitivity study and approximation of static stress range. Applied Ocean Research, 48, 148-161.
71. de Pina, A. A., da Fonseca Monteiro, B., Albrecht, C. H., de Lima, B. S. L. P., & Jacob, B. P. (2016). Artificial Neural Networks for the analysis of spread-mooring configurations for floating production systems. Applied Ocean Research, 59, 254-264.
72. Mahfouz, A. B. (2007). Predicting the capability-polar-plots for dynamic positioning systems for offshore platforms using artificial neural networks. Ocean Engineering, 34(8-9), 1151-1163.
73. Dagli, B.Y:, Gokkus, U., Yildirim, M.S., (2019). A new approach for the calculatıon of hydrodynamıc forces actıng on lattıce steel structures. Int. J. of Adv. Res. 7 (2). 32-37] (ISSN 2320-5407).
74. López, I., & Iglesias, G. (2014). Efficiency of OWC wave energy converters: A virtual laboratory. Applied Ocean Research, 44, 63-70.
75. Amundarain, M., Alberdi, M., Garrido, A. J., & Garrido, I. (2011). Neural rotational speed control for wave energy converters. International Journal of Control, 84(2), 293-309.
76. Valério, D., Mendes, M. J., Beirão, P., & da Costa, J. S. (2008). Identification and control of the AWS using neural network models. Applied Ocean Research, 30(3), 178-188.

THE IMPORTANT COMPONENTS OF ULTRA-WIDEBAND TECHNOLOGIES: DIRECTIONAL AND OMNIDIRECTIONAL ANTENNAS

Ali Recai ÇELİK [1]

[1] Dr., Dicle University, Electrical and Electronics Engineering, Diyarbakir, Turkey.

1. Introduction

Energy is a size that can be sensed and calculated by the effects of the sound, heat, light etc. There are many energy types such as kinetic, potential, electrical, heat and nuclear which can be turned into each other (Demirel, 2012). Two important methods of transferring an existing energy from one point to another are using mechanical waves and electromagnetic (EM) waves. Mechanical waves express the vibrations that occur in solid, liquid, gas and plasma materials, while EM waves refer to the wave type which occurs not only in the material environment but also in the cavity, which can be expressed by the movement of the charged particles. The diagram showing the frequency ranges of all EM wave types is called the EM Spectrum. EM radiation types are gamma-rays, infrared light, ultraviolet light, X-rays, microwaves and radio waves as shown in Figure 1 (Cyberphysics, 2019).

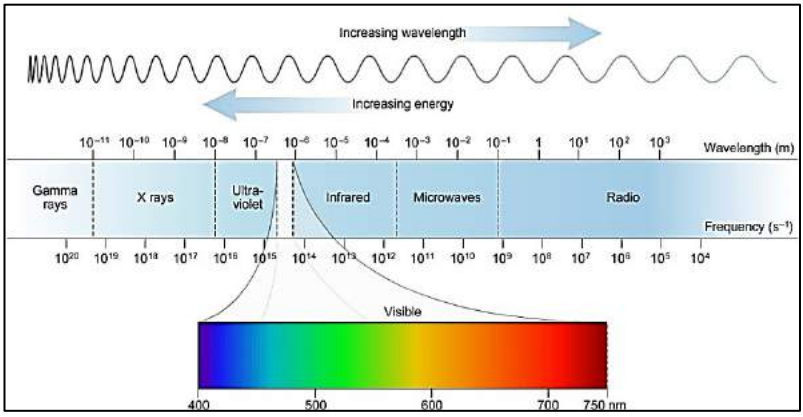

Figure 1. EM spectrum showing the properties of EM waves

In this chapter, we focus on the 'microwaves' that have the frequencies ranging from about 0.3 gigahertz (GHz), up to about 300 GHz and wavelengths of about 1 meter to 1 millimeter (Jones, Layer, & Osenkowsky, 2013), (Pozar, 1993). This waves have a range of applications including communications, radar and perhaps best known by most people, cooking.

Of course, there is a need for some devices in order to transmit and receive microwaves and all EM waves. Electronic circuit elements that used for this function, in other words devices used for transmitting and receiving informations at certain frequency values, are called antennas. The antennas that convert the electrical energy into the EM wave are called transmitting antennas, while the antennas that convert the EM wave into the electrical energy are called receivers (Graf, 1999).

The most important definition which can be used to characterize the impedance matching and determine the working frequency range in the design process is 'Return Loss' of the antenna. This is a measure in decibels (dB) meaning how much of the sent power is returned to the antenna. In which frequency range the antenna wants to operate, the Return Loss value in that frequency band must be below -9.55 dB.

'Bandwidth (BW)' is a term that defines the frequency band in which the antenna can operate efficiently. BW is generally expressed by fractional bandwidth and bandwidth ratio definitions. The fractional bandwidth is defined as given in Equation (1), and the bandwidth ratio is defined as given in Equation (2):

$$BW = \frac{f_h - f_l}{f_c} \times 100\% \quad (1)$$

$$BW = \frac{f_h}{f_l} : 1 \quad (2)$$

where, f_l express the lower frequency, f_h express the higher frequency and f_c express the center frequency of the operation band (Balanis, 2015).

Since US Federal Communication Commission and European Telecommunications Standards Institute allocated of unlicensed use of the bandwidth starting from 3.1 to 10.6 GHz in 2002 and starting from 3.4 to 8.5 GHz in 2008, respectively (FCC, 2002), (ETSI, 2008), an interest to the ultra-wideband (UWB) technology is increased significantly. For the reception of an antenna as broadband; BW should be at least 20% of the *fc*, if the central frequency (fc) is less than 2.5 GHz. And, the BW should be at least 500 MHz while the *fc* is greater than 2.5 GHz. An example graphic of BW versus return loss is given in Figure 2 which shows the UWB range of 3 GHz – 8 GHz.

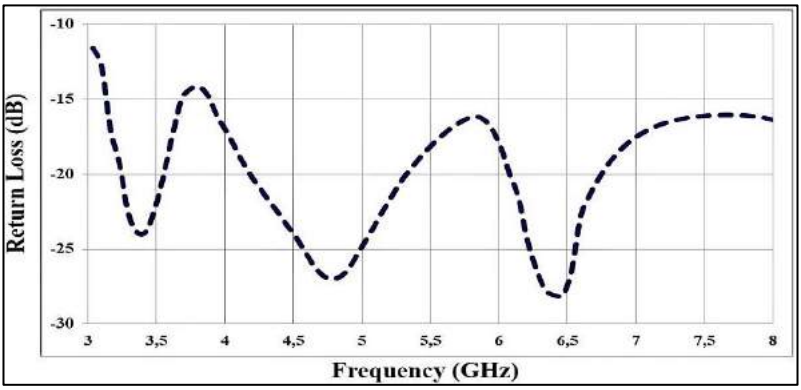

Figure 2. Return loss variation plot for an UWB antenna

The UWB technology is used in many areas such as communication, wireless and measurement systems, imaging systems, radar-based systems, indoor and hand-held systems etc. The reason why the UWB system is preferred in many areas is that it has many advantages such as spectrum reuse, high data rate in short range, multipath immunity, low power, low cost, adequate depth of penetration and high resolution radar. In parallel with the increasing interest in the UWB systems, the development of the antennas which are the key components and important parts of these systems has also improved (Liang & et al, 2005), (Ryu & Kishk, 2009), (Ahmed, Elboushi, & Sebak, 2012). Log periodic, vivaldi, bi-conical, spiral, printed monopole, planar monopole and array antennas are some of the antenna types having broad working frequency ranges.

These antennas differ from each other in terms of the size, shape, gain, directivity, radiation characteristic and purpose of use. Some working areas require using compact-sized antennas, while others may require using large-sized antennas. Similarly, in several UWB applications the omnidirectional radiated antennas are used, whereas some other UWB applications need the directional antennas.

In this chapter, it is aimed to review the directional and omnidirectional UWB antenna types and explain the characteristics of these antennas in detail.

2. Omnidirectional Antennas

A type of antennas that emits uniform wave power in all directions in a plane is called omnidirectional antenna. The radiation pattern of this antenna is generally showed as doughnut shaped as given in Figure 3.

The omnidirectional antennas are preferred in the devices which don't have a fixed orientation and don't need to favour any specific direction. There are many types of UWB omnidirectional antennas such as duck antenna, cloverleaf antenna, dipole antenna, discone antenna which are given in Figure 4 (ChangHong, 2019), (Alaris, 2019), (Wiki, 2018).

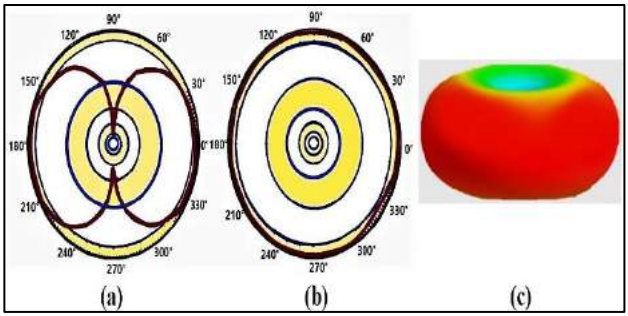

Figure 3. Omnidirectional radiation pattern
a) Vertical, b) Horizontal, c) Three dimensional

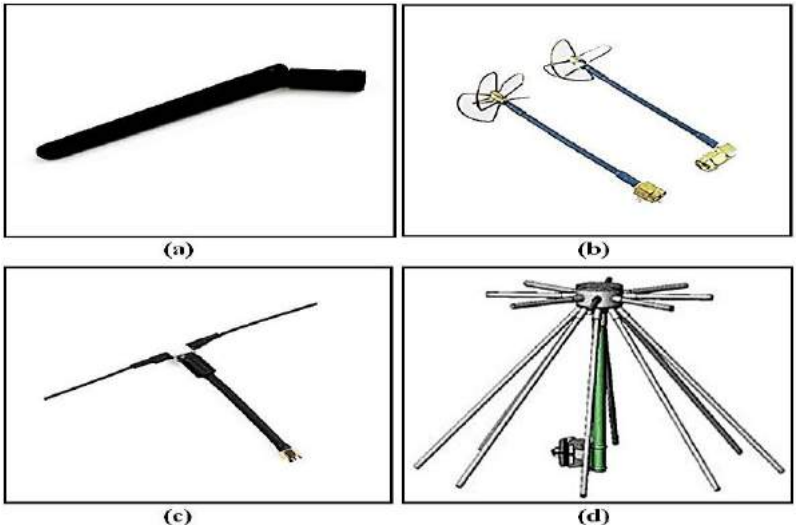

Figure 4. Different omnidirectional antenna types
a) Duck, b) Cloverleaf, c) Dipole, d) Discone

Although there are several types of these antennas, planar and printed monopole antennas have become widespread in recent years due to their compact size and easy integration into the systems. The configurations of these types antennas are seen in Figure 5 (Chou & Su, 2007), (Celik, Kurt, & Helhel, 2018). Planar monopole antenna is perpendicular to a large ground plane whereas printed monopole antenna is parallel to a partial ground plane. Impedance matching of these antennas can be controlled by shaping antenna geometry and/or adjusting antenna structure around feeding.

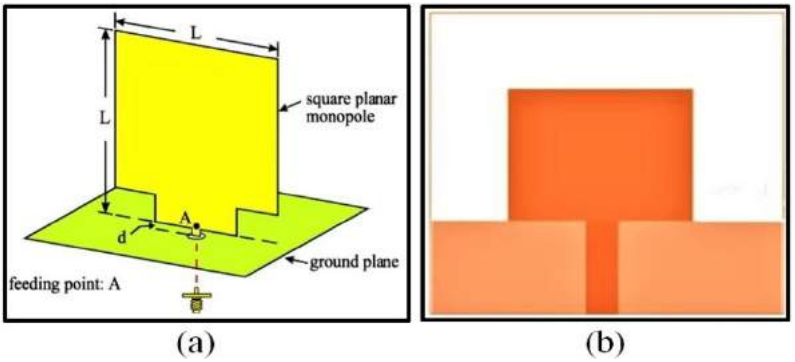

Figure 5. a) Planar monopole, b) Printed monopole antenna

3. Directional Antennas

Directional antennas focus the energy in a particular direction. In other words, these antennas pull out the signals better to one direction and pull in the signals better from one direction. Directional antennas do not have symmetry in the radiation pattern and typically have a main lobe in one direction. However, back lobe and side lobes can be seen in the radiation pattern as given in Figure 6. Pencil-beam radiation pattern of a directional antenna is also shown in Figure 7.

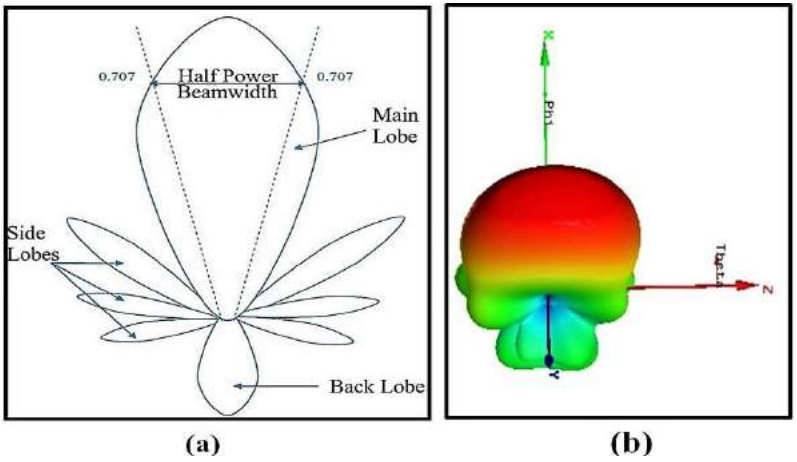

Figure 6. Directional radiation pattern terms
a) Two dimensional, b) Three dimensional

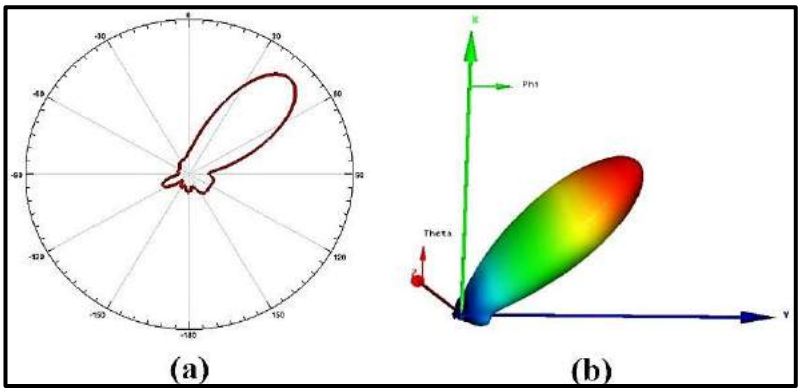

Figure 7. Directional pencil-beam radiation pattern
a) Two dimensional, b) Three dimensional

There are many types of UWB antennas having directional radiation patterns such as horn, vivaldi, dish, dual-ridge horn etc. Some of these antennas are given in Figure 8 (Amitec, 2015) (Wiki, 2018).

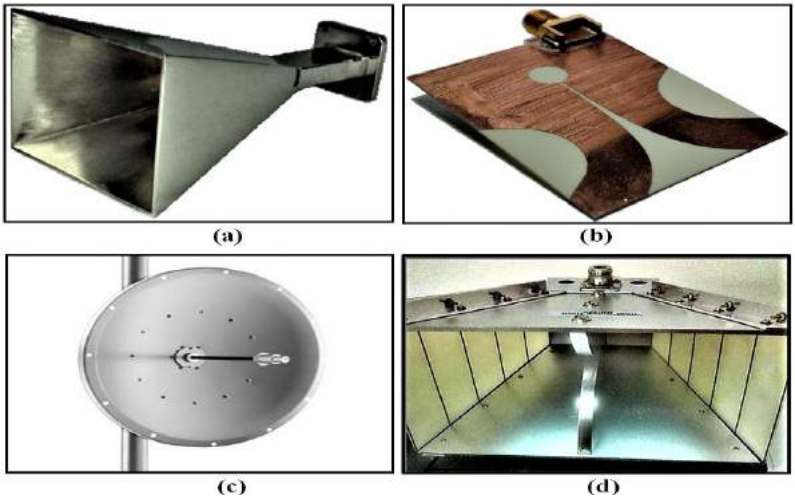

Figure 8. Different directional antenna types
a) Horn, b) Vivaldi, c) Dish, d) Dual-ridge horn

Although there are several types of these antennas, modified planar and printed monopole antennas have become widespread in recent years due to their compact size and easy integration into the systems. The configuration of a modified printed monopole antenna is shown in Figure 9 as an example.

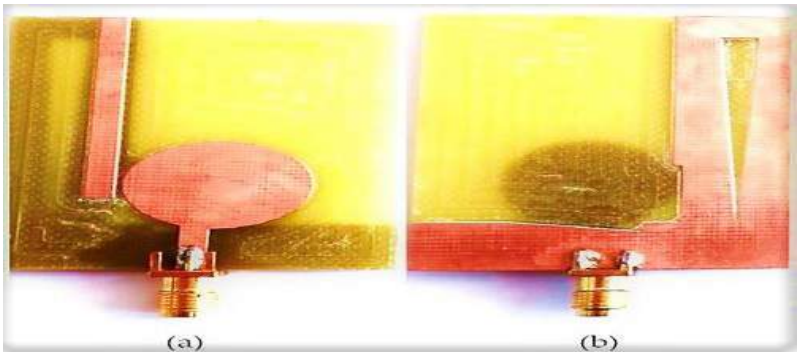

Figure 9. A modified printed monopole antenna
a) Front view, b) Back view (Celik & Kurt, 2018)

4. Modification Techniques

The return loss, gain, directivity, bandwidth and beamwidth are some of the antenna parameters. The values of these parameters are determined according to the applications and using areas of the antennas. As it can be seen from the antenna given in Figure 9, various changes can be made on an antenna in order to change the characteristics of it according to a desired purpose.

There are various modification techniques to improve the performance of the antenna. Some of these techniques are changing feeding technique, adjusting the position of feedline, adding parasitic element, slotting and notching on the patch or using defected ground structure approach on the ground (Ahn, et al., 2001), (Guha, Biswas, & Antar, 2005), (Dong, Li, & Deng, 2017).

Slot and notch mean part ejection and provide creating new resonance. Hence, the method of using slot or notch can be pefferred for bandwidth and return loss improvement of a compact UWB antennas (Wani & Kumar, 2015), (Bah, Hong, & Jamro, 2015). Parasitic element means adding part around the patch and provides changing radiation pattern, directivity and gain (Abdelaziz, 2006), (Tseng, Huang, & Hsu, 2009). In Figure 10, some modification terms are shown on the antenna.

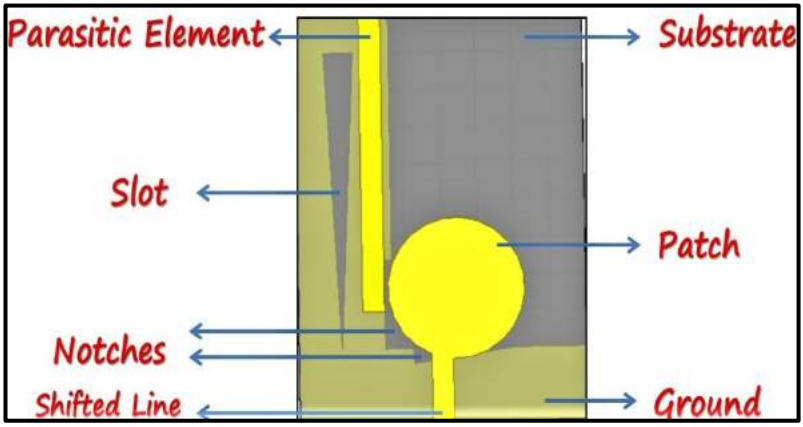

Figure 10. Some parameters and modification techniques

5. Conclusions

In this chapter, it was aimed to mention about EM waves, show the frequency range of UWB, and introduce basic terms such as BW, return loss, gain and radiation pattern to the readers. Furthermore, the types and characteristics of the directional and omnidirectional UWB antennas are explained. The subjects mentioned for these purposes can be summarized as follows:

- There are many types of EM radiation that make up the EM spectrum.
- Microwaves are one of the important types of EM waves. They have the frequency range of 0.3–300 GHz and the wavelengths of 1m–1mm.
- There is a need for some devices in order to transmit or receive EM waves. Antenna is an electronic device which is used for this aim.
- BW defines the frequency band in which the antenna can operate efficiently. Broad frequency range is described as UWB.
- FCC and ETSI allow the unlicensed use of UWB microwaves in the frequency range of 3.1–10.6 GHz and 3.4–8.5 GHz, respectively.
- The UWB technology is used in many areas and they have many advantages. UWB antennas are the key components of this system.
- In order to transmit and receive UWB microwaves, generally two types of antennas are used. These are named as directional or omnidirectional according to their radiation patterns.
- There are various types of omnidirectional antennas. Among them, planar and printed monopole antennas have become widespread in recent years due to their many advantages.
- Omnidirectional antennas can be transformed to directional antennas by using some modification techniques for the patch or ground plane.

References

1. Abdelaziz, A. (2006). Bandwidth Enhancement of Microstrip Antenna. Progress In Electromagnetics Research, 63, 311-317.

2. Ahmed, O. M., Elboushi, A. & Sebak, A. R. (2012). Design of Half Elliptical Ring Monopole Antennas with Elliptical Slot in Ground Plane for Future UWB Applications. Microwave and Optical Technology Letters.

3. Ahn, D., Park, J., Kim, C., Kim, J., Qian, Y., & Itoh, T. (2001). A Design of the Low-Pass Filter Using the Novel Microstrip Defected Ground Structure. IEEE Transactions on Microwave Theory and Techniques, 49, 86-93.

4. Alaris. (2019). High-Powered Wideband (100 – 400 MHz) Discone Antenna User Manual.

5. Amitec. (2015). 5G Ready 40 MHz - 12.4 GHz RF & Microwave Antenna Lab User Manual. Amitec Corporation.

6. Bah, M., Hong, J. & Jamro, D. (2015). Ground Slotted Monopole Antenna Design for Microwave Breast Cancer Detection Based on Time Reversal MUSIC . Progress In Electromagnetics Research C, 59, 117-126.

7. Balanis, C. (2015). Antenna Theory: Analysis And Design. New Jersey, USA: Wiley.

8. Celik, A. R. & Kurt, M. B. (2018). Development of an Ultra-Wideband, Stable and High-Directive Monopole Disc Antenna for Radar-Based Microwave İmaging Of Breast Cancer. Journal of Microwave Power and Electromagnetic Energy, 52:2, 75-93.

9. Celik, A.R., Kurt, M.B & Helhel, S. (2018). Mikrodalga Görüntüleme Uygulamaları için Bir Düzlemsel Dikdörtgen Monopol Anten Tasarımı ve Optimizasyonu. Dicle Üniversitesi Mühendislik Dergisi, 9:1, 1-12.

10. ChangHong Corporation. (2019). Global System for Mobile Communication 900/1800MHz Phone Antenna User Manual.

11. Chou, J.H. & Su, S.W. (2007). Internal Ultra-wideband Metal-plate Monopole Antenna for a Wireless USB Dongle. IEEE Antennas and Propagation Society International Symposium . Honolulu, USA.
12. Cyberphysics.(2019). Open Access:
13. https://www.cyberphysics.co.uk/topics/light/emspect.htm
14. Demirel. (2012). Energy Production, Conversion, Storage, Conservation, And Coupling. Springer.
15. Dong, J., Li, Q. & Deng, L. (2017). Compact Planar Ultrawideband Antennas with 3.5/5.2/5.8 GHz Triple Band-Notched Characteristics for Internet of Things Applications. Sensors, 17, 349.
16. ETSI. (2008). Ultra Wideband (UWB) Technologies For Communication Purposes. European Telecommunications Standards Institute.
17. FCC. (2002). Revision of Part 15 of the Commission's Rules. Federal Communications Commission .
18. Graf, R. F. (1999). Modern Dictionary of Electronics. Newnes.
19. Guha, D., Biswas, M. & Antar, Y. (2005). Microstrip Patch Antenna With Defected Ground Structure for Cross Polarization Suppression. IEEE Antennas and Wireless Propagation Letters, 4, 455-458.
20. Jones, G. A., Layer, D. H., & Osenkowsky, T. G. (2013). National Association of Broadcasters Engineering Handbook,. Taylor & Francis.
21. Liang, J., & et al, C. (2005). Study of a printed circular disc monopole antenna for UWB systems. IEEE Transactions on Antennas and Propagation.
22. Pozar, D. M. (1993). Microwave Engineering Addison. Wesley Publishing Company.
23. Ryu, K., & Kishk, A. (2009). UWB Antenna with Single or Dual Bandnotches for Lower WLAN Band and Upper WLAN Band. IEEE Transactions on Antennas and Propagations.
24. Tseng, C., Huang, C., & Hsu, C. (2009). Microstrip-Fed Monopole Antenna With a Shorted Parasitic Element for Wideband Application. Progress In Electromagnetics Research, 7- 115-125.
25. Wani, Z., & Kumar, D. (2015). Dual-band-notched Antenna for UWB MIMO Applications. International Journal of Microwave and Wireless Technologies, 35, 1-6.
26. Wiki.(2018). Open Access:
27. https://en.wikipedia.org/wiki/Omnidirectional_antenna

EXPERIMENTAL AND COMPUTATIONAL DESIGN OF GASOLINE CAR ENGINE'S SUPER HIGH STRENGTH STEEL MATERIAL ADVANCED CRANKSHAFT AND STRUCTURAL ENGINEERING ANALYSIS BY FINITE ELEMENT ANALYSIS FOR BETTER MANUFACTURING

Özdoğan KARAÇALI [1]

[1] Doç. Dr., Department of Mechanical Engineering, Engineering faculty, İstanbul University-Cerrahpaşa, Avcılar, Istanbul, 34320 Turkey.

1. Introduction: Crankshaft technology and research

The Crankshaft technology and research is important to consider the new technologies developed in the automobile industry and the minimum production costs to be implemented. Necessary products, such as the connecting rod, crankshaft and engine block, are required to be extensively surveyed to meet market competitiveness in the automobile field [1]. In the efficient operation of engine's combustion section, the crankshaft is the essential and critical components that pushes the piston's piston movement to the rotational movement and pushes the vehicle forward. It is subjected to various stresses and loads [2]. Crankshaft manufacturers need new methodology and technology research to make crankshafts better, stronger and more dynamic [3]. The design and mechanical-static analysis of the advanced crankshaft made of super-high-strength steel on a crankshaft in a four-cylinder engine with four-stroke was investigated in the ANSYS for a stronger and better design.

A three-dimensional engine crankshaft was created by the SOLIDWORKS modelling method. FEA-finite element assessment was accomplished to ensure the alternative of the strain size at the risky points of the crankshaft. The behaviour of the crankshaft under static and variable loads was performed with ANSYS 19.0 commercial software. These loads were tested to the FEA modelling in ANSYS. The boundary environment was determined regarding to the motor installation circumstances. Von Mises stress analysis was performed for analysis, critical areas for damage to the crankshaft, cracking or fracture control. The stress change on the engine speed was investigated to compute bending load and the torsion effect in the finite element computational analysis. Crankshaft stress analysis of is complex and adjustment is needed studying strain concentration factors [3]. Afterward defining the loading and boundary conditions, the crankshaft loading stresses were analysed to determine the critical locations.

The force magnitude bases on many considerations, such as the connecting rod dimensions, the connecting rod, crank radius, the piston, the piston rings and weight of the pin. As the combustion gas force and inertial force, two types of force are applied on the crankshaft, including the torsional load and the buckling load. The material of the crankshaft must be strong enough to be able to drive downwardly without excessive buckling due to the applied force, therefore, the life and dependability of the inner combustion engine is greatly build upon to the force of the crankshaft. [4].

The crankshaft is similar to a cantilever beam with a load distributed along its length varying in relation to the crank locations. Each part of the shaft is subject to bending and twisting. Bending moment and torsional moment which cause tensile and compressive stresses cause shear stress. The crankshaft may cause engine failure. The usual crankshaft failures are fatigue at the junction zone as the bending force due to combustion [5-8]. The moment of combustion causes the load from the piston to be transmitted to the crank pin, resulting in a large torsional torque over the entire geometry

of the crankshaft. The crankshaft areas have stress concentrations at the root, and the positions of this high stress array are the specific area where repeated loads can trigger cracks due to weakness cranking to breakage [6]. Figure 1 displays the three-dimensional crankshaft solid model discussed in this study.

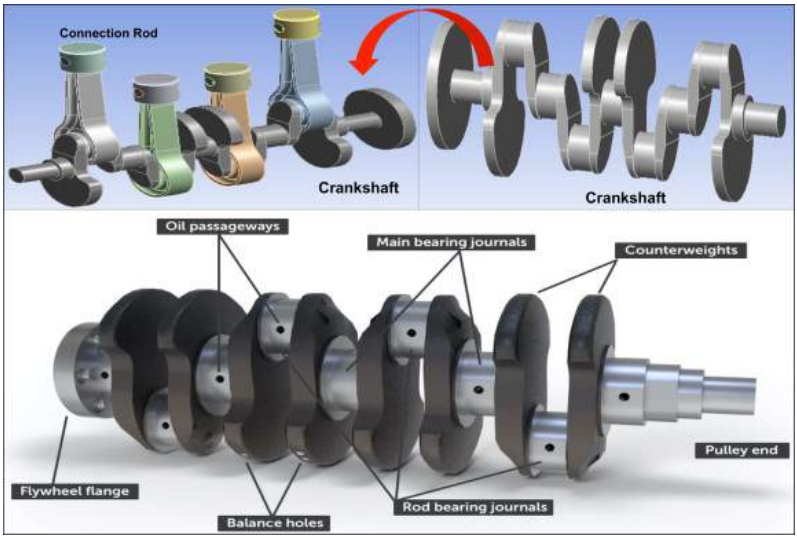

Figure 1: Crankshaft model of crankshaft in SOLIDWORKS

This study examined the dynamic loads acting on the crankshaft during operation. The presence of maximum stress for critical stresses and cranking is calculated by SEA. In the design of the crankshaft, it has been optimized for dynamic loading [1]. The maximum deformation has been observed at the crankshaft centre surface. The peak strain is seen on the surface between the crankshaft journal and the crankshaft side surfaces and also adjoining the central point. The main shaft edge is a extreme stress area. The crankshaft deformation is often the bending distortion below low frequency [8]. The determined extreme deformation was found on the shaft amid the main bearing journal and the crank pin and the crank sides. Thus, this area revealed bending fatigue cracking.

P. Arcos [2] is a three-dimensional engine crankshaft model by Pro-Engineering (ProE) software. The FEA for the crankshaft was performed beneath severe operative situations. The stress distribution of the crankshaft was offered for the crank stress change model. The crank tension was found by using the finest element analysis of the greatest danger point. The enhancement approach for crankshaft structural design is specified. The crankshaft was modelled with point mass and rods in the study. Hydrodynamic (HD) equations are solved in the main bearing connections.

Then the driving forces of the motor and the response of the developed analysis were computed and related with experimental tests. The engine block and the crankshaft was modelled, made an HD connection between them and analysed the simple model they obtained from the main bearing caps due to the ease of measurement. Tests were performed on the same motor to verify the crankshaft model, and components in the test signal were estimated to come from other parts in order to find the vibrations from the crank mechanism. The results of the tests were compared with the answers obtained from the same locations. This research combined the motion equations of the cylinder block and the crankshaft mechanism components, all of which were rigid, to obtain a combined numerical model.

This displays that the great stress zone is mostly concentrated on the arm joints of the crank and the crankshaft central body. The connecting rod centre and crank arm are the maximum easily shattered area. P.Thejasree [3] analysed the 3D FEA model crankshaft of the 380 diesel engine by ANSYS and ProE. Then, the solid model was transferred to the FEA or CFD ANSYS. The material properties boundary conditions and 380 diesel engine crankshaft mechanical boundary conditions of have been resolved. Lastly, the stress and strain values of the crankshaft have been computed with the highest stress point and the hazardous zone. This study has proved the fatigue evaluations and static strength of the crankshaft. It has provided a theoretical basis for development and optimization of the engine design. Greatest deformation occurred in the cylinder balance end weight.

M. Fonte [4] investigated a 3D engine crankshaft by the ProE. By the ANSYS, it showed that the great stress zone primarily focuses on the crank arm and the joints of the main body on arm journal of arm and the connecting rod. the uppermost easily cracked area is between the journal arm and connecting rod. F. Summer [5] analysed the crankshaft model and crank throw performed by the ProE software and then transferred to the ANSYS software. The deformation of the crankshaft has found that it often produces torsional distortion below low frequency. The extreme distortion is found on the shaft amid the main bearing journal, the crank pin then the crank sides.

J. A. Villanueva described the stress concentration in the crankshaft model for the static analysis [6]. The stress concentration showed that the sidewall and crank pin surface tension were comparatively large. According to the stress analysis, the fatigue strength calculation for the crankshaft was able to meet the requirements of the design. Natural frequency values showed that the crankshaft resonance was not the same. This article has shown that it is all about the dynamic analysis of the crankshaft. B. Kareem provided a comprehensive literature review of the crankshafts [7]. His research has presented a literature survey focusing on fatigue assessment and comparison of nodular cast iron and forged steel crankshafts. The Crankshaft features, working environments and several fault causes are considered. The usual crankshaft material and production process tools used were compared in terms of durability performance.

L. Witeka [8] presented crankshaft optimization design research on a literature review. Failure analysis of materials, production process, design evaluation etc. has been assessed. The design of the crankshaft has taken into account dynamic loading, and optimization has been carried out to meet automobile requirements for cost and dimension efficiency of specifications. The middle part of the fissure front became flatter and they concluded that the crack grew sooner on the crank free surface. Fatigue established that the crankshaft the failure was coming from mechanism of the loading.

A. Albers [9] discussed modal analysis and stress analysis of an engine 4-cylinder mechanical crankshaft. The FEA models developed in ANSYS was used to evaluate the modal and stress analysis of the crank shot vibration. The correlation between vibration modal and frequency is explained by the modal analysis of the crankshaft. This delivers a reliable theoretical basis for engine design optimization.

B. Bellakhdhar [10] used the forged steel and cast iron crankshaft for a four-stroke cylinder engine. A CMM laser-measuring machine measured these crankshafts. Modelling of the engine provided load analysis and validation of the results. In the next step, geometry and production cost optimization are done. Given the torsional load under general dynamic loading conditions, it has shown that there is no effect on the stress of von Misses in the region of the critical tension occurring. All of the critical positions on the crankshaft have been found in the side surface areas due to the great stress rise in these positions. The optimization of geometry resulted in a decrease of 18% by weight of forged steel. Surface rolling showed that the surface areas caused a residual stress, which resulted in a 165% expansion in the fatigue potency of the crankshaft.

The other coming section deals with the material and method used in this research. The experimental and theoretical computational ANSYS analysis method is presented.

2. Material and method in crankshaft research

In this study, crankshaft fatigue test and theoretical computational simulation method was compared. The advanced crankshaft design and ANSYS analysis of the gasoline automobile engine made of super-high-strength steel were carried out. In this case, the device for the fatigue test shown in Figure 2 is presented. As a result of this experiment, the forces to the crankshaft have been defined.

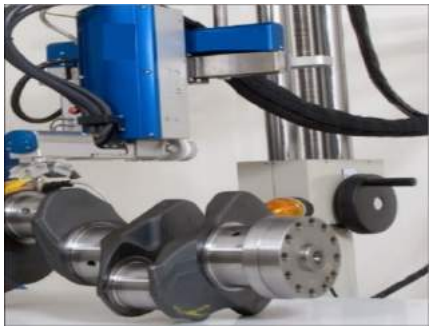

Figure 2: Crankshaft and fatigue experimental test

The crankshaft is subjected to various forces, and it has been analysed in two positions in this study. First, it can be a failure in the maximum torsion position; this may be at the centre or at both ends of the crank. In such a case, bending causes the pressure and the breakdown in the mechanical part of the crank is maximum level. Another, the pin of crank can collapse resulting from torsion; therefore the crankshaft must be controlled periodically for slip at the maximum bending zone location. The pressure at this position is the maximum pressure, but only the maximum pressure ratio. A crankshaft includes two or more centrally located coaxial cylindrical main shafts and one or more offset cylindrical lower crankshafts. The two-plane crankshaft shown in Figure 1 has five main spindles and four lower spindles each spaced 90 °. By rotating the crankshaft main part in a series of support bearings, the offset causes the drop journals of shaft to spin in a rounded path about the principal shaft centres, which is double the diameter of the lower parts. The diameter of this line pathway is the motor's "course stroke": the piston distance of travels up and then goes down in the crankshaft cylinder. The connection bottom shaft consists of the lower spindle bearings whose bearings are located in the lower shaft offset rod jacks. In Figure 3, the maximum equivalent stress was found to be 908.61 MPa in the finite element analysis in ANSYS.

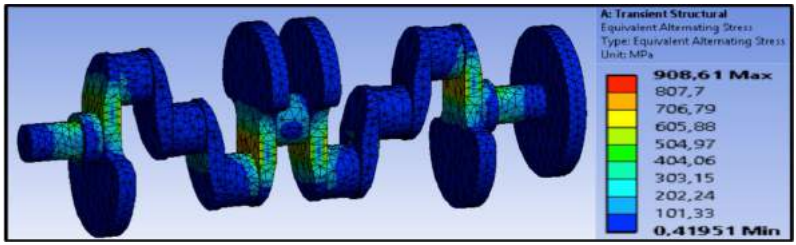

Figure 3: Crankshaft analysis with finite elements

Using the crankshaft SOLIDWORKS software modelled in ANSYS according to the forging process, the crankshaft was solid-modelled. Static analysis was performed by using ANSYS-19 software. ANSYS is a broad-spectrum drive SEA (Finite Element Analysis) commercial package. SEA is a computational method of dividing into very small pieces, called complex system elements. The software is applied to the equations that govern the crankshaft behaviour [11] and solves all of them; the crankshaft has produced a comprehensive report on how the system acts as a whole. Crankshaft total deformation analysis in Figure 4

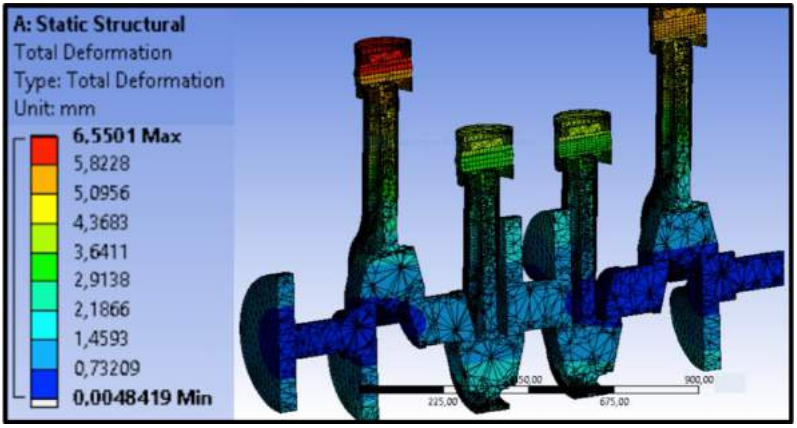

Figure 4: Crankshaft total deformation analysis

The ANSYS application environment was used in this study as a preliminary finite element analysis tool in pre-production design by using pre-modeling in conjunction with SOLIDWORKS systems. ANSYS is a software environment for conducting analyses such as structural and thermal. For this reason, the crankshaft design has focused on adding the existing geometry, adjusting the finite element model, solving and reviewing the results. Figure 5 presents a crankshaft safety factor analysis.

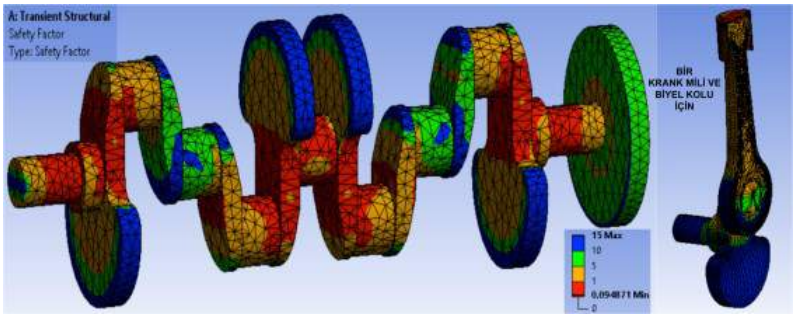

Figure 5: Crankshaft safety factor analysis

Structural static analysis of crankshaft described stresses, forces and displacements in construction of components triggered by loads. Those all mechanical behaviours do not generate substantial damping and inertia consequences [13]. It is assumed that the constant loading and response conditions, the response of the structure and the loads change slowly over time. The load types that may be employed in a mechanical static evaluation incorporate outsider affected pressures and forces, stable state inertia dynamisms such as rotational speed with gravity, displacements, heats for thermal stress. Figure 6 shows the static analysis of the crankshaft connecting rod connecting rod.

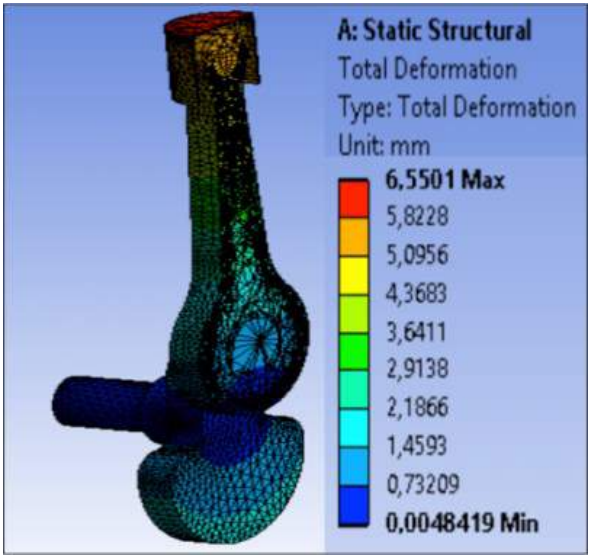

Figure 6: Static analysis of crankshaft connecting rod connecting rod

4. Mesh model of crankshaft, loading and boundary conditions

The finite element method has arisen from the following requirements in the crankshaft modelling: reducing the number of prototypes, virtual modelling for the prototype test beforehand, cost savings, reducing the time spent in modelling.

Mesh process, continuous environment or structure to cut into several elements or smaller squares to create a node is formed. Subsequently, the assembly between the elements outlined as nodes holding the knot parts together are established. These outcomes was generated from a series of concurrent algebraic equations [9]. The higher the number of nodes or the optimal nodes gave the better the results of the analysis, the greater the accuracy of the results. The type of lattice selected for the model has the element number 79452 and the node number 117685, as shown in the figure below. As the fineness of the pattern increases, the result is improved. To analyse the crankshaft strength, the model material property must be defined. The QT-800 was selected as the material of the gray cast iron crankshaft. The Young's modulus as 210 GPa, Bulk density as 8900 kg / m3, Poisson's ratio as 0.30, and tensile strength as 345 GPa were taken as physical parameters. The crankshaft is mounted on the one side with a ball bearing and on the further adjacent on a spigot and they are firmly seated on the engine crankshaft. This condition can not permit the engine crankshaft any movement except for revolution about its leading axis. Then only bearing surfaces 180 degrees confronting the load path restrict the crankshaft movement, this restriction is stated as a set semicircle to the width of the bearing seat. The crankshaft other side is the journal bearing. Consequently, this side is modelled for semicircle confronting the weight below the radius, which is stationary in a surface vertical to the principal axis and unrestricted to transfer in the direction of the centre axis. Figure 7 shows the equivalent stresses during the operation on the crankshaft. The delivery of the weight on the linking rod is equal compression over the contact area of 120 degrees. Since the crankshaft interacts with the joining rod, the equal loading sharing is transferred to the crankshaft. In this analysis, a pressure of 10.6 MPa was affected to the crank pin in the upper dead centre position of the piston.

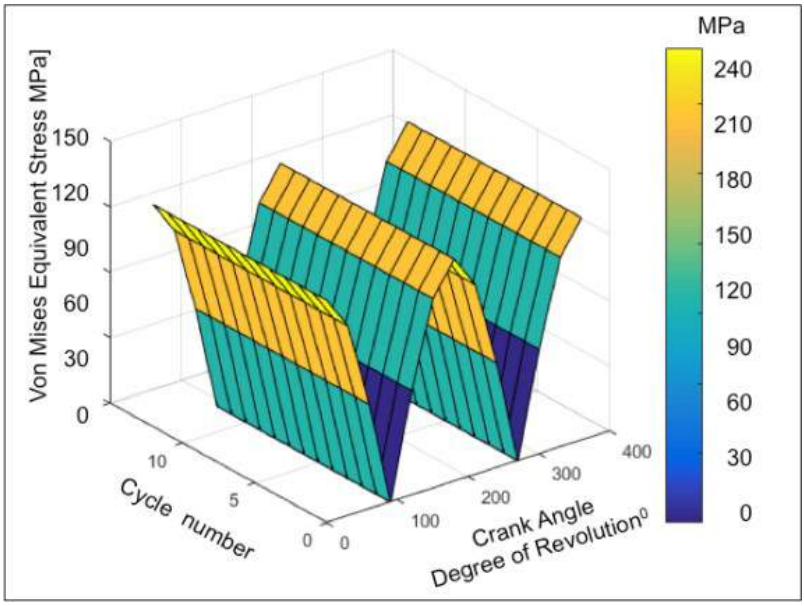

Figure 7: Equivalent stresses occurred during crankshaft operation

In the step of making the mesh, the number of small parts divides the component or part. The total nodes occurred wss 136492 and the amount of elements was 7339. The force effect on each part of the component is not the same. The purpose of the parsing process is to perform the analysis in each small section separately. For this purpose, the ANSYS modelling software was used to model the four-cylinder engine crankshaft to determine the maximum probability of crack formation and to find a possible solution.

5. Results and discussion

The crankshaft is critical, important, essential, component of cars and must work smoothly. Otherwise, the pistons will not run and the vehicle will not move. For this reason, the crankshaft is located in the engine, with the cylinder head; the camshaft and the pistons are among the most critical parts. The aim of the study is to model the metal crankshaft and fatigue analysis. The behaviour of the crankshaft under static and variable loads is modelled using the ANSYS 19.0 software. A comparative study was conducted to estimate the structural behaviour of the mechanical crankshaft by the three-dimensional finite element evaluation and to estimate the critical regions. Stress and fatigue life of the crankshaft was found to be better than the crankshaft made of cast iron material. ANSYS stress values were compared with theoretical stress and unit deformation values obtained by numerical

calculations. The characterization of boundary conditions provides a direct relationship with the mesh type. So the engine crankshaft was carefully defined parallel to the real working circumstances. In order to establish the boundary condition, the reason for some simplified assumptions was investigated: The torque acting on the crankshaft was neglected. In this analysis only the bending moment is taken into consideration. The engine crankshaft is often affected by the torsional moment and causes stress and stress stresses. Mass power is added to modelling to automatically determine the value of the mass depending on the density of the crankshaft material. Therefore, the mass weight limit situation is omitted. According to the value acquired by the analysis, it can be concluded that the crank pin of the crankshaft in research was a high voltage danger zone. The crankshaft of the engine was maintained on both the flywheel mounting flash and the crank edge. Crankshaft movement as shown in Figure 8, the effect of the combustion force change and the impact on the crankshaft is shown.

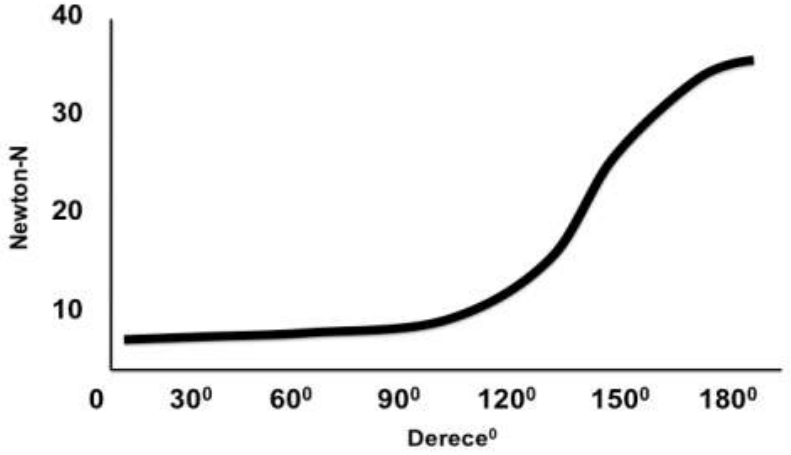

Figure 8: Combustion force change and its effect on crankshaft

In the analysis, under 70 bar pressure, the results show that the crankshaft maximum tension is 94.61 MPa and occurs at the crank pin edge. Maximum shear stress was 60.28 MPa. Maximum stress analysis is performed.

From this study, the working force of the crankshaft is due to the interaction between the main force on the crankshaft and the piston as a result of the air combustion mixture of the fuel. A connecting rod on the crank pin and the piston connected to the crankshaft have moved. The torsional load acts on the crankshaft via the direct connection path and the high rotational movement of the crankshaft acts. This has been studied in the

crankshaft gasoline engine analyzed in the study. Completing a cycle requires a four-stroke stroke for a four-stroke spark ignition engine [9]. After the engine piston was started, the engine produced four different value pressures acting on the crankshaft. The maximum or maximum pressure produced by the power stroke was 60 bar, while the induction stroke was 0.14 bar, the stroke 14 bar and the exhaust stroke produced a pressure of 6 bar.

6. Conclusions

The dynamic system of the crankshaft is very difficult to model. The main problem is that the model is accurate and the metal has high fatigue resistance to torsion. The proposed model takes into account both geometry and load corresponding to the actual drive systems of the crankshaft.

The maximum distortion develops at the centre of neck surface of the crankshaft. The crankshaft design according to the results concluded was safe as von-Misses stresses within the limits. Maximum deformation between the crank cheeks and main bearing journal of crankshaft was detected during analysis.

In this study, a crankshaft model was constructed using SOLIDWORKS and then analysed using ANSYS. Maximum stress occurred on the surface between the crankshaft and the crank cheeks at the crankshaft centre. High stresses occurred at the edge of the crankshaft.

Experimental stress-fatigue and finite element analysis results showed a close fit within 3% difference. These results show that the crankshaft bearing is not symmetrical bending stresses, while the analytical approach calculates that the distortion, buckling and bending stresses will be symmetrical at this time. Due to the comparatively crankshaft multifaceted geometry, SEA modeling was required to compute the geometry deformation outcome.

When the results of experimental fatigue examination and ANSYS simulation studies were compared, it was observed that parallel results were obtained. Finite element analysis is the best method for analysis of permissible stresses.

8. Acknowledgements

The Istanbul University-Cerrahpaşa BAP-scientific research unit supported this research with the project number 481520.

References

1. Z. Yu, X. Xu, "Failure analysis of a diesel engine crankshaft" Engineering Failure Analysis 12 (2005) 487–495, doi:10.1016/j.engfailanal.2004.10.001
2. P. Arcos, P. M. Fontea, V. Infanteb, M. Freitas, L. Reis, "Failure mode analysis of two diesel engine crankshafts" Procedia Structural Integrity 1 (2016) pp:313-318 doi: 10.1016/j.prostr.2016.02.042
3. P.Thejasree, G.Dileep Kumar, S. Leela Prasanna Lakshmi "Modelling and Analysis of Crankshaft for passenger car using ANSYS" Materials Today: Proceedings 4 (2017) 11292–11299
4. M. Fonte, P. Duarte, V. Anes, M. Freitas, L. Reis "On the assessment of fatigue life of marine diesel engine crankshafts" Engineering Failure Analysis 56 (2015) 51–57 doi:10.1016/j.engfailanal.2015.04.014
5. F. Summer, F. Grün, "Tribological study of crankshaft bearing systems: Comparison of forged steel and cast iron counterparts under start–stop operation" Wear 338-339 (2015) 232–241 doi: 10.1016/j.wear.2015.06.022
6. J.A. Villanueva, F. Espadafor, "A methodology for cracks identification in large crankshafts" Mechanical Systems and Signal Processing 25 (2011) 3168–3185 doi:10.1016/j.ymssp.2011.02.018
7. B. Kareem "Evaluation of failures in mechanical crankshafts of automobile based on expert opinion" Case Studies in Engineering Failure Analysis 3 (2015) 25–33 doi: 10.1016/j.csefa.2014.11.001
8. L. Witeka, M. Sikorab, F. Stachowicza, T. Trzepiecinskia "Stress and failure analysis of the crankshaft of diesel engine" Engineering Failure Analysis 82 (2017) 703–712 doi:10.1016/j.engfailanal.2017.06.001
9. A. Albers, N. Leon-Rovira, H. Aguayo, T. Maier "Development of an engine crankshaft in a framework of computer-aided innovation" Computers in Industry 60 (2009) 604–612 doi:10.1016/j.compind.2009.05.017
10. R. Metkara, V. Sunnapwarb, S. Hiwasec, V. S. Ankid, M. Dumpa "Evaluation of FEM based fracture mechanics technique to estimate life of an automotive forged steel crankshaft of a single cylinder diesel engine" Procedia Engineering 51 (2013) 567 – 57 doi:10.1016/j.proeng.2013.01.080
11. B. Bellakhdhar, A. Dogui, J.-L. Ligier, "A simplified coupled crankshaft–engine block model" C. R. Mecanique 341 (2013) 743–754 doi: 10.1016/j.crme.2013.09.008

CAN HUMAN BEINGS PRODUCE EVERYTHING? THE LIMITS OF THE 3D PRINTERS

Abdurrahman AYDIN [1] , Fatih KAHRAMAN [2] , Vjekoslav IVKOVIC [3]

[1] Dokuz Eylül University, Faculty of Engineering, Department of Mechanical Engineering, Izmir, Turkey.
[2] Dokuz Eylül University, Faculty of Engineering, Department of Mechanical Engineering, Izmir, Turkey.
[3] The University of Salford, School of Computing, Science and Engineering, Department of Mechanical Engineering, Manchester, United Kingdom.

1. INTRODUCTION

The effects of developing technology and the industrial 4.0 are seen in all of the areas, from education to industry. One of the modern methods of manufacturing with a significant growth in big array of applications is three-dimensional printing. 3D printing can also be reffered to as additive manufacturing (AM), rapid prototyping (RP), solid free form fabrication or layered manufacturing [1]. Examples of areas where 3D printers are used include, industrial manufacturing, medicine and health sector, aerospace, architecture and construction, military applications, textiles, food, education, and the list keep on growing [2].

The three-dimensional printer is a machine that produces solid objects based of a three-dimensional CAD (Computer Aided Design) file prepared using design software. These machines can be compared to traditional CNC (Computer Numeric Control) machines as they have similar principle of tool trajectory movement throughout the workspace. With the 3D printers, the models designed in digital environment can be produced and tested in a short amount of time compared to traditional manufacturing methods [3].

Additive manufacturing is the production method in which the physical mass is formed in layers using metal or polymer materials with its geometrical shape designed in CAD software. 3D printing technologies are one of the most common areas where additive manufacturing is applied [4]. The strength of the printed parts changes, depending on the thermoplastic material and the selected printing parameters used in 3D printers [4]. Spoerk et al. stated that the optimum layer design is one of the basic parameters affecting the strength of the printed part. They also stated that, with the increase in cohesion, the mechanical properties of the printed part increased significantly [5].

3D printer technologies allow detection of possible problems before manufacturing and accelerate solution to problems that may occur in the development process of a new product. Prototypes should be prepared and tested before the serial production phase of all designs drawn in digital environment. The traditional prototyping process involves both costly and time-consuming activities. The desired prototypes can be produced in shorter periods using 3D printers [6].

2. 3D PRINTING PROCESS

The 3D printing process begins with a 3D model of the object, usually designed by CAD software or a scan of an existing artifact. Special software slices this 3D model into cross-sectional layers, creating a digital file that is sent to the 3D printer. The 3D printer produces the object by forming each layer via the selective placement (or forming) of material [7]. The generalized steps of AM technologies are shown in Figure 1.

Figure 1. Generalized steps of 3D printing process [7]

The advantages of three-dimensional printers are as follows [8]:

- The design can be easily transferred or shared
- Changes and corrections can be made quickly
- Personalized products can be produced easily
- 3D printers are efficient in terms of investment and production
- Relatively low initial investment cost
- Product price can be calculated before production
- Recyclable materials can be used
- Minimum waste from material

2.1. STEREOLITHOGRAPHY – SLA

Model created in CAD designing software is divided into thin layers that will be applied on top of each other. Each of the layers is hardened by application of ultraviolet laser aimed at the desired points. The photopolymer solidifies under UV light. After each layer is cured, according to the shape of the CAD part and thickness set by the energy of the ultraviolet laser, the platform with cured layer is lowered into the resin. This way it gives room to a new liquid layer that yet must be solidified [9]. The SLA processing principle is shown in Figure 2.

Modernized version of Stereolithographic printing is called Micro stereolithography (MSL) and is used for extremely thin layers of thickness less than 10μm. Dynamic pattern mask for this process is created using liquid crystal display (LCD) screen or digital micro mirror device (DMD) chip and a light source through or across the mask into the photopolymerizable resin solidifying it to desired shape. This process is used for production of nano/microscale composite scaffolds which found application in a field of cartilage regeneration [10].

2.2. DIGITAL LIGHT PROCESSING – DLP

Digital Light Processing is a novel method used for production of microproducts of high resolution. The process can use conventional projector that can be used as a source of digital picture sent through a digital micromirror (DMD) projecting millions of optical patterns of UV light onto transparent resin. This way entire layer of resin can be cured at once, significantly reducing production time [11]. The DLP principle is shown in Figure 3.

2.3. FUSED DEPOSITION MODELING – FDM

In FDM technique, the thermoplastic material is extruded from a nozzle which is heated to a temperature above the melting temperature of the plastic. During extrusion, the head of the 3D printer moves along the x-y plane. Plastic material flowing through the nozzle is laid in a sequence of layers of desired thickness. After each completed layer, the printing platform descends down the z axis by the desired layer thickness. This process continues until the part is completed [12]. The working principle of a 3D printer using FDM technology is shown in Figure 4.

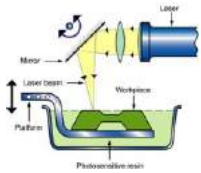

Figure 2. SLA [9]

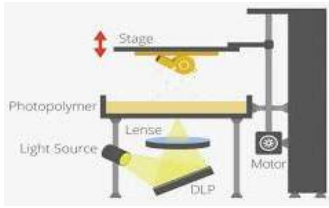

Figure 3. DLP [11]

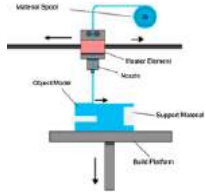

Figure 4. FDM [9]

2.4. SELECTIVE LASER SINTERING – SLS

Selective Laser sintering is additive manufacturing process introduced soon after Stereolithographic process. It works on a principle of laying the thin powder layer on the printing table where high – power CO2 laser beam is focused on creating a solid 2D pattern of previously CAD designed part. Tiny particles of plastic, ceramic or glass are fused together by heat from a high-power laser to form a solid, three-dimensional object [9,10]. Quality of each of the layers and in the end the finished part depends on the laser beam energy, bed temperature, and layer thickness. Sintering has a big advantage over other methods because almost any material in powder form can be processed. Materials commonly used in sintering process are polymers, metals, ceramics, but it is not limited to them. Composite materials such as glass reinforced polymers, metal/polymer composites and metal/metal composites can be used [1]. Also, the density of the products produced in this

manner is extremely high which makes them stronger and less susceptible to fractures due to imperfections inside the structure of material. Downside is price of powder materials because of their production process and also storing of powder materials, which can be potentially dangerous. Once produced, parts are left inside the powder to cool down to room temperature [9,10]. The working principle of a 3D printer using SLS technology is shown in Figure 5.

2.5. LAMINATED OBJECT MANUFACTURING – LOM

Laminated Object Manufacturing (LOM) is a very fast and inexpensive way to 3D print objects in several kinds of materials. Sheets are bonded together and cut in the right geometry according to the 3D model. LOM is mainly used for prototyping, not for production shown in Figure 6 schematically [13,14].

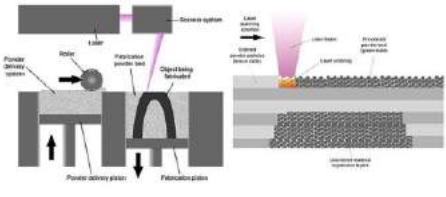

Figure 5. SLS [15]

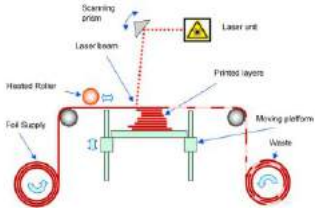

Figure 6. LOM [9]

3. MATERIALS USED IN 3D PRINTERS

Depending on the purpose, branch of industry and requirements of the user, types of materials used for additive manufacturing can change. In general, they can be divided into biomaterials, metals and their alloys, bio-ceramics and bioactive glasses, polymers and hydrogels. With advancement of technology the list of materials keeps on growing. In this research only some of the materials are covered.

ABS (Acrylonitrile Butadiene Styrene) and PLA (Polylactic Acid) materials are widely used in three-dimensional printers. ABS plastic is a rigid and hard thermoplastic polymer. ABS is a type of material that is frequently preferred in 3D printers due to its high strength and impact resistance [6,16]. PLA is the most widely used three-dimensional printer material according to the current statistics. Easy to work because of its low melting temperature is the main reason of choosing this material [17].

Materials used in medicine are usually Titanium and its alloys due to their physical, chemical and biological properties. They are usually corrosion resistant, have high specific strength and are biocompatible. Downside of them is that they have near-inert properties which makes their use limited to

certain areas. Products made of Titanium may be dental implants, pacemaker cans, ribs, heart valves and many more [1, 10].

Figure 7. Titanium Jaw Implant [18]

Figure 8. Titanium ribs used by a cancer patient [19]

Hydroxyapatite (HA) is a glass-ceramic composite. When 3D printed it manages to obtain Young's modulus between 7 and 30 [GPa] and a 3-point bending strength in the range between 50 and 150 [MPa]. It has significantly higher strength than it would have when produced using traditional manufacturing methods. Sintering of the same material could obtain porosity of just over 50 %, but when 3D printed it can obtain porosity of just 2.5 %. This high density makes it eligible for use as bone implant material [20].

Poly(3-Hydroxybutyrate) is a natural thermoplastic polyester produced by microorganisms under imbalanced growth conditions. It has similar properties of conventional thermoplastics. Its use is mostly in area of biomedical areas for production of scaffolds for tissue engineering [21].

Figure 9. Skeletal reconstructive surgery [22]

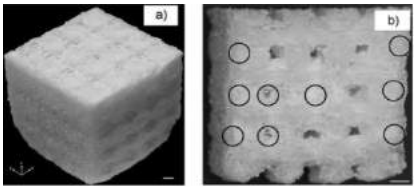

Figure 10. 3D printed PHB model of porous cube a) isometric view b) internal view [21]

4. AREAS OF APPLICATION

With scientists, engineers, artists and in general researchers with a background from different areas of life, new ideas of application of 3D printing are rapidly emerging. To start with, three dimensional printing of biological devices is based on biomimicry, biologically inspired engineering approach to creating identical duplicates of the native tissue or organ, independent self-assembly, using embryonic organ development as a process

guide, and miniature-tissue building blocks, structural and functional components of a tissue that can later on be assembled into a larger tissue constructed by self-assembly or regulated design [10]. Simplified models of in vitro liver and kidney have been successfully produced using bioprinting [23].

Using traditional methods, it is extremely expensive to create molds just to make one part, but using 3D printing each part can be different. As an example, orthopedic grafts can be created without the waste of material, money and designed specifically for the user.

Three dimensional printed parts can also serve as surgical templates. Using this technology, surgeon can perform surgery without guessing and encountering surprises throughout the surgery. Exact drilling pathway, angles and locations of nerves can be predicted. Of course, there are certain limitations due to CT scans which are used to build the 3D CAD model, but with development of technology, the accuracy has been increasing constantly.

Bioprinting has potential to recapitulate the disease models and become a reliable tool for drug screening and understanding fundamental models of mechanisms contributing to disease [10].

It is possible to enable fabrication of various structural aspects of tumor microenvironment using 3D printing. Up to date, blood vessels, of different diameters, used for studying of cancer cell migration have successfully been created [23].

According to D. Choudhury and S. Anand et al., integration of bioreactor and bioprinter would be a key for natural maturation of printed tissue constructs [23].

New digital models can be successfully produced with CAD programs via computer tomography data/image. Computer tomography scan images can be used to assist surgical operations. In a study conducted by Çelebi et al., they printed the damaged skull structure obtained from the computer tomography image with the use of a 3D printer. Then, they performed the implant design in accordance with the defective region. The implant produced from the Ti6Al4V material is attached to the damaged skull bone [24]. Skull implant production is shown in Figure 11.

The ankle foot orthosis (AFO), which are extremely important for human walking, are produced to prevent deformations and control the movement of the ankle. An AFO is often used to protect a weak leg, keep the wrist and foot in the correct position, and better the stepping. Since the end user may have different sizes of wrists and different types of deformations, an AFO should be produced in full compliance with the end user's foot. Therefore, serially produced AFOs may not be suitable for each end user. Considering this situation, 3D printers stand out in the production of personalized biomedical equipment. Considering this situation, three-dimensional printers become prominent in the production of personalized biomedical equipment. In a study by Aydın et al., example was modeled using a special AFO with CAD

software. Later, example was produced with the 3D printer that was built by the researchers who developed the model [25]. The ankle foot orthosis production is shown in Figure 12.

Figure 11. Skull implant production [24]

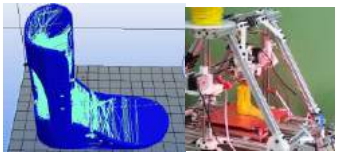

Figure 12. The ankle foot orthosis production [25]

Another area of use of 3D printers, is casts accommodating fractured limbs. In the past, casts were made from plaster and they had many limitations to them. Once placed on the broken limb they cannot be removed unless destroyed. Plaster casts limit the user in everyday activities and especially hygiene because they cannot get wet. They can cause discomfort and even infection or rash underneath it. 3D printed casts are easy to put on, easy to use, waterproof, adjustable for swelling and made from high temperature thermoplastic. The design is done individually for each patient by use of 3D mapping and design softwares. The only downside is the time patient has to wait for it to be printed [26,27].

Figure 13. Fractured hand 3D printed casting [26]

Figure 14. 3D printed upper limb casts of different sizes and shapes [27]

3D printing also found its use in prosthetic limb production. World's first medically certified 3D-printed bionic arm has been 3D printed. Commercially available for below-elbow upper limb difference people from the early age of 8 years old. This bionic arm is controlled using biomimetic sensors, by contraction and relaxation of muscles the digits are moved accordingly. It

completely changed life of people in need of prosthetics because of its low price compared to similar prosthetics created using traditional methods [28].

Food industry has also experienced breakthrough of 3D printing. Intriguing shapes for molds that would be extremely hard maybe even impossible to create using traditional methods are now created without spending extremely high amount of money. New shapes are limited only by the imagination of the artist behind the idea [29].

Figure 15. Bionic 3D printed arm [28]

Figure 16. 3D printed model and silicone mold created according to it [29]

Architects and urban planners can analyze the land wit using 3D printouts. This is a fast solution when they need topographic models. 3D printing process is an application that will be very useful in prototyping works, architectural modeling presentations and architectural modeling studies [30]. It is also shown in Figure 5 to use the topographic data for printing of minimized city scenes.

Figure 17. Use of 3D technology in land modeling [30]

5. THE FUTURE OF 3D PRINTERS

Future shaped by 3D printing technologies seems to become more likely. Rapid advancement of 3D printing technologies opens doors to a world of products and ideas that were previously hard to imagine and impossible to produce. People involved in different aspects of industry are trying to implement 3D printing technologies on existing products, taking them one step further.

Additive manufacturing is also used to explore new combinations of materials and their behaviors related to their surroundings. 4D printing is new term that is used for 3D printed objects that change their shape and structure when exposed to different factors such as heat, magnetic forces, water or other sources of energy [31].

Scientists from "Foundation for Research and Development of Science" presented their idea of creating bionic pancreas. According to Michał Wszoła, head of project, pancreas would have to be created from pancreatic tissue or cells that produce insulin allowing people with diabetes to have a functional pancreas [32].

Startup from San Francisco states that 3D printing and nanotechnology combined are going to have an enormous impact on destruction of cancer cells, nerve regeneration and drug delivery. Nanoparticles inserted into the aimed areas of the body would be created from special bio ink responsive to special wavelength or laser. Particle would act as nano surgical tool [34].

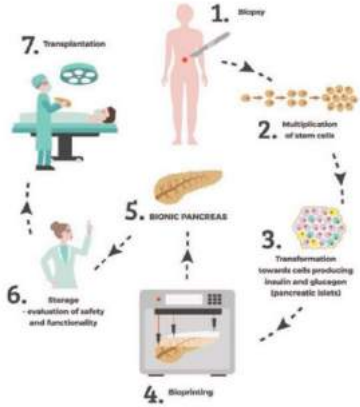

Figure 18. Bionic pancreas transplantation process [32]

Figure 19. 3D printed robot [33]

University of Arizona scientists are working on development of 3D printed bone that would contain adult stem cells. This way in case of a fractured bone, either as an sports injury or especially in explosion injuries where bone is shattered, process of healing would be quicker. Even in the situations where usually limb would have to be amputated, this process would make it a possibility for a bone to heal [35].

Atlas, robot fully capable to run, jump and avoid obstacles with precision uses 3D printing technologies to make it lighter and increase its agility. Further development of robots using additive manufacturing will improve their specifications and areas of use. Boston Dynamics, company producing this robot have stated that use of 3D printing has helped them to get rid of excess material. It is expected that in couple of years robots will be used as home or company assistants [33].

From the examples used above it can be concluded that additive manufacturing will lead a significant role in future of technology, world and people. With new technologies, needs are satisfied and new solutions to problems open.

6. RESULTS

In this study, existing systems, patents and literature research about 3D printers has been obtained. At the same time with the developing technology in material science and 3D printers, it was concluded that simple products that we use in daily life in the near future can be produced in homes.

It is obvious that the use of 3D printers will accelerate the new product development process, as it provides an opportunity to produce prototype for the inventors, engineers and industrial designers in a significantly less time and with less resources.

Architects and city planners can use the 3D printers to print the architectural presentation, architectural modeling and topographic modeling work will be very useful.

With the increase in the widespread use of 3D printing technology, the interaction between the educator and the student will increase and the students' ideas and concepts will be transformed into tangible objects and the creativity and innovative thinking ability will be developed.

In order to prevent the use of 3D printers in the production of negative and harmful products, it is necessary to make the legal arrangements and production should be kept under control.

It can be offered as a suggestion for the works that can be done about this technology by making faster and high-quality printing, producing strong parts, narrowing the production tolerances and making the design optimization.

REFERENCES

1. U. K. Roopavath, D. M. Kalaskar. ”Introduction to 3D printing in medicine”. 3D printing in medicine, 2017.
2. S. Kökhan, U. Özcan, "3D Yazıcıların Eğitimde Kullanımı", Bilim Eğitim Sanat ve Teknoloji Dergisi 2, 2018.
3. B. Güler, K. Çetinkaya, "Endüstriyel Boyutlu Çift Başlı Kartezyen Tipi Üç Boyutlu Yazıcı Tasarımı ve Prototip Üretimi", International Journal of 3D Printing Technologies and Digital Industry 2, 2018.
4. Ö. Öz, M. Aydın, A. Kara, M. Sancak, "Üç Boyutlu Yazıcılarda Kullanılan Doluluk Oraninin Hasar Yüküne Olan Etkisinin Belirlenmesi", International Journal of 3D Printing Technologies and Digital Industry 2, 2018.
5. M. Spoerk, F. Arbeiter, H. Cajner, J. Sapkota, C. Holzer, “Parametric optimization of intra- and inter-layer strengths in parts produced by extrusion-based additive manufacturing of poly(lactic acid)”, Journal of Applied Polymer Science, 134(41):1-15, 2017.
6. D. Çelik, K. Çetinkaya, "Üç Boyutlu Yazıcı Tasarımları, Prototipleri ve Ürün Yazdırma Karşılaştırmaları", İleri Teknoloji Bilimleri Dergisi 5, 2016.
7. T. Campbell, C. Williams, O. Ivanova, B. Garrett. Could 3D Printing Change the World? Atlantic Council, Strategic Foresight Report, 2011.
8. K. Şahin, B. Turan, “Üç Boyutlu Yazıcı Teknolojilerinin Karşılaştırmalı Analizi”, Stratejik ve Sosyal Araştırmalar Dergisi, 2 (2), 97-116, DOI: 10.30692/sisad.441648, 2018.
9. J. R. C. Dizon, A.H. Espera, O. Chen, “Advincula RC. Mechanical characterization of 3D-printed polymers”, Additive Manufacturing, 20:44–67, 2018.
10. P. Elena, M. Deepak, “3D printing families: laser, powder, nozzle based techniques”, 3D printing in medicine (pp. 25 – 28), ISBN 987-0-08-100717-4, 2017.
11. Magimages 2016. Digital Light Processing Printing. http://www.magimages.org/digital-light-processing-3d-printing/ (Accessed Date: 10.02.2019).
12. Y. Gür, “3 Boyutlu Masa Üstü Yazıcı ile Matematiksel Bir Modelden Gerçek Bir Nesnenin Dijital Üretimi”, Balıkesir Üniversitesi Fen Bilimleri Enstitüsü Dergisi, 19 (2), 237-245, 2017.
13. G. Suresh, K. L. Narayana, M. K. Mallik, “A Review on Development of Medical Implants by
14. Rapid Prototyping Technology”, International Journal of Pure and Applied Mathematics, Volume 117 No. 21 2017, 257-276.
15. J. B. B. Vaupotic, M. Brezocnik, “Use of PolyJet technology in manufacture of new product”,J. Achiev. Mater. And Manufacturing Eng., 18 (1–2), 319–322, 2006.
16. Live Science 2013. What is Selective Laser Sintering? https://www.livescience.com/38862-selective-laser-sintering.html (Accessed Date: 08.04.2019).
17. B. N. Turner, R. Strong, S. A. Gold, “A review of melt extrusion additive manufacturing processes: I. Process design and modeling”, *Rapid Prototyping Journal*, 192- 204, 2014.
18. M. Chhabra, R, Singh, “Rapid casting solutions: a review”, Rapid Prototyping Journal, 328 -350, 2011.
19. All3dp 2017. CADSkills Develops 3D Printed Titanium Jaw Implant to Reduce Surgical Time. https://all3dp.com/cadskills-develops-amsji-3d-printed-titanium-jaw-implants-to-save-time/ (Accessed Date: 11.02.2019).
20. Forbes 2015. How Surgeons Implanted 3D-Printed Titanium Ribs In A Cancer Patient. https://www.forbes.com/sites/amitchowdhry/2015/09/19/how-

surgeons-implanted-3d-printed-titanium-ribs-in-a-cancer-patient/#29f3ac162a9b (Accessed Date: 11.02.2019).
21. R. Gmeiner, U. Deisinger, J. Schönherr, B. Lechner, R. Detsch, A. Boccaccini, J. Stampfl, "Additive Manufacturing of Bioactive Glasses and Silicate Bioceramics", Journal of Ceramic Science and Technology, 6, 75-86, 10.4416/JCST2015-00001, 2015.
22. F. Pereira, M. Oliveira, I. A. Maia, Izaque, J. Silva, M. Costa, R. Thiré,"3D Printing of Poly(3-hydroxybutyrate) Porous Structures Using Selective Laser Sintering", Macromolecular Symposia, 319, 10.1002/masy.201100237, 2012.
23. Cellular3D 2015. Xilloc Introduces 3D Printed "Real" Bone Implant Solutions. https://www.cellular3d.com/index.php/medical-bioprinting/46-xilloc-introduces-3d-printed-real-bone-implants (Accessed Date: 15.03.2019).
24. D. Choudhury, S. Anand, N. M. Win, "The Arrival of Commercial Bioprinters - Towards 3D Bioprinting Revolution", International Journal of Bioprinting, 2018.
25. A. Çelebi, H. Tosun, A. Önçağ, "Hasarlı Bir Kafatasının Üç Boyutlu Yazıcı İle İmalatı ve İmplant Tasarımı", International Journal of 3D Printing Technologies and Digital Industry , ,2017
26. L. Aydın, S. Küçük, "Üç Boyutlu Yazıcı ve Tarayıcı ile Hastaya Özel Medikal Ortez Tasarımı ve Geliştirilmesi", Politeknik Dergisi, 2017.
27. Calvertjournal 2019. These delicate 3D-printed casts from Latvia could be the future of personalised healthcare. https://www.calvertjournal.com/articles/show/11070/latvia-startup-castprint-stop-plaster-casts-3D-printed-waterproof (Accessed Date: 13.04.2019).
28. All3dp 2019. 3D Printed Cast – The Most Promising Projects in 2019. https://all3dp.com/2/3d-printed-cast-the-most-promising-projects (Accessed Date: 13.04.2019).
29. Havaslynx 2017. Open Bionics – The prosthetic pioneers making science fiction a reality. https://www.havaslynx.com/open-bionics-the-prosthetic-pioneers-making-science-fiction-a-reality (Accessed Date: 13.04.2019).
30. Dinara Kasko. Silicone Molds. http://www.dinarakasko.com (Accessed Date: 10.04.2019).
31. A. Aydın, F. Kahraman, "3B Baskı Teknolojisi Kullanılarak Hızlı Prototipleme Yapımı ve Nesnelerin Üretimi", 6th International Symposium on Innovative Technologies in Engineering and science, 2018.
32. 3D Natives 2019. 4D printing reconfigurable materials for use in aerospace, medical and robotics fields. https://www.3dnatives.com/en/4d-printing-materials-030420195 (Accessed Date: 13.04.2019).
33. 3D Natives 2019. 3D Bioprinted Bionic Pancreas to Fight Diabetes https://www.3dnatives.com/en/bionic-pancreas-080420194 (Accessed Date: 13.04.2019).
34. 3D Natives 2019. Atlas, the 3D printed robot that strolls through the park. https://www.3dnatives.com/en/atlas-3d-printed-robot310520184 (Accessed Date: 13.04.2019).
35. 3D Natives 2019. 3D Printing Nanostructures Could Fight Cancer. https://www.3dnatives.com/en/3d-printing-nanostructures-aether-300120195 (Accessed Date: 13.04.2019).
36. 3D Natives 2019. 3D printing bone, a way to treat fractures? https://www.3dnatives.com/en/3d-printing-bone-treat-fractures-170120195 (Accessed Date: 13.04.2019).

INVESTIGATING THE EFFECT OF SUCCESSIVE LAUNDERINGS ON THE STRENGTH OF SOCKS PRODUCED BY DIFFERENT FIBERS

Züleyha DEĞİRMENCİ [1] , Mehmet TOPALBEKİROĞLU [2]

[1] Gaziantep Üniversitesi, Mühendislik Fakültesi, Tekstil Mühendisliği Bölümü, Gaziantep, Türkiye.
[2] Gaziantep Üniversitesi, Mühendislik Fakültesi, Tekstil Mühendisliği Bölümü, Gaziantep, Türkiye.

1.Introduction

Socks have an important place among the textile products which are indispensable for our daily lives. The socks obtained by the knitting method should provide the user with psychological and physiological comfort during use. While socks selected for winter are expected to keep the user warm, socks that do not sweat and smell in summer are preferred. Athletes' socks must have high water vapor and air permeability. It is important to produce anti-bacterial for military because they will remain in the airless environment for a long time. In addition, medical and/or diabetic socks and varicose hosieries are of vital importance to users. Silver-ion anti-bacterial socks produced in this area are also very popular. The mentioned properties of the socks vary according to the type of yarn production, raw material and applied finishing.

On the other hand, socks are classified as short socks, long socks and pantyhose. These socks can also be classified within themselves in different ways: nose-noseless; corset-without corsets etc. For consumers socks are varied in accordance with the yarn fineness, color, hairiness, patterns and of course fashion socks. Among them, while buying the consumer is the most attractive fashion, the performance of socks during use is also very important. They shoud be resistant to wear and pilling, dimensional stable, soft and, of course, durable. The product must have high performance during washing and using life. Since they are obtained by knitting for socks, they are expected to have high bursting strength.

Socks are subjected to washing in a domestic washing machine for their cleaning regardless of their production and raw materials. Since the washing process is a mechanical process, this process is also predicted to wear down the socks and reduce their useful life. Since they are used by consumers in a mostly closed shoe all day long, the washing process should be done frequently in order to remove bacteria from the surface and to remove the stains from the surface. For these reasons, it is thought that the socks will wear down and their strength will decrease. During the washing and drying processes, fiber migration can occur and the unit weight and thickness in the area can reduce. On the other hand, it is assumed that the washing process can increase the weight and thickness in the unit area by inflating the cross-sectional areas of the fibers and the shortening / shrinking in the area and length. For these reasons, changes in the strength of the washings should be explained in relation to the changes caused by the structural properties of the washing.

Some researches about the performance and thermal comfort properties of socks can be summarized as follows. Akaydın and Can examined the abrasion resistance and air permeability characteristics of cellulose based socks (modal, viscous, linen-modal, bamboo, cotton, tencel). They reported that fibers such as linen-modal and modal have very high abrasion resistance and air permeability values (Akaydın & Can, 2012). Ertekin and Marmaralı applied performance tests to cotton, acrylic and myabi fiber knitted fabrics.

The results show that miyabi fabric has higher air permeability, thermal resistance and relative water vapor permeability values compared to 100% cotton and 100% acrylic fabrics. The miyabi fabric provides better heat insulation and a warmer feel at the first touch with lower heat absorption value. Miyabi fabric is also resistant to abrasion. According to the authors' comments, miyabi fabric can be used in summer or high activity clothing with high thermal resistance, air permeability and relative water vapor permeability to provide better moisture management (Ertekin & Marmaralı, 2014). Cimilli et al. examined the thermal comfort properties of socks made of new generation yarns (modal, micro modal, bamboo, soybean and chitosan) as well as traditional yarns (cotton, viscose). They stated that they affected the comfort related properties of fabrics beside the fiber type, thickness and fabric characteristics. Chitosan, modal and viscose fabrics have performed relatively better than other fabrics considering all the properties examined (Cimilli et al, 2010). Demiroz Gun et al examined the structural and physical properties of cotton / bamboo, viscose / cotton and modal / cotton blended knitted fabrics. The results showed that the structural properties and air permeability were independent of the fiber type. The highest strength values were made of modal / cotton fiber knitted fabrics, while the least pilling was observed in bamboo / cotton fabrics (Demiroz Gun et al, 2008). Özdil investigated the thermal comfort properties of socks produced by wool, acrylic, cotton and PA. Author reportes that the thermal conductivity values of woolen socks are lower than acrylic socks. The thermal resistance values of wool acrylic socks are higher than 100% acrylic socks and have a warm feeling in the first contact. Socks with PA fibers have high thermal conductivity and thermal absorption (Ozdil, 2008). Iukas and Abramaviči investigated the air permeability properties of socks produced using the yarns of new fiber types such as soybeans, bamboo, cotton / Seacell and bamboo / linen. They reported that the air permeability values of natural fibers were the determining factor (Iukas & Abramaviči, 2010). Çelik et al produced 10 different knitted socks in 2 different numbers produced by different fibers (cotton, organic cotton, acrylic, bamboo and modal) and examined their air permeability values after repeated washing. The highest permeability values are obtained with modal fabrics before and after washing while the lowest air permeability belongs to organic cotton fabrics (Çelik et al, 2014). Değirmenci and Topalbekiroğlu investigated the dimensional behaviour of socks produced by different raw materials after successive launderings. They reported that increasing washing cycles the change in length and width increases (Değirmenci & Topalbekiroğlu, 2018).

The aim of this study is to examine the effects of the successive washing process on the strength loss of the socks. For this purpose, raw material selection during sample production was made according to the preferences of the users. Cotton is a natural fiber of cellulose origin. These fibers are frequently used in socks production because of their permeability, absorbency and softness. Although these fibers are thin, they are good in strength. Also; their strength increases even more when they get wet. This can be advantageous during washing (Eberle et al, 2014;Waite, 2009). Modal

is a regenerated cellulosic fiber obtained by the modified viscose process. It has good wet and dry strengths compared to other regenerated cellulosic fibers. This is because chemicals added to the coagulation bath during production cause prolongation of cellulose molecules. It is a more absorbent fiber than cotton. These fibers are also preferred because they are thin and soft (Eberle et al, 2014;Waite, 2009). Organic cotton is the kind of cotton which is produced without the use of pesticides and fertilizers during the production. Organic cotton is produced by completely natural methods according to conventional cotton and supports the conservation of nature and enables sustainable agriculture. There are no chemicals harmful to health on the products. On the other hand, the physical properties are the same as conventional cotton (Eberle et al, 2014;Waite, 2009). Bamboo is an anti-bacterial natural fiber with high moisture transmission. The rapid growth of the fiber during the production without the need for pesticide and other chemicals is also effective on the antibacterial behavior of the fiber. However, its production is more expensive than organic cotton. At the same time, products made from this fiber keep cool in the hot summer season. It is a soft, UV resistant, anti-static and biodegradable fiber. It is popular because of its features (Eberle et al, 2014;Waite, 2009). Acrylic is a synthetic fiber that is generally used in staple form. Due to its similarity to the wool, it is often used in place of wool or as a mixture with wool. It has a soft and voluminous structure that makes the user feel warm. This thermoplastic fiber is wrinkle resistant and machine washable (Eberle et al, 2014;Waite, 2009). Nylon/Polyamide is used for strength increase and flexibility in many sock we buy. Nylon fiber has very little absorbency, but its capillary cavities provide rapid transport of liquid water. The strength is very high. The wet strength of it is approximately 2 times the dry strength. And it is machine washable, quick-dried, wrinkle resistant and very flexible fiber (Eberle et al, 2014;Waite, 2009).

2.Material and method

In this study, socks were produced by using 10 different ring yarns in Ne 20/1 and Ne 30/1 numbers from organic cotton, cotton, modal, bamboo and acrylic fibers in a conventional mill. One part of the socks were washed in a domestic washing machine and dried on a flat surface. Three separate groups of sample socks were formed. The first group was not washed, the second group had five successive washings and the third group had fifteen successive washings. TS 5720 standard and 5A option were selected for washing. The samples were completed at a total load of 4 kg and washed at 30 ºC and 400 cycles were applied for the spin cycle. Drying was carried out on a flat surface. Thirty different sock samples were conditioned in accordance with the standards in laboratory conditions. The thickness, unit weight and bursting strength of all socks were then measured in accordance with international standards. The TRUBURST test device was used for the bursting strength test and the average test results were obtained after the diaphragm correction. The test results were analyzed by means of graphs.

The statistical significance of the results was tested by one-way variance analysis with Design Expert 11th Package program.

3.Results and discussions

In the study, carded ring yarns obtained from different raw materials with same numbers (Ne20 / 1 and Ne 30/1) were used and the twist alpha was kept constant at αe:3.5. Quality test results applied to yarns are given in Table 1.

Table 1. Quality test results of yarns of samples

		Strength RKM	Elongation %	Unevennes %	CVm %	Thin place -50 % /km	Thick place -50 % /km	Neps +200% /km
	Cotton	17,68	6,05	8,7	10,95	0	1,3	6,3
	Organic Cotton	13,93	7,13	11,61	14,68	0	72,5	115
	Bamboo	16,46	15,27	8,33	10,56	0	3,8	16,3
	Modal	26,16	11,36	7,92	10,04	0	8,8	20
NE 20/1	**Acrylic**	21,89	19,71	8,77	11,07	0	7,5	7,5
	Cotton	16,97	5,12	9,54	12,01	0	7,5	15
	Organic Cotton	16,88	5,84	13,27	16,91	46,3	345	312,5
	Bamboo	18,42	16,19	10,51	13,3	3,8	32,5	77,5
	Modal	23,09	10,69	9,98	12,69	2,5	71,3	343,8
NE 30/1	**Acrylic**	20,24	18,94	10,52	13,22	2,5	15	16,3

When the table is examined in detail, Modal yarn has the highest strength among the selected samples. The strength of organic cotton is the lowest. As the yarn becomes thinner, the resistance is reduced. Acrylic fibers are the most elongated fiber. This elongation value is 2 times that of cotton and 2 times of modal. The strength and elongation level of the bamboo yarn is proportional and moderate. As the yarn becomes thinner, the mass variation increases; and the number of thin-thick places and neps increased considerably. Compared to cotton and organic cotton, there is no significant difference between strength and elongation; this is caused by the short fiber content and the organic lumps formed during carding. Increased number of neps is also a serious quality problem for knitted fabrics since it will cause serious problems during the dyeing process.

The quality tests were completed with 10 types of yarn blended with 19% polyamide and 2% elastane. The purpose of this blending is to increase

the strength of cellulosic raw materials and to provide comfort to the consumer in terms of flexibility during use. The proportion of polyamide and elastane used during the production was kept constant in percentages, regardless of the yarn count. For this reason, the effects of these fibers will be ignored. The resulting yarns are knitted with a single jersey pattern, 3-inch diameter, 10-feed, 168-needle, single-bed, industrial type Sangiacomo branded circular knitting machine. The yarn loop length has been kept constant. The stitch density of the samples is given in Table 2.

Table 2. Stitch density (wpc*cpc) of the samples

	Ne 20/1 Samples				
Washing type	**Organic Cotton**	**Cotton**	**Acrylic**	**Modal**	**Bamboo**
Unwashed	102,2	99,3	98,6	104,5	107,7
5 Times Washed	107,6	107,5	108,5	111,8	114,4
15 Times Washed	107,6	107,5	108,5	111,8	92,7
	Ne 30/1 Samples				
Washing type	**Organic Cotton**	**Cotton**	**Acrylic**	**Modal**	**Bamboo**
Unwashed	103	109,5	101	98,1	114,4
5 Times Washed	115	102,9	109,8	115	114,3
15 Times Washed	115	102,9	109,8	115	114,3

When the table is examined, it is seen that the first cause tightening of the loops but after five washings there is no change in the stitch density because the fabric reaches balanced state. Thus, in the relationship analysis between structural properties and strength the stability of the fabric structure will be taken into account after the five washings.

As the thickness of the produced socks is thought to be related to strength, the thickness measurement results before and after washing are given in Figure 1and 2 respectively.

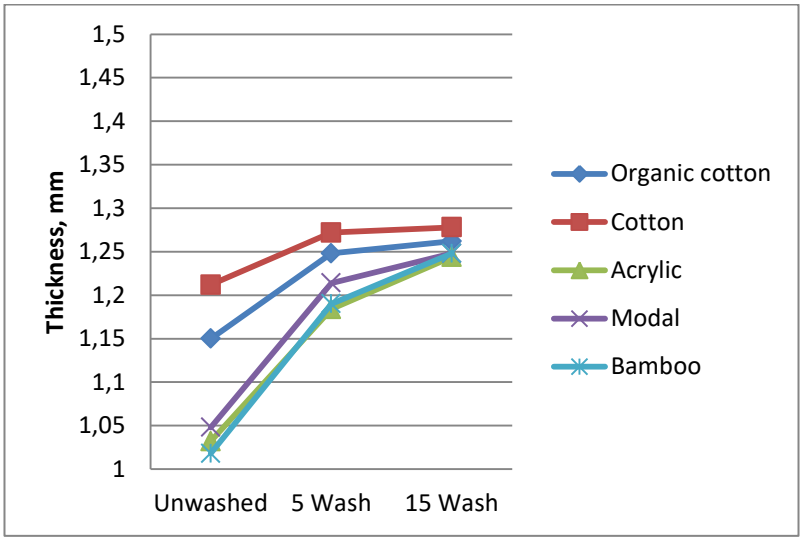

Figure 1. Thickness of samples produced by Ne 30/1 yarn

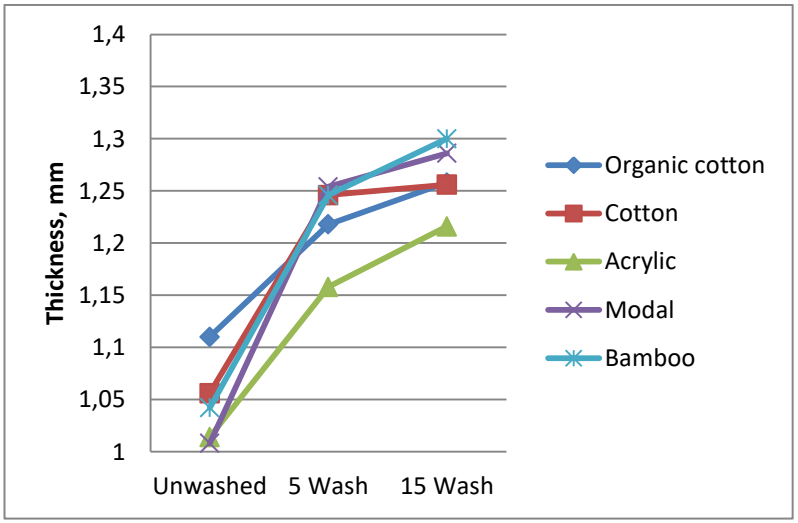

Figure 2. Thickness of samples produced by Ne 20/1 yarn

The thickness of the socks of Ne 20/1 and Ne 30/1 yarns increased in direct proportion to the washing. However, when the results are examined in detail, it is seen that the change in thickness of the first five was higher, and

even in cotton after 5 washings. When it is considered that all the fibers except acrylic are of cellulosic origin, it is understood that the water easily penetrates into the fiber due to the hydroxyl group of the fiber and changes the structure. Due to the nature of organic and normal cotton fibers, the lumen in its sections becomes smaller as they are treated with water and the fiber in the form of beans is rounded. After reaching this level, there is no more shrinkage due to the fact that there is no space for the fiber to swell and there is no thickness change after this level. For these samples, this level was also reached after 5 washes and no change was observed in the thickness of the socks after 5 washes. On the other hand, it was observed that socks made of fibers other than cotton were thinner at the beginning but were much thicker due to the effect of washing. In addition, Ne 30/1 yarns were thicker before washing, but after the washing, the socks obtained from Ne 20/1 yarns became thicker. This was caused by the attempt to knit the same stitch thread length of the two groups and the same density, but the samples were thicker as was the case after the fibers were released after washing.

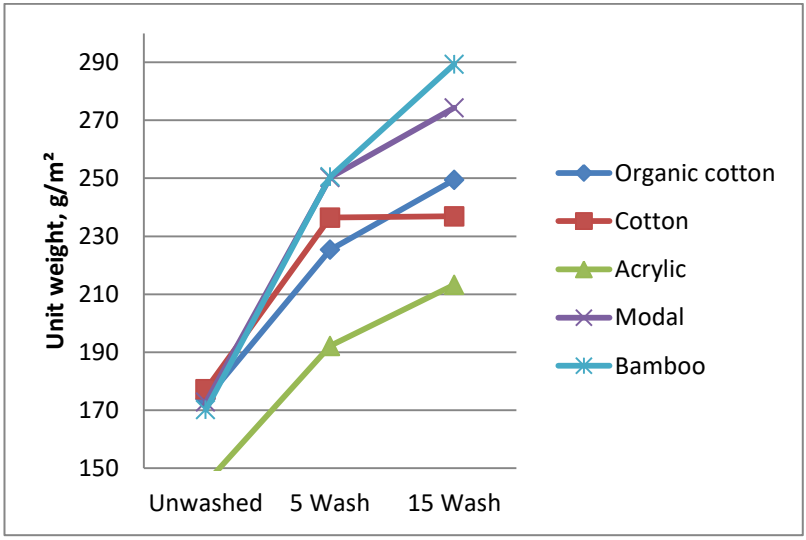

Figure 3. Unit weight of samples produced by Ne 30/1 yarn

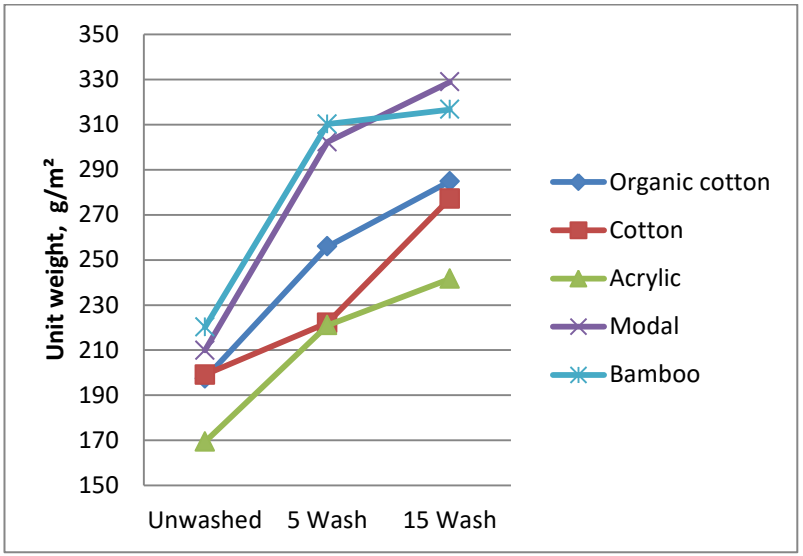

Figure 4. Unit weight of samples produced by Ne 20/1 yarn

Figure 3 and 4 show the changes in the weights of the samples after washing. All samples were become thick after washing. The highest increase was in modal and ba1mboo socks. Unit weights increased due to tightening of fabrics. Samples from Ne 20/1 yarns are heavier depending on the yarn count. However, depending on the number of washings, the weight differences increased. The weight increasing is proportional to number of washes. The changes in the strength of the knitted socks due to washing are shown in Figures 5 and 6.

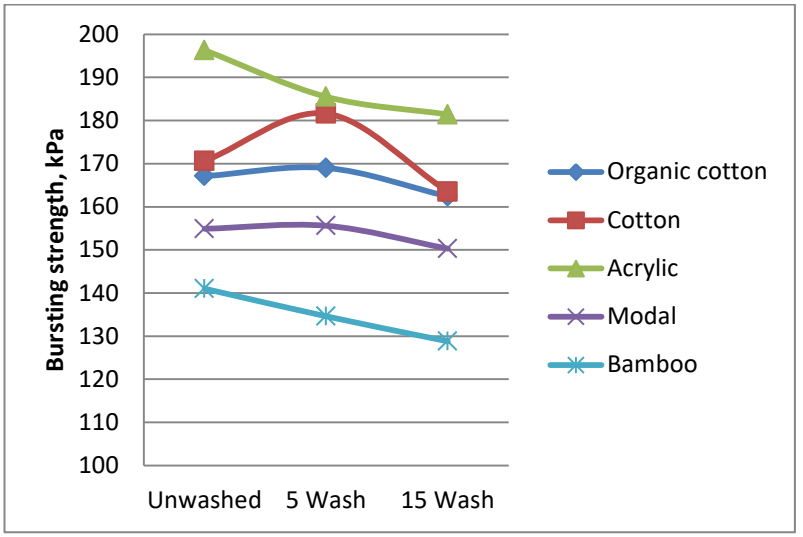

Figure 5. Bursting strength of samples produced by Ne 30/1 yarn

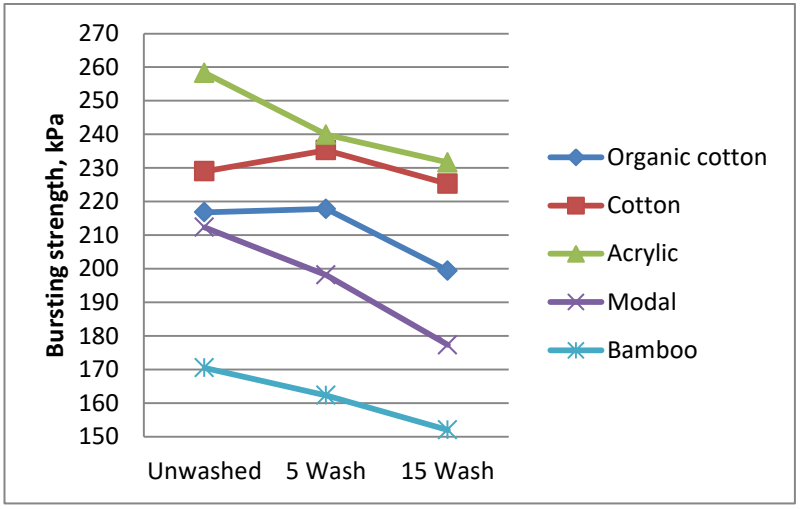

Figure 6. Bursting strength of samples produced by Ne 20/1 yarn

When the unwashed strengths of the socks made of 20/1 and Ne 30/1 yarns are examined, it is seen that the highest strength value is acrylic and the lowest strength is bamboo. According to the literature, the bursting strength is related to the yarn strength and elongation percentage. The

pressure of the knitted fabrics during the strength test causes a certain area of the fabric to swell and break the loop from the weakest point. This results points that the knitted fabrics obtained from flexible and durable yarns will be more resistant. Strength order of the samples independent from the yarn count is as Modal> Acrylic> Cotton> Bamboo> Organic Cotton and that of elongation percentage order is as Acrylic> Bamboo> Modal> Organic Cotton> Cotton. However, when we look at the strength of the fabrics, it is in the form of Acrylic> Cotton> Organic Cotton> Modal> Bamboo. In this case, it may not always be correct to comment on the strength by looking at the yarn strength or elongation alone for knitted fabrics. Furthermore, the fact that the polyamide and elastomeric yarns, which were ignored but added during the production of the samples, were highly flexible and durable, led to different results for each raw material used as a blended. According to the mentioned graphs, it can be said that washing of knitted socks leads to a decrease in strength. Only the first 5 washings in normal and organic cotton samples caused an increase, then a decrease occurred. The weights and thickness of the samples increased depending on the number of washings. There have been no significant changes in the length and density of yarn stitches. This shows that there is an increase in the number of fibers in the unit area and that the fabric is tightened. Flexibility decreases as the fabric tightens. This may explain the reduction in strength. As a result, the washing reduces the resistance of the socks.

3.1 Statistical analysis

In this study Design Expert 11 statistical package program was used. The dependent one-way ANOVA test was used as the analysis method. In analysis design, full factorial and 2FI model was selected. The raw materials, yarn number and number of washes were chosen as independent variables. As a result, the effects of independent variables on the thickness, unit weight and bursting strength chosen as dependent variables were investigated. As a result of the one-way analysis of variance, it was decided that the effect of independent variable on the dependent variable was significant or insignificant when the p value was greater than or equal to 0.005 in the 95% confidence interval. If the value in question is small, it is not significant. If the result is smaller than 0.001, the level of significance is higher and the confidence interval is 99%. The results are given in Table 3.

Table 3. Directional variance analysis-ANOVA

ANOVA	Model	Significance	Raw material	Yarn count	Number of washes
Thickness	<0,0001	Significant	0,1626	0,8271	<0,0001
Unit weight	<0,0001	Significant	<0,0001	<0,0001	<0,0001
Stitch density	0,6695	Insignificant	0,9336	0,0553	0,9955
Loop yarn length	0,0006	Significant	0,0004	0,0972	0,0623
Bursting strength	<0,0001	Significant	<0,0001	<0,0001	0,008

When Table 3 is examined, it can be said that the change in raw material and yarn number on the thickness does not have a significant effect but the washing has a significant effect. That is, as the number of washes increased, a significant change in the thickness of the socks occurred. On the unit weights of socks, all three independent variables have significant effects. All the independent variables on bursting strength are also significantly effective, but the effect of raw materials and number is greater than the effect of washing. The stitch density of the samples are independent of the number of raw materials, numbers and washes. Raw material has a significant effect on the loop yarn length. Statistical analyzes are consistent with graphical results.

4. Conclusion

The aim of this study is to explain the importance of raw material selection on the strength of sock selection by relating it with the number of washing. Since socks have not an alternative method for cleaning, they are continuously washed in the washing machine. The washing causes the fabric to be tightened and the number of fibers in the unit area increased. At the same time, washing causes thickening and heavy fabric. Fiber migration occurs during washing and drying processes. In fact, this fiber migration can reduce the unit weight and thickness. However, the length and width of the loop decreses by swelling the cross-sectional areas of the fibers. The results show that washing resulted in a significant reduction in the strength of all fibers. As the number of successive washings increases, the losses in strength increase. However, cotton is the most resistant to washing. Modal and bamboo, which are the new generation fibers, can be preferred when they are produced by coarse yarns. In terms of cost, cotton fiber is both cheap and durable, and it explains the reason for using this fiber in the first choice for the production of socks.

References

1. Akaydın, M., Can, Y. (2012). A Research of strength properties of socks knitted from new cellulose-based fibers, Tekstil Teknolojileri Elektronik Dergisi, Cilt:6, No:2, 28-36.
2. Çelik, Z., Topalbekiroğlu, M., Değirmenci, Z. (2014). Farkli hammaddelerden üretilmiş çoraplarin hava geçirgenliğine ardişik yikamalarin etkisi. 2.Uluslararası Tekstil Zirvesi, 22-24 Ekim,124-125, Kahramanmaraş, Türkiye.
3. Cimilli, S., Nergis, B.U., Candan, C., Özdemir, M. (2010). A Comparative study of some comfort-related properties of socks of different fiber types. Textile Research Journal, 80, 948-957
4. Čiukas, R., Abramavičiūtė, J. (2010). Investigation of the air permeability of socks knitted from yarns with peculiar properties. Fibres & Textiles in Eastern Europe, Vol. 18, No. 1 (78), 84-88.
5. Degirmenci, Z., Topalbekiroğlu, M., (2018). The Effect of successive laundering on the dimensional properties of hosiery produced from different raw materials. Ejons V – International Conference On Mathematics – Engineering – Natural & Medical Sciences, November 22-25,183-189, Gaziantep, Türkiye
6. Demiroz, Gun, A., Unal, C., Unal, B. T. (2008). Dimensional and physical properties of plain knitted fabrics made from 50/50 bamboo/cotton blended yarns. Fibers and Polymers, Vol.9, No.5, 588-592.
7. Ertekin, G., Marmaralı, A. (2014). Performance and thermal comfort properties of knitted fabrics produced by cotton, acrylic and miyabi yarns. XIIIth International Izmir Textile and Apparel Symposium, April 2-5, 237-243,İzmir, Turkey.
8. Eberle, H., Gonser, E., Hermeling, H., Hornberger, M., Kilgus, R., Kupke, R., Menzer, D., Moll, A., Ring, W. (2014). Clothing Technology:... from Fibre to Fashion. Verlag Europa-Lehrmittel.
9. Özdil, N. (2008). A study on thermal comfort properties of the socks. Tekstil ve Konfeksiyon, 8(2), 154-158.
10. Waite M. (2009). Sustainable Textiles: the role of bamboo and a comparison of bamboo textile properties-Part 1. Journal of Textile and Apparel, Technology and Management, 6 (2), 1-21.

AN OVERVİEW OF MARİTİME CLOUD FOR THE BİG DATA MANAGEMENT İN MARİTİME TRAFFİC BY PROJECT "THE EFFİCİENSEA2"

Meriç Burçin ÖZER [1] , Veysel TATAR [2]

1

2

1.INTRODUCTION

From early time of humanity, the maritime transport over the sea has been important to carry people and develop business. Carrying goods is performed by tankers, bulk carriers and container ships which every year transport billions of tones along a few principal trade routes (Figure 1).

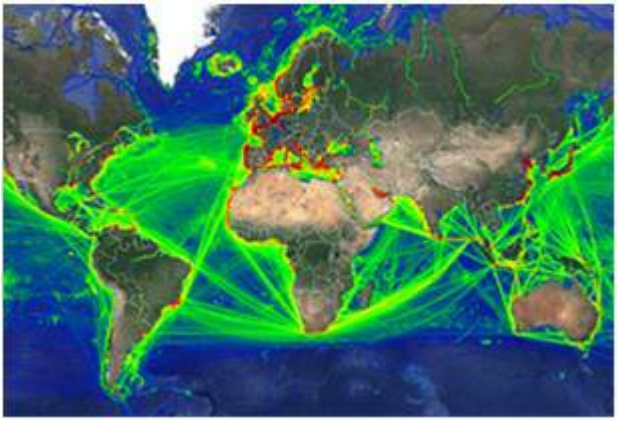

Figure 1. International trades routes and density.

The containerization has also revolutionized the global cargo shipping, bringing vast improvements in efficiency. The growth of the world population and the need of food have requested to increase the float of fishing ships to answer this demand. As markets became increasingly globalized, world trade has more than trebled since the 2000-2017(Figure 2) [1].

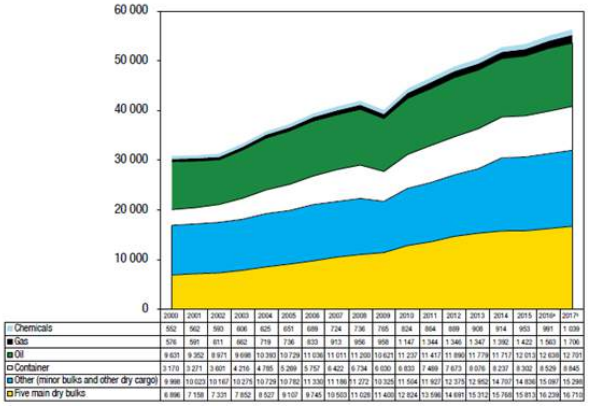

	2000	2001	2002	2003	2004	2005	2006	2007	2008	2009	2010	2011	2012	2013	2014	2015	2016*	2017*
Chemicals	552	562	593	606	625	651	689	724	736	765	824	864	889	906	914	953	991	1 039
Gas	576	591	611	662	719	736	833	913	956	958	1 147	1 344	1 346	1 347	1 392	1 422	1 503	1 706
Oil	9 631	9 352	8 971	9 696	10 393	10 729	11 036	11 011	11 200	10 621	11 237	11 417	11 896	11 779	11 712	12 013	12 606	12 707
Container	3 170	3 271	3 601	4 255	4 785	5 289	5 757	6 422	6 734	6 030	6 835	7 489	7 673	8 076	8 237	8 392	8 529	8 845
Other (minor bulks and other dry cargo)	9 998	10 023	10 167	10 275	10 729	10 782	11 330	11 186	11 272	10 325	11 504	11 927	12 375	12 952	14 703	14 836	15 087	15 299
Five main dry bulks	6 896	7 156	7 331	7 852	8 527	9 107	9 745	10 503	11 028	11 402	12 824	13 596	14 691	15 312	15 766	15 813	16 239	16 710

Figure 2. World seaborne trade in cargo ton-miles by type of cargo, 2000–2017 (Billions of ton-miles)

Maritime communications will experience major changes during the next two decades. Not only will the evolution of e-Navigation require higher digital data exchange capacities, but new connectivity solutions for the crew will also increase bandwidth needs. New potential digital VHF services are envisioned [2] while other innovative digital VHF implementations are also in the pipeline. These are only some examples of emerging trends, technologies or demands.

In the modern globalized economy, ocean shipping becomes the most efficient method for transporting commodities over long distance. The persistent growth of the world economy leads to increasing demand of maritime transportation with larger ship capacity and higher sailing speed [3]. In this circumstance, safety and security become key issues in maritime transportation. Intelligent maritime navigation system using Automatic Identification System (AIS) data improves the maritime safety with less cost compared with conventional maritime navigation system using human navigators. The AIS is a maritime safety and vessel traffic system imposed by the Interna-tional Maritime Organization (IMO). Autonomously broadcasted AIS messages con-tain kinematic information (including ship location, speed, heading, rate of turn, des-tination and estimated arrival time) and static information (including ship name, ship MMSI ID, ship type, ship size and current time), which can be transformed into useful information for intelligent maritime traffic manipulations, e.g. vessel path prediction and collision avoidance, and thus plays a central role in the future autonomous mari-time navigation system. Over the last several years, receiving AIS messages from vessels and coastal stations has become increasingly ordinary.

The requirement of the International Maritime Organization (IMO) to install the Automatic Identification System (AIS) on-board ships, together with the use of other self-reporting systems based on Global Positioning System (GPS)-quality navigation information [4], contribute to the overabundance of information. This information is potentially of great value and importance but typically the resources are not fully exploited. In such circumstances, there is a challenging issue of how to extract/discover valuable knowledge from the available large volumes of maritime traffic information usually stored in a database (DB).

AIS technology broadcast ship information and voyage information at regular time interval. The information can be received by onboard transceiver and terrestrial and/or satellite base station. There are some important attributes of AIS data: longitude, latitude, speed over ground (SOG), course over ground (COG), vessel's maritime mobile service identity (MMSI), base date time, vessel type, vessel dimension, rate of turn (ROT), navigation status and heading.

In this section, we design a new model shown in Figure 3 for the index of maritime traffic situation (Imts). This model combines three dynamic features, namely rate of encounter, rate of turn and speed acceleration from

AIS data and the Imts is visualized on the Electronic Chart Display and Information System (ECDIS).

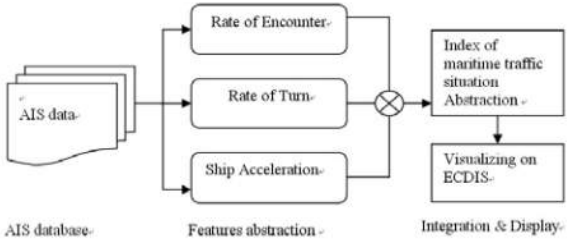

Figure 3. The flowchart of AIS data visualization model [5]

This paper gives an update of the recent development and status of the Maritime Cloud. It presents the main conceptual ideas and its core elements for the implementation and usage of the Maritime Cloud, evolved in the context of the projects EfficienSea2.

2.THE PROJECT: "EFFICIENSEA2 EfficienSea2"

Today, information exchange between ships and shore is unstable, costly and marked by old technology and non-standardised solutions. This increases the risk of accidents, inefficiency and administrative burdens. Furthermore, incentives to comply with emission regulations are limited, which adversely impacts the environment. The need for operational solutions in the maritime domain is significant. The overall aim of the EfficienSea2 project is to deal with these challenges by creating and deploying innovative and smart solutions for efficient, safe and sustainable traffic at sea through improved connectivity for ships.

EfficienSea2 develops the essential solutions that are the prerequisites for taking e-Navigation from testbeds to real-life implementation. EfficienSea2 is a demonstrator in the Arctic and Baltic Sea and the first generation of a coherent e-Navigation solution. Through global collaboration, use of open source software and an explicit aim for standardised solutions, Efficiensea2 is paving the way for a global roll out of e-Navigation.

The EfficienSea2 four areas of focus are:

End user services – smart navigation and administration

EffcienSea2 identifies, develops, tests and, where possible, standardises and implements solutions that reduce the risk of accidents, increase the efficiency of the transport chain and lower the administrative burdens and environmental impacts.

Output: 15 e-Navigation and e-Maritime services

EfficienSea2 develops more than 15 end user services, though at different stages of maturity. Some services, like basic navigation and weather solutions, will be tested and implemented in real world platforms. Other more advanced services will be tested at experimental levels. Focus is on open source software and providing input to relevant standardisation bodies. Services, such as Maritime Safety Information and Notices to Mariners, are anticipated to reach new global standards within the project scope.

Platform displays – web and onboard equipment

EfficienSea2 makes services available for the end user by developing webbased platforms focusing on the Arctic and Baltic areas. For the long term roll-out, services will also be prototyped and tested in commercial onboard and shore equipment.

Output: Implementation of BalticWeb

EfficienSea2 provides a working prototype of a cloud embedded single point of access to e-Navigation and e-Maritime services in the Baltic Sea (based on the existing ArcticWeb). With five to six integrated e-Navigation services, BalticWeb will be accessible on all internet connected systems, e.g. tablet and PC.

Communication framework – The Maritime Cloud

EffcienSea2 creates and implements a communication framework that enables efficient, secure and reliable information exchange in and around the maritime sector. The Maritime Cloud connects all maritime stakeholders with maritime information services of all kinds. The Maritime Cloud includes an Identity Registry for secure identity management, a Service Registry for registering, discovering and using relevant services and a Messaging Service for intelligently exchanging information between communications systems connected to the cloud. The Maritime Cloud has potential to break ground by enabling the maritime internet of things.

Output: Implementation of The Maritime Cloud

EfficienSea2 provides a working prototype of the communication framework with operational functions such as a single logon for all services, identity management and discovery of maritime services. Elements of The Maritime Cloud will be made operational in the Arctic and Baltic Sea.

Communication channels – smart roaming and VDES EfficienSea2 develops, prototypes and tests concepts for cost-effective and seamless roaming between communication channels, as well as, the new communication channel VDES (VHF Data Exchange System). Thereby, it addresses the challenge of weak connectivity and high cost communication.

Output: Maturation of VDES – VHF Data Exchange System

EfficienSea2 provides field testing of the on-air parameters performed on a dedicated test platform of a new, globally interoperable and potentially cost free ship-to-ship and ship to shore digital communication link that is dedicated to data transfer via radio channels.

3.THE CONCEPT OF THE MARITIME CLOUD

The growing demands for data links capacity in maritime vessels and high costs of satellite communication links through mandatory GMDSS Inmarsat equipment emphasize the possibility of optimizing data traffic routes through alternative service providers either satellite or terrestrial [6]. E-navigation is the harmonised collection, integration, exchange, presentation and analysis of marine information on board and ashore by electronic means to enhance berth to berth navigation and related services for safety and security at sea and protection of the marine environment. Shipping is the most prevalent transportation type worldwide and accounts for 80% of all transportation and it plays a crucial role in maritime safety culture [7]. International shipping, although considered a safe and environment-friendly form of transportation [8]. Maritime accidents are rare occurrences with the potential to result in significant human casualty [9]. Development towards increased safety, sustainable environment, and higher profits within shipping cannot be enabled without Sea Traffic Management (STM).

International Maritime Organization (IMO) has decided to introduce an e-navigation in order to improve safety of navigation and to reduce errors. In spite of the huge development of Technologies in navigation and communication systems, there is a need to coordinate systems and more use of harmonized standards. IMO defined e-navigation as “the harmonized collection, integration, exchange, presentation and analysis of marine information on board and ashore by electronic means to enhance berth to berth navigation and related services for safety and security at sea and protection of the marine environment” [10].

The Maritime Cloud is a dynamic concept derived from a user-driven process based on experience gained from several e-navigation testbed projects. It is a scalable enabler of seamless information exchange between a variety of available systems and across different physical communication links in the Maritime Domain, as explained graphically in the Annex of this document. With reference to the report of the Correspondence Group on e-navigation to the first session of the NCSR Sub-Committee (NCSR 1/9), the Maritime Cloud is to be considered as part of Task T15 on the proposed e-navigation Strategy Implementation Plan and, more specifically, as a communication infrastructure supporting the five prioritized solutions for e-navigation, as well as other non-prioritized potential solutions to be developed in the future.

Shipboard navigational system of non-SOLAS ships are relatively poor in comparison with SOLAS ships which are carrying advanced navigational

equipment in accordance with the provisions of SOLAS. Shipboard navigational systems and equipment for all ships are described in Regulation 19, Chapter V of SOLAS. Unless expressly provided otherwise, the chapter V shall apply to all ships on all voyages. However the Administration shall determine to what extent the provisions of regulations on carriage requirements for shipborne navigational systems and equipment do not apply to the domestic voyage ships and fishing vessels [11].

The digital communication system is a key for the implementation of e-navigation. It will consist of digitalized GMDSS (Global Maritime Distress and Safety System) and LTE–M (Long Term Evolution for Maritime). The digitalized communication system will be developed based on the existing GMDSS for SOLAS ships, such as AIS Application Specific Messages (AIS-ASM) and VHF Data Exchange System (VDES). AIS-ASM transmitted in binary format will be increasingly used to digitally communicate maritime safety information between participating vessels and shore stations. Together with AISASM, VDES will have a significant beneficial impact on the maritime information services including Aids to Navigation and VTS in the future.

The Maritime Cloud can be applied to the future of e-navigation in terms of its core components, its applicability to the prioritized e-navigation solutions, relationship with GMDSS Development of GMDSS was initiated by the International Maritime Organization (IMO) and the system represents a significant improvement in maritime communications. Vessel Traffic Services (VTS) aim to improve the safety and efficiency of vessel traffic and to protect the environment [12]. The Maritime Cloud could support e-navigation infrastructure and trials are underway. Vessel Traffic Service (VTS) can be defined as a service implemented by a competent authority, designed to improve the safety and efficiency of vessel traffic and to protect the environment. The Maritime Cloud consists of standards, infrastructure and service reference implementations. The concept of Maritime Cloud is shown in Figure 4.

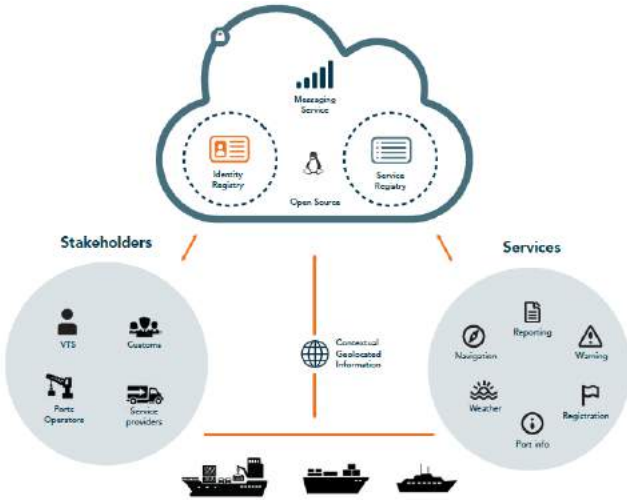

Figure 4. The Maritime Cloud System

The e-navigation operation system will include central and regional operation centre(s), bigdata system of marine information, ship position information, information exchange, maritime cloud system and data back-up system. The e-navigation operation system will consist as shown in Figure 5.

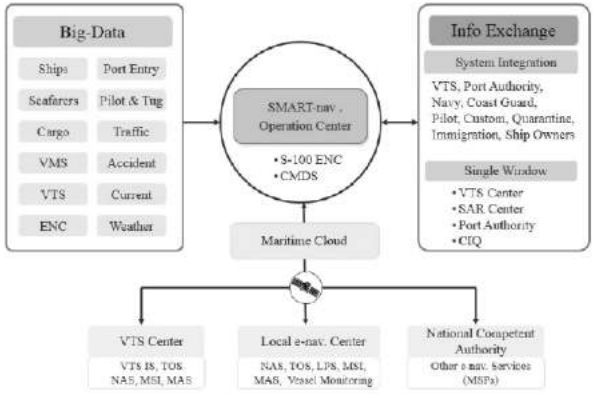

Figure 5. E-navigation Operation System [13]

The Maritime Cloud consists of standards, infrastructure and service reference implementations, that together with governance enable the

efficient exchange of information between qualified maritime parties via interoperable information services, utilizing highly automated interfaces to different communication options, enhancing general communications related to berth to berth navigation and related services for safety and security at sea and protection of the marine environment. Existing as well as new communication links may serve to provide information exchange using the Maritime Cloud (Fig 6). Existing as well as new communication links may serve to provide information exchange using the Maritime Cloud. Provision of mandatory information services, such as the MSI service under the Global Maritime Distress and Safety System (GMDSS), is currently provided using the NAVTEX and SafetyNet communication services. However, the TELEX based NAVTEX and SafetyNet technologies do not allow the distribution of S-100 structured data, which can be presented on geographically oriented display systems. Mandatory reporting for the purpose of interaction with VTS may utilize VHF voice communication and AIS. Application Specific Messages via AIS or a future VHF Data Exchange System (VDES) could support such functions, and these communication services should remain cost free for ships.

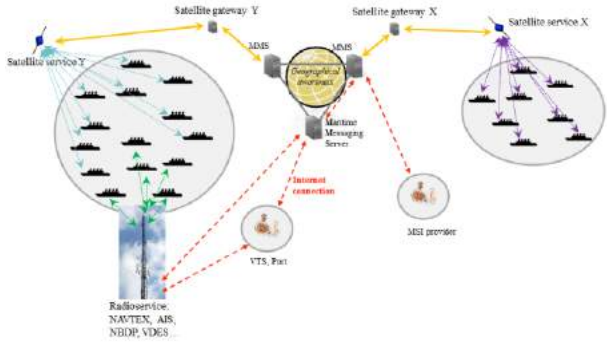

Figure 6. Global Maritime Cloud Communication System

4.CONCLUSION

The fourth, industrial revolution is about fundamentally rethinking the way we produce goods and deliver services. And it is also about thinking about what qualifications we need to equip our workforce with. It is about using digitalization and technology in new ways to retain employment, to create and develop new types of competences and employment and thereby promote new growth. It is about strengthening productivity and increasing our competitiveness. Shipping of the future must be approached the same way.

This revolution in ship connectivity will reduce existing barriers and enable the implementation of many new applications for maritime users. These new applications will include condition monitoring, energy efficiency,

and autonomy, making shipping smarter and more cost-efficient. Yards, maritime equipment vendors, classification societies, and new players will identify opportunities for improving maintenance schemes and developing new services based on operational data that will be transferred to shore on a live basis. As more and more vessels become "connected" via broadband, concepts such as "Big Data" and the "Internet of Things" will soon become a reality in the maritime business.

The benefits of the Maritime Cloud include:

- Ability to reuse existing communication systems, while communicating seamlessly across different digital systems, and further facilitating transition to new Technologies and systems.
- Availability of prioritized messaging queuing systems for addressing mobile actors.
- Automatic Quality Assurance of communication links and information delivery through request for automated acknowledgements, when using the Maritime Messaging Service.
- Verification of authenticity of origin and content of information as an additional service (not generally required).
- Enabling automated access from one ship borne single window to multiple National Single Windows for reporting, further enabling a reduction in the administrative burden and cognitive load on mariners.
- Enabling the development of a unified communication terminal able to switch automatically between a multitude of different channels to identify and address a specific actor, thereby reducing the complexity in choosing the right communication system depending on purpose of use.
- Facilitation of the future definition of new and improved information services, based on an open architecture allowing alternatives for distribution of information storage or service points.
- A framework enabling secure ship to ship, ship to shore data exchange, as well as shore to shore data exchange between MRCCs, VTS, ports, agents, National Single Window systems for reporting, etc.
- Further facilitate logistics chain integration with other modes of transport, promoting an efficient and Sustainable Maritime Transportation System.
- Secured private and public communication links supported by the Maritime Cloud, taking into account issues of Cyber-Security.

REFERENCES

1. UNCTAD, (2017). Revıew Of Marıtıme Transport.
2. CEPT. (2013). Information Paper on VHF Data Exchange System (VDES), CPG PTC(13) INFO 16. Electronic Communications Committee, Tech. Rep.
3. P. Kaluza, A. Kölzsch, M. T. Gastner, and B. Blasius. (2010). The complex network of global cargo ship movements. In: Journal of the Royal Society Interface, vol. 7, no. 48, pp. 1093–1103.
4. T. Hammond, M. McIntyre, D. Chapman, and L. Lapinski, (2006). The impact of self-reporting systems on maritime domain awareness. ser. Proceedings of the 11-th International Command and Control Research and Technology Symposium.
5. Jiacai, P., Qingshan, J., Jinxing, H., Zheping, S. (2012). An AIS data Visualization Model for Assessing Maritime Traffic Situation and its Applications, Procedia Engineering, vol.29, pp.365-369
6. Sumić, D., D. Peraković, and M. Jurcević, Optimizing Data Traffic Route for Maritime Vessels Communications.
7. Arslan, V., et al., (2016). Safety Culture Assessment and Implementation Framework to Enhance Maritime Safety. Transportation Research Procedia, 14: p. 3895-3904.
8. Coomber, F.G., et al., (2016). Description of the vessel traffic within the north Pelagos Sanctuary: Inputs for Marine Spatial Planning and management implications within an existing international Marine Protected Area. Marine Policy, 69: p. 102-113.
9. Nordström, J., et al., (2016). Vessel TRIAGE: A method for assessing and communicating the safety status of vessels in maritime distress situations. Safety Science, 85: p. 117-129.
10. International Maritime Organization (2009a), Strategy for the Development and Implementation of enavigation. Report of the Maritime Safety Committee on its Eighty-fifth Session (MSC 85/26/Add.1), Annex 20. https://docs.imo.org/
11. Annex 20. https://docs.imo.org/ International Maritime Organization (2009b), International Convention for the Safety of Life At Sea, 1974, as amended (SOLAS 1974), London.
12. Van Dam, S., M. Mulder, and M.M. van Paassen, (2006). Ecological Interface Design For Vessel Traffic Management: A Theoretical Overview. IFAC Proceedings Volumes, 39(12): p. 193-198.
13. Kwang An, (2015). A Study on the Collision Prevention Support System for Small Ships based on e-navigation, Graduate School of Mokpo National Maritime University.

BIOMASS POTENTIAL FOR A SUSTAINABLE ENVIRONMENT AND ENERGY PRODUCTION IN TURKEY

Zuhal AKYÜREK [1] , Sevnur TURGUT [2]

[1] Burdur Mehmet Akif Ersoy University, Faculty of Engineering and Architecture, Department of Polymer Engineering, Burdur, Turkey.
[2] Burdur Mehmet Akif Ersoy University, Graduate School of Natural and Applied Sciences, Department of Material Technologies Engineering, Burdur, Turkey.

1. Introduction

Energy is the vital element for sustainable development of nations. In the last decades, rapid increase in the world population, industrialization and technological developments have fostered energy demand and the concerns on negative environmental impacts of energy generation from fossil fuels. According to International Energy Agency, global energy demand grew by 2.1 % in 2017, more than twice of the growth rate in 2016. Utilization of excessive amount of fossil fuel resources to meet the growing energy demand on one hand, and the climate change threat of fossil fuel combustion on the other, have risen the interest on alternative, environmentally friendly energy options (Panwar et al., 2011; Huang and Yuan, 2015.; Akyürek, 2019a).

Renewable energy sources have gained importance in this manner to cope with growing energy demand. The main forms of renewable energy used today are biomass energy, hydroelectricity, wind energy, solar energy, and geothermal energy. Their availability, energy conversion efficiency, technical and economic potential and impacts on climate change and environmental sustainability, determine their share in the world energy mix (Moriarty and Honnery, 2019). Renewables are predicted to show rapid growth in the electricity production by supplying about 30 % of total power demand in 2023. The prediction of the share of renewables in electricity, heating and transportation sectors are demonstrated in Figure 1 (IEA, 2018).

Biomass is the largest and most important renewable energy option that can be used to produce various forms of energy. It is also considered as one of the most promising energy source in the near future due to its abundancy and potential to reduce global warming problem (Panwar et al., 2012; Akyürek et al.,2019b). Biomass potential can be exploited with existing technologies to shift the energy mix from fossil fuels to renewables (Ladanai and Vinterbäck, 2009).

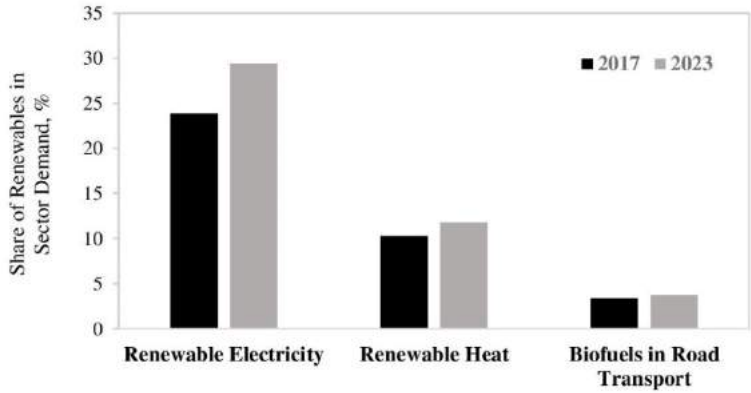

Figure 1. Comparison of the share of the renewables by sector between 2017 data and 2023 projections.

2. Biomass

Biomass can be defined as organic materials derived agricultural residues, forestry residues, livestock manure, industrial waste and municipal solid waste (Al-Hamamre et al., 2017; Akyürek, 2018b). Biomass stores its energy directly from solar radiation. It is considered as a carbon dioxide neutral fuel, because the amount of carbon that is released to the atmosphere during energy production is equivalent to the amount it has absorbed during its life time via photosynthesis (Figure 2). Therefore, net greenhouse gas emissions from biomass energy becomes neutral in the biomass cycle (Yan et al., 2019).

Biomass structure mainly composed of cellulose, hemicellulose, lignin, starch and proteins (Parmar, 2017). Biomass differs from coal by its higher volatile matter and lower ash contents and higher reactivity. Table 1 shows characteristic properties of some biomass types with respect to coal.

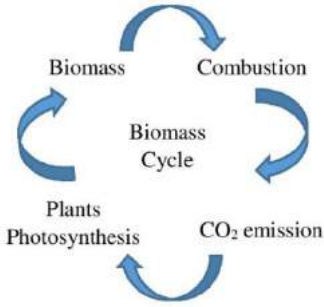

Figure 2. Biomass cycle, net zero CO_2 emissions.

Table 1. Elemental analysis of biomass and coal (wt %) (Demirbaş, 2004; Vassilev et al., 2010).

	C	H	N	S	O
Coal	81.5	4.0	1.2	3.0	3.3
Pistachio Shell	50.9	6.4	0.7	0,2	41.8
Wheat Straw	41.8	5.5	0.7	-	35.5
Walnut Shell	49.9	6.2	1.4	0.1	42.4
Corn Stover	48.7	6.4	0.7	0.1	44.1

2.1. Biomass Conversion

Biomass can be converted to electricity, heat, biofuels and chemical though various conversion technologies. Several factors have impact on selection of conversion process such as the type, quantity, and characteristics of biomass feedstock, end-use requirements, environmental regulations, economic conditions, location and transportation requirements (Adams et al., 2018). Figure 3 illustrates the conventional energy conversion technologies for biomass fuels.

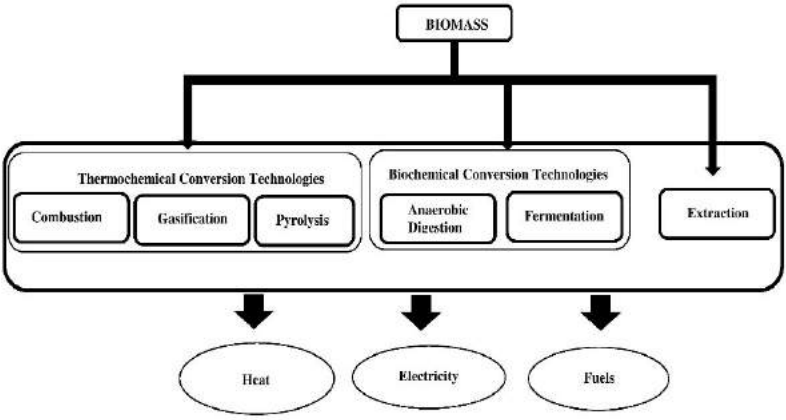

Figure 3. Biomass conversion technologies.

Energy recovery from biomass can be carried out through direct combustion, gasification and pyrolysis applications. Thermochemical processes aim to convert high moisture and low energy content biomass to

more valuable fuels with higher energy efficiency and easily transportable, environmentally friendly and low ash content products (Boyles, 1984).

During combustion, biomass primarily loses its moisture content at temperatures up to 100°C. As temperature increases, volatiles release and combustion occur. In the end, char oxidizes and final product ash remains. (IEA, Bioenergy Task 32). Biomass combustion can be effective for both small and large scale operations. Large-scale power plants are operated for electricity production from biomass and they are generally able to supply 100 to 3000 MW energy (McKendry, 2002). Biomass combustion can be an alternative to coal combustion, however, some operational problems may occur due to the formation of undesirable side reactions. The resulting biomass ash compositions generally cause operational problems such as agglomeration, slagging and corrosion due to low melting point constituents in biomass ash for instance, K, Na, Cl, etc. (Agrela, 2019). For effective electricity production from biomass, co-firing with coal in existing thermal power plants can be an effective solution to ash melting problems of biomass combustion (Göğebakan, 2007).

Gasification process converts biomass into producer gas by the partial oxidation of the solid fuel at high temperature, in the range of 800-1000 °C (Akyürek et al., 2019b). The gasification performance depends on the biomass characteristics and operational parameters such as moisture content of biomass, gasifying agent, equivalence ratio, gasifier temperature, particle size of biomass, etc. (La Villetta, et al., 2017). Gasification can be carried out by using air, oxygen and/or steam as a gasifying agents. Product gas from gasification is the syngas which contains hydrogen, carbon monoxide, carbon dioxide, methane and nitrogen.

Pyrolysis is another promising thermochemical conversion technology for conversion of waste materials into energy and valuables, such as bio-oil, synthetic gas, and biochar products (Akyürek, 2019). In pyrolysis, biomass energy is extracted to produce; (a) stabilized pyrolysis oil which has potential to be used as fuels in furnaces, turbines, and diesel engines or feedstock for many chemicals; (b) combustible syngas for power generation; and (c) biochar to be used as soil fertilizer and adsorbent green chemicals (Uzoejinwa et al., 2018). Pyrolysis process can be classified into three groups according to reaction temperature and heating rate as slow (200-600 °C), fast (500-950 °C) and flash (1050-1300 °C) pyrolysis (Kambo and Dutta, 2015).

Anaerobic digestion process is a widespread biochemical conversion technology to convert organic wastes into renewable energy and to effectively mitigate the greenhouse gas emissions. In anaerobic digestion, biogas composed of methane (35-75 %), carbon dioxide (25-65 %), hydrogen (1-5 %) is produced. Biogas can be upgraded to bio-methane which is a valuable energy carrier similar to natural gas (Akyürek, 2018, Yentekakis et al., 2017). Biogas could be a potential energy source for heat and electricity production. In addition, anaerobic digestion of waste materials produces organic fertilizer, which can be used in agricultural areas. Anaerobic digestion (AD) of animal waste can be advantageous as it provides

prevention of waste problems, unpleasant odors and microbial pathogens in livestock farms, production of renewable energy.

2.2. Biomass Potential in Turkey

Agricultural activities and livestock farming have high contribution to economic development in Turkey. Turkey has 8.6 MTOE of biomass energy potential generated from agricultural, animal and urban wastes (General Directorate of Renewable Energy, 2018). The abundancy of agricultural residues and livestock manure signify their potential for renewable energy production in Turkey. Utilization of biomass through conversion technologies can help to prevent waste disposal problems in livestock waste, agricultural residues, municipal solid waste, industrial waste having organic content and to produce renewable energy on one hand, and to reduce the greenhouse gas emissions and contribute the climate change combat, on the other. Renewable energy production supports local, regional and national economic development.

Turkey is one of the fastest growing economies in Europe. Europe has targeted 40% reduction in greenhouse gas emissions by year 2030 (Scarlat et al., 2018). In Turkey, power generation and industrial activities are responsible for most of the greenhouse gas emissions. According to Turkey's Intended Nationally Determined Contribution covering the period 2012-2030, total greenhouse gas emissions will be reduced up to 21% with the improvements in energy, industrial processes and products use, agriculture, land use land-use change and forestry, and the waste sectors.

In the view of above requirements for biomass utilization, biomass energy potential has gained more importance to reach the emission reduction targets of Turkey. Therefore, in this study biomass sources in Turkey have evaluated in terms of energy production potentials.

3. Materials and Methods

Turkey has high biomass potential generating from agricultural and forestry residues, and municipal solid waste. Table 2 shows the production amount of agricultural residues, forestry residues and municipal solid waste inventory in Turkey that have collected from Turkish Statistical Institute and General Directorate of Renewable Energy (2018). Energy content of the biomass types are presented in Table 3. The production and heating value data have used to calculate the total energy potential of biomass.

Table 2. Agricultural, forestry and MSW production in Turkey (2018)

Product	Tons/year
Wheat	20,000,000
Barley	26,119,403
Rye	1,109,025
Oats	1,058,254
Rice	940,000
Sugar Cane	167
Wood	5,000,000
Maize	5,700,000
Olive	1,500,467
Tea	1,500,000
Almond	100,000
Apricot	750,000
Walnut	215,000
Hazelnut	515,000
Sunflower	1,949,229
Peanut	173,835
Cotton	2,570,000
Banana	498,888
Orange	1,900,000
MSW	31,583,553

Table 3. Heating values of agricultural residues, forestry residues and municipal solid waste. (Avcıoğlu et al., 2019; McKendry, 2002; Toklu, 2017; Öztürk et al., 2017)

Biomass	Lower Heating Value, MJ/kg
Wheat Straw	17.3
Barley Straw	16.1
Rye Straw	14.0
Oat Straw	14.0
Rice Straw	14.9
Sugar Cane Bagasse	15.4
Wood Bark	18.6
Maize Cobs	17.6
Olive Husk	17.7
Tea Waste	17.1
Almond Shell	16.9
Apricot Stone	17.3
Walnut Shell	16.8
Hazelnut Shell	16.8
Sunflower Residue	13.2
Peanut Shell	16.5
Cotton Stalk	17.0
Banana Peel	13.1
Orange Peel	17.6
MSW	14.4

4. Results and Discussion

Biomass have become one of the global sources of renewable energy in the world today. Biomass have potential to meet the growing energy needs for electricity and heating. In this study, energy potentials of biomass sources in Turkey were evaluated. Waste potential of agricultural residues, forestry residues and MSW in Turkey and energy potential that can be acquired from different biomass has presented in Table 4.

Table 4. Waste and Energy potential of biomass in Turkey

Biomass	Waste Potential (Tons/year)	Energy Potential, TJ/year	Energy Potential MW/year
Wheat Straw	14,000,000	242,200	7,680.1
Barley Straw	17,761,194.04	285,955	9,067.6
Rye Straw	776,317.5	10,868.4	344.6
Oat Straw	740,777.8	10,370.9	328.9
Rice Straw	470,000	6,989	221.6
Sugar Cane Bagasse	50.1	0.77	0.02
Wood Bark	3,500,000	65,100	2,064.3
Maize Cobs	4,560,000	80,256	2,544.9
Olive Husk	900,280.2	15,935	505.3
Tea Waste	1,050,000	17,955	569.3
Almond Shell	50,000	848	26.9
Apricot Stone	142,500	2,469.5	78.3
Walnut Shell	107,500	1,806	57.3
Hazelnut Shell	412,000	6,921.6	219.5
Sunflower Residue	1,364,460.3	18,011	571.1
Peanut Shell	86,917.5	1,436.7	45.6
Cotton Stalk	2,184,500	37,180	1,179.0
Banana Peel	199,555.2	2,614.2	82.9
Orange Peel	380,000	6,688	212.1
MSW	31,583,553	453,539	14,381.7

As can be depicted from the table, Turkey has annual 40,181 MW energy recovery potential from various biomass sources. Biomass energy potential is equivalent to 50 million tons of bituminous coal combustion. The results revealed that utilization of available of different types of biomass in Turkey can contribute to sustainable energy production, environment and economic development.

5. Conclusion

Turkey is an energy importing country, therefore indigenous energy sources in Turkey is of great importance. Agricultural residues, forestry residues and municipal solid waste energy potential can be exploited to provide energy needs of country by using suitable conversion technologies. In Turkey biomass has annual 40,181 MW energy generation potential as a substitute to 50 million tons of bituminous coal combustion. Biomass is a worthwhile energy option to be utilized in Turkey for economic and environmental sustainability.

Acknowledgement

This research did not receive any specific grant from funding agencies in the public, commercial, or not-for-profit sectors.

References

1. Adams, P., Bridgwater, T., Lea-Langton, A., Ross, A., Watson, I. (2018). Cpt 8 Biomass Conversion Technologies, *Greenhouse Gas Balances of Bioenergy Systems*, 107-139
2. Agrela, F., Cabrera, M., Morales, M. M., Zamorano, M., & Alshaaer, M. (2019). Biomass fly ash and biomass bottom ash. New Trends in Eco-Efficient and Recycled Concrete, 23–58. doi:10.1016/b978-0-08-102480-5.00002-6
3. Akyürek, Z. (2018a). Potential of Biogas Energy from Animal Waste in the Mediterranean Region of Turkey*, Journal of Energy Systems*, 2(4), 159-167.
4. Akyürek, Z. (2018b). Valorization of Agricultural and Industrial Wastes Through Pyrolysis: Thermal Behavior and Kinetic Analysis. *Current Academic Studies in Engineering Sciences-2018*, IVPE.
5. Akyürek, Z. (2019). Sustainable Valorization of Animal Manure and Recycled Polyester: Co-pyrolysis Synergy. *Sustainability,* 11, 2280. doi:10.3390/su11082280
6. Akyürek, Z., Akyüz, A.Ö., Güngör, A. (2019a). Optimizing the Tilt Angle of Solar Panels to Reduce Carbon Footprint: Case for the West Mediterranean Region of Turkey. *International Journal of Engineering, Design and Technology*, 1(1), 10-15.
7. Akyürek, Z., Güngör A., Akyüz, A.Ö. (2019b). Energy potential from gasification of agricultural residues in Burdur, Turkey, *Techno-Science*, 2(1), 15-19.
8. Al-Hamamre, Z., Saidan, M., Hararah, M., Rawajfeh, K., Alkhasawneh, H.E., Al-Shannag, M. (2017). Wastes and biomass materials as sustainable-renewable energy resources for Jordan. *Renewable and Sustainable Energy Reviews*, 67, 295-314. Doi: 10.1016/j.rser.2016.09.035
9. Avcıoğlu, A.O., Dayıoğlu, M.A., Türker, U. (2019) Assessment of the energy potential of agricultural biomass residues in Turkey. *Renewable Energy*, 138, 610-619.
10. BP Statistical Review of World Energy. (2018). Retrieved from https://www.bp.com/content/dam/bp/business-sites/en/global/corporate/pdfs/energy-economics/statistical-review/bp-stats-review-2018-full-report.pdf
11. Boyles, O. (1984) Bio-Energy, Ellis Horwood Limited, England.
12. Demirbaş, A. (2004) Combustion Characteristics of Different Biomass Fuels. *Progress in Energy and Combustion Science*, 30, 219-230.
13. Gogebakan, Z. (2007) Co-firing Biomass with Coal in Bubbling Fluidized Bed Combustors, *PhD Thesis*, Middle East Technical University.
14. Huang, H., Yuan, X. (2015). Recent progress in the direct liquefaction of typical biomass, *Progress Energy Combustion Science,* 49, 59-80.
15. International Energy Agency (2018). *Task 32, Biomass Combustion and Co-firing.* Retrieved from http://task32.ieabioenergy.com/overview/basic-principles-biomass-combustion/
16. International Energy Agency (2018). *Renewables 2018 Market analysis and forecast from 2018 to 2023*. Retrieved from https://www.iea.org/renewables2018/
17. Kambo, H.S., Dutta, A. (2015). A Comparative Review of Biochar and Hydrochar in Terms of Production, Physico-Chemical Properties and Applications. *Renewable and Sustainable Energy Reviews*, 45, 359–378.
18. Ladanai, S., Vinterbäck, J. (2009). Report No: 013. *Global Potential of Sustainable Biomass for Energy*. Retrieved from https://pub.epsilon.slu.se/4523/1/ladanai_et_al_100211.pdf
19. La Villetta, M., Costa, M., Massarotti, N. (2017). Modelling approaches to biomass gasification: A review with emphasis on the stoichiometric method.

Renewable and Sustainable Energy Reviews, 74, p. 71-88, DOI: 10.1016/j.rser.2017.02.

20. McKendry, P. (2002). Energy Production from Biomass (Part II): Conversion Technologies. *Bioresource Technology*, 83(1), 47-54.
21. Moriarty, P., Honnery, D. (2019). Global renewable energy resources and use in 2050. *Managing Global Warming. An Interface of Technology and Human Issues*, 221-235. Doi:10.1016/B978-0-12-814104-5.00006-5
22. Ozturk, M., Sabab, N., Altay, V., Iqbal, R., Hakeem, K.R., Jawaid, M., Ibrahim, F.H. (2017) Biomass and bioenergy: An overview of the development potential in Turkey and Malaysia. *Renewable and Sustainable Energy Reviews,* 79, 1285-1302.
23. Panwar, N.L., Kaushik, S.C., Kothari, S. (2011). Role of renewable energy sources in environmental protection: A review *Renewable and Sustainable Energy Reviews,* 15, 1513–1524. doi:10.1016/j.rser.2010.11.037
24. Parmar, K. (2017). Biomass- An Overview on Composition Characteristics and Properties. *IRA-International Journal of Applied Sciences*, 7, 2455-4499.
25. Republic of Turkey Ministry of Energy and Natural Resources, General Directorate of Renewable Energy, Biomass Energy Potential Map (2018). Retrieved from http://bepa.yegm.gov.tr/
26. Scarlat, N., Fahl, F., Dallemand, J.F., Monforti, F., Motola, V. (2018). A spatial analysis of biogas potential from manure in Europe, *Renewable and Sustainable Energy Reviews* 94: 915–930.
27. Statistical Institute of Turkey, TUIK. (2018). Retrieved from http://tuik.gov.tr/
28. Toklu, E. (2017) Biomass energy potential and utilization in Turkey. *Renewable Energy*, 107, 235-244.
29. Uzoejinwa, B.B., He, X., Wang, S., Abomohra, A.E.F., Hu, Y., Wang, Q. (2018). Co-pyrolysis of biomass and waste plastics as a thermochemical conversion technology for high-grade biofuel production: Recent progress and future directions elsewhere worldwide. *Energ. Convers Manag.* 163, 468–492.
30. Vassilev, S.V., Baxter, D., Andersen, L.K., Vassileva, C.G. (2010) An Overview of the Chemical Composition of the Biomass. *Fuel*, 89, 913-933.
31. Yentekakis, I.V. and Grammatiki, G. (2017) Biogas Management: Advanced Utilization for Production of Renewable Energy and Added-value Chemical, *Frontiers in Environmental Science*, 5, 1-18

OPTIMIZATION OF HYBRIDIZATION FACTOR IN HYBRID ELECTRIC VEHICLES

Emre ARABACI[1], Bayram KILIÇ[2], Ali Özhan AKYÜZ[3], Afşin GÜNGÖR[4]

[1] Dr. Burdur Mehmet Akif Ersoy University.
[2] Dr. Burdur Mehmet Akif Ersoy University.
[3] Dr. Burdur Mehmet Akif Ersoy University.
[4] Dr. Akdeniz University.

INTRODUCTION

Vehicles usually use a single propulsion source. The propulsion sources used in today's cars are internal combustion engines and the main source of energy is oil-based fuels. In hybrid vehicles, the combination of two propulsion sources with different characteristics is used. These two propulsion sources for hybrid electric vehicles are internal combustion engine and electric motor (Arabaci, 2018). Approximately $1.3x10^{12}$ barrels of oil reserves are found in the world while oil consumption is $8.5x10^{7}$ barrels/day. According to this scenario, there are approximately 42 years of oil reserves. On the other hand, it is possible to say that the consumption of oil will be exhausted in a shorter period when the consumption is continuously increasing. Because of the new reserves, the increase in the rate of consumption unfortunately can not meet (Mi and Masrur, 2017). Approximately 60% of the oil is used for transportation (Owen et. al., 2010). During this use of oil, CO_2 concentration increases rapidly and causes global climate changes. For this reason, much effort has been made to reduce the use of electric vehicles, especially in recent years. Hybrid-electric vehicles are likely to become indispensable in the future due to the advantages they offer, although hybrid-electric vehicles are considered to be an important alternative for the use of electric vehicles in the future.

Today, the use of hybrid vehicles is two types. The first is an electric motor structure added to conventional vehicle technology and requires only gasoline or diesel as the energy source. In such vehicles, the electrical energy is generated by the generator in the vehicle and the main drive source in the vehicle is the internal combustion engine. The second is a complete combination of conventional vehicle and electric vehicle. For such vehicles, gasoline or diesel for the internal combustion engine, electrical energy is required to externally charge the batteries required for the operation of the electric motor. In these vehicles called plug-in hybrid, the main drive source is the electric motor. In short, hybrid electric vehicles are designs between conventional vehicles and electric vehicles (Figure 1).

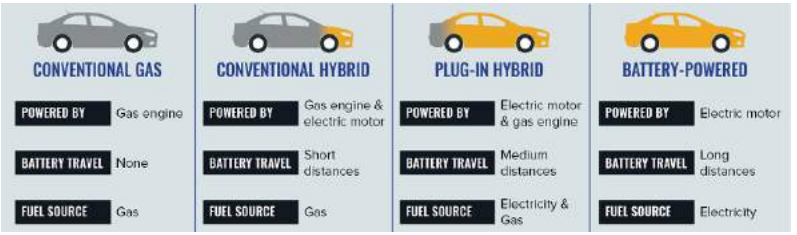

Figure 1. From conventional vehicles to electric vehicles (NYSERDA, 2019)

Hybrid vehicles have various configurations of the internal combustion engine and electric motor. These are called series, parallel and combined (or series-parallel). The main propulsion source in the series hybrid-electric

vehicles is the electric motor. The internal combustion engine only drives to a generator to charge the battery used to operate the electric motor. In parallel hybrid-electric vehicles, the internal combustion engine either moves the vehicle or charges the battery. Series-parallel hybrid-electric vehicles are combined with the advantages of series and parallel systems. Power-split mechanism is used for the system to work in series and/or parallel (Ehsani et. Al., 2018).

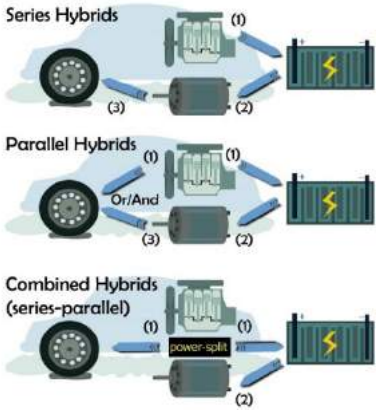

Figure 2. Electric motor-internal combustion engine configurations in hybrid electric vehicles

Although the exceptions are the main target in hybrid electric vehicles, fuel economy and the environment. Although electric vehicles today are considered as zero-emission, this situation may vary according to the way of production of electrical energy. The electric vehicle is considered as zero-emission because electrical energy is used. However, in order for these vehicles to be truly zero-emission, there must also be zero emission in the production of electrical energy. Today, industrial electricity is produced from various sources such as coal, natural gas, hydraulic, wind and solar. On the one hand, efforts are made to reduce the oil consumption, while on the other hand, efforts are made to produce the electricity we need most in clean ways. Figure 3 shows the annual CO_2 emissions equivalent to vehicle types for the USA. It is important to note that there is an indirect release of emissions from electric vehicles. If all of the electrical energy was obtained from clean energy sources, then the emission value for electric vehicles would be fueled to zero. When we look at the emission values of hybrid vehicles, it is seen that it is lower than the emission values of conventional vehicles.

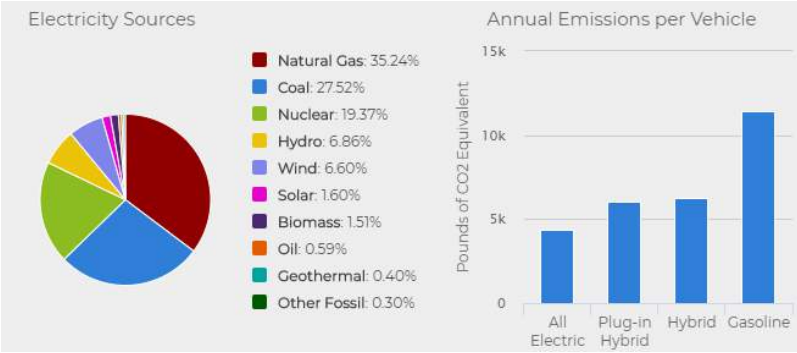

Figure 3. CO_2 equivalent emissions according to vehicle propulsion types (USDOE, 2019)

As long as the vehicles are operating internal combustion engines, pollutant exhaust gases (emissions) occur. Therefore, a vehicle standing in the red traffic light occurs a heavy emission (Yousef et al., 2010). It is known that CO_2 equivalent emissions are much more intense where there is traffic light. For this reason, various algorithms are developed for the coordination of traffic lights, and instant intelligent scenarios are created for traffic lights depending on traffic flow with the help of artificial intelligence applications. (Ferreira and d'Orey, 2012, Li and Shimamoto, 2011, Krajzewicz et al., 2015). One thing that is more dangerous than CO_2 in electricity production, especially in electric vehicles, is the process of recycling or disposal of the battery used in electrical storage. Recycling or disposal processes are applied to the batteries whose work life expires due to their chemical structures (Elwert et. Al., 2016, Ahmadi et. Al. 2017, Manzetti and Mariasiu, 2015).

Hybrid electric vehicles are a combination of the advantages of conventional vehicles and electric vehicles. The fact that hybrid electric vehicles have characteristics close to conventional vehicles or electric vehicles depends entirely on the strategies of the manufacturers. For this reason, hybrid electric vehicles have been categorized in a certain way (Figure 4).

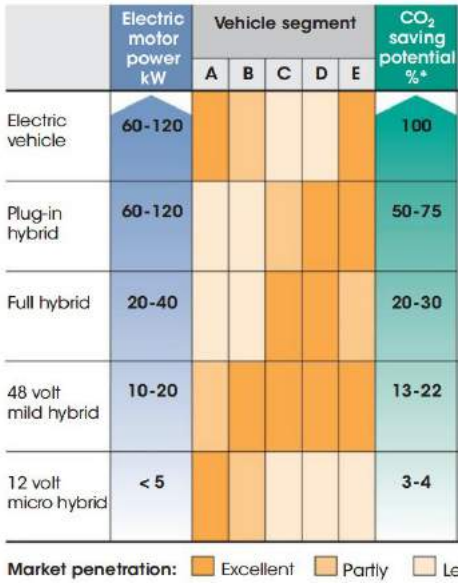

Figure 4. Categorization of hybrid-electric vehicles (X-engineer, 2019)

As is known, the reduction of CO_2 emissions in hybrid electric vehicles (with reduced fuel consumption), reduction of exhaust gas emissions and improvement of the power transmission system dynamics are the three main reasons for the development of these vehicles. Hybrid electric vehicles can be examined in four parts: micro, mild, full and plug-in. In micro hybrid electric vehicles which are accepted as the starting phase, idle stop-start system is used. The main purpose here is to stop the engine for a short time instead of idling the vehicle for short periods of time especially in the urban use. An economical and environmental contribution is made in terms of fuel burned during idle time. CO_2 emissions savings in micro hybrid electric vehicles are approximately 3-4%. At present, the electrical system in all cars, including micro-hybrid vehicles, has a voltage of 12V. In Mild hybrid vehicles, the electrical system is in the range of 48-160V. In this type of vehicles, besides the idle stop start system, electric torque assistance and regenerative braking systems are available. In the electric torque assistance system, the electric motor produced by the internal combustion engine of the vehicle also supports the electric motor. However, this torque support is only short-lived due to the operation of the electric motor with the battery. Regenerative braking system is used to charge batteries by using kinetic energy on wheels when the vehicle is wanted to slow down. In full and plug-in hybrid electric vehicles, the electrical system is in the range of 200-400V. In such hybrid electric vehicles, only electric motors can be driven without the use of an

internal combustion engine (Mi and Masrur, 2017). The comparison of hybrid electric vehicles according to various features is as in Table 1.

Table 1. Comparision of the hybrid electric vehicles

Parameter	Micro Hybrid	Mild Hybrid	Full Hybrid	Plug-in Hybrid
Battery voltage [V]	12	48–160	200–300	300–400
Motor power [kW]	2–3	10–15	30–50	60–100
Generator power [kW]	<3	10–12	30–40	60–80
EV mode range [km]	0	0	5–10	<50
Minimum battery state of charge [%]	80–90	40–60	30–50	10–20
Battery chemistry	lead-acid	Li-ion–NiMH	Li-ion	Li-ion

The classification of hybrid electric vehicles is a very superficial comparison. For this reason, the concept of hybridization factor has emerged for comparison of hybrid electric vehicles. Hybridization factor (*HF*) is a simple indicator of how much of the vehicle's power is supplied by an electric motor. The hybridization factor is definitely not a performance indicator and is only used for comparison of hybrid electric vehicles. The hybridization factor can be formulated as the ratio of electric motor power (P_{EM}) to total rated power of the vehicle ($P_{ICE} + P_{EM}$) of the vehicle (Mi and Masrur, 2017).

$$HF = \frac{P_{EM}}{P_{ICE} + P_{EM}} \tag{1}$$

Although the hybridization factor is expressed in such a simple manner, other parameters need to be considered for optimization of the hybridization factor.

NEW PERSPECTIVE FOR THE HYBRIDIZATION FACTOR

In order to examine the effects of the hybridization factor, catalog information of the vehicles used today is used as a reference (Ford, 2019, Toyota, 2019, Honda, 2019, Kia, 2019, Hyundai, 2019) (Table 2).

Table 2. Some of today's hybrid electric vehicles

Brand Model	Stroke volume (dm^3)	Maximum Power (kW)			*HF* (%)		
		Total Power	Internal Com. Engine	Electric Motor	Desired	Actual	Success
Toyota Yaris	1.5	74	54	45	60.8	45.5	74.8
Toyota Auris	1.8	90	72	53	58.8	42.4	72.1
Toyota Prius	1.8	90	72	53	58.8	42.4	72.1
Ford Fusion	2.0	138	104	88	63.8	45.8	71.7
Hyundai Ioniq	1.6	104	77	32	30.8	29.4	95.5
Kia Niro	1.6	104	77	32	30.8	29.4	95.5
Honda Accord	2.0	156	105	133	85.3	55.9	65.5

The total power (P_{tot}) value is expected to be equal to the maximum power (P_{EM}) of the electric motor and the maximum power (P_{ICE}) of the internal combustion engine. However, Table 2 shows $P_{tot} < P_{ICE} + P_{EM}$ (Figure 5).

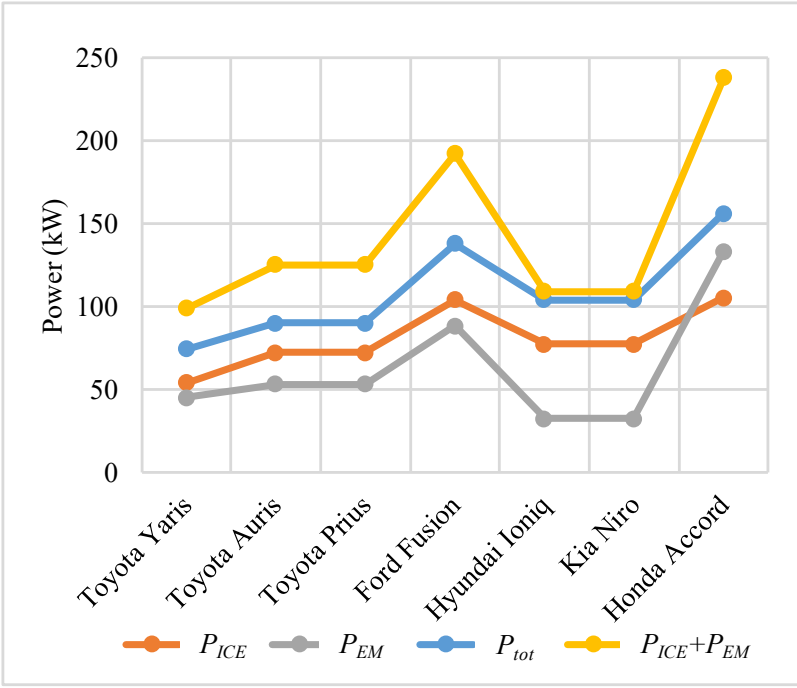

Figure 5. Power components in hybrid electric vehicles

When calculating *HF* according to Eq. 1, $P_{ICE} + P_{EM}$ is used instead of P_{tot}. This is due to the characteristic structure of internal combustion engine and electric motor. While the electric motors can operate at a constant power after a certain engine speed, the maximum power in the internal combustion engines corresponds to a single engine speed. Given the advantageous operating conditions of the electric motor and the internal combustion engine, this is never possible when both internal combustion engine and electric motor are desired to operate in maximum power. Theoretically, in the case of $P_{tot} < P_{ICE} + P_{EM}$, *HF* reaches the maximum value. Therefore, the *HF* value calculated by Equation 1 is actual *HF* (HF_{actual}). However, although such a description is not included in the literature, P_{EM} / P_{tot} is the desired *HF* ($HF_{desired}$), and the ratio of these two HFs ($HF_{actual} / HF_{desired}$) can be called *HF* success ($HF_{success}$) (Figure 6). $HF_{success}$ value here is a relative definition. Therefore, the high $P_{ICE} + P_{EM}$ value of the vehicle does not indicate that the vehicle will perform well.

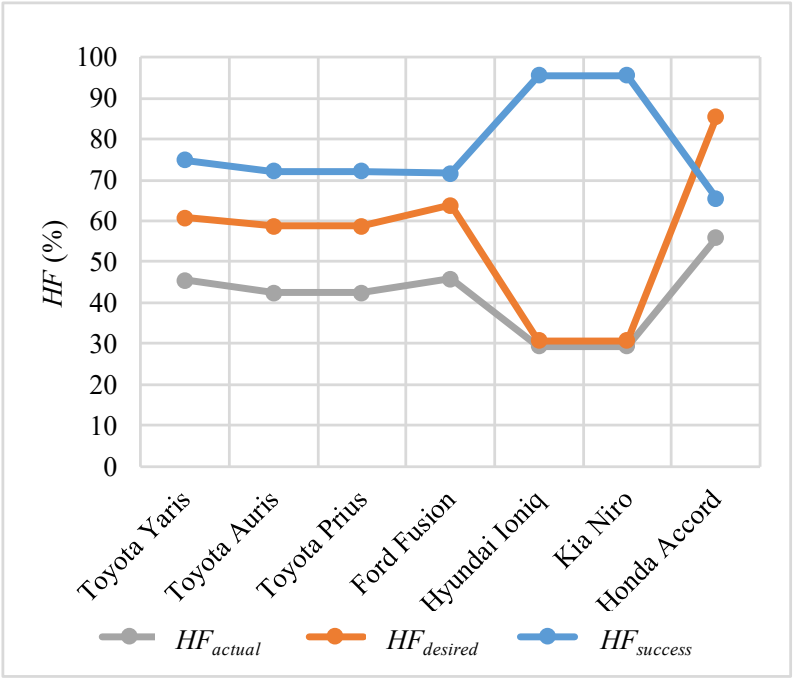

Figure 6. Hybridization factors

As shown in Figure 6, the Hyundai Ioniq and Kia Niro's HF_{actual} values are lower than others but the $HF_{success}$ values are higher than others. However, although the HF_{actual} value of the Honda Accord is higher than the others, the $HF_{success}$ value is lower than the others. For high HF_{actual} value, P_{ICE} / P_{EM} should be as low as possible (Figure 7).

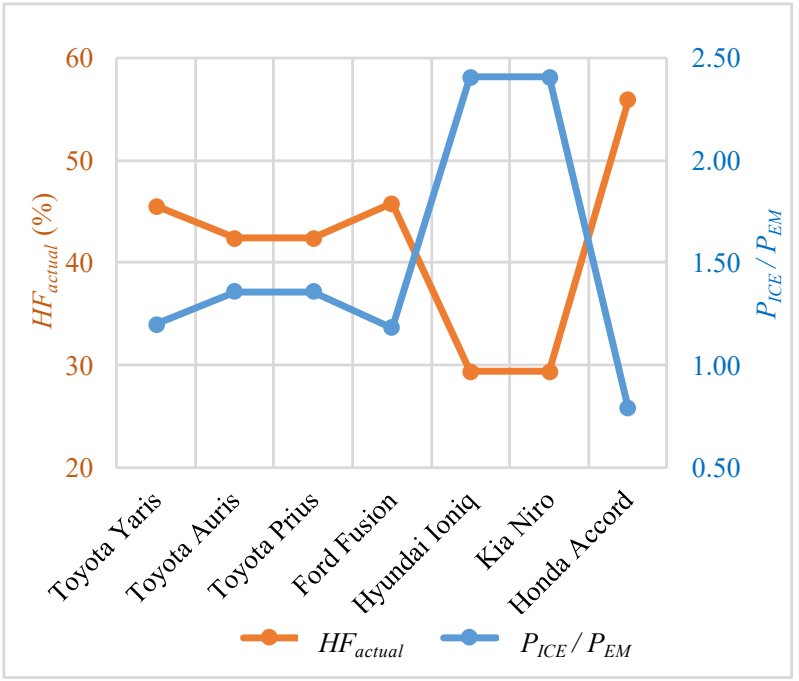

Figure 7. Effect of power ratio (P_{ICE} / P_{EM}) on actual hybridization factor (HF_{actual})

Fuel economy is the foremost in hybrid vehicles. The lower the dependence on the internal combustion engine, the more fuel economy is improved. However, since the electric motor is connected to the battery, the range of the vehicle that can be obtained by the electric motor varies according to the battery capacity. In this case, it is necessary to increase the battery capacity while fuel economy is desired. Battery capacity and volume increase with increasing battery capacity. Therefore, only the improvement of the fuel economy of a hybrid electric vehicle with an electric motor seems to be partly mulled. In order to eliminate this problem, the internal combustion engine must have a high economy. Studies on internal combustion engines continue at high speed. These studies are followed for the production of hybrid electric vehicles. As is known, internal combustion engines are tried to be optimized in the performance-economy-environment triangle. To improve one side of the triangle, the other two may have to be sacrificed in part. In hybrid electric vehicles, Atkinson cycle gasoline engines are especially preferred for their high thermal efficiency. However, although such engines are advantageous in terms of fuel economy, their power relative to the stroke volume is not as high as expected. In engine technology, the ratio of maximum engine power to stroke volume is defined as power

density. Atkinson cycle gasoline engines have high fuel economy, but their power density is low. In today's conventional gasoline engines, the power density is between 60-65 kW/L and in conventional gasoline engines with overfill power density is between 70-85 kW/L. However, the power density in hybrid electric vehicles is quite low compared to conventional engines as shown in Figure 8.

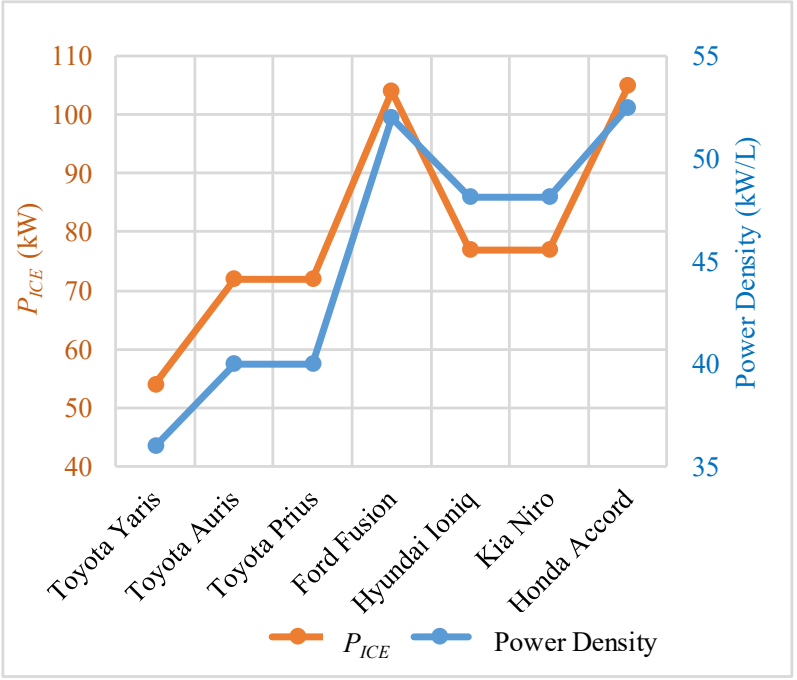

Figure 8. Power density of internal combustion engines in hybrid electric vehicles

Although the power density does not directly affect *HF*, P_{EM} may be lower as the weight decreases as the engine volume decreases for the same power, and therefore the lower capacity battery can be used. In this case, a hybrid electric vehicle with the same fuel economy but low *HF* is obtained.

CONCLUSION

Although a large part of today's vehicles are condemned to petroleum-derived fuels, it is inevitable that we are not fully ready for electric vehicles. While fuel economy in hybrid electric vehicles is at the forefront, high performance demand is also expected. For this reason, the internal combustion engine must work in perfect harmony with the electric motor. Although the characteristics of the electric motor and the internal

combustion engine do not resemble each other, this characteristic is as similar as possible in the particular operating range in terms of both fuel economy and performance. Although the concept of hybridization factor has been developed for this purpose, this concept alone can be misleading about the economy and performance of hybrid electric vehicle. In addition to the hybridization factor, the evaluation of other important details is of vital importance for optimization of the hybridization factor.

REFERENCES

1. Arabaci, E. (2018) Investigation of The Power Split Mechanism in Serial-Parallel Hybrid Electric Vehicle Depending on The Engine Speed Variation. *Ömer Halisdemir University Journal of Engineering Science*, *8*(1), 394-404.
2. Mi, C., & Masrur, M. A. (2017). *Hybrid electric vehicles: principles and applications with practical perspectives*. John Wiley & Sons.
3. Owen, N. A., Inderwildi, O. R., & King, D. A. (2010). The status of conventional world oil reserves—Hype or cause for concern?. *Energy policy*, *38*(8), 4743-4749.
4. NYSERDA, New York State Energy Research and Development AuthorityAbout electric cars, https://www.nyserda.ny.gov/All-Programs/Programs/Drive-Clean-Rebate/About-Electric-Cars/Types-of-Cars, accesed: May 10, 2019.
5. Ehsani, M., Gao, Y., Longo, S., & Ebrahimi, K. (2018). *Modern electric, hybrid electric, and fuel cell vehicles*. CRC press.
6. USDOE, Electric vehicle emission, https://afdc.energy.gov/vehicles/electric_emissions.html, accesed: May 10, 2019.
7. Yousef, K. M., Al-Karaki, M. N., & Shatnawi, A. M. (2010). Intelligent traffic light flow control system using wireless sensors networks. *J. Inf. Sci. Eng.*, *26*(3), 753-768.
8. Ferreira, M., & d'Orey, P. M. (2012). On the impact of virtual traffic lights on carbon emissions mitigation. *IEEE Transactions on Intelligent Transportation Systems*, *13*(1), 284-295.
9. Li, C., & Shimamoto, S. (2011). An Open Traffic Light Control Model for Reducing Vehicles'$\hbox {CO} _ {2} $ Emissions Based on ETC Vehicles. *IEEE transactions on vehicular technology*, *61*(1), 97-110.
10. Krajzewicz, D., Wagner, D., Woelki, M., & Dippold, M. (2015). Driving patterns reducing pollutant emission at traffic lights. In *ITS World Congress*.
11. Elwert, T., Goldmann, D., Römer, F., Buchert, M., Merz, C., Schueler, D., & Sutter, J. (2016). Current developments and challenges in the recycling of key components of (hybrid) electric vehicles. *Recycling*, *1*(1), 25-60.
12. Ahmadi, L., Young, S. B., Fowler, M., Fraser, R. A., & Achachlouei, M. A. (2017). A cascaded life cycle: reuse of electric vehicle lithium-ion battery packs in energy storage systems. *The International Journal of Life Cycle Assessment*, *22*(1), 111-124.
13. Manzetti, S., & Mariasiu, F. (2015). Electric vehicle battery technologies: From present state to future systems. *Renewable and Sustainable Energy Reviews*, *51*, 1004-1012.
14. X-engineer, 2019, categorization of hybrid-electric vehicles, https://x-engineer.org/automotive-engineering/vehicle/hybrid/mild-hybrid-electric-vehicle-mhev-introduction/, accesed: May 10, 2019.
15. Toyota, https://www.toyota-europe.com/#, accessed: May 10, 2019.
16. Ford, https://www.ford.com/cars/fusion/models/fusion-hybrid-se/, accessed: May 10, 2019.
17. Hyındai, https://www.hyundai.com/worldwide/en/eco/ioniq-hybrid/highlights, accessed: May 10, 2019.
18. Honda, https://global.honda/products/automobiles.html, accessed: May 10, 2019.
19. Kia, http://www.kia.com/worldwide/main.do accessed: May 10, 2019.

STARCH USAGE IN PAPER INDUSTRY

Öznur ÖZDEN [1], Sinan SÖNMEZ [2]

[1] Asst. Prof. Dr., Istanbul University-Cerrahpasa, Faculty of Forest, Forest Products Chemistry and Technology, Istanbul, Turkey.

[2] Assoc. Prof. Dr., *Corresponding author*, Marmara University, School of Applied Sciences, Department of Printing Technologies, İstanbul, Turkey.

INTRODUCTION

Paper and paper products have been a great facilitator for humanity since the beginning of use. Paper is an important product that has entered our lives in many fields from daily life to industrial products.

For the production of paper, firstly suitable fibers are needed for end use. Then the filling material, binder and additional materials are required. The most commonly used fillers are kaolin and calcium carbonate. Resins are used as binder. In the beginning, while natural resins were used and Alkyl Ketene Dimer (AKD) ve Alkenyl Succinic Anhydride (ASA) resins were used today (Roberts, 1991).

Besides these, one of the most used chemical substances is starch. The starch is highly used in the paper industry due to the features listed below

- Being a low cost and renewable connector
- Viscosity can be controlled
- Water retention properties
- Specific electrostatic charge
- Film formation and bonding after drying

These performances of starches are increased by chemical or physical modification (Maurer, 2001).

Parts of starch used during paper making and features gained on paper are shown in Table 1.

Table 1: Starch and papermaking

Cellulose Fillers Starch additives	Wet End	Spray starch	Surface starch	Coating
Process	Paper formation Retention Dry strength	Improve surface strength Improve ply bond Improve internal bond	Improve printing Improve surface strength Fill voids	Improve optical Printing and Functional properties
Starch	Cationic Amphoteric	Unmodified starch Polymers	Oxidized Enzyme converted Other modified Specialty	Starch and Latex mixtures with fillers
Typical Uptake	0.3-2%	1-4%	2-6%	0.5-2.0%

Sources:http://www.tongaathulettstarch.co.za/downloads/Papermaking%20surface%20size%20starch.pdf

Basic application areas during paper making process for starch;

- Starch, flocculation agent during the creation of paper draft, helps retention and drainage, carrier for alkali glue. It also increases internal resistance.
- Surface binder on the surface plate are used as a binder to improve the stiffness of the fibers and to improve the hardness, resistance properties and dimensional stability of the paper, and to improve the printability of offset printing.
- It is used in conjunction with latex-type connectors to connect pigments to each other and to the surface in coating. This increases surface brightness and smoothness for high print quality (Johnston, 2002).

1. STARCH

Starch is a natural polymer whose molecular weight is very high which molecule formula is $(C_6H_{10}O_5)_n$. Color varies between white and camel hair. They are sold in powder, bead or crystal form. It is used in paper mills to improve dry strength and paper surface (Biricik et al., 2011). The native starch has a very high viscosity.

On the other hand, modified starch has a lower viscosity. The main sources of starch are regular maize, tapioca, waxy maize, wheat and potatoes. After cellulose fiber and mineral filler, starch is the third most common raw material in paper mill industries (Holik, 2006).

Starch is produced as a result of photosynthesis from the leaves of green leafy plants and stored as spare nutrients. Starch, which is one of the renewable agricultural products, is stored in the roots, tubers and seeds of easily grown plants. Starch, which is a carbohydrate depot of plants, is a high molecular weight polymer of α-β glucose.

It forms in the form of thin white granules in various parts of plants. Enzyme-catalyzed, called the process of photosynthesis as a result of starch (Pérez et al, 2009).

$$6H_2O + 6CO_2 \xrightarrow{\text{light / chlorophyll}} C_6H_{12}O_6 + 6O_2$$

Water + carbon dioxide → Glocose + oxygen

$$nC_6H_{12}O_6 \xrightarrow{\text{enzymes}} (C_6H_{12}O_6)_n + H_2O$$

Glucose → Starch + Water

The main sources of commercial starch are corn, potatoes and waxy maize. The components of some starch sources are shown in Table 2.

Table 2: Composition of starch sources

Source	**Moisture %**	**Starch %**	**Protein %**	**Fiber %**	**Fat %**	**Ash %**
Corn	16,7	60,0	8,3	2,2	4,0	1,2
Grain sorghum	15,5	62,0	9,5	2,2	3,1	1,3
Wheat	12,5	59,0	10,4	2,2	1,7	1,7
Rice, polished	12,0	75,0	7,5	0,6	1,7	1,1
Potatoes	78,0	16,5	2,2	0,4	0,1	-
Sweet Potatoes	64,5	25,5	1,5	0,9	0,6	0,9
Tapioca roots	68,0	25,0	3,0	2,0	0,5	1,0
Sago palm, palm trunk	50,0	40,0	-	-	-	-
Bananas, green	77,6	14,6	1,6	-	-	-

(Do not total 100% because of water-soluble and unidentified materials) **Source:** Maurer, 2001

Amylase and amylopectin ratios in the structure of starches are also an important feature that affects their behavior. Table 3 shows the contents of amyloses and amylopectin of some starches.

Table 3: Amylose and amylopectin content of starches

Starch	Amylose Avg. %	Degree of Polimerization	Amylopectin, %
Corn	28	800	72
Potato	21	3000	79
Wheat	28	800	72
Tapioca	17	3000	83
Waxy maize	0	-	100
High-amylose corn	40-70	600	30-60
Grain sorghum	25	800	75
Waxy grain sorghum	0	-	100
Rice	17	-	83
Sweet potato	20	-	80
Sago palm	27	740	83
Banana	20	-	80

Source: Maurer, 2001

All starches are usually a combination of two basic fractions, a linear molecule amylose and a highly branched polymer amylopectin (Figure 1 and 2) Each glucose unit constituting the starch potentially has three reactive hydroxyl groups which form the basis of all derivatization.

Amylose contains almost all 1-4α-glycoside chains. Amylopectin contains is mostly 1-6α glycosidic chains with 1-4α-glycoside chain at the branching point. As good as for polymerization, average ratio of Amylopectin to amylose for various starches is different (Bello-Perez et al. 2010).

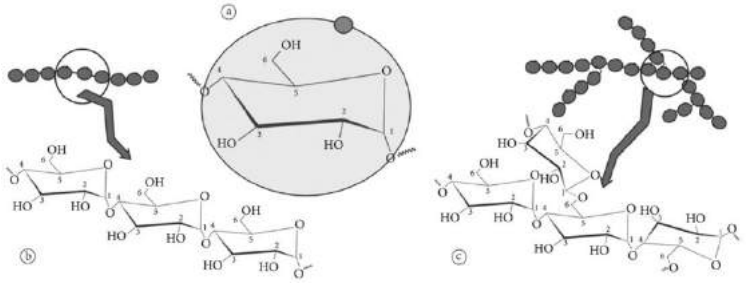

Figure 1. (a) Glucose units, (b) Amylose and (c) Amylopectin structure.of starch (Alcázar-Alay and Meireles, 2015)

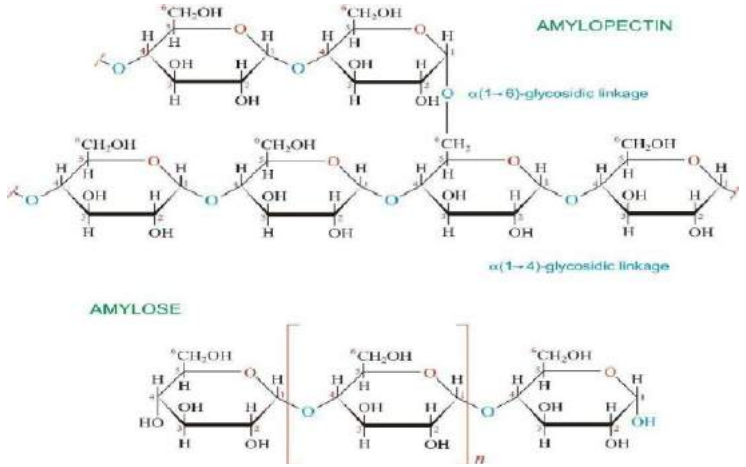

Figure 2. Amylopectin and Amylose structure of starch (Korma et al., 2016)

The presence of both linear (amylose) and branched (amylopectin) molecules in starch has a different structure than cellulose, with molecular weight of several hundred thousand to several million, respectively. Amylopectin is branched through the primary hydroxyl, which is a branching point for the mainly each 18 to 27 glucose units (Tester et al., 2001).

By means of starch hydroxyl groups provides resolution in polar solvents, including hot water. However, the molecular size and the amount of the amylose component to form gels or precipitates depending on the concentration.

The high molecular weight and hydrogen bonding properties of starch are effective in internal bonding (interfiber). In general, the conditions used in the dissolution of the starch, which are normally dispersed in water for 15 to 30 minutes at 92 ° C do not cause significant hydrolysis (Hofreiter, 1981).

The use of starches in natural form, high viscosity in low dry matter and poor viscosity stability (retrogradation) affect. Modified starch and derivatives are used to overcome these.

2. RETROGRADATION

Starch granules in a living plant are formed result by enzymatic synthesizes. Glucose molecule chains are arranged in a regular structure. This H-bound regular structure needs to be disturbed for to cook and disperse starches. As a result of cooking, this structure breaks down and water molecules are introduced into starch molecules. At this point the molecular speed is quite high and the gelatinized starch is in liquid form. Retrogradation is a process which occurs when the starch dispersion is reversed and the temperature decrease and the starch pastes age. Retrogradation is the reversion of this process (Figure 3) In another sense,

recycling process is a starch molecules are reorganized and the water molecules are removed and the new H-bonds are formed. But, the most important point here is that reorganization will not take place in a systematic manner and that the starch can never return to the original granule structure.

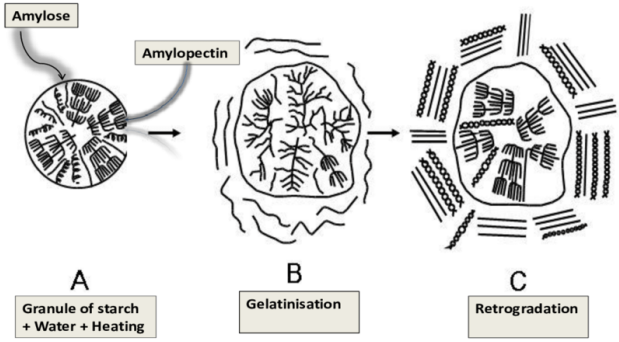

Figure 3: Starch retrogradation (Sukhija et al., 2015).

Retrogradation trends should also be taken into consideration in the selection of starches to be used.

The gelling formed as a result of retrogradation is completely dependent on the molecular structure. The flat chain amylose is independent of branched points. Therefore, another amylose molecule with immediately it can form H- bonds (Wagoner and van der Burg, 1990). Modification processes are oxidation, acidification, hydroxylation and enzyme (Higham, 1963).

3. MODIFIED STARCHES

Although natural starch is cheap and abundant, it is not suitable for the requirements of modern industrial processes due to limitations in physicochemical properties. The industrial problems caused by natural starches are mostly composed of their solutions and flakiness viscosity, the change in temperature, the pH and the salinity. These problems can be ameliorative and in some cases chemically modified starch by using or using alternative plant, algae and microbiol polysaccharides to overcome problems (Cleary, 1980). Although the natural starch is consumed in large quantity, the majority of the starch produced is chemically modified to meet special industrial requirements.

3.1. Modified Starch Varieties

3.1.1. Acid modified starch

The acid modified starch is produced by hydrolytic degradation of the starch molecules with a strong acid in low concentration (~% 3 HCI) treatment (Wurzburg, 1986). Acid modified starches show an unstable structure. This is due to the production of low molecular weight straight chain molecules in acid hydrolysis.

3.1.2. Oxidized starch

As suggested, the mechanism of gel formation and retrogradation degradation are due to the association (hydrogenation) of hydrogen bonds between hydroxyl groups in amylose chains. (Elder and Schoch,1959).

Oxidation of only a few of these hydroxyl groups appears to be sufficient to prevent intramolecules fusion for merger. As a result, oxidized starch gelation is weaker than the actual starch, but the solutions are less sensitive to retrograde.

The oxidized starch is generally produced by treatment with an alkali starch suspension by means of an oxidation to form carboxyl and carbonyl groups (Figure 4) The oxidation agent generally sodium hypochlorite. However other markers are used. The most well-known are periodic acid and potassium permanganate (Knight J.W.,1969). However, the products of hypochlorite oxidation are complex and irregular, the periodic acid specifically binding the oxidized starch between the 2nd and the 3rd carbons of the D-Glucopyranose unit to the dialdehyde products.

The paper industry is the consistently the largest consumer of dialdehyde starch. Starch is used in the paper industry to increase the wet strength of special papers such as wrapping paper, paper towels, sanitary towels and map papers (Radley, 1976). Wet strength and improved structure consist of cross-linking between hydroxyl groups of cellulose and carbonyl groups of dialdehyde starch (Kennedy et al., 1990).

The oxidation process is obtained by treating the starch suspension with sodium hypochlorite solution having 6-9% of the available chlorine. The presence of carboxyl and carbonyl groups substantially hinders the retrogradation event. The reaction mechanism is shown in the Figure 4 .

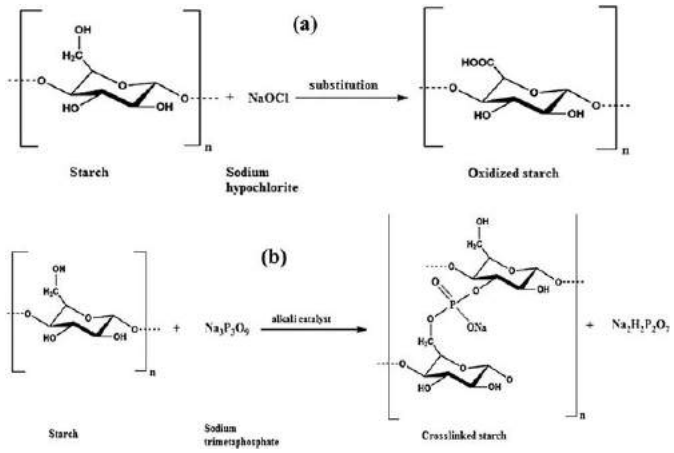

Figure 4: Oxidation of Starch with NaOCI (Sukhija et al., 2015).

Oxidation results in a decrease in the degree of oxidation of the starch in the gelation temperature compared to the degree of oxidation. In a decrease of peak viscosity parallelism showed. The dispersed starch is characterized by a more stable structure and a decrease in viscosity.

4. STARCH DERIVATIVES

In some chemicals of the 3-OH groups in each glucose unit, displacement reactions take place. In these reactions, starch group OH- and group H are replaced by starch ether or esters.

4.1. Hydroxyethylated Starch

The hydroxyethylation process takes place in a reaction as follows.

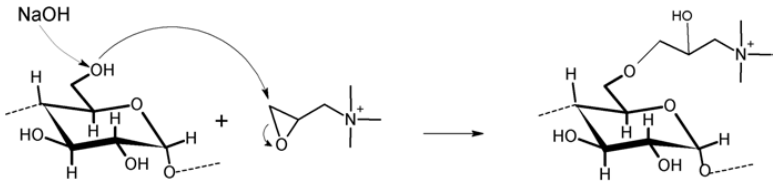

Figure 5: Synthesis of 2-hydroxy-3-(trimethylammonium) propyl starch (López et al., 2008).

These reactions can be catalyzed with alkaline metal hydroxide. Hydroxyethylated treated starches have a great tendency to swell. Gelling temperatures are also reduced according to the degree of hydroxyethylation.

4.2. Cationic Starch Ethers

Cationic starches are similar way with obtained by starch process with chemicals which give cationic substitution group to the OH group via ether linkage (Figure 6). This reaction is carried out as follows.

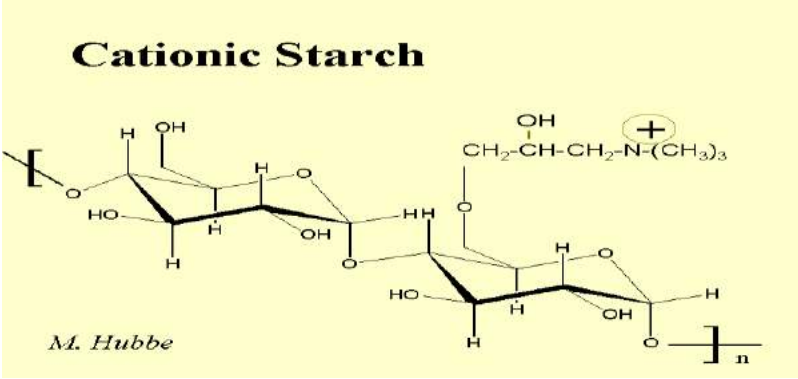

Source: https://projects.ncsu.edu/project/hubbepaperchem/CST.htm

Figure 6: Cationic starch

Cationic starches are important industrial derivatives in which starch yields a positive ionic charge, including ammonium, amino, imino, sulfonium or phosphonium groups. Cationic starches exhibit higher solubility and dispersibility with improved clarity and stability.

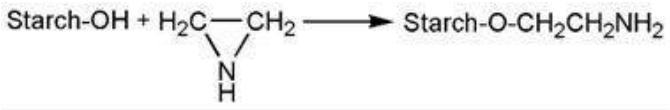

Figure 7: Starch reacts with ethyleneimine to produce amino-ethylated Starches (Xie et al., 2005)

Common usage cationic starches are quaternary amino derivatives that are naturally cationic with quart amino derivatives (the acidic medium is desired to generate cationic charge). These starches have a lower gelling temperature than the starch they produce.

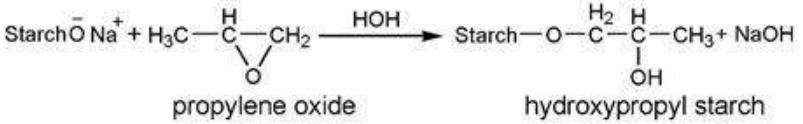

Figure 8: The reaction of propylene oxide with starch under alkaline conditions (Xie et al., 2005)

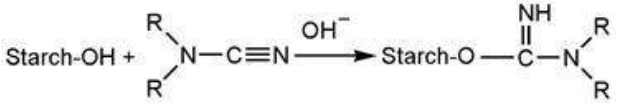

Figure 9: Reaction of starch and dialkyl cyanamides at pH 10 to 12 to produce iminoalkyl starches (Xie et al., 2005)

4.3. Starch Esters

The starch ester is a modified starch in which some hydroxyl groups are substituted with ester groups. The esterification is to give hydrophobic properties to starch products thanks to the free available hydroxyl groups. (Xie et al., 2005) Most commonly used are acetylated starch esters. This starch is obtained by treatment with acetic anhydride. Acetate groups largely to hinder starch retrogradation. Starch esters have a tendency to diesterify under acidic and alkaline conditions and form acetic acid. Starch esters, acid anhydrides, octenyl succinic anhydride (OSA), dodecenyl succinic anhydride (DDSA) are synthesized with various reagents such as fatty acids and fatty acid chlorides.

Figure 10: Starch acetates prepared by reacting starch with acetic anhydride (Yan and Zhengbiao, 2010).

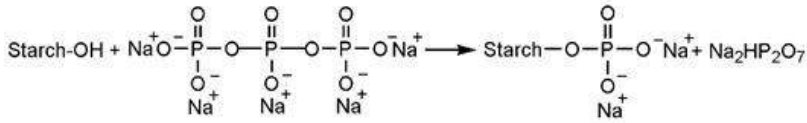

Figure 11: Phosphate monoester of starch prepared by reacting starch with sodium tripolyphosphate (Xie et al., 2005)

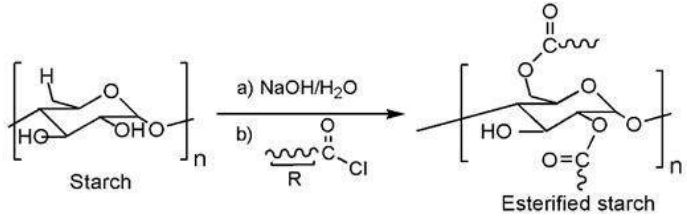

Figure 12: Scheme for reaction of starch with fatty acid chlorides (R: C8, C12, C16) (He et al, 2007).

5. MODIFIED STARCH PROPERTIES

The natural properties of the starches are changed to make a polymer suitable for coating. Each process offers different features. We can explain them as described below.

Hydroxy ethylated starches have excellent water retention and film-forming properties and are flexible. They are used in high quality glossy paper types (Guarás, 2017).

Starch esters are mostly used in surface sizing. But they are also used as coating binder. They have good film outcome properties and attitude. They cannot penetrate well into the laminate (Maurer, 2009).

Cationic starches significantly affect anionic pigments and fibers. They react with anionic materials and clearly increase viscosity in the coating paint. Therefore, it is necessary to apply special methods to minimize this effect.

Oxidized starches are a good coating binder and assist in the coating balance. Oxidized starches give good films. They have very good resistance properties and ease of penetration into laminate (Higham, 1963).

Acid modified starches are low in binder due to fast retrogradation and unstable coating viscosity (Radley, 1954). Therefore, they are not widely used in coating. Although thermally generated (thermal) enzymes are suitable for coating, they reduce to results strength due to their low molecular weight.

6. AREAS USED IN PAPER AND PROPERTIES

Industrially produced starches for use in paper and cardboard are also chemically modified. Thinned starches with the acid are of low viscosity. This restricts the use in paper mills, but firstly surface gluing and oxidized starches are used more as surface glue in the press.

Different types of starches have been used in paper machines for years to increase the resistance properties of paper. Initially, natural starches were added to the wet portion to improve resistance, but this type of starch showed a low affinity for cellulosic fibers. It also causes a high BOD load in the waste water. For this reason, the use of cationic starch is preferred for strength

improve. The most commonly used cationic starches cause a significant improvement in dry strength. Cationic starches are added to the system in stock for maximum strength improvement.

The use of high levels of anionic starch in new systems developed for the use of anionic starches is achieved by a combination of PAC / polyDADMAC (Johnston, 2002).

During the production of paper, cereal products at wet-end are used root and tuber starches, gums and their chemical derivatives. The use amounts of these substances continue to increase in parallel with paper production.

In these substances, starch is a complex but very valuable material. Industrially used in a many areas of starch is the most widely used paper industry.

Starch is a basic substance used in various stages of paper production (bleached, unbleached, coating, uncoated, mechanical or chemical, printing paper or wrapping paper) It is used as glue are used corrugated cardboard as binder for bonding, glomeration and reaction matter. It is used during the production and after surface treatments to improve the properties of the paper. It is also used as glue in corrugated cardboard production (Bajpai, 2015).

According to CEPI data, the largest starch user in Europe is the paper industry. In 2002, about 2 million tons of maize, wheat and potato starch were used in the paper and cardboard production and recycling products in the European paper industry. In the coming years, the consumption of starch will continue in parallel with the glossy paper and paper recycling.

Starch and other additives improve the properties of paper and paperboard. It is used in papermaking processes, for coating purposes or for bonding. It strengthens the packaging products or improves the surface smoothness, gloss and opacity of the paper for better printability (CEPI, 2003).

7. STARCH USAGE IN THE CORRUGATED CARDBOARD PRODUCTION

Corrugated cardboard consists of gluing a corrugated sheet of paper between two flat layers. In the corrugated cardboard production is a need for a glue to bond the layers together. For the bonding of these layers, starch is used as adhesive. The corrugated cardboards are one of the most important implementation areas of starch glues (Chenier, 2002). It is the main component of adhesives used in the construction of corrugated cardboard.

The starch and dextrin adhesives are not preferred because due to their slow adhesion rate and contain excess water. Therefore, The Stein Hall process is used which a two-phase system. Accordingly, in the first phase, starch is mixed with water and caustic so that the gelatinized starch adhesive is formed.

In the second phase, starch is cooked with water and borax mixture to form starch adhesive and then two phases are mixed (Cornell and Hoveling, 1998).

Here, glue of %20 dry material content is used in the mixture of uncooked starch (4 part) and cooked starch (1 part). In addition, the sodium hydroxide in the formula allows the starch to be easily gelatinized in the hot pan portion of the corrugated cardboard machine. The borax ratio of sodium hydroxide is also important at this time.

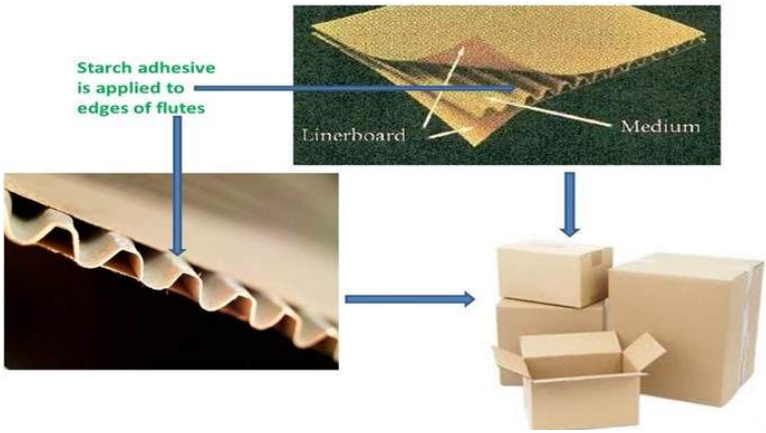

Source: https://polymerinnovationblog.com/second-generation-biomass-feedstock-7-past-prologue/

Figure 13: Processing of starch glue on corrugated cardboard

8. STARCH USAGE IN PAPER AND CARDBOARD SURFACE SIZING

Surface sizing is the process of applying a sizing agent material to the paper or cardboard surface using suitable systems. The task of surface sizing is to improve the appearance and printable properties of paper and cardboard products (Zijderveld and Stoutjesdijk, 1976). Natural or synthetic binders are used as surface sizing agent. Sodium Carboxymethyl Cellulose (SCMC) and Polyvinly Alcohol (PVOH) as well as starches are naturally used.

Today, size presses are the most widely used machine for surface sizing on the machine. Today, they are made more useful by making additions to the size presses. The use of starch as a surface binder improves the quality of paper or cardboard.

REFERENCES

1. Alcázar-Alay, S. C., Meireles, M. A. A. (2015). Physicochemical properties, modifications and applications of starches from different botanical sources, Food Science and Technology, 35 (2), 215-236.
2. Bajpai, P. (2015). Pulp and paper chemicals, in Pulp and paper industry: chemicals, Chapter 3, Elsevier, U.S., 82-87.
3. Bello-Perez, L. A., Rodriguez-Ambriz, S. L., Sanchez-Rivera, M. M. and Agama-Acevedo, E. (2010). Starches characterization, properties, and applications: Starch macromolecular structure, Chapter 3, Andréa C. Bertolini (ed.), CRC Press, USA, 33-58.
4. Biricik, Y., Sonmez, S. and Ozden, O. (2011). Effects of surface sizing with starch on physical strength properties of paper, Asian Journal of Chemistry, 23 (7), 3151-3154.
5. CEPI (Confederation of European Paper Industry) (2003), The European Paper Industry & the Starch Issue www.cepi.org
6. Chenier, P. J. (2002). Coating and adhesives, in Survey of industrial chemistry, Chapter 19, Springer Science+Business Media, USA, 360
7. Cornell, H. and Hoveling, A. W. (1998). Chemically modified wheat starches and their uses, in Wheat: chemistry and utilization, Chapter 6, Technomic Publishing AG, Switzerland, 226-227.
8. Elder, A. L. and Schoch, T. J. (1959). Measuring the useful properties of starch, Cereal Science Today 4(7), 202-208.
9. Guarás, M. P., Luduena, L. N. and Alvarez V. A. (2017), Development of biodegradable products from modified starches, in Starch-based materials in food packaging: Processing, characterization and applications, Chapter 4, Silvia E. Barbosa, Maria A. García, Luciana Castillo, Olívia V. Lopez (eds.), Academic Press, London, 80-81.
10. He, J., Liu, J. and Zhang, G. (2007). Slowly digestible waxy maize starch prepared by octenyl succinic anhydride esterification and heat–moisture treatment: Glycemic response and mechanism, Biomacromolecules, 9 (1), 175-84.
11. Higham, R. R. A. (1963), A Handbook of papermaking, the technology of pulp, paper and board manufacture, Second Edition, Business Books Limited, London, England.
12. Hofreiter, B. T. (1981). Natural products for wet-end addition, starch for wet-end, in Pulp and paper chemistry and chemical technology, James P. Casey (ed.), Chapter 3, Third Edition, Volume III, John Wiley&Sons, USA, 1475-1500.
13. Holik, H. (2006). Handbook of paper and board, Wiley, Germany, 358-359.
14. Johnston, H. (2002). A novel approach to improve dry strength, APPW2002 (African pulp and paper week2002)" Adding value in a global industry", TAPPSA Journal Papers, Durban.
15. Kennedy, J. F., Stevenson, D. L. and Junel, K. (1990). An objective illustration of the inadequacy of the official EC "Ewers" method for the determination of starch, Starch, 42 (1), 8-12.
16. Knight J. W. (1969). The starch industry, Pergamon Press, Oxford.
17. Korma, S. A., Alahmad, K., Niazi, N., Ammar, A.F., Zaaboul, F., and Zhang, T. (2016). Chemically modified starch and utilization in food stuffs, International Journal of Nutrition and Food Sciences, 5(4), 264-272.
18. Lopez, O. V., Garcia, M. A. and Zaritzky, N. E. (2008). Film forming capacity of chemically modified corn starch, Carbohydrate Polymers, 73 (4), 5, 573-581
19. Maurer, H. W. (2009). Starch in the paper industry, in Starch chemistry and technology, Chapter 18, James BeMiller and Roy Whistler (eds.), Academic Press, USA, 693-695.

20. Maurer, H. W. (2001). Manufacture and composition of unmodified starch, in Starch and starch product in surface sizing and paper coating, Chapter 4, Tappi Press, USA, 25-29.
21. Pérez, S., Baldwin, P. M. and Gallant, D. J. (2009). Structural features of starch granules I, in Starch chemistry and technology, Chapter 5, James BeMiller and Roy Whistler (eds.), Academic Press, USA, 149-188.
22. Radley, J. A. (1954). The paper industry, in Starch and its derivatives, Chapter 2, John Wiley & Sons Inc., USA, 243-261.
23. Roberts, J. C. (1991). Paper chemistry: Neutral and alkaline sizing, John Christopher Roberts (ed.), Blackie, Newyork, USA,114-130.
24. Robles-Ramírez, M. C., Flores-Morales, A, and Mora-Escobedo, R. (2012). Corn Tortillas: Physicochemical, structural and functional changes, in Maize cultivation, uses and health benefits, Chapter 7, Jose C. Jimenez-Lopez (Ed.), Nova publishers, Newyork, USA, 98.
25. Sukhija, S., Singh, S., Riar, C. S. (2015). Effect of oxidation, cross-linking and dual modification on physicochemical, crystallinity, morphological, pasting and thermal characteristics of elephant foot yam (Amorphophallus paeoniifolius) starch, Food Hydrocolloids 55, 56-64.
26. Tester, R. F., Debon, S. J. J., Qi, X., Sommerville, M.D., Yousuf, R. and Yusuph, M. (2001). Amylopectin crystallisation in starch, in Starch advances structure and function, Tina L. Barsby, Athene M. Donald and Peter J. Frazier (eds.), Royal Society of Chemistry, U.K., 97-102.
27. Xie, S. X., Liu, Q., and Cui, S. W. (2005), Starch modifications and applications, in Food carbohydrates: Chemistry, physical properties, and applications, Chapter 8, Steve W. Cui (Ed.), CRC Press, Boca Raton, 368-369.
28. Wagoner, J. A. and van der Burg, L. F. (1990), Unmodified starches: Sources, composition, manufacture and properties, in Starch and starch products in paper coating, Robert L. Kearney and Hans W. Maurer (eds.), Tappi Press, Atlant, USA, 2-30.
29. Wurzburg, O. B. (1986). Modified starches: Properties and uses, CRC Press, Boca Raton, Fl., 19-21.
30. Yan, H. and Zhengbiao, G. U. (2010). Morphology of modified starches prepared by different methods. Food Research International, 43 (3), 767-772.
31. Zijderveld, A. H. and Stoutjesdijk, P. G. (1976). The paper industry, in Industrial uses of starch and its derivatives, Chapter 5, J. A. Radley, Applied Science Publishers Ltd., London, 199-209.
32. https://projects.ncsu.edu/project/hubbepaperchem/CST.htm (Accessed date 14.05.2019).
33. https://polymerinnovationblog.com/second-generation-biomass-feedstock-7-past-prologue/ (Accessed date 14.05.2019).
34. http://www.tongaathulettstarch.co.za/downloads/Papermaking%20surface%20size%20starch.pdf (Accessed date 14.05.2019).

THE USE OF ARTIFICIAL NEURAL NETWORKS (ANNS) IN GEOTECHNICS

Yeşim TUSKAN [1], Begüm Y. DAĞLI [2], Dilay UNCU [3]

[1] Civil Engineering Department, Manisa Celal Bayar University, Manisa, Turkey.
[2] Vocational School of Technical Sciences, Manisa Celal Bayar University, Manisa, Turkey.
[3] Civil Engineering Department, Manisa Celal Bayar University, Manisa, Turkey.

Introduction

In recent decades, the usage of artificial neural networks (ANNs) has increased in many engineering area. Especially, ANN has been practiced in many geotechnical engineering issues and has been highly successful. The literature review shows that; pile capacity estimation, soil behavior modeling, land characterization, settlement, slope stability, design of retaining structures, pile design and tunnels were the most effective areas of this issue. In all studies these problems were investigated using an overview of artificial neural networks. The current complexity of these problems has led researchers a new modeling style to overcome with this complexity of geotechnical behavior. The traditional structure of engineering design was modeled by using ANN. This technique is an approach known as artificial neural networks (ANNs), which ideally model complex problems. The study aims to detail some features of ANN in the framework of the compilation of some usages of artificial neural networks involved in geotechnical engineering.

PILE DESIGN

Goh [1] studied an ANN that estimates the pile friction capacity in clayey soils. The ANN developed has been trained with the in-situ data obtained from the current case records. Input parameters of the model were selected as pile diameter, undrained shear strength, pile length and average effective stress. The only output of the model was surface friction resistance. The outcomes obtained using ANN developed was compared with those obtained from the Burland [2] and, Semple-Rigden method [3]. The regression analysis with the error rate was shown in the Table 1.

Table 1 Comparaison of regression analysis with the error rate of ANN, Semple and Rigden [3] and Burland [2] method.

Method	Correlation Coefficient		Error Rate	
	Training	Testing	Training	Testing
ANN	0.985	0.956	1.016	1.194
Semple and Rigden (1986)	0.976	0.885	1.318	1.894
Burland (1973)	0.731	0.704	4.824	3.096

Goh [4,5] applied ANN to estimate the final load capacity on piles. The outcomes of the developed model were obtained out off the existing load tests on steel piles in sandy soils, namely; hammer weight, pile length, pile group index, pile cross-sectional area, pile elasticity modulus and hammer type were utilized as model input. The only model output is pile load capacity. The study also compares the results of ANNs with the relationship of the past traditional studies. The Table 2 below indicates that the pile load

capacity obtained from the ANN estimates the best result compared to the other methods.

Table 2 Comparaison of regression analysis with the error rate of ANN, Hiley [6] and Janbu [7] method.[5]

	Correlation Coefficient	
Method	Testing data	Training data
ANN	0.97	0.96
Hiley (1992)	0.76	0.48
Janbu (1953)	0.89	0.82

Lee and Lee [8] investigated ANNs to estimate the final pile bearing capacity. The model is situated on the simulation using the data maintained from the pile loading test results on the field. Model inputs were selected as: the penetration depth ratio, the average normal stress and pulse number of the calibration chamber. The final carrying capacity is the output given by the model. Two ANN models have been developed as shown in Figure 1.

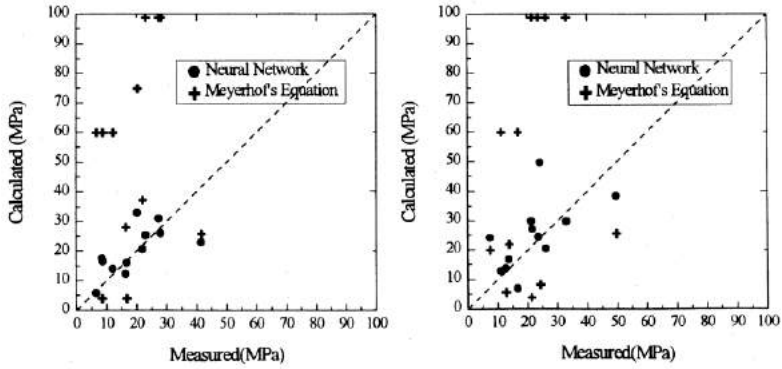

Figure 1 ANN model prediction of pile bearing capacity versus Meyerhof's [9] equation[8]

Teh et al.[10] demonstrated a static pile capacity ANN model for the prefabricated square section concrete pile, which provides estimation from dynamic stress - wave data.

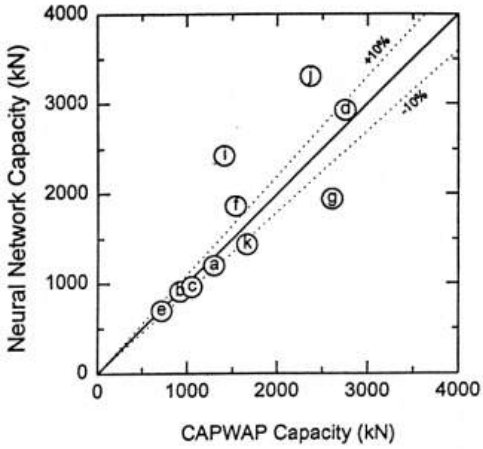

Figure 2 Estimated pile capacity by ANN model and actual pile capacity obtained by CAPWAP [10]

Neural networks are trained with the capacity data obtained by CAPWAP computer code by associating the stress-wave inputs [11]. This study aims to compare the CAPWAP (Figure 2) estimated capacity and actual piling capacity. It learns the artificial neural network training set data in an almost perfect. The trained neural network was evaluated because it was in a form to be generalized with the test data set.

Abu-Kiefa [12], modeled two ANNs to estimate the capacity of piles on cohesionless soils. The total pile capacity was predicted in the first model. The second model is utilized to predict the pile tip capacity. In the first ANN, five parameters were utilized as model inputs. These variables were the shear strength angle, pile resistance angle, effective tip tension, and equivalent pile cross-sectional area with pile length. There is only one output that defines the pile capacity.

Kim and Kim [13] have studied back-propagation ANN and sequential ANN to estimate the horizontal load-deflection relationship in piles.

Adel et al. [14] identified an ANN model to generate the resistance ratios in a group of pile. The outcomes generated by the developed ANN model were checked against the current laboratory and in-situ analysis. As a result, the ANN model presented a suitable design to assist geotechnical engineers in determining resistance ratio of pile group.

Lee et al. [15] adopted an ANN to overcome the complication of jetty pile design. Finite element analysis was performed for 50 different design cases to generate ANN model. The outcomes of the ANN model gives similar resılts compared by results of FE analysis saving design time and cost.

Momeni et al.[16] implemented ANN for solving geotechnical problems such as pile design. An ANN-based predictive model for predicting ABC of piles was trained by a feed forward back-propagation as depicted in Figure 3. Results of the statistical parameters demonstrated that the ANN model has high accuracy to estimate the bearing resistances of piles.

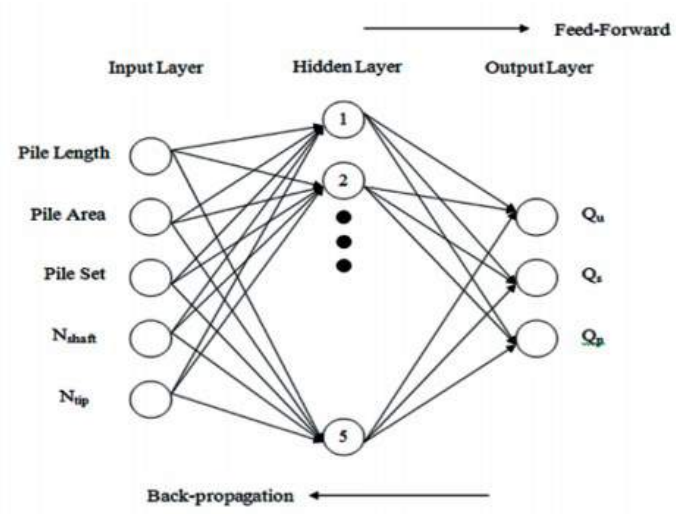

Figure 3 Structure of the ANN-based predictive model for predicting ABC of piles [16]

SETTLEMENT

Goh [17] developed an ANN to model the settlement estimation of horizontally loaded piles in the homogeneous soil layer. Input parameters in the proposed ANN were the ratio of the pile elasticity modulus to the ground shear modulus, the length of the pile, the shear modulus of the ground, the poison's ratio of the ground and the pile radius. The pile settlement is the only output. The comparison of theoretical and predicted settlement was depicted in Figure 4.

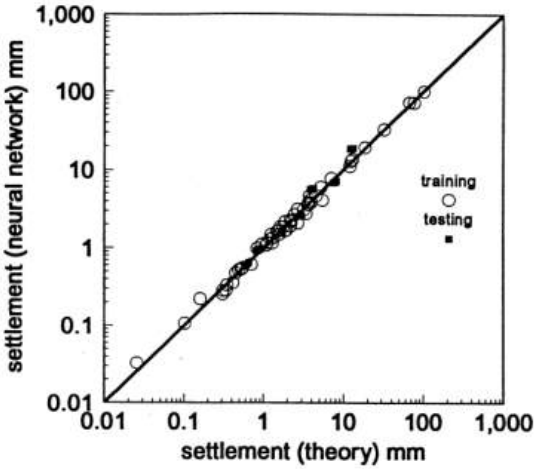

Figure 4 The comparison of theoretical and predicted settlement [17]

Sivakugan et al. [18] proposed an ANN to estimate foundation settlement on granular soils. The proposed ANN was trained with five inputs: Stress, standard penetration test number, thickness, shape and depth of foundation. This ANN output was selected as settlement of foundation. Outcomes from ANN were compared with Terzaghi and Peck [19] and Schmertmann [20] methods as depicted in Figure 5.

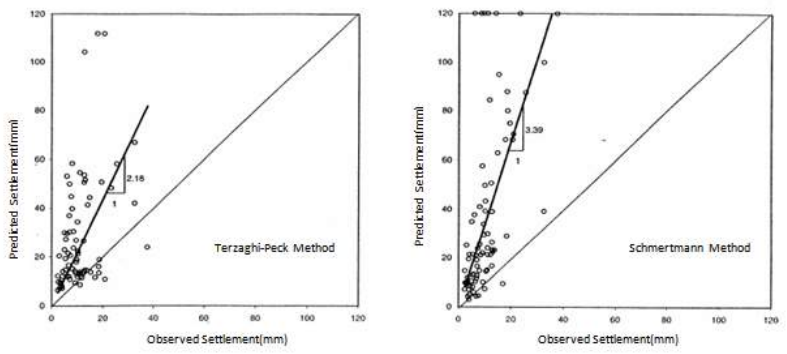

Figure 5 Settlement of foundation from ANN model versus Terzaghi and Peck (1967) and Schmertmann (1970) methods [18]

Shahin et al. [21] conducted similar studies in the prediction of settlement on shallow foundations in cohesionless soils. 272 compiled data

were utilized to model the proposed algorithm. ANN results were compared with the most commonly utilized three conventional approches as shown in Table 3. ANN has more applicability and gives better performance than traditional methods.

Table 3 Comparaison of regression analysis with the error rate of ANN, Meyerhof [22], Schultze and Sherif [23] and, Schmertmann et al. [24] methods.

Category	ANN	Meyerhof (1965)	Schultze and Sherif (1973)	Schmertmann et al. (1978)
Correlation,*r*	0.99	0.33	0.86	0.70
RMSE	3.9	27.0	23.8	45.2
MAE	2.6	20.8	11.1	29.5

Goh and Kulhawy [25] were used an ANN to estimate the safety analysis in limit state surface modeling of foundation settlement.

Shahin et al. [26] applied probabilistic analysis on an ANN model to estimate settlements occurred on granular soils. The implementation of the probabilistic analysis on ANN of the models has been also used in many cases in civil engineering.

An ANN model for settlement estimation was proposed by Kanayama et al. [27] from results of a test embankment in The Netherlands. Predicted settlements were found to be in perfect agreement with the measurements.

A database of 47 published case histories about earthquake-induced crest settlement were used by Zeroual et al. [28] to obtain an ANN model for the rockfill dams. The developed ANN model has been able to predict earthquake-induced settlement in rockfill dams with a precision of more than 99%, thus indicating the effectiveness of this model in this practice.

SOIL BEHAVIOUR

The cone penetration test (CPT) and relative density was modeled by using ANN interpreted by Goh [29]. The only outcome is CPT cone penetration resistance. The ANN model finds high correlation coefficients for training and test data, such as 0.97 and 0.91, respectively, indicating that the nonlinear link between the other parameters and CPT cone penetration resistance is successfully modeled.

Cal [30] utilized an ANN model to generalize a quantitative ground classification system based on three basic factors (plasticity index, clay content and liquid limit).

Attoh-Okine and Fekpe [31] developed an ANN to examine the strength characteristics of iron and aluminum-containing soils. The traditional back-propagated network model was compared with the adapted Artificial Neural Network applied to model the California Bearing Ratio (CBR) land strength value and characteristics. Two neural network approaches based on the

existing field experiments and laboratory data selected for the study were examined and used to calculate the CBR value. Both models gave good results in modeling the strength characteristics of soils.

Najjar et al. [32] demonstrated that ANN based models could accurately assess ground swelling and provided significant achievements in predictive accuracy over statistical models.

Ghaboussi and Sidarta [33] are drained and subjected to triaxial pressure testing used artificial neural networks modeling non-drainage behavior.

Zhu et al. [34, 35] modeled an ANN model to investigate Hawaii volcanic floor, dune and fine-grained residual soils in predicting their behavior.

The shear modulus and damping ratio of sand–mica mixtures were investigated by Cabalar ve Cevik [36]. An ANN model was proposed containing input variables namely; the mica content, effective stress and strain. The outputs of the model were the damping ratio and shear modulus. A quite satisfactory performance were obtain with both moels.

An ANN model was proposed by Zhao et al. [37] to estimate soil texture from accessible soil maps combined with hydrographic variables generated from a digital elevation model. Results indicated that The Levenberg–Marquardt algorithm was found to be most accurate model in association with back-propagation algorithm.

An ANN estimation model containing a large data set of compaction characteristics, permeability, and soil shear strength to predict the soil index parameters was developed by Tizpa et al. [38]. The results of the prediction model demonstrate that a high accurate estimation was provided by developed ANN model.

Correlation between matric suction and volumetric water content of unsaturated soils was investigated by Zainal and Fadhil [39]. Problems including seepage, bearing capacity, volume change were studied to observe considerable effects of matric suction and volumetric water content on unsaturated soils.

LIQUEFACTION ASSESMENT

Goh [40] used an ANN to model the combined correlation between seismic data and ground parameters for liquefaction potential research. In this study, data of 13 earthquake records obtained from Japan, the United States and some parts of the Americas during 1891-1980 were used in artificial neural network architecture. In the study, only one output is obtained when using eight input variables.

Goh [41] has also resorted to the use of ANNs to obtain the liquefaction potential by utilizing the results of CPT and evaluating the resistance data. The results obtained from the silty sand deposits of sandy soils used in the study represent the five earthquakes that occurred in the period 1964-1983.

Rahman and Zahaby [42] used fuzzy variables in the probabilistic liquefaction risk analysis.

Rahman and Wang [43], using the neural network model with the fuzzy model has made liquefaction estimates. The model they developed was tested using a large liquefaction database. In the second phase of two different test algorithms, membership degrees of fuzzy sets were developed for single parameters and input variables were expressed.

Goh [44] utilized a probabilistic neural network (PNN), with an implementation of Bayesian classification approach. The algorithm was utilized to develop separate research of CPT and shear wave velocity data.

A seismic wave energy-based method with back propogation ANN to define the liquefaction probability was presented by Juang et al. [45]. The ability in generating the probability of soil liuefaction was observed in proposed method.

Baziar and Nilipour [46], utilized a reliable CPT data with a wide range of variables to generated in a program called STATISTICA tarined by ANN algorithm. The back propagation algorithm with a multilayer perceptron ANN was used to investigate the liquefaction assesment as shown in Figure 6.

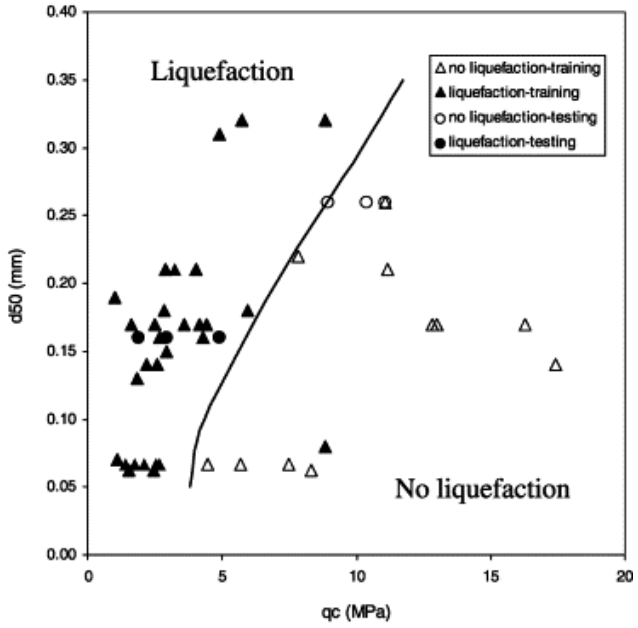

Figure 6 Liquefaction assesment evaluated by ANN model using CPT data [46]

The liquefaction assessment was investigated by Baziar ve Ghorbani [47] using lateral spreading at ground failure at a given site. An ANN model called STATISTICA was utilized to caused by liquefaction in both ground slope and free face conditions were estimated by predict the magnitude of resulting deformations and the horizontal ground displacement as depicted in Figure 7.

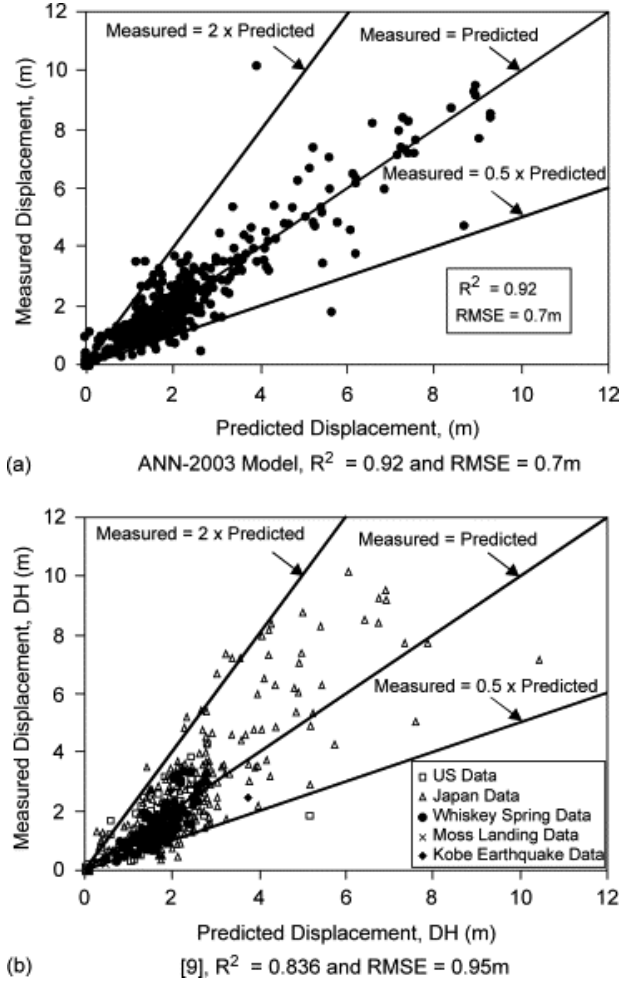

Figure 7 Liquefaction assesment evaluated by ANN model using STATISTICA [47]

Baziar ve Jafarian [48], presented an ANN model to form a connection between soils initial variables and the strain energy required in liquefaction

assesment. A data set containing 284 compiled shear test data were utilized to obtain the model. the accuracy to develop an ANN-based model for soil capacity energy was observed as depicted in Figure 8.

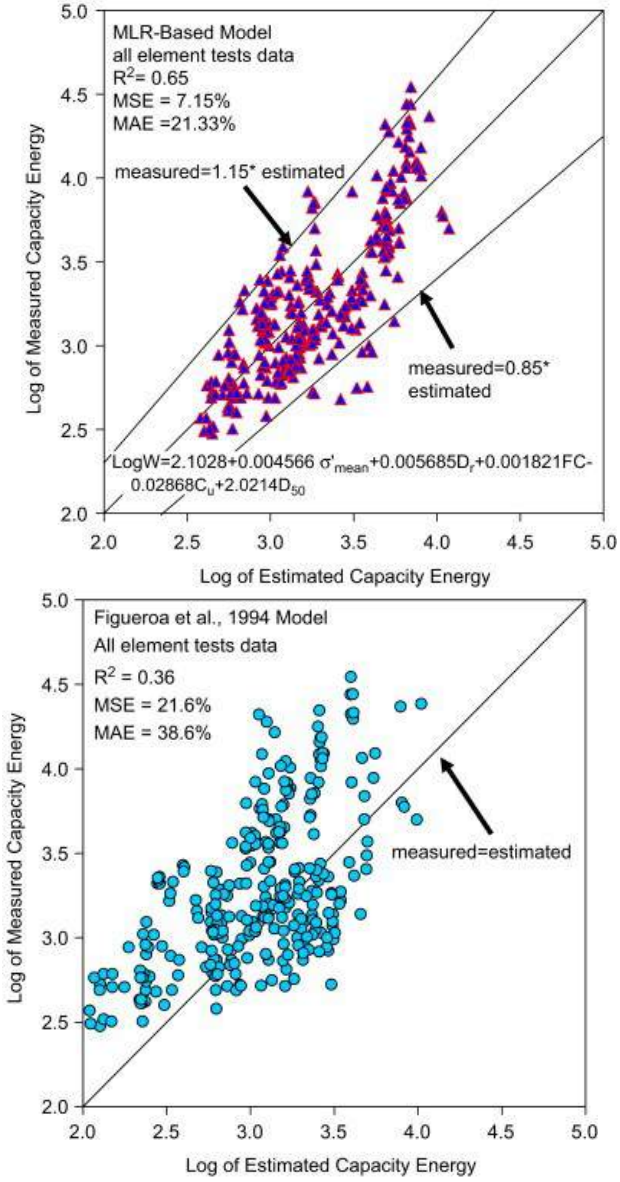

Figure 8 Soil capacity energy prediction to model liquefaction assesment by utilizing developed ANN-based model [48]

Baykasoğlu et al. [49] presented a new approach which is based on classification on data mining to predict liquefaction assessment. A multi-layer perception ANN which is one of the most widely utulized ANN is considered for classification of the liuefaction occurance.

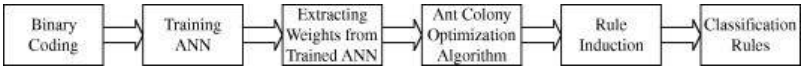

Figure 9 Architecture of the proposed method [49]

Lee and Hsiung [50] studied a new approach to quantify the sensitivity of the system of key parameters influencing liquefaction recognition in the field with the ANN model. A new index obtained from the mathematical formulation of the neural network was proposed to quantify the result of the sensitivity analysis.

Tsompanakis et al. [51] simulated the seismic response of a typical embankment by utilizing ANN as depicted in Figure 10. ANNs were trained to replace the time-consuming behaviour of the embankment problem.

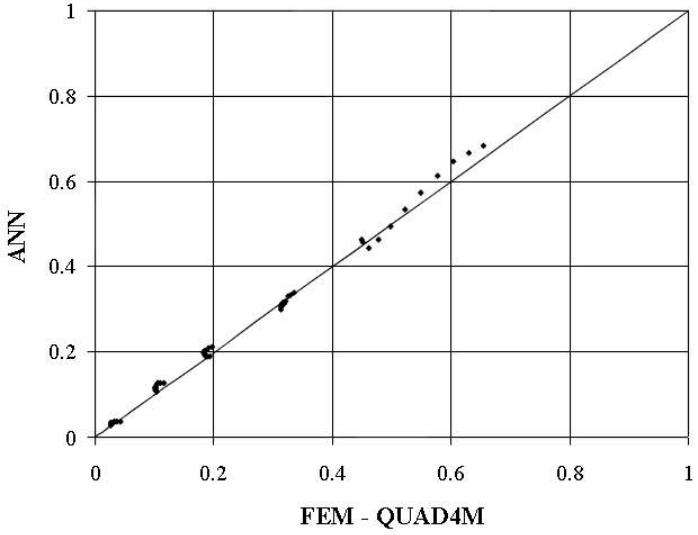

Figure 10 Computed (FEM-QUAD4M) versus predicted (ANN) seismic response [51]

Farrokhzad et al.[52] utilized a data set of 2500 sampling points from 30 boreholes to train the proposed ANN model. The liquefaction microzonation map for the Babol city was assessed by utilizing artificial neural network. In

this ANN model, a back-propagation learning algorithm was used for the training process. The geotechnical and seismic parameters were used as input data to estimate liquefaction potential. The accuracy between the ANN estimation and in-situ data for all cases was found to be over 91%.

Sharafi and Jalili [53] developed a back-propagation ANN in order to estimate the liquefaction cyclic resistance ratio (CRR) of sand-silt mixtures. A database of laboratory cyclic triaxial, torsional shear and simple shear tests results was collected and generated in the ANN model (Figure 11). The proposed ANN model was founded to be suitable to serve as an accurate tool for understanding liquefaction assessment.

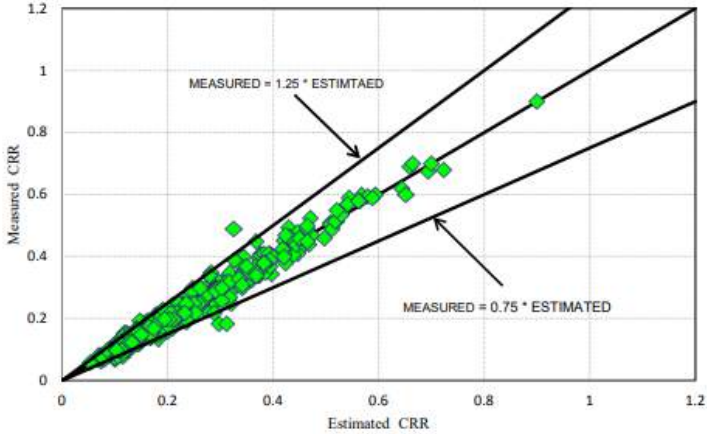

Figure 11 Predicted CRR by ANN model versus measured values for training data [53].

An ANN model was trained by Choobbasti et al. [54] to estimate and classify the soil layers gathered from boreholes at different depths with a multi layer ANN model.

Xue et al. [55] presented a hybrid probabilistic ANN and particle swarm optimization (PSO) algorithms to estimate the liquefaction assesment. Seven earthquake and soil parameters were selected as the evaluating indices.

ENVIRONMENTAL GEOTECHNICS

Capodaglio et al. [56] used the forward-feed, back-propagation ANN model for analysis of the volume conditions at the waste water treatment center. The sediment volume index was utilized to predict the conditions of bulk change due to blistering, and the data was introduced in the artificial neural network using the time series input scheme.

McAvoy et al. [57] conducted studies on the biological treatment with biological C, N vr P inhibitors. Three processing units were utilized with proposed three feed back feed-in ANN: anaerobic pre-treatment unit, aeration tanks and a deposition reservoir.

Blais et al. [58] used the technique of artificial neural network to reveal the kinetic model structure due to heavy metal reduction in the sludge in the activation process. The task of the artificial neural network model is to estimate the maximum specific growth rate according to the different combinations of heavy metals in waste water.

Tabak and Govind [59] have proposed an artificial neural network for predicting kinetic biodegradation in the compound based on the number and type of chemical groups in the composition of the compound.

Rogers and Dowla [60] presented a new approach for optimization of an aquifer improvement with the ANN method to estimate the nonlinear groundwater model. In this new approach, the ANN model was trained to predict flows. A back propagation algorithm was used in the training of ANN model.

An existing mechanistic model for a large scale activated sludge treatment process was developed by Coté et al.[61]. Subsequently, a feed-forward, back-propagation ANNs were utilized to optimized mechanistic model. The coupling of the mechanistic model with theANNmodel were obtain as a result of a hybrid model.

Dan et al. [62] used ANNs to investigate contaminant concentration in soil profiles of polluted sites. The prediction of the heavy metals in soils polluted by a mining accident were observed to forecast the pollutant levels in the selected area.

Lallahem and Mania [63] selected an area of 70000 km^2 in the north of Paris to model a leakage in the groundwater basins with certain infiltration parameters A mathematical model to obtain artificial neural networks for underground flow detection have been also modeled with the linear approach MERO.

Shang et al. [64] investigated the presence and type of heavy metals in soils by using an intrinsic electrical property of materials. The complex permittivities of the soil specimens are measured in the laboratory using a custom-developed apparatus to obtain a database. Two ANN models were then developed to identify and distinuish the metal type contained in soil specimen. The identification using the The first ANN model to predict the presence of heavy metals was determined with accuracy in 90% of cases. The second ANN model was utilized to classify the type of the heavy metal in 95% of cases.

El-Din,et al. [65] investigated an in-situ case that noticed some comprehensive study to derivate nonlinear ANN estimation for a waste water treatment plant. The prediction performance to model the by using the

performance of the propesed ANN model was reviewed to model waste water assesment.

Nasr et al. [66] provided a reliable model for wastewater treatment to estimate its performance and minimize the operation costs. An ANN model with a feed forward to estimate the performance of of the propesed ANN model was reviewed to model waste water assesment as shown in Figure 12.

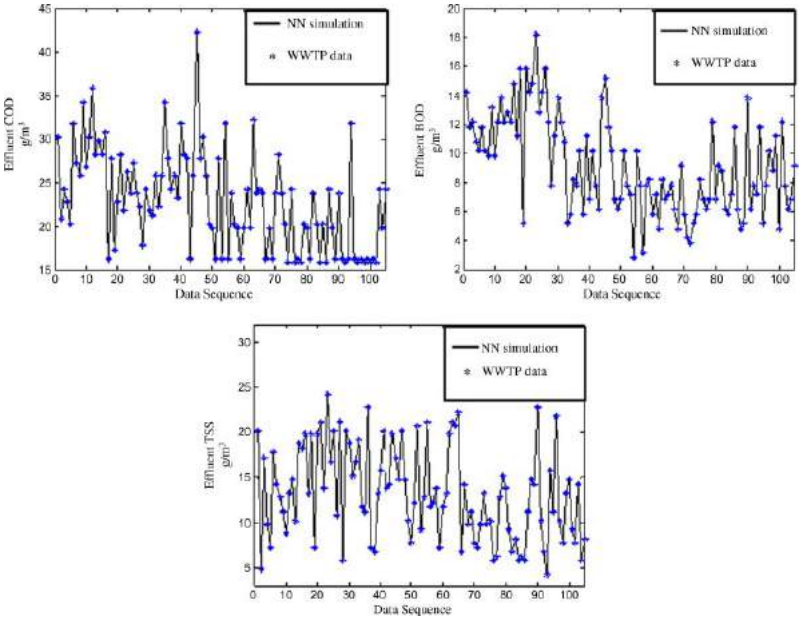

Figure 12 Simulation results of waste water traitment by using ANN model [66]

Abba and Elkiran [67] employed an ANN to generate and predict the waste chemical oxygen demand from the wastewater treatment plant. Statistical techniques were utilized to evaluate the ANN performance. The accuracy revealed that ANNs model exhibited better performance in estimating chemical oxygen demand over the multiple linear regresşon model.

SITE CHARACTERIZATION

Pezeshk et al. [68] utilized ANNs in geophysical log mapping to interprete boreholes test results in terms of formation aspects in groundwater modeling in presence of simple geotechnical and hydrological data.. A trained neural network was develeoped effectively and efficiently to complete the

interpretation of logs. The applied model provides information about the under ground layers.

Huang and Williamson [69] were utilized the offshore borehole data in Canada to conduct the permeability and porosity of the ground determined by ANN model.

Marmo et al. [70] studied rock samples from the San Lorenzello during the Lower Cretaceous period. In this study, 215 thin layers of carbonates in rock samples taken from the San Lorenzello were examined to developed an ANN model based on rock classification.

Garcia and Shigidi [71] investigated acase study under steady-state conditions to model ground water flow equation with an ANN. The result was then inverted to show its capability to estimate the aquifer response.

Samui and Thallak [72] investigated the site characterization in presence of a compiled data from SPT in three-dimensional subsurface. An ANN model utilizing multilayer perceptrons was developed to investigate the site characterization.

REFERENCES

1. A.T.C. Goh, *Back-propagation neural networks for modeling complex systems*, Artificial Intelligence in Engineering, vol. 9, pp143-151. 1995a.
2. J.B. Burland, *Shaft friction of piles in clay – a simple fundamental approach*. Ground Engineering. Vol 6(3) pp.30-42. 1973.
3. R.M Semple, and W.J. Rigden, *Shaft capacity of driven pipe piles in clay: Analysis and design of pile foundations*, ASCE, West Conshohocken, pp. 59–79. 1984.
4. A.T.C. Goh,. *Empirical design in geotechnics using neural networks*, Geotechnique, Vol. 45(4), pp. 709-714. 1995b
5. A.T.C. Goh, *Pile driving records reanalyzed using neural networks,* Journal of Geotechnical Engineering, vol. 122(6), pp. 492- 495. 1996b.
6. A. Hiley, *The efficiency of the hammer blow, and its effects with reference to piling*., Engineering, vol.2, pp.673.1922.
7. N. Janbu, *Une analyse energetique du battage des pieux a l'aide de parametres sans dimension*.,.Norwegian Geotech. Inst., Oslo, Norway, vol. 3, pp. 63-64. 1953.
8. I.M., Lee, J.H. Lee,. *Prediction of pile bearing capacity using artificial neural networks.* Computers and Geotechnics, vol. 18(3), pp.189-200. 1996
9. G. G. Meyrehof, *Bearing capacity and settlement of pile foundations*. J. Geotech. Engrg., ASCE, vol.102(3), pp.196- 228. 1976.
10. C.I., Teh, K.S Wong,., A.T.C., Goh, S. Jaritngam, *Prediction of pile capacity using neural networks*, Journal of Computing in Civil Engineering, vol. 11(2), pp.129-138. 1997.
11. F., Rausche, F., Moses, and G.G. Goble, *Soil resistance predictions from pile dynamics*., J. Soil Mech. and Found. Div., ASCE,vol. 98, pp.917-937. 1972.
12. M.A. Abu-Kiefa, *General regression neural networks for driven piles in cohesionless soils*, Journal of Geotechnical and Geoenvironmental Engineering, vol.124(12), pp.1177-1185. 1998.
13. B.T., Kimand, Y.S. Kim, *Lateralload – deflectiom Modeling of groups of piles using artificial neural networks.InDeepFoundations*: Proceedings of the International Deep FoundationsCongress, Orlando, Fla.,pp. 14–16, 2002.
14. H., Adel, G., Morcous and M. Helmy, *Efficiency of pile groups installed in cohesionless soil using artificial neural Networks*. Canadian Geotechnical Journal. Vol.41(6) pp.1241-1249.2004
15. E Momeni, R Nazir, DJ Armaghani, H Maizir, *Application of Artificial Neural Network for Predicting Shaft and Tip Resistances of Concrete Piles.* Earth Sciences Research Journal vol.19 (1), pp.85-93, 2015.
16. Y., Lee S., Lee and H.K Bae. *Design of Jetty Piles Using Artificial Neural Networks.* Scientific World Journal. 1-12. 2014
17. A.T.C. Goh, *Nonlinear modelling in geotechnical engineering using neural networks*, Australian Civil Engineering Transactions, CE3 vol. 6(4), pp.293-297, 1994a.
18. N., Sivakugan, J.D Eckersley and H. Li, Settlement predictions using neural networks, Australian Civil Engineering Transactions, CE vol.40, pp.49-52, 1998.
19. K. Terzaghi and R.B.,Peck, *Soil Mechanics in Engineering Practice,* John Wiley and Sons, 729p. 1967.
20. J.H., Schmertmann, *Static Cone to Compute Static Settlement over Sand*, Jnl. Soil Mech. & Found. Div., ASCE, Vol. 96, No. SM3, pp. 1011-1043. 1970.
21. M.A. Shahin, H.R. Maier, M.B. Jaksa *Predicting settlement of shallow foundations using neural Networks*, Journal of Geotechnical and Geoenvironmental Engineering, vol. 128 (9) pp. 785-793. 2002.

22. G. G. Meyerhof, *Shallow foundations.* J. Soil Mech. & Found. Div., ASCE, vol.91(SM2), pp.21-31,1965.
23. E., Schultze, and G. Sherif, *Prediction of settlements from evaluated settlement observations for sand.* Proc., 8th Int. Conf. Soil Mech. & Found. Engrg., vol.1(3), pp.225-230. 1973.
24. J. H., Schmertmann, J. P Hartman, and P. B Brown,. *Improved strain influence factor diagrams*. J. Geotech. Engrg., ASCE, vol.104(GT8), pp.1131-1135. 1978.
25. A. T. C., Goh, and F. H. Kulhawy, *Neural network approach to model the limit state surface for reliability analysis*. Canadian Geotechnical Journal, vol. 40, pp.1235-1244, 2003.
26. M. A., Shahin, M. B Jaksa,., and H. R Maier,. *Neural network based stochastic design charts for settlement prediction.* Canadian Geotechnical Journal, vol.42(1), pp.110- 120. 2005a
27. M, Kanayama, H, Yamashita, T, Higashi, M Ohtsubo *Examination for predicting consolidation settlement by measurement records –prediction of settlement by using neural network model-.* Trans Jpn Soc Irrigation Drain Reclam Eng vol 259:pp.61–69 (in Japanese) 2009.
28. A., Zeroual, M., Djeddou and A. Fourar *Artificial neural network application for the Prediction of earthquake-induced crest settlement in rockfill dams.* First International Conference on Dams. ICDBiskra. Pp. 355-361. 2018
29. A. T. C. Goh, *Neural network modeling of CPT seismic liquefaction data. Journal of Geotechnical Engineering*, American Society of Civil Engineers, USA, vol. 122(1), pp.70-73. 1996
30. Y. Cal, *Soil classification by neural-network.* Advances in Engineering Software, 22(2), 95-97. 1995
31. N.O. Attoh-Okine Edward S.K. Fekpe, *Strength characteristics modeling of lateritic soils using adaptive neural networks* Construction and Building Materials vol. 10(8) pp.577-582. 1996
32. Y. M., Najjar, I. A Basheer,., and R. McReynolds, *Neural modeling of Kansan soil swelling.* Transportation Research Record, No. 1526, pp.14-19. 1996
33. J., Ghaboussi, and D. E. Sidarta, *New nested adaptive neural networks (NANN) for constitutive modeling.* Computers and Geotechnics, vol. 22(1), pp.29-52. 1998
34. J. H., Zhu, M. M., Zaman, and S. A. Anderson, *Modeling of soil behavior with a recurrent neural network.* Canadian Geotechnical Journal, vol.35(5), pp.858-872. 1998a
35. J. H., Zhu, M. M., Zaman, and S. A. Anderson, *Modeling of shearing behaviour of a residual soil with recurrent neural network*. International Journal of Numerical and Analytical Methods in Geomechanics, vol. 22(8), pp.671-687. 1998b
36. A.F Cabalar. and A. Cevik *Modelling damping ratio and shear modulus of sand–mica mixtures using neural Networks.* Engineering Geology. Vol.104(1) pp.31-40. 2009
37. Z., Zhao, T.L., Chowb, H.W., Rees, Q., Yang Z., Xing, F.R. Meng, *Predict soil texture distributions using an artificial neural network model*. computers and electronics in agriculture vol.65: pp.36–48 2009
38. P., Tizpa, R.J., Chenari, M.K., Fard, S.L. Machado *ANN prediction of some geotechnical properties of soil from their index parameters.* Arab J Geosci DOI 10.1007/s12517-014-1304-3. 2014
39. A.E.., Zainal, S.M. Fadhil, *Prediction of soil water characteristic curve using artificial neural network: a new approach*. MATEC Web of Conferences. p162. 2018
40. A. T. C. Goh, *Seismic liquefaction potential assessed by neural network.* J. Geotech. & Geoenv. Engrg., ASCE, vol.120(9), pp.1467-1480. 1994b

41. A. T. C. Goh, *Neural-network modeling of CPT seismic liquefaction data.* J. Geotech. Engrg., ASCE, vol. 122(1), pp.70-73. 1996a
42. M.S. Rahman and K.E. El-Zahaby *Inclusion of fuzzy variables in geotechnical risk analysis. Computer methods and advances in geomechanics*: Proceedings of the Ninth international conference of the association for computer methods and advances in geomechanics. Pp.567-572. 1997.
43. M.S Rahman,, J., Wang, Fuzzy neural network models for liquefaction prediction. Soil dynamics and earthquake engineering. Volume vol. 22, pp.685-694. 2002.
44. A.T.C., Goh,. *Probabilistic neural network for evaluating seismic liquefaction potential*, Can. Geotech. J., vol.39: pp.219-232. 2002
45. C. H Juang,., T. Jiang, and R. D. Andrus. *Assessing Probability-Based Methods for Liquefaction Potential Evaluation.* Journal of Geotechnical and Geoenvironmental Engineering vol.128 (7): pp.580-589. 2002.
46. MH, Baziar, N. Nilipour *Evaluation of liquefaction potential using neural-networks and CPT results.* Soil Dyn Earthq Eng vol.23:pp.631–636 2003
47. MH, Baziar, A Ghorbani, *Evaluation of lateral spreading using artificial neural networks*. Soil Dyn Earthq Eng vol.25:pp1–9. 2005
48. M.H. Baziar, and Y. Jafarian, *Assessment of Liquefaction Triggering Using Strain Energy Concept and ANN Model: Capacity Energy*. Soil Dynamics and Earth-quake Engineering, vol.27, pp.1056-1072. 2007
49. A., Baykasoğlu, A., Çevik, L Özbakır, S. ,Kulluk, Generating prediction rules for liquefaction through data mining. Expert Systems with Applications vol.36, pp. 12491– 12499. 2009.
50. C.J. Lee and T.K. Hsiung, *Sensitivity analysis on a multilayer perceptron model for recognizing liquefaction cases*. Computers and Geotechnics vol.36(7):pp.1157-1163, 2009
51. Y Tsompanakis., N Lagaros., P. Psarropoulos., and E.C. Georgopoulos, *Simulating the seismic response of embankments via artificial neural networks* Advances in Engineering Software vol.40(8):pp.640-651.2009
52. F. Farrokhzad, A.J. Choobbasti , A. Barari. *Liquefaction microzonation of Babol city using artificial neural network* Journal of King Saud University – Science. Vol.24, pp.89–100. 2012.
53. H. Sharafi., S. Jalili, *Assessment of Cyclic Resistance Ratio (CRR) in Silty Sands Using Artificial Neural Networks*. Open Journal of Civil Engineering, vol.4, pp.217-228. 2014
54. A J Choobbasti, F Farrokhzad, S Rahim Mashaie, P H Azar, *Mapping of soil layers using artificial neural network (case study of Babol, northern Iran)* Journal of the South African Institution of Civil Engineering vol.57(1), pp.59–66. 2015
55. X. Xue, X. Yang , P. Li, *Application of a probabilistic neural network for liquefaction assessment*.Neural Network World. Vol.6: pp.557–567. 2017
56. A.G Capodaglio., H.V Jones., V. Novotny, *Sludge bulking analysis and forecasting: application of system identification and artificial neural computing technologies,* Water Research, vol. 25(10), pp.1217–1224. 1991
57. D. C McAvoy., W. S Eckhoff. and R. A. Rapaport, *Fate of linear alkylbenzene sulfonate in the environment*. Environ. Toxicol. Chem., vol.12, pp.977-987. 1993
58. JF Blais, RD Tyagi, JC Auclair. *Bioleaching of metals from sewage sludge: microorganisms and growth kinetics*. Water Res; vol.27 (1): pp.101-110. 1993
59. HH Tabak, R Govind, *Prediction of biodegradation kinetics using a nonlinear group contribution method*. Environmental toxicology and chemistry vol.12 (2),pp.251-260. 1993
60. L.L. Rogers and F.U. Dowla, *Optimization of groundwater remediation using artificial neural networks with parallel solute transport modeling.* Water resources research. Vol.30(2) pp.457-481. 1994

61. M Cote., P.A Bernard., P. Lessard and, J. Thibault, *Dynamic modeling of the activatedsludge process*. Water Research vol.29(4) pp.995-1004. 1994
62. A Dan., J Oosterbaan., and P. Jamet *Contribution des réseaux de neurones artificiels (RNA) à la caractérisation des pollutions de sol. Exemples des pollutions en hydrocarbures aromatiques polycycliques (HAP) Artificial Neural Networks (ANNs) characterisation of soil pollution: the Polycyclic Aromatic Hydrocarbons (PAHs) case study.* Comptes Rendus Geosciences. 2002
63. S, Lallahem, J Mania *A nonlinear rainfall-runoff model using neural network technique: example in fractured porous media*. Math Comput Model vol.37:pp.1047–1061. 2003
64. J Q Shang, W Ding, R K Rowe,L Josic, *Detecting heavy metal contamination in soil using complex permittivity and artificial neural networks.* Vol. 41(6): pp. 1054-1067. 2004
65. A.G El-Din., D.W. Smith and M.G El-Din. *Application of artificial neural networks in wastewater treatment*. Journal of Environmental Engineering and Science, vol3(1): pp.81-95.2004
66. M S. Nasr, A.E. Medhat M. Hamdy A.E. Seif, Application of Artificial Neural Network (ANN) for the prediction of EL-AGAMY wastewater treatment plant performance-EGYPT Alexandria Engineering Journal vol51, pp.37–43 2012
67. S. Isa, A.G Elkirana, *Effluent prediction of chemical oxygen demand from the astewater treatment plant using artificial neural network application.* Procedia Computer Science 1877-0509 9th International Conference on Theory and Application of Soft Computing, Computing with Words and Perception, ICSCCW 2017, 22-23 August 2017, Budapest, Hungary. Vol.120: pp.156–163 2017.
68. S., Pezeshk, C.C Camp., S Karprapu,., Geophysical log interpretation using neural network. J. Comput. Civil Eng. Vol.10, pp.136. 1996.
69. Z., Huang M.A Williamson. *Artificial neural network modeling as an aid to source rock characterization*. Marine and Petroleum Geology vol.13(2): pp.277-290. (1996)
70. R., Marmo, S. Amodia., R., Tagliaferri, G. *Longo Textural identification of carbonate rocks by image processing and neural network: Methodology proposal and examples.* Computers & Geosciences vol.31(5): pp.649-659. (2005)
71. L.A., Garcia, A., Shigidi, *Using neural networks for parameter estimation in ground water*. Journal of Hydrology, vol.318 (1–4), pp.215–231. 2006.
72. P., Samui, S.G. Thallak, *Site Characterization Model Using Artificial Neural Network and Kriging*. International Journal of Geomechanics. Vol. 10(5): pp.171-180 DOI:10.1061/(ASCE)1532-3641(2010)10:5(171) 2010

AIR TEMPERATURE ESTIMATION BASED ON ARTIFICIAL NEURAL NETWORKS

Kazım KUMAŞ [1] , Onur İNAN [2] , Ali Özhan AKYÜZ [3] , Afşin GÜNGÖR [4]

[1] Öğr. Gör., Burdur Mehmet Akif Ersoy University, Bucak Emin Gulmez Vocational School of Technical Sciences, 15300, Burdur, Turkey.
[2] Öğr. Gör., Burdur Mehmet Akif Ersoy University, Bucak Emin Gulmez Vocational School of Technical Sciences, 15300, Burdur, Turkey.
[3] Dr. Öğr. Üyesi., Burdur Mehmet Akif Ersoy University, Bucak Emin Gulmez Vocational School of Technical Sciences, 15300, Burdur, Turkey.
[4] Prof. Dr., Burdur Mehmet Akif Ersoy University, Bucak Technology Faculty, 15300, Burdur, Turkey. (Akdeniz University, Engineering Faculty, Antalya, Turkey)

INTRODUCTION

Temperature is an important climate parameter affecting daily life. Temperature is depending on many factors such as sunshine time, latitude, altitude and vegetation. Temperature is evaluated from a climatic and meteorological point of view. Therefore it is analyzed according to the maximum, minimum and average values. Depending on this situation, meteorological units estimate the temperature daily, monthly and yearly. Daily estimates take from one day to ten days. Classical synoptic, statistical and dynamic methods are used in the estimation process [1].

Air temperature forecasting has been increasingly become important for areas such as environment, industry, agriculture and livestock. This is because global climate change is a threat to the world and humanity. As a result of the industrial activities, global warming has progressed further. Extreme changes in air temperature negatively affect plants and animals. Due to this fact, it has become more crucial to know the ambient temperature variability for agricultural activities [2].

Temperature is very effective in the growth and development of plants. A certain temperature value is required for each plant to grow. This value should be continually optimal. Therefore, the vegetation adapts to the temperature zones. All plants are affected from high temperature. Heat-resistant zone maps were firstly started by the American Horticultural Society using data from 4745 meteorological measurement centers of 1974-1995. [3]. Nowadays, many methods are used to estimate the air temperature. Artificial Neural Networks (ANN) and Adaptive Network Based Fuzzy Inference System (ANFIS) are some of these methods.

Tasadduq, et al. in their study, have used ANN to estimate the air temperature of Jeddah located in Saudi Arabia. Using the back propagation algorithm in their ANN model, they have reached the desired weather forecast results with only one input parameter [4]. In their study, Smith et al. have built ANN model for the weather forecast using the data of the University of Georgia in 2005. In their model, they intended to determine the air temperature estimate of 12 hours before [5]. In their study, Dombaycı and Gölcü have established an ANN model to estimate the average daily temperature of Denizli province located in Turkey. They have used the General Directorate of State Meteorological Services (DMI) data for years 2003-2005 as training and for year 2006 as test data. They have tried different algorithms and different neuron numbers in their model. Finally they have found the correlation (R^2) and Root Mean Square Error (RMSE) values of model and made their comparisons. They have specified that the ANN is an efficient method for estimating ambient temperature [6]. Dr. S. Santhosh Baboo and I.Kar Shereef have used back propagation neural network (BPN) technique as a learning algorithm for estimating temperature. They have stated that the BPN neural network can approach a large class of functions and have the potential to capture complex relationships. They have compared the results of meteorological units with the results they obtained

and have showed that their method is successful in the estimation of the temperature [7]. In their study, Erkaymaz and Yaşar have estimated the air temperature by using feed forward neural network method from meteorological data from Elazığ province. They have used water vapor pressure, relative humidity, wind power and air pressure as input units. They have taken the temperature as output. They have shown that the average temperature can be used for other meteorological parameters by means of the software they developed in MATLAB with the smallest error [8]. In their study, Piyush Joshi and A. Ganju have estimated the maximum and minimum temperature according to the meteorological data they observed in the observation houses in Western Himalaya regions. In their ANN models, they have used back propagation learning algorithm. Approximately twenty five years old data has been used for the training of the network. They have estimated the temperature of the winter months between 2005 and 2010 in their network [9].

In their study, Kisi and Shiri have used ANN and ANFIS methods to estimate long-term monthly air temperature. As the input parameters of both methods, the number of months, station latitude and station longitude and altitude has been used. Long-term monthly temperature has been taken as the output parameter. They have shown that ANFIS method is better than ANN method in training phase. But in the test phase, they have specified that ANN method is better than ANFIS method by means of error values such as root-mean-square error (RMSE) and Mean Absolute Error (MAE). As a result, they have stated that ANFIS method could be a good alternative in weather forecasting [10].

In this study, an ANN model has been built to determine the air temperature by using meteorological data taken from the years 2000-2016 in Burdur province. From measured data monthly average relative humidity, monthly average steam pressure, month and year parameters have taken as input parameters and by using model it has been tried to estimate monthly average air temperature.

MATERIAL AND METHOD

Artificial neural networks (ANNs) are connected to each other by weighted links similar to human neural networks and have a specific memory in itself is a parallel data processing system. The core information in the ANN is processed in the nerve cell. Artificial nerve cells produce one or more inputs. Artificial nerve cells come together with various connections to form a network component. This structure is similar to the neural networks created by neurons. Each cell column is called a layer. The weights are the values located in the connections between cells. These weights represent intercellular interaction and activity. The network structure creates a set of algorithms between the input and output data, allowing input data to generate an inference. Modeling is based on the learning principle of the network [11]. The connection of a typical ANN structure is shown in Fig. 1 [12].

As seen in Figure 1, layers are formed by connecting artificial nerve cells to each other. An ANN composed of three layers: input, hidden and output layer. The input layer is responsible for forwarding the incoming information to the intermediate (hidden) layer. Intermediate layer processes information coming from the input layer and transmits to the output layer. More than one intermediate layer can be found in an ANN. In the output layer, the information coming from the intermediate layer is processed and the output corresponding to the information in the input layer is generated and transferred to the external environment [12]. Figure 2 shows the general structure of the ANN [13].

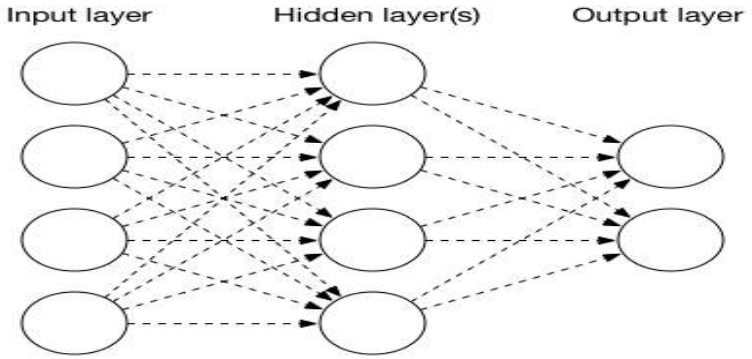

Figure 1. ANN connections

ANNs as in Figure 2 are composed of five basic structures: input (xi), weight (wi), transfer function, activation function and output [13].

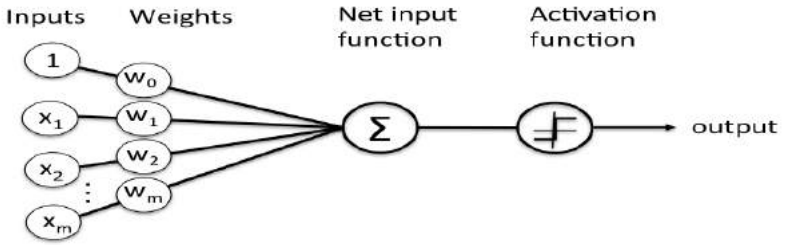

Figure 2. General structure of ANN cell

The weights in Figure 2 are the mathematical values that indicate the importance and effect of the input information to the cell. Each input has its own weight. The positive or negative values of the weights indicate the direction of the effect and the large or small values of the weights state the strength of the effect. If the weight has a zero value, it means that there is no

effect. Transfer function calculates the net input information coming to the cell. The sum of each weight multiplied by the inputs is added by the threshold value and sent to the activation function. The activation function operates the net input coming from the transfer function and generates the output corresponding to the cell input [11, 14].

For optimal solution in ANN method, it is very important to determine the number of operating elements in the layers and the number of hidden layers to be used [15]. In this study, ANN has been tested with different algorithms and neuron numbers in order to estimate with the smallest error value. The optimum results have been achieved with feed forward ANN having 10 neurons along with one hidden layer at the end of 1000 iterations shown in Figure 3.

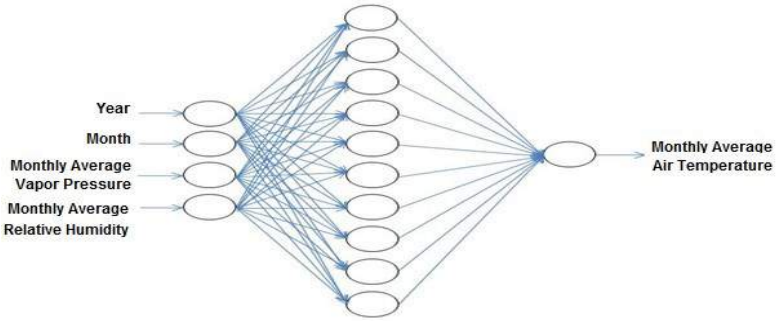

Figure 3. ANN architecture used in the application

Levenberg Marquardt (LM) as a back propagation algorithm and Logistic Sigmoid as activation function have been utilized for the training of ANN. As network structure, Feed-Forward Back Propagation type has been preferred because of its good prediction on linear and nonlinear models. Mean Squared Error (MSE) has been used as the performance function. The Matlab interface used in the training of ANN model is shown in Figure 4. The number of neurons ranging from 3 to 12 in the secret layer has been used. In the ANN model, the number of input and output neurons has been determined and then the values have been set to 0-1 range for the usage of dependent and independent variables in the system. 1000 iterations, 0 error 1.00e.-07 gradient value and 1000 validation error number have been used for stop criterion in training phase. Training phase has stopped at 1000 iterations in 20 seconds. The data taken from General Directorate of State Meteorological Services (DMI) has been separated %70, %15 and %15 as training, verification and test respectively. In the training of ANN model, input and output parameters as specified in Figure 3 have been used for the years 2000-2014 for Burdur province. According to the data of the input parameters given in Figure 3 for the years 2015-2016, the output values have been estimated.

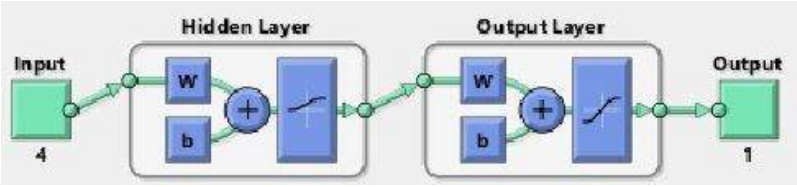

Figure 4. Matlab ANN tool interface

The performance of the model for training and test data has been evaluated according to statistical methods such as Root Mean Squared Error (RMSE), Covariance (COV) and Correlation Coefficient (R^2). These statistical methods have been used to compare actual data with estimated data. The error in the training phase is estimated by Formula 1. The detection coefficient (R^2) and the coefficient of variation (COV) in percent are expressed in Formula 2 and 3, respectively [16].

$$\mathrm{RMSE} = \sqrt{\frac{\sum_{m=1}^{n}(y_{p.m} - t_{m.m})}{n}} \quad (1)$$

$$R^2 = 1 - \frac{\sum_{m=1}^{n}(t_{m.m} - y_{p.m})^2}{\sum_{m=1}^{n}(t_{m.m} - \bar{t}_{m.m})^2} \quad (2)$$

$$\mathrm{cov} = \frac{\mathrm{RMS}}{|\bar{t}_{m.m}|}\ 100 \quad (3)$$

In the equals $y_{p.m}$ is the estimated value, $t_{m.m}$ is the measured value, $\bar{t}_{m.m}$ is the actual value, and n is the number of data. The high performance of ANN model is evaluated according to the lower RMS and COV values and with R^2 value is close to 1 along with the mean square error is close to 0 [16].

RESULTS AND DISCUSSION

Monthly air temperature values of Burdur province have been estimated with artificial neural network model. In order to obtain the best results, different neuron numbers have been tried in the hidden layer and the obtained statistical values are given in Table 1. The best R^2 results for the monthly air temperature values of Burdur have been obtained from the Levenberg Marquardt (TRAINLM-11) algorithm.

Table 1. Statistical analysis of estimated monthly average air temperatures

Algorithm-Neuron	RMSE	COV	R^2
LM-3	0,038132	0,074996	0,981484
LM-4	0,032472	0,063863	0,986407
LM-5	0,030904	0,060780	0,987800
LM-6	0,034815	0,068473	0,984682
LM-7	0,051883	0,102041	0,965466
LM-8	0,038970	0,076645	0,983340
LM-9	0,035194	0,069218	0,984290
LM-10	0,054823	0,107823	0,961677
LM-11	**0,028915**	**0,056867**	**0,989238**
LM-12	0,033721	0,066320	0,985448

Training and testing phase has been started after the ANN model. In order to reach the least error level in the ANN model, a training set network has been presented. In the training of ANN model, the values of learning and momentum have been taken as 0.01 and 0.4, respectively. In the selection of the weight value where the performance is the best, the error values of the validation set obtained as a result of the training have been used.

In the test phase, all of the values given during the training have been presented to the network, thus the synaptic weight matrix and input values have been presented to the network and the program is estimated with the least margin of error. During the test, whether the algorithm has been converging to the actual values has been checked. The change in the performance of training, verification and test data in each iteration during the training of the network is given in Figure 5.

The lowest error value was observed in the 12th iteration of the model. At this point, the MSE value was found to be 0.0009352.

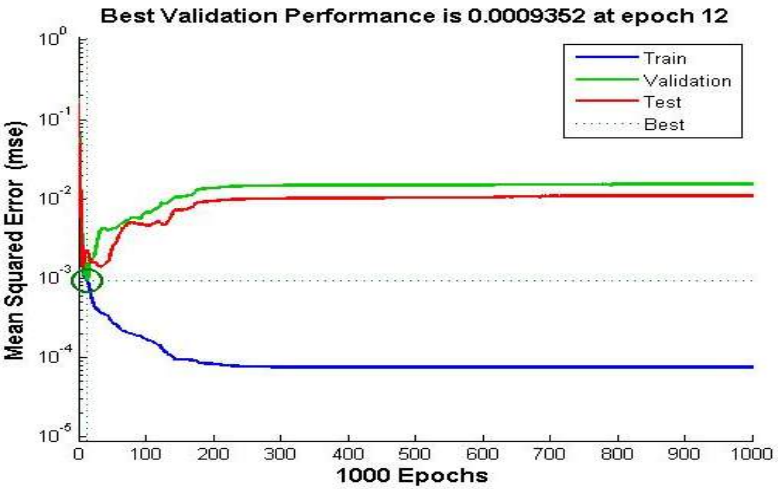

Figure 5. Performance evaluation of training, verification and test data

Figure 6 shows another type of graph showing validation error and learning rate changes. Validation check value is 993 in 1000 iterations. As the difference between the actual data and the estimated data started to increase after 7 iterations, the cycle has been stopped at 1000 iterations.

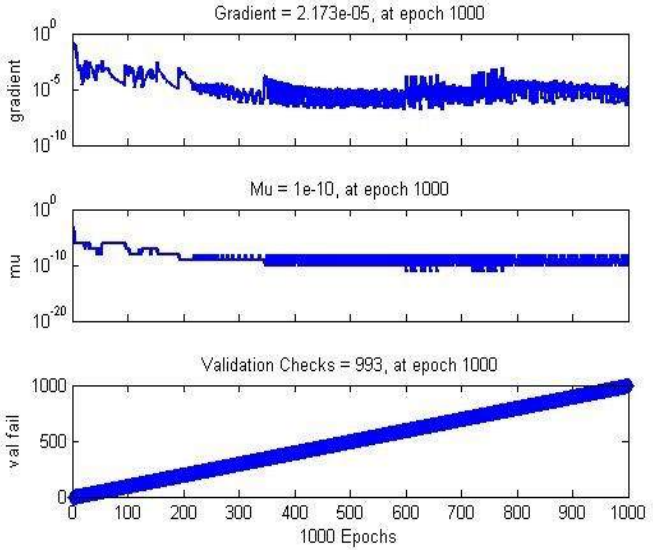

Figure 6. Gradient value, validation error and learning rate changes

Regression (R) graphs showing the performance of the model are given in Figure 7. For training data, R value has been obtained as R = 0.99316 and for the test data, it is R = 0.99577 using Mean Square Error (MSE). According to the graph, the data accumulates around the linear lines. This shows that the values tested and tested are compatible with validation. Figure All, R = 0.99394 indicates that this ANN model can be used in the estimation of surface roughness values with a very high confidence interval. In brief, the learning process of the network is very successful. For all data, it is seen that the values are close to 1 and converging to the actual data with ANN model output.

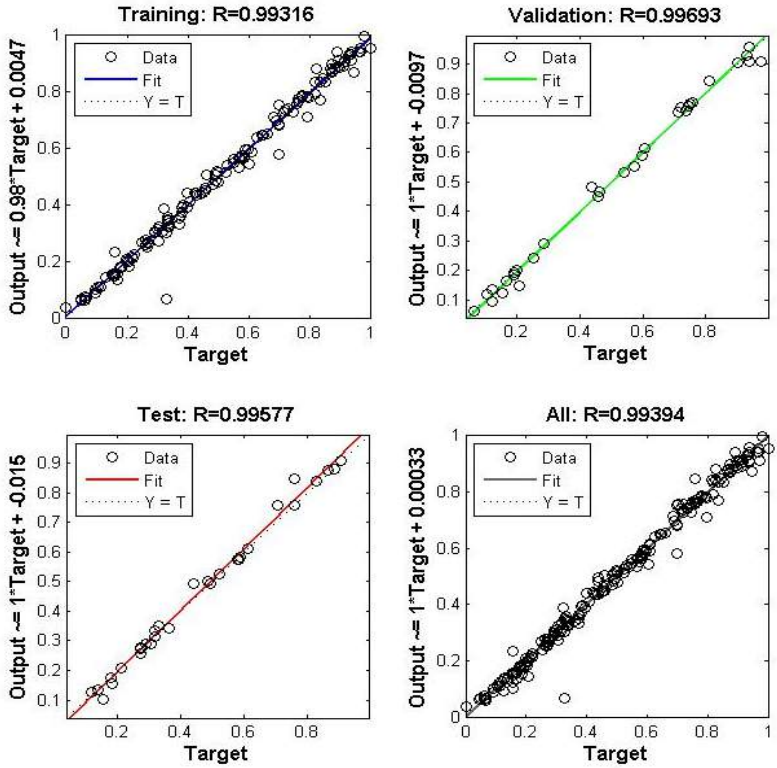

Figure 7. Regression graphs of training, verification and test sets

Table 2 shows the mean monthly average air temperature values obtained from the General Directorate of Meteorology for the years 2015 and 2016 in Burdur.

Table 2. Comparison of actual and estimated monthly average air temperature values

Year	Month	Actual Average Air Temperature (^{0}C)	Estimated Average Air Temperature with ANN Method (^{0}C)
2015	1	3,30	3,03
2015	2	4,10	4,37
2015	3	7,30	7,9
2015	4	10,60	12,21
2015	5	14,30	15,03
2015	6	19,50	16,96
2015	7	26,40	26,71
2015	8	25,90	25,67
2015	9	23,60	22,06
2015	10	16,00	16,10
2015	11	9,90	9,62
2015	12	2,60	3,11
2016	1	2,40	2,77
2016	2	8,50	7,87
2016	3	8,70	9,06
2016	4	16,20	16,90
2016	5	16,70	15,64
2016	6	24,10	24,25
2016	7	27,70	26,27
2016	8	26,90	25,20
2016	9	20,50	21,45
2016	10	15,90	16,58
2016	11	8,30	8,54
2016	12	0,70	0,66

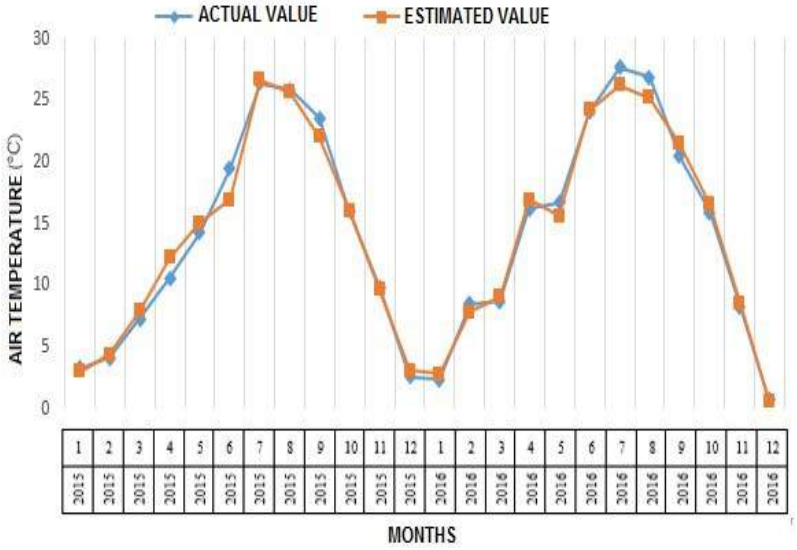

Figure 8. Comparative graphical representation of monthly average temperature data and real meteorological values estimated by ANN

Figure 8 shows the comparison of the average monthly air temperature estimates obtained from ANN for the years 2015-2016 and actual meteorological values. There are some minor differences in 2015 year 4, 6 and 9 months and 2016 year 7 and 8 months. As a result, it is seen that the actual values tested are close to each other with the predicted values.

CONCLUSION

In this study, the average monthly air temperature of Burdur has been estimated with the ANN model using various data of 2000-2016 years. Estimation values have been compared with the actual data. The accuracy of the results has been tested with high precision and it has been found that ANN model is very successful for estimating the average air temperature. The Logistic Sigmo Regression values of the results of training, validation and test data have been found to be close to 1 according to the air temperature values predicted by ANN model along with actual air temperature values.id function has been used to estimate the ANN model and the best result has been obtained in the LM11 algorithm. The training of the network has been completed in the 12th iteration and the MSE value for this point is 0.0009352. It has been observed that ANN can be used as an alternative to traditional forecasting methods in future planning for areas such as agriculture, animal husbandry and industry, where air temperature estimation is important.

REFERENCES

1. Demircan, M. Arabacı, H. Coşkun, M. Türkoğlu, N. Çiçek, İ. (2016). Sıcaklıkların Aylık Dağılım Desenleri, Tucaum 2016 Uluslararası Coğrafya Sempozyumu,Ankara.
2. Gill, E.J. Singh, E.B. Singh, E.S. (2010). Training back propagation neural networks with genetic algorithm for weather forecasting. IEEE 8th International Symposium on Intelligent Systems and Informatics, Subotica, Serbia, 465-469.
3. Peşkircioğlu, M. Özaydın, K. A. Özpınar, H. Nadaroğlu, Y. Dokuyucu, Ö. Aytaç Cankurtaran, Günal, S. Şimşek, O. (2016). Bitkilerin Sıcağa ve Soğuğa Dayanıklılık Bölgelerinin Türkiye Ölçeğinde Coğrafi Bilgi Sistemleri ile Haritalanması, Tarla Bitkileri Merkez Araştırma Enstitüsü Dergisi, 25 (1):11-25.
4. Tasadduq, I. Rehman, S. Bubshait, K. (2002). Application of neural networks for the prediction of hourly mean surface temperatures in Saudi Arabia", Renewable Energy, 25,545-554.
5. Smitha, B. A. Hoogenbooma, G. McClendon, R. W. (2009). Artificial neural networks for automated year-round temperature prediction,Computers and Electronics in Agriculture, 68, 52-61.
6. Dombayci, Ö. A. Gölcü, M. (2009). Daily means ambient temperature prediction using artificial neural network method: A case study of Turkey, Renewable Energy, 34(4),1158-1161.
7. Dr. S. Santhosh Baboo and I. Kadar Shereef, (2010). An Efficient Weather Forecasting System using Artificial Neural Network, International Journal of Environmental Science and Development 1(4), 321-326.
8. Erkaymaz H. Yaşar Ö. (2011). Yapay Sinir Ağı İle Hava Sıcaklığı Tahmini,5th International Computer & Instructional Technologies Symposium, Fırat University, Elazığ- Turkey.
9. Joshi, P. Ganju, A. (2012). Maximum and Minimum Temperature Prediction Over Western Himalaya Using Artificial Neural Network, Mausam, 63, 283-290.
10. Kisi, O. Shiri, J. (2014) Prediction of long-term monthly air temperature using geographical inputs', International Journal of Climatology,34(1),179–186.
11. Elmas, Ç. (2003). Yapay sinir ağları, Seçkin Yayıncılık, Ankara.
12. Çuhadar, M. (2013). Modelıng And Forecastıng Inbound Tourısm Demand To Turkey BY MLP, RBF AND TDNN Artıfıcıal Neural Networks: A Comparatıve Analysıs, Journal of Yasar University, 8(31) 5274-5295.
13. Aslay, F. Özen, Ü. (2013). Meteorolojik Parametreler Kullanılarak Yapay Sinir Ağları ile Toprak Sıcaklığını Tahmini, Politeknik Dergisi,16(4),139-145.
14. Öztemel, E. (2003). Yapay sinir ağları, Papatya Yayıncılık, İstanbul.
15. Şahan, M. Okur, Y. (2016). Akdeniz Bölgesine Ait Meteorolojik Veriler Kullanılarak Yapay Sinir Ağları Yardımıyla Güneş Enerjisinin Tahmini, SDU Journal of Science (E-Journal),11(1), 61-71.
16. Yılmaz, F. Selbaş, R. Şencan Şahin, A. Efficiency analysis of organic Rankine cycle with internal heatexchanger using neural network, Heat Mass Transfer,52, 351–359.

AUTONOMOUS ROAD VEHICLES AND ELECTRICAL-ELECTRONIC EQUIPMENT

Hayrettin GÖKOZAN [1] , Mehmet TAŞTAN [2]

[1] Dr. Manisa Celal Bayar University, Turgutlu Vocational School, Department of Electric & Energy, Manisa, Turkey.
[2] Dr. Manisa Celal Bayar University, Turgutlu Vocational School, Department of Electronic & Otomation, Manisa, Turkey.

1. INTRODUCTION

The digitalization process in vehicles has started with the use of electronic ignition systems and electronic speed indicators in the vehicles. This process, reverse vision cameras, parking assistants etc. equipment continued. It has also come to the end point known with autonomous vehicles without driver intervention.

Smart vehicles are vehicles equipped with cameras, sensors, computers, wireless communication materials Global Positioning System (GPS) which are added to the conventional vehicles used today and produced as a result of rapid development of digital technology [1]. These devices regularly send information to satellites, making it possible to identify the exact location of the vehicle on the earth. At the same time, the vehicles communicate with each other, with the control center as well as with smart traffic signs, determine speed distance information, the status of vehicles with transition priority, and the traffic and road conditions of motorways [2,3]. This is seen in figure 1.

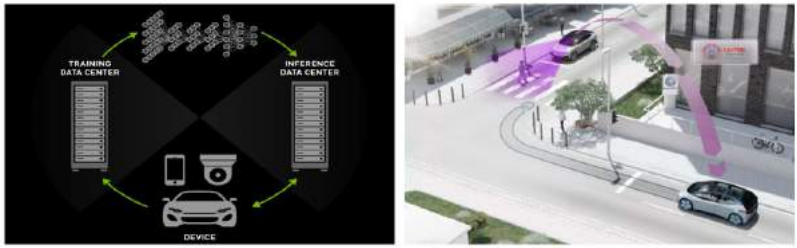

a b

Figure 1. (a) Communication of Vehicle to Data center [4] (b) Communication of Vehicle to Vehicle [4]

With the help of satellite assisted navigation systems, direction determination can be made easily today. Especially, in the parking car park, the parked vehicle is developed to provide parking facility by sending the location of the parking place. Moreover, vehicles that can automatically park when necessary are also widely used today [5]. These systems, combined with artificial Intelligence algorithms, determine their own way. The drive determines the start and end points and allows the car to select its own path [6]. Vehicles with black box-like devices similar to those intended to be placed on vehicles, the behavior of vehicles can be examined, in case of traffic violations can be easily controlled vehicles [7].

The first experiments on autonomous vehicles began in the 1920s. Between 1987 and 1995, he continued with the DARPA Autonomous Land Vehicles project between Mercedes-Benz and the US Department of Defense.

To date, all companies producing automobiles have been developing their research and trials in this area.

1.1. Some Advantages of self driving cars:

- Since 81 percent of car crashes are the result of human error, computers would take a lot of danger out of the equation entirely. 94% of accidents are caused by driver errors.
- Passencers can carry on with other things.
- Speed limits could be increased to reflect the safer driving, shortening journey times.
- Eases parking woes.
- Potential for more powerful vehicles.
- Efficient travel also means fuel saving, cutting costs.
- Travelers would be able to journey overnight and sleep for the duration.
- Nearly no error.
- There are no opportunities for a computer to be «distracted», which is a leading cause of accident.
- Mobility for disabled individuals.
- Traffic could be coordinated more easily in urban areas to prevent long tailbacks at busy times. Commute times could be reduced drastically.
- Drunk driving incident should decrease.
- Self-aware cars would lead to a reduction in car theft.

1.2. Some disadvantages of self driving cars

- The very security behind self-driving cars would be a major obstacle, especially because the technology would be of very high interest to hackers.
- Driverles cars would likely be out of price range of most ordinary people when generally introduced, likely costing over $100,000.
- Potantial loss of privacy.
- Personal injury lawyers may see a reduction in their earnings.
- Reading human road signs is challenging for a robot.
- Self-driving cars would eliminate many jobs in the transportation sector, especially taxi drivers.
- What happens if a sensor or sensors goes out?
- There are problems currently with autonomous vehicles operating in certain types of weather. Heavy rain interferes with roof-mounted laser sensors, and snow can interfere with its cameras.
- The gasoline industry is likely to suffer because the self-driving cars would be electric.
- Self-driving cars would be a great news for terrorist, as they could be loaded with explosives and used as moving bombs.

2. SELF-DRIVING CAR LEVELS

Until the present day, cars have become fully autonomous by going through various stages. These stages are respectively; No Automation, Driver Assistance, Partial Automation, Conditional Automation, High Automation and Full Automation. These levels are shown in the Figure 2.

SAE level	NAME	Narrative Definition	Execution of Steering and Acceleration/ Deceleration	Monitoring of Driving Environment	Fallback Performance of Dynamic Driving Task	System Capability (Driving Modes)
Human driver monitors the driving environment						
0	**No Automation**	The full time performance by the human driver of all aspects of the dynamic driving task, even when enhanced by warning or intervention systems	Human driver	Human driver	Human driver	n/a
1	**Driver Assistance**	The driving mode-specific execution by a driver assistance system of either steering or acceleration/ deceleration using information about the driving environment and with the expectation that the human driver perform all remaining aspect of the dynamic driving task	Human driver and system	Human driver	Human driver	some driving modes
2	**Partial Automation**	The driving mode-specific execution by one or more driver assistance system of both steering and acceleration/ deceleration using information about the driving environment and with the expectation that the human driver perform all remaining aspect of the dynamic driving task	**System**	Human driver	Human driver	some driving modes
Automated driving system ("system") monitors the driving environment						
3	**Conditional Automation**	The driving mode-specific performance by an automated driving system of all aspect of the dynamic driving task with the expectation that the human driver will respond appropriately to a request to intervene.	System	**System**	Human driver	some driving modes
4	**High Automation**	The driving mode-specific performance by an automated driving system of all aspect of the dynamic driving task, even if a human driver does not respond appropriately to a request to intervene	System	System	**System**	some driving modes
5	**Full Automation**	The full-time performance by an automated driving system of all aspect of the dynamic driving task under all roadway and environmental condition that can be managed by a human driver	System	System	System	**All driving modes**

Figure 2. Self-Driving Car Levels Explained [8].

3. CONTROL ELEMENTS USED IN VEHICLES

A wide variety of sensor-based auxiliary elements are used in autonomous vehicles. While some of these devices are used for measuring distance, some of them are effective in determining the physical properties of the objects. In addition, there is a computer used to evaluate the information received and to perform the necessary operations and other equipment that provides the movement of the vehicle. Figure 3 shows the general algorithm of the smart vehicle system.

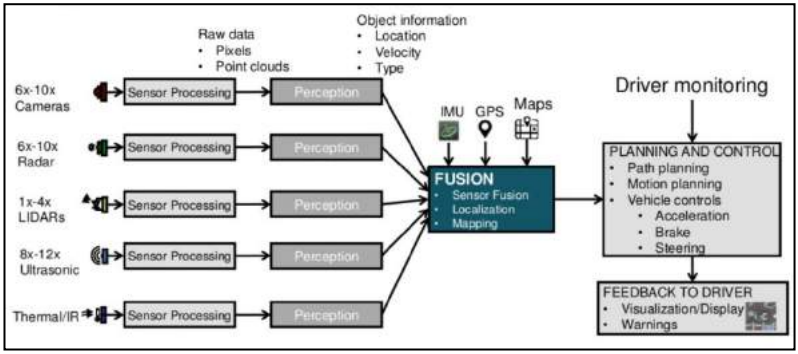

Figure 3. General algorithm of smart vehicle system [9]

Information from the sensors is transmitted to the control center. Data that is combined with sensor information, location and map information is transferred to the planning and control unit. Here, the task (road and movement planning, speed values, braking and management) of the vehicle is determined and implemented. The display and warnings are also displayed as feedback, if required for instant situations.

The electrical-electronic equipment used in smart vehicles are as follows:

- Radar (electromagnetic wave based-77/79 GHz 28 nm CMOS) sensors,
- Lidar (Laser beam based) sensors,
- Ultrasonic (Sound-wave based) sensors,
- Normal / Infrared (thermal) cameras and sensors,
- GPS,
- Computer and Software,
- Vehicle Control,
- Battery group,
- Inverter and Traction Motor.

3.1. Radar

(Radio Detection and Ranging): It is a system that enables us to understand, detect or measure the moving or stationary objects that are further away from our vision by means of electromagnetic (radio) waves. The system has a unit that detects a rotating signal by hitting the target with a signal emitter. When calculating the distance, the travel time of the electromagnetic beam is divided into two and multiplied by the speed of the beam.

3.2. Lidar

(Light Detection And Ranging): Lidar systems determine the distance from the road lines, people, traffic signs, roadside and obstacles with the laser distance sensor. This; similar to the radar system, but by sending light beams, it calculates the rotation time of the reflection from surrounding objects. The LIDAR instrument fires rapid pulses of laser light at a surface, some at up to 150,000 pulses per second.

Generally there are two types of LiDAR detection methods. Direct energy detection, also known as incoherent, and Coherent detection. Coherent systems are best for Doppler or phase sensitive measurements and generally use Optical heterodyne detection. This allows them to operate at much lower power but has the expense of more complex transceiver requirements.

In both types of LiDAR there are two main pulse models: micropulse and high-energy systems. Micropulse systems have developed as a result of more powerful computers with greater computational capabilities. These lasers are lower powered and are classed as 'eye-safe' allowing them to be used with little safety precautions. High energy systems are more commonly used for

atmospheric research where they are often used for measuring a variety of atmospheric parameters such as the height, layering and density of clouds, cloud particles properties, temperature, pressure, wind, humidity and trace gas concentration[10]. Principle of a lidar and distance measurement is seen in figure 4.

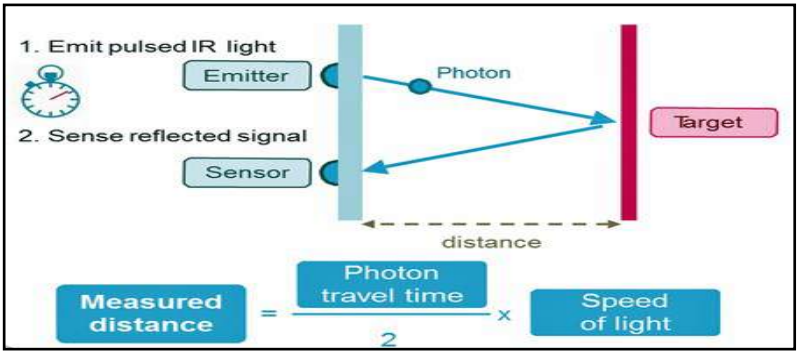

Figure 4. Principle of a lidar and distance measurement [11]

It is expensive and requires very powerful computers due to high data flow. Figure 5 shows the LIDAR, operating principle of LIDAR and the visualization of LIDAR data.

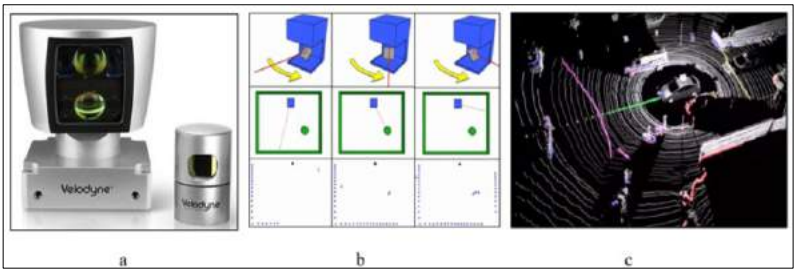

Figure 5. (a)LIDAR, (b) the operating principle of LIDAR and (c) the visualization of LIDAR data [10]

3.3. Ultrasonic Sensor

It is used for detecting objects and measuring distance with the help of sound waves. It consists of a sound source and a receiver that detects an echo. When calculating the distance, the sound is multiplied by the sound speed by dividing the sound when it hits the obstacle. The sensors are used together to turn their superiority into a more comprehensive sense. While the camera system detects the color of the surface, the lidar determines the material type of the surface of the body. When used together, the system can

detect the green surfaces corresponding to the grass and give a more detailed information about the environment.

3.4. Cameras

Used to transfer images around and inside the vehicle to the host computer in the vehicle. Infrared cameras, unlike normal cameras, are used to detect the temperature of objects. Keeping cameras and sensors clean is important for data quality.

3.5. GPS

It is the sensor used to locate the vehicle on earth. The GPS system identifies its own spherical coordinates by taking signals from satellites around the world. These coordinates are mapped to the road map coordinates and the position of the vehicle on the road is determined. The GPS system is used in conjunction with a gyroscope and accelerometer which is continuously used to measure the position, displacement and speed of the vehicle.

3.6. Computer and Software

Of course, the most important element in the use of autonomous vehicles, computers and software used in the control of the system. It takes place via a computer and running software (Controller Area Network, Local Area Network etc.) that provides control and interaction with GPS signals, data transmissions, traffic signs and other vehicles. Artificial Intelligence supported software evaluates the information coming from the system's input units and determines the movement of the vehicle by giving output according to the situation. The Control board can process 24 trillion operations every second. Figure 6 shows the Control board with different number of input-output units.

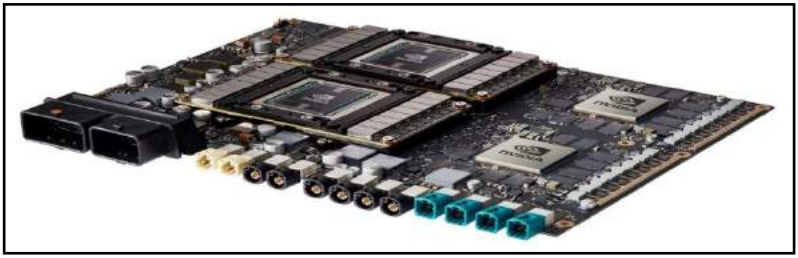

Figure 6. Control board with different number of input-output units[4]

3.7. Vehicle Control

The desired speed of the vehicle according to road and traffic conditions is carried out by speed control system (Cruise Control and Adaptive Cruise Control). The vehicle is also guided by the stepper, servo or hydraulic motors mounted on the vehicle's steering system. The user decides the time and shape of the starting and stopping of the vehicle (remotely or closely). Other operations (in case of emergency) are automatically activated by the controlling computer.

Figure 7. Identification of objects in autonomous vehicles[4]

In Figure 7, it is seen that the objects around the vehicle are determined as a result of the information received from the sensors. According to their properties, objects are differentiated in different color categories and the situation is evaluated. Here; vehicles are defined by green, people are defined by light blue, signalization, direction and speed plates are also defined in dark blue.

3.8. Battery

The main battery technologies commonly used in electric vehicles are Lead-Acid, Nickel-Iron, Nickel-Cadmium, Nickel-Metal Hybrid, Lithium-Ion, Lithium-Polymer, Lithium-Iron, Sodium-Sulfide, Sodium-Metal-Chloride batteries. Recently, Aluminum-Air and Zinc-Air batteries have been developed. Although batteries have a history of about 160 years, a suitable battery type for electric vehicles is still not fully developed.

Performance criteria of batteries; specific energy, energy density, specific power, nominal voltage, amp-hour efficiency, energy efficiency, commercial producibility, cost, operating temperature, self-discharge rate, life (how many times can be charged) and charging time. A designer also needs to consider how existing battery energy varies according to ambient temperature, charge and discharge speed, battery geometry, optimum temperature, charging method and cooling requirement.

A wide range of battery technologies are used, from simple electronic devices to electric vehicles. Although their usage areas are different, their performance and lifespan depend on the safe working area. This field of work improves the performance of the batteries by avoiding the dangers that may occur in the cases of overcharging and discharging. More efficient battery groups are being developed, which will be charged in a short time and allow the vehicle to travel longer. The battery management system is the unit that enables the batteries to operate in this safe area in terms of safety and performance.

3.9. Inverter and Traction Motor

Autonomous vehicles are usually electric vehicles. Electric vehicles are equipped with an electric traction motor that can drive the car on pure electric power. The inverter is a device used to convert the DC voltage from the battery inside the vehicle to the AC voltage required for the traction motor to be used. Permanent Magnet Synchronous Motors (PSM) and Asynchronous Motors (ASM) are the two main motor principles currently driving electric traction motors.

The traction motor is suitable for a range of vehicle applications, from medium size passenger cars to light duty commercial vehicles. Multiple drive systems per vehicle can be supported due to the safety case and levels of torque integrity employed. This electric motor has position and speed sensors. These sensors help to work properly. The motor operates like a dynamo during braking, generating electricity and charging the batteries. Principle of an inverter and Traction Motor is seen in figure 8.

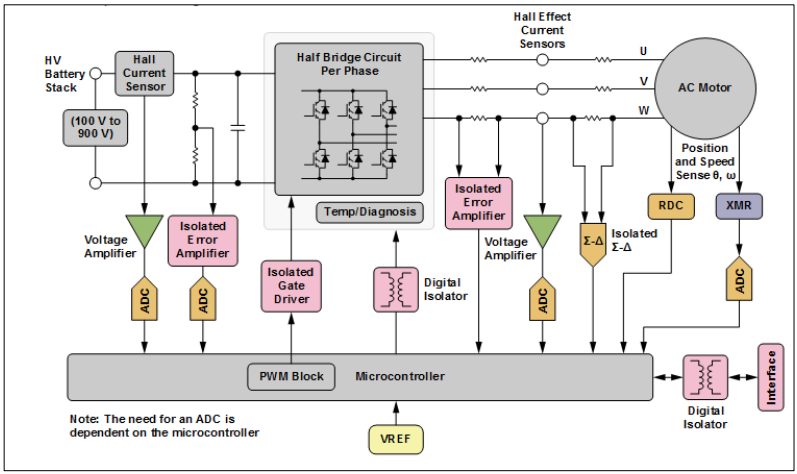

Figure 8. Principle of a Inverter and Traction Motor[12]

4. CONCLUSION

In the 2020s, autonomous vehicles are expected to become commonplace when the technologies used in intelligent and autonomous vehicles increase by 20% each year, and their production and use increases day by day. By this way, a more regular traffic flow on the roads will be possible thanks to artificial intelligence and deep learning, which can be prevented from traffic accidents caused by human errors, by means of communication of the vehicles with each other and with the hardware forming the smart traffic system (IoT-Internet of Things Internet). If desired, the images during the trip will be recorded and camera recordings related to accidents and adverse events will be created.

The ratio of the number of sensors and sensitivity to be placed on vehicles will also affect the price of the vehicles. As long as the machines are always active as long as they are not energized, the accident rates will be much less than the vehicles used by the drivers. If any technical error occurs in the course of navigation, the system takes measures to ensure safety, regardless of the main control unit, through special equipment equipped with the necessary sensors.

The biggest problem that can be encountered in driverless vehicles is a possible traffic accident, the use of the vehicle in terrorist incidents, the presence of cyber-attacks on vehicle software etc. in cases where the responsible person is determined by legal arrangement. The necessary legal arrangements in this regard have been completed to a large extent in the countries where the instruments are widely used, and are about to be completed in our country.

References

1. Gökozan, H., Taştan, M., Sarı, A., (2017), "Smart Cities and Management Strategies", International Strategic Research Congress (ISRC2017), Antalya.
2. Kerem, A., (2014), "Development of Electric Vehicle Technology and Future Expectations", The Journal of Graduate School of Natural and Applied Sciences of Mehmet Akif Ersoy University 5 (1), 1-13.
3. Ekinci, O. A., (2013), "Multi-Agent Based Large Scale Traffic Flow Simulation of Intelligent Transportation Systems", M.Sc. Thesis, Istanbul Technical University, Graduate School of Science.
4. https://www.youtube.com/watch?v=0rc4RqYLtEU, NVIDIA DRIVE Autonomous Vehicle Platform, Date of Access: 21.02.2019.
5. Gökozan, H., Taştan, M., Sarı, A., (2017), "Smart Cities and Management Strategies", LAP LAMBERT Academic Publishing, Chapter 8, Page(s): 115-126, Socio-Economic Strategies, (Extended Version).
6. Tepeköylü, S., (2016), "Mobil Lidar Applications, Data Processing Software and Models", Journal of Geomatic Engineering Research, 1(1), 1-7.
7. Okutkan, O., Maktav, D., (2014), "Use of Remote Sensing of Mobile Robots in Urban Area Navigation", 5. Symposium of Remote Sensing (UZAL-CBS 2014), Istanbul.
8. https://www.youtube.com/watch?v=EzylsrXtkxI, Date of Access: 10.01.2018.
9. https://www.slideshare.net/PeterLabaziewicz/perceiving-and-understanding-the-world-for-adas-and-autonomous-peter-labaziewiczv4/slide 11 of 19, Date of Access: 10.01.2018.
10. http://www.lidar-uk.com/how-lidar-works/, Date of Access: 14.02.2018.
11. https://www.sensorsmag.com/components/three-sensor-types-drive-autonomous-vehicles
12. https://www.analog.com/en/applications/markets/automotive-pavilion-home/ev-and-hevpowertrain/inverter-and-e-motor-systems.html, Date of Access: 16.03.2019.

APPLICATION OF COMBINED ULTRASOUND AND FENTON REAGENT IN SUGAR INDUSTRY WASTEWATER TREATMENT

Şefika KAYA [1] , Yeliz AŞÇI [2] ,

[1] Ph. D. Department of Chemical Engineering, Eskisehir Osmangazi University, Eskisehir, Turkey.
[2] Assoc. Prof. Ph. Department of Chemical Engineering, Eskisehir Osmangazi University, Eskisehir, Turkey.

1. INTRODUCTION

In the sugar factories producing crystal white sugar, a large amount of water is used during the production process and thus the amount of water coming out of the process at the end of production is also high (Akın, 2010). A significant part of this wastewater is the washing water which is formed as a result of washing the sugar beets carried to the factory. Another big part is the diffusion water in the sugar production plant and the waters of the press.

Sugar factory wastewaters contain various organic and inorganic substances. Organic substances are in the diffusion wastewater and inorganic substances in sugar beet wash wastewater (Hutnan et al., 2000; Sharma and Kumar, 2015). The high content of organic matter content (nitrogen and phosphorus) in the diffusion wastewater negatively affects soil fertility, plant growth and aquatic life. For this reason, the treatment without leaving the recipient environment is very important. Physicochemical and biological methods are widely used for the treatment of sugar beet wash wastewater. However, there is a need for advanced wastewater treatment methods to break down organic substances (Sahu and Chaudhari, 2015).

Advance oxidation processes (AOPs), which produces ·OH radicals that oxidize a wide range of organic substances quickly and selectively, has gain importance as an alternative process to classical treatment methods. AOPs are known as environmentally friendly in the treatment of wastewater by oxidizing biodegradable organic pollutants into a more harmless form (such as carbon dioxide, water and inorganic salts) (Primo et al., 2008).

The use of ultrasound as an AOPs has become one of the most interesting research topics in recent years. When the ultrasonic sound waves and Fenton reagents are used together, the oxidation efficiency, mass transfer rate and catalytic properties increases considerably (Voncina and Marechal, 2003). The chemical effect of the ultrasound is based on acoustic cavitation. Acoustic cavitation is defined as the formation, growth and collapse of the bubbles caused by the sound waves generated in a liquid in a very small time period by creating a large amount of energy (Eren, 2018).

In this study, it was aimed to treat the sugar industrial wastewater by combining ultrasound and Fenton reagents ($Fe(II)/H_2O_2$). In experimental studies, the effect of parameters such as pH, iron ion concentration, H_2O_2 concentration and reaction time on color and COD removal were investigated.

2. MATERIALS AND METHOD

2.1. Materials

Experimental studies were carried out with industrial wastewater which was obtained from Eskisehir Sugar Factory. Fenton reagents; iron(II) sulfate heptahydrate ($FeSO_4.7H_2O$) was supplied form Merck and hydrogen peroxide (30 wt%) was supplied from Sigma Aldrich.

2.2. Method

Experimental studies were performed with brand of Sonics VCX 750 ultrasonic homogenizer (20 kHz and 750 W). After adjusting the pH of the wastewater sample to the desired value, Fe(II) and H_2O_2 solutions were added. The instrument was operated by immersing the 13 mm probe of the ultrasound device into a 4 cm sample. At the end of the reaction time the analyzes of color and COD of sample were performed. The experimental setup of the ultrasound/Fenton process was shown in Figure 1.

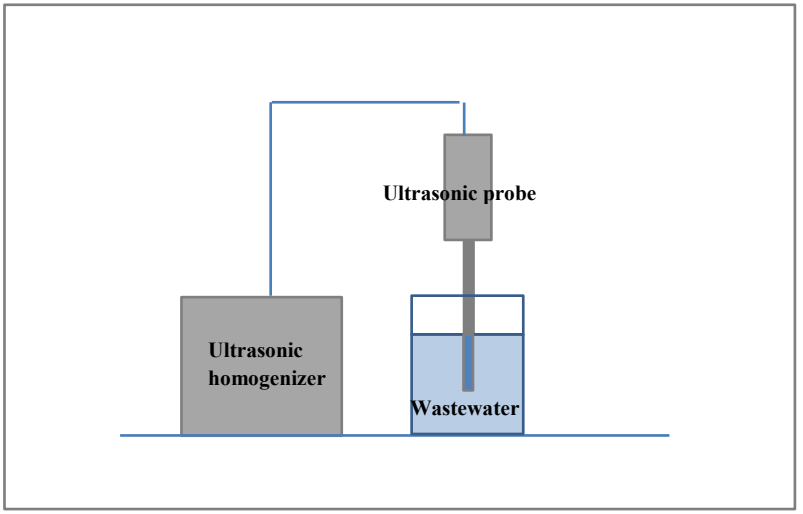

Figure 1. Ultrasound/Fenton process experiment setup.

2.3. Analyzes

The analyzes were performed by Hach Lange DR 3900 brand spectrophotometer. In color analysis, wavelength and maximum absorbance value (λ_{max}=327 nm) of the wastewater samples were determined by scanning in the wavelength range between 320-900 nm. The measurements were made at this wavelength and color removal efficiencies were calculated. COD analysis was performed with Hach Lange LCK 514 brand 13 mm diameter COD test kits. 2 ml of samples were put into the kits and kept in thermoreactor for 2 hours at 148^{o}C. Then, COD removal efficiency was calculated by spectrophotometer measurements. The initial COD of the wastewater was 478 mg/l.

3. RESULTS AND DISCUSSION

3.1. Effect of pH

The pH value, which is one of the most important parameters in the advance oxidation process, was changed between 2 and 5. The experimental results obtained by keeping the concentration of Fe(II) and H_2O_2 constant were given in Figure 2.

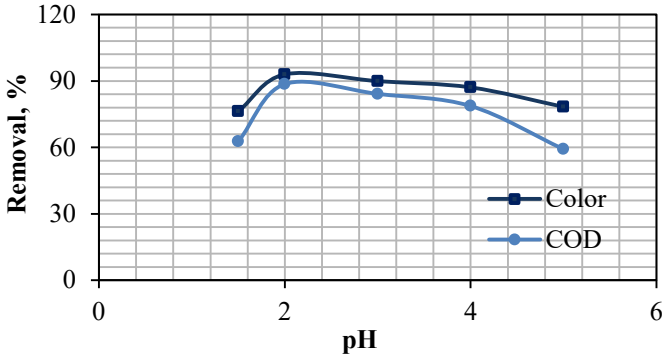

Figure 2. Effect of pH on color and COD removal (Fe(II)=200 ppm, H_2O_2=200 ppm and reaction time 120 minutes).

Fenton processes are highly effective under acidic conditions and the oxidation ability of the hydroxyl radical was very strong (Burbano et al., 2005). However at very low pH values, the formation of $Fe_2(H_2O)^{2+}$ occurs producing less hydroxyl radicals (Masomboon et al., 2010). When the experimental results were examined, the optimum pH value was determined as 2. After pH 2, color and COD removal efficiencies started to decrease. This can be explained by the decrease in oxidation potential of ·OH radicals at high pH values (Vajhandl and Marechal, 2007).

3.2. Effect of Fe(II) concentration

Another important parameter, iron ions, catalyzes H_2O_2 in the environment and provides the production of ·OH radicals. It is therefore important to determine the optimum concentration of Fe(II). In this study, the pH and H_2O_2 values were kept constant and the experiments were carried out with Fe(II) concentration of 50-100-150-200-250-300 ppm.

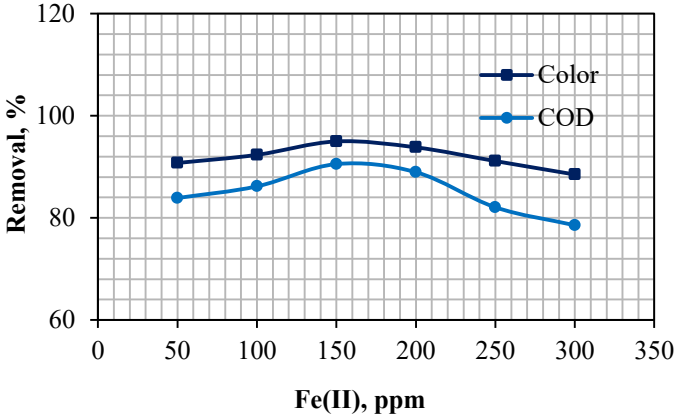

Figure 3. Effect of Fe(II) concentration on color and COD removal (pH=2, H_2O_2=200 ppm and reaction time 120 minutes).

When Figure 3 is examined, color and COD removal efficiencies increased by up to 150 ppm value with increasing iron concentration. 95.0% color and 90.5% COD removal efficiencies were achieved at 150 pmm. Due to the catalytic effect of iron ions on H_2O_2, when the iron ions concentration increases, the amount of ·OH radical in the environment increases (Tamimi et al., 2008). According to the results, as the Fe(II) concentration increased, color and COD removal efficiencies decreased. This is due to the inhibition effect shown by excess iron ions acting as scavengers (Brink et al., 2017).

3.3. Effect of H_2O_2 concentration

In order to determine the optimum H_2O_2 concentration, experiments were performed by constant pH and Fe(II) concentration at different H_2O_2 concentrations (50-300ppm).

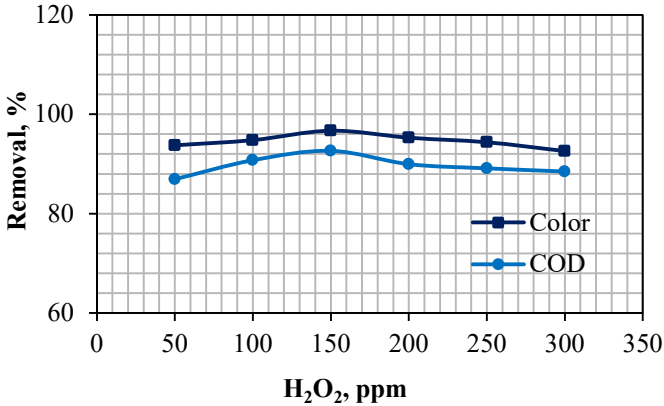

Figure 4. Effect of H_2O_2 concentration on color and COD removal (pH=2, Fe(II)=150 ppm and reaction time 120 minutes).

As shown in Figure 4, the color and COD removal efficiencies increased with increasing of H_2O_2 concentration. This is related to the fact that H_2O_2 is the source of the ·OH radical. The addition of more H_2O_2 to the solution will increase the amount of radicals ·OH increases so the efficiency of the treatment (Mahamallik and Pal, 2017). However, when the concentration of H_2O_2 is higher, the radicals such as peroxyl (HO_2·) and oxygen (O_2) which are non-active and act as cleansers occur. HO_2· is much less reactive and reduces removal efficiency. In addition, hydroxyl radicals produced at high concentrations can easily be converted to H_2O_2 (Firdous et al., 2018). For this reason, the optimum H_2O_2 concentration was chosen as 150 ppm.

3.4. Effect of reaction time

The effect of the reaction time was investigated by changing from 5 minutes to 240 minutes. The results obtained at constant pH, Fe(II) and H_2O_2 concentrations were given in the Figure 5.

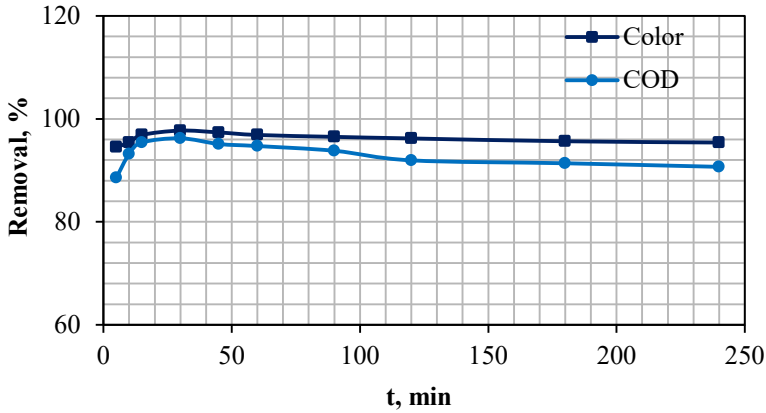

Figure 5. Effect of reaction time on color and COD removal (pH=2, Fe(II)=150 ppm and H_2O_2=150 ppm).

According to Figure 5, 94.6% color and 88.6% COD removal efficiencies were obtained in the first 5 minutes of the reaction time. At the 30th minute, maximum color (97.7%) and COD (96.2%) removal were obtained. In course of time, it was observed that the reaction was decelerated due to the decrease of ·OH radicals produced by decreasing Fe(II) and H_2O_2 concentrations. For this reason, the optimum reaction time was chosen as 30 minutes in working conditions.

4. CONCLUSION

In this study, sugar industry wastewater treament studies were carried out by applying the ultrasound/Fenton process. The parameters, which effected on color and COD removal, such as pH, Fe(II) and H_2O_2 concentrations and reaction time were investigated. The optimum conditions for the ultrasound/Fenton process were determined pH 2, Fe(II) concentration 150 ppm, H_2O_2 concentration 150 ppm and reaction time 30 minutes. Under these experimental conditions, 98% color and 96% COD removal efficiencies were achieved. According to the results of high color and COD removal obtained from this study, it was concluded that the combined use of Fenton reagents and ultrasonic sound waves was highly effective in the increase of wastewater.

REFERENCES

1. Akin, B.A. (2010). Chemical coagulation of sugar industry wastewater investigation of the treatment of the method and determination of optimum operating conditions. *M.Sc. thesis*, Ankara University, 110p.
2. Brink, A., Sheridan, C.M. and Harding, K.G. (2017). The Fenton oxidation of biologically treated paperand pulp mill effluents: A performance andkinetic study. *Process Safety and Environmental Protection*, 107, 206-215.
3. Burbano, A.A., Dionysiou, D.D., Suidan, M.T. and Richardson, T.L. (2005). Oxidation kinetics and effect of pH on the degradation of MTBE with Fenton reagent, *Water Research*, 39, 107-118.
4. Eren, Z. (2018). The study of treatability of residual pharmaceutical in water sources via Advanced Oxidation Technologies: A review. *Academic Platform Journal of Engineering and Science*, 6, 153-163.
5. Firdous, N., Shaikh, I.A. and Shahid, R. (2018). Decolorization of Reactive Azo Dye Remazol Black B by Using Advanced Oxidation Processes (AOPs). *Journal of The Chemical Society of Pakistan*, 40, 828-833.
6. Hutnan, M., Drtill, M. and Mrafkova, L. (2000). Anaerobic Biodegradation of Sugar Beet Pulp. *Biodegradation*, 11, 203-211.
7. Mahamallik, P. and Pal, A. (2017). Degradation of textile wastewater by modified photo-Fenton process: Application of Co(II) adsorbed surfactant-modified alumina as heterogeneous catalyst. *Journal of Environmental Chemical Engineering*, 5, 2886-2893.
8. Masomboon, N., Ratanatamskul, C. And Lu, M.C. (2010) Chemical oxidation of 2,6-dimethylaniline by electrochemically generated Fenton's reagent. *Journal of Hazardous Materials*, 176, 92-98.
9. Primo O., Rivero M.J. and Ortiz I. (2008). Photo-Fenton process as an efficient alternative to the treatment of landfill. *Journal of Hazardous Materials*, 153, 834-842.
10. Sahu, O.P. and Chaudhari, P.K. (2015). The characteristics, effects, and treatment of wastewater in 18 sugarcane industry. Water Quality, *Exposure and Health*, 7, 435-44.
11. Sharma, C. and Kumar, V. (2015). Analysis of the volume of the main water and wastewater in a sugar manufacturing process followed by the suggestion regarding the reutilization of the waste water. *International Journal of Current Engineering and Technology*, 5, 1757-61.
12. Tamimi, M., Qourzal, S., Barka, N., Assabbane, A. and Ait-Ichou, Y. (2008). Methomyl degradation in aqueous solutions by Fenton's reagent and the photo-Fenton system. *Separation and Purification Technology*, 61, 103-108.
13. Vajhandl, S. and Marechal, A.M.L. (2007). Case study of the sonochemical degradation of textile azo dye Reactive Black 5. *Journal of Hazardous Materials*, 141, 329-335.
14. Voncina, D.B. and Marechal, A.M.L. (2003). Reactive dye decolorization using combined ultrasound/H_2O_2. *Dyes and Pigments,* 59, 173-179.

AN EXPERIMENTAL COMPARISON OF STEEL WIRE ROPE SERVICE LIFE USED IN HOISTS

Abdurrahman AYDIN [1], Erdem KURTMEN [2], Fatih KAHRAMAN [3], Vjekoslav IVKOVIC [4]

[1] Güralp Vinç ve Makina A.Ş., Research and Development Center, Izmir, Turkey.
[2] Güralp Vinç ve Makina A.Ş., Research and Development Center, Izmir, Turkey.
[3] Dokuz Eylül University, Faculty of Engineering, Department of Mechanical Engineering, Izmir, Turkey.
[4] The University of Salford, School of Computing, Science and Engineering, Department of Mechanical Engineering, Manchester, United Kingdom.

1. INTRODUCTION

Wire rope is an interesting and complex, but yet such a simple structural element combining both flexibility and strength. Broad range of use, of a wire rope, requires extreme diversity in rope types. Throughout its lifetime, it is expected that wire rope withstands repeated axial and bending stretch loads [1]. In order to produce requirement satisfying wire ropes, there are certain procedures that have to be considered for it to have desired mechanical properties [2]. One of the most important characteristics of a wire rope is their helical winding that gives them the strength and rigidity for their purpose of use. It is inevitable that after a certain number of working cycles and due to gradual deterioration, wire rope has to be retired from service and replaced. There are several types of failures that can be considered while observing the working life of a rope wire. Some of the types of failures are, high contact stresses and longitudinal sliding stresses at contacting points between ropes outside surface and sheaves. Even though sometimes maximum strength of a wire rope is not exceeded, it is possible for a wire rope to fail due to fatigue stresses that come in different forms according to Mourady, El Barkany and Biyaali [3]. Wire rope lifetime can be prolonged immensely by taking into consideration some of the failure mechanisms and act against them before the consequences have already occurred. Some of the protection mechanisms are lubrication, zinc coating (galvanizing) and plastic shielding [3].

The fatigue strength of wires used in steel ropes depends on the following parameters [4]:

Manufacturing related:

- Chemical composition of wire
- Wire diameter
- Wire section shape
- Surface quality
- Surface coating condition

Use related:

- Drive type and equipment type
- Sheaves material, diameter and groove shape
- Case and size of loading
- Environmental conditions
- Maintenance

Wire ropes operate under high stress conditions and are almost always subject to variable loads. One reason for the stress changes in the continuous working wire ropes is the repeated bending over the sheaves and drums [5].

Compared with textile ropes, wire ropes have the advantage of greater strength and longer service life. The quality of the ropes and the degree of wear significantly affect cranes in terms of safety and reliability [1, 6].

This article presents a practical example of duration of a steel wire rope lifetime through tests based on 4 different specimens. Each of the specimens of the same type has been tested twice, giving 8 sets of results presented in tables. All of the calculations presented use equations extracted from ISO 4308-1 and FEM 9.661 standards. The wire ropes used for tests are all of the same nominal diameter and are compacted and galvanized. Throughout this text, the test procedures used have been presented and explained along with the possible reasons for failures. It should be noted that failure of a wire rope in practice is considered once inspection determines that it is not safe and will not last until next inspection. While performing this testing, rope was used until fractured completely. Corrosion, lubrication, abrasion, groove material, shape of the grooves, fleet angle are the factor of influence which are not taken into account while performing tests. All of the wire ropes are tested in same conditions and compared their service life.

2. MATERIALS AND METHODS

For the fatigue test, 5000 kg capacity hoist and the testing platform used were designed and manufactured. Hoist has been designed according the FEM and ISO standards. Using four rope specimens, constant weight was applied and repeatedly lifted and lowered, each time completing one full lifting cycle. This process was performed until complete failure of the tested specimen. The number of cycles until the rope has fully fractured have been recorded using a PLC software in the machine control panel.

There are 3 different types of ropes according to type of core; fiber core, strand core and steel core are shown in figure 2. The wire ropes used in this study are all steel cored wire rope [7]. As the metal cross-sectional area of steel cored wire ropes is more durable than others, the tensile strength is higher.

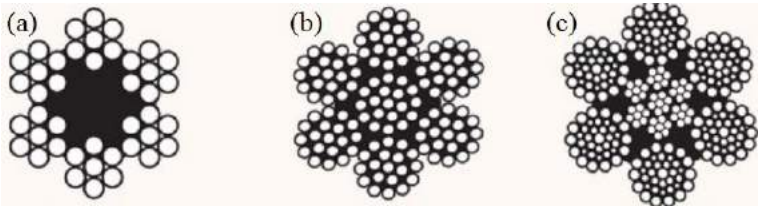

Figure 1. Steel wire rope cores; (a) fiber core, (b) strand core, (c) steel core

Steel wire ropes used in this study are produced using high quality wire materials by following the relevant international standards. The most important factor for selecting the suitable wire rope which is used for the

hoist is deciding whether a rope type is to be rotation resistant or non-rotation resistant [8]. This point needs to be considered very carefully as using the non-rotation resistant ropes must not be used with a swivel [8]. The wire ropes used in this study are all non-rotation resistant rope, galvanized, containing polimers (plastic) and compacted. The polimer (plastic) layer between steel core and the outer strands acts like a cushion reducing the contact stresses and prevents steel to steel friction. This way internal wire rope failure is prevented, and wire rope work life is significantly prolonged [9]. Steel wire rope constructions are shown in figure 2.

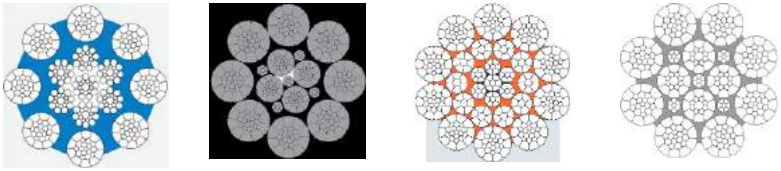

WR-A WR-B WR-C WR-D

Figure 2. Steel wire rope construction

One of the other factors that affect the life of the wire rope is lubrication. Generally, steel wire ropes are lubricated during production, but it is not sufficient for long term use [10]. Wire ropes must be lubricated at regular intervals with a suitable lubricant to increase their service life and avoid the formation of rust [11]. Advantages of wire rope lubrications are protection from abrasion, increasing service life, protecting against corrosion, providing better slide of wires and strands during work [10].

3. THEORY AND CALCULATION

The rope diameter is determined according to FEM 9.661 and ISO 4308-1:2003 standards by the following formula:

$$d_{min} = C.\sqrt{S} \quad (1)$$

Where:

d_{min}: Minimum rope diameter in mm

S: Maximum force of the rope in N

C: Coefficient is calculated as a function of the cable construction and the group of mechanism is calculated according to FEM 9.661 and ISO 4308-1:2003 standards by the following formula:

$$C = \sqrt{\frac{Z_p}{\gamma . f . R_0 . \frac{\pi}{4}}} \quad (2)$$

Where:

Z_p: Partial safety coefficient according to the group of mechanism

R_0: Tensile strength of the individual wire in N/mm²

f: Filling factor

$$f = \frac{metallic\ cross\ section}{area\ of\ the\ circumscribed\ around\ rope\ cross\ section} \quad (3)$$

γ: Spin (loss) factor

$$\gamma = \frac{minimum\ breaking\ strength\ of\ the\ rope}{calculated\ breaking\ strength\ of\ the\ rope} \quad (4)$$

General specification of the hoist is given in Table 1.

Table 1. General specifications of hoist

	Capacity [kg]	**Rope falls**	**Max. rope force [N]**	**The group of mechanism**
1	5000	4/1	12262,5	FEM 2m / ISO M5

Four different types of wire ropes are used in this experimental study. Partial safety coefficient of the rope (Z_p value) is selected according to classification of mechanism from Table 1. in FEM 9.661 standard and Table 1. in ISO 4308-1:2003 standard [11,12]. If the crane is used for dangerous conditions or transporting dangerous material, for example the handling of molten metal or chemical material the Zp value shall be increased by 1,25 times up to a maximum 9 [11,12]. For cranes transporting dangerous materials, the classification of mechanism shall not be less than FEM 2m or ISO M5 [11,12]. Technical specifications of the wire ropes and results of minimum rope calculation which are used in the test hoist are given in Table 2. The safety factor of selected rope must be greater than the Z_p value given in the standards, so the selected rope diameter must be greater than D_{min}. As

can be seen from the calculation results in the table, the maximum safety factor is found in WR-B.

Table 2. Technical specifications of wire ropes

	Wire rope Code	Rope Grade (R_0) [N/mm²]	Filling Factor (f)	Spin (Loss) Factor (γ)	Partial safety coefficient of ropes (Z_p)	Calculated coefficient (C)	Min. rope dia. d_{min} [mm]	Selected rope dia. d_{wr} [mm]	Safety factor of selected rope
1	WR-A	2160	0,659	0,847	4,5	0,06894	7,63	8	4,94
2	WR-B	2160	0,7403	0,84	4,5	0,06531	7,23	8	5.5
3	WR-C	2160	0,732	0,83	4,5	0,06608	7,32	8	5,4
4	WR-D	2160	0,71	0,86	4,5	0,06591	7,3	8	5,4

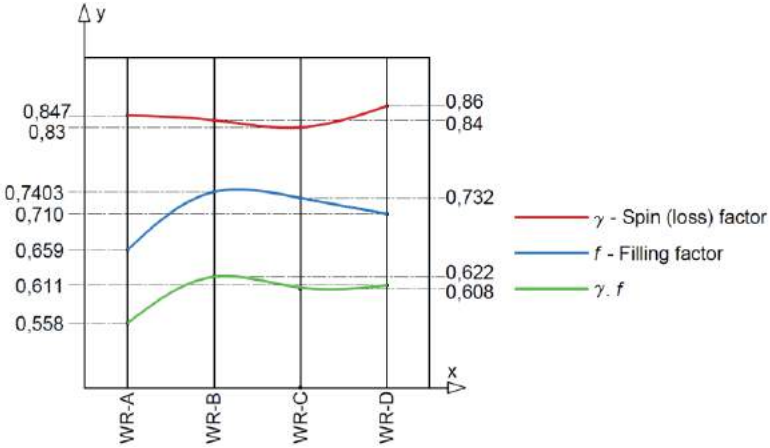

Figure 3. Technical specifications of wire ropes

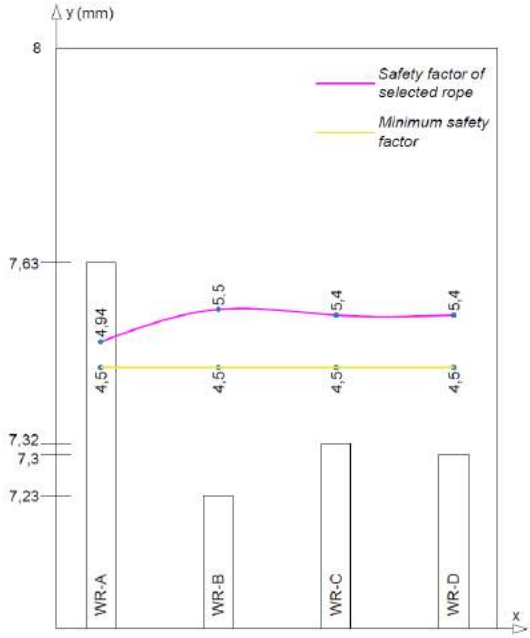

Figure 4. Comparison of safety factors

Rope reeving components (drum, sheave, compensating sheave) are selected depending on the minimum rope diameter by the following formulas:

$$D_1 \geq h_1 . d_{min} . t \quad (5)$$

$$D_2 \geq h_2 . d_{min} . t \quad (6)$$

$$D_3 \geq h_3 . d_{min} . t \quad (7)$$

Where:

D_1: Drum diameter in mm

D_2: Sheave diameter in mm

D_3: Compensating sheave diameter in mm

t: The factor of wire rope type according to Table 3. (Rope type factor t for various rope types) in ISO 4308-1:2003 standard.

The factor of wire rope type (t) takes into account the different bending fatigue performance of different types of wire rope [12]. The minimum pitch circle diameter of the rope reeving components (drum, sheave, compensating

sheave) is calculated using formula 5,6 and 7 and the factor of rope type (t) is taken into account as 0,95 depending on the number of outer strands in the rope according to ISO 4308-1:2003 [12]. The diameter of drum, sheave, compensating sheave and the pressure between wire rope and groove affects the service life of rope [11]. The service life of the wire rope increases as the pressure decreases [11]. Creating spiral grooves along the drum, machined in a continuous spiral around the barrel, gives a degree of support to the rope, making it coil correctly and reducing the unit contact pressure [11]. The groove radius (r) has to be adapted to the actual rope diameter. The minimum recommended radius of groove according to FEM 9.661 is determined by the following equation:

$$r = 0{,}53.d_{wr} \tag{8}$$

Table 3. Diameter calculation of the rope reeving components

	Wire rope Code	Min. rope dia. d_{min}[mm]	Selection factor for drum (h_1)	Selection factor for sheave (h_2)	Selection factor for compensating sheave (h_3)	Rope type factor (t)	Min. dia. of drum $D_{1,min}$ [mm]	Min. dia. of sheave $D_{2,min}$ [mm]	Min. dia. of compensating sheave $D_{3,min}$ [mm]
1	WR-A	7,63	18	20	14	0,95	130,47	144,97	101,48
2	WR-B	7,23	18	20	14	0,95	123,63	137,37	96,16
3	WR-C	7,32	18	20	14	0,95	125,17	139,08	97,36
4	WR-D	7,3	18	20	14	0,95	124,83	138,7	97,09

Under one and the same rope pull S, ropes having a diameter of up to 1,25 times the calculated diameter (d_{min}) may be provided without affecting their life if the rope reeving components have the diameters D calculated as Table 3 [11].

When calculating, the design working period (DWP) of a hoist, the estimated duty from the history shall be increased by a safety factor according to ISO 12482:2014 [13]. Safety factor f_1 for duty counting is 1 from Table 1 in ISO 12482:2014 standard because the hoist which is used in this study has an automatic recording system and manual documentation. Total operation time is 1600 hours for FEM 2m and ISO M5 classification of mechanism [14].

4. RESULTS AND DISCUSSION

Eight tests were carried out using a 5000 kg (49 kN) capacity hoist which is located on special test platform. The tests were performed with a dynamic test load. Dynamic load coefficient is 1,10 therefore, the test was carried out using 5500 kg load. Two tests were performed for each wire rope. Test results are given in Table 4.

Table 4. Test results

	TYPE	HOURS	MONTH
TEST-1	WR-A	116	8,7
TEST-2	WR-A	102	7,65
TEST-3	WR-B	178	13,35
TEST-4	WR-B	205	15,375
TEST-5	WR-C	80	6
TEST-6	WR-C	216	16,2
TEST-7	WR-D	132	9,9
TEST-8	WR-D	138	10,35

The highest safety factor is calculated for WR-A type as seen from Table 3 and Figure 4. But, as seen from the test results, the best results were WR-B and WR-C ropes.

The highest safety factor was calculated as 5,5 for WR-B ropes, and the lowest safety factor was calculated as 4,94 for WR-A ropes. In parallel with these calculations, the highest service life of the rope was WR-B, the lowest service life of the rope is WR-A.

Although the WR-C rope broke after 80 hours in the first test, it was broken after 216 hours in the other test. The reason for the low lifetime of the first test may be that the rope is damaged before it was wound up on the hoist. Because the tests for the other 3 ropes gave approximately similar results in the same type of ropes.

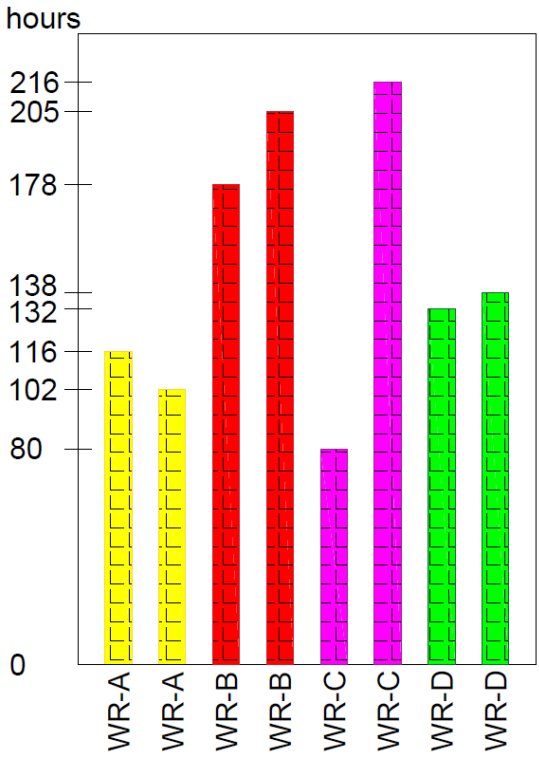

Figure 5. Test results diagram

5. CONCLUSIONS

Hoist operation data should be recorded by a special software when the hoist is in use. The possibility of switch off the recording system of the crane operator must be eliminated.

The hoist duty history should be calculated based on a regular process on which the hoist operates and the time remaining to maintenance must be known to the user. Accordingly, it should be possible to calculate the time of the rope change according to the estimated wire rope service life.

The ropes are expected to use the rope that is best suited to their operating conditions in order to perform their duties safely. Factors affecting the life of the rope should be known.

The steel wire ropes used in hoists are one of the most critical elements. The choice of rope types and diameter must be made in accordance with relevant and updated international standards. Maintenance and controls should be carried out periodically.

In order to get the most out of the selected wire rope, user should strictly apply the relevant international standards for the particular type of use. The operating conditions are extremely important in order to use wire ropes efficiently and with a minimal risk of danger. One of the means of control is the constant onboard software control that always has to remain on. Also, by monitoring the duty history of the hoist, user should be aware of the number of remaining cycles until maintenance and capable of calculating time of the rope change depending on the estimated wire rope service time.

REFERENCES

1. P. Peterka, J. Krešak, S. Kropuch, G. Fedorko, V. Molnar, M. Vojtko, "Failure Analysis of hoisting steel wire rope", Engineering Failure Analysis, Volume 45, pages 95-105, 2014.
2. K. Feyrer, "Wire Ropes: Tension, Endurance, Reliability", Springer-Verlag Berlin Heidelberg, 2007.
3. H. Mouradi, A. E. Barkany, A. E. Biyaali, "Investigation on the Main Degradation mechanisms of Steel Wire Ropes: A Literature Review", Journal of Engineering and Applied Sciences 11(6): 1206-1217, 2016.
4. M. N. Gerger, M. Tayanç, "Çelik Tel Halatlarda Tel Çapı ve Redüksiyon Oranının Yorulma Dayanımına Etkisi", Makina Tasarım ve İmalat Dergisi, Cilt 3, Sayı 4, 1998.
5. A. S. Anıl, "Eksenel Yüklü Tel Halat Demetlerinin Bilgisayar Ortamında Yorulma Ömürlerinin İncelenmesi", Yüksek Lisans Tezi, İstanbul Teknik Üniversitesi, 2011.
6. M. Giglio, A. Manes, "Life Prediction of a Wire Rope Subjected to Axial and Bending Loads", Engineering Failure Analysis, 12:549–68, 2005.
7. Technical information, Important Things About Steel Wire Rope, http://www.celsancelik. com/en/teknik-bilgiler/ (Accessed date: 03.03.2019).
8. Diepa, Special Wire Ropes Catalogue, http://www.diepa.de/files/diepa/Kataloge/ Katalog%20englisch%2003_2016.pdf, (Accessed Date: 03.03.2019).
9. Casar Special Wire Ropes, Steel Wire Ropes for Cranes, Problems and Solutions, http://fastlift.co.za/pdf/CASAR%20%20Rotation%20characteristics%20of%20steel%20wire%20rope.pdf.
10. G. A. Costello, "Theory of Wire Rope, Second Edition", Springer Science+Business Media New York, 1997.
11. Fédération Européenne de la Manutention, Rules for the design of series lifting equipment, Dimensions and design of rope reeving components, FEM 9.661, 2nd edition, 1998.
12. International Standard, Cranes and Lifting Appliances – Selection of Wire Ropes, Part 1: General, ISO 4308-1, 2003.
13. International standards, Cranes – Monitoring for Crane Design Working Period, ISO 12482, 2014.
14. International standards, Cranes – Classification – General, ISO 4301-1, 2016.

ALGINATE GEL-COATED KAOLIN ADSORBENT FOR REMOVAL OF CR (VI): *MECHANISMS AND FACTORS AFFECTING THE ADSORPTION*

Şerife PARLAYICI [1] , Erol PEHLİVAN [2]

[1] Dr., Department of Chemical Engineering, Konya Technical University, Campus, Konya, Turkey.
[2] Prof. Dr., Department of Chemical Engineering, Konya Technical University, Campus, Konya, Turkey.

1. Introduction

The cleaning process of contaminated metal from industrial leakage is one of the most important environmental issues that have not been solved in recent years. Surface water pollution by toxic metals is common in developing countries due to waste discharge (Norgate et al. 2007; Bonanno et al. 2017; Ogata et al. 2012). Significant amounts of harmful ions in the water sources increases in the aquatic environment emerged from industrial activities evry year. For this reason, clean water is essential for most plants, animals and human life (Tchounwou et al. 2012; Qu et al. 2013; Khan et al. 2014; Pehlivan and Altun 2008).

Kaolinite can be found as a silicate material in deep rock soil, and rocks. The mass ratio is 1:1 dioctahedral aluminosilicate clay mineral (Deng et al. 2017; Brigatti et al. 2006). It became completely bonded to the tetrahedral silica film on an octahedral sheet via oxygen atom sharing between silicon and aluminum atoms in neighboring layers (Khan et al. 2017). The following identical layers bring them together and hydrogen bonds form layers between adjacent silica and alumina. A tetrahedral sheet with a small negative charge was produced without any form defined by Si^{4+} and Al^{3+} substitution so that the negative charges were received for each replacement.

This study has developed an environmentally friendly novel kaolin/alginate composite for the application of Cr (VI) removal from aqueous solution. Alginate is one of the most functional polymers and alginate belongs to a large group of sugars which are mainly produced from brown algae. The relative amounts of each alginate vary with the source of the alginate (Escudero et al. 2006). Alginate consists of (1-4)-linked b-D-Mannuronic acid and a-L-guluronic acid monomer residue, which form block structures (Volesky 2003; Vijaya et al. 2008). Most of the alginate application is based on the ability to assemble gel by binding positive charge ions. Alginate is effective to remove toxic, easy to use and was reported as a suitable adsorbent to be worthwhile due to its efficiency in toxic metal removal, easy usage, economic, and due to the fact that it's obtained easily from oceans. Different forms of alginate such as gels, pastes, fibers and solid structures have been evaluated for use in many applications. The most popular process is living cell immobilization in alginate gels. Most current studies on improving adsorption capacity of kaolin focus primarily on the study of the effects of pH, mass dose, and time. Little attention was taken after treatment of kaolin with alginate.

Many removing methods such as chemical precipitation, adsorption, electro-deposition, ion exchange, photo-catalytic reduction, ultrafiltration and membrane filtration are now used to remove Cr (VI) from the wastewater systems (Parlayıcı et al. 2016; Altun et al. 2016; Dong et al. 2014; Mu et al. 2010; Duan et al. 2017; Wang et al. 2016). However, these technologies are ineffective or expensive when Cr (VI) is present in the wastewater at a low concentration. The new adsorbent has an interesting alternative adsorbent properties and it is cheap and easily available material.

Therefore, we should pay close attention to the use of natural materials available in large quantities. However, many of the adsorbents are not always able to perform a good adsorption efficiency and capacity for Cr (VI). The aim of this study was to investigate the adsorption properties of Alg©Ka towards Cr (VI). Different parameters of the adsorption process such as stirring time, metal concentration, pH and amount of adsorbent material were tested in the treatment process.

2. Materials and methods

2.1. Materials

All of the chemicals used in the experiments were analytical grade and ultra-pure was used to prepare the necessary solutions. Cr (VI) stock solution was prepared by dissolving $K_2Cr_2O_7$ salt (Merck) in ultra-pure water. $CaCl_2$, NaOH and HCl solutions were obtained from Merck.

2.2. Preparation of alginate coated kaolin

5% sodium alginate suspension (w/v) was prepared by mixing the sodium alginate powder with ultra-pure water. This suspension was hold in distilled water and the gel was formed in 2 hours. 5% kaolin suspension (w/v) was prepared and dispersed in distilled water. Kaolinite suspension was added to the alginate gel in the form of 1/1 mass ratio (kaolin/alginate) and the solution was stirred for 6 hours with a magnetic stirrer to form a homogeneous slurry. The solution was kept in the dark overnight. The resulting suspension was added dropwise by using a 5 mL syringe (needle size 0.6 mm) into 0.5 M $CaCl_2$ solution (1 ml gel/5 ml $CaCl_2$) with continuous stirring (100 rpm). The Alg©Ka beads were formed and the suspension was filtrated and washed with distilled water until neutral condition was obtained. The produced adsorbent was then dried at room temperature (Fig. 1.).

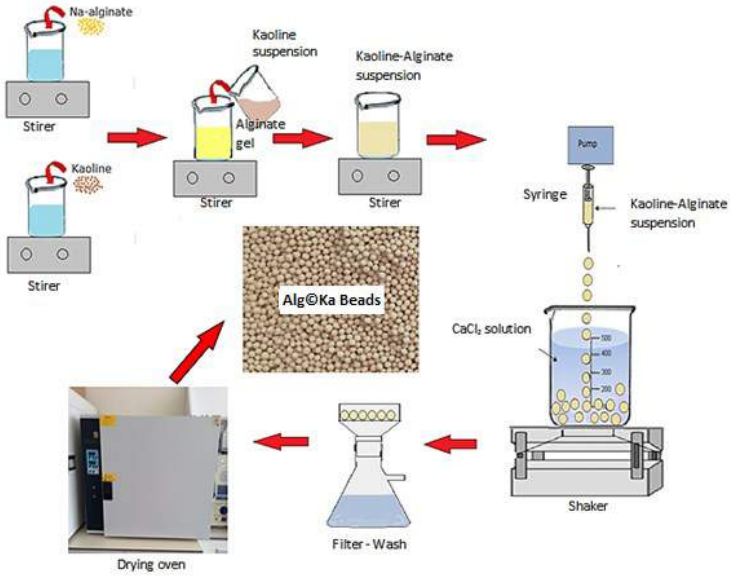

Fig. 1. Preparation of Alg©Ka beads

2.3. Characterization of the adsorbent

During the adsorption experiments, the pH measurement was adjusted with Orion 900S2 Model pH meter. A thermostated shaker of GFL 3033 model and IKAMAG- RO15 model magnetic stirrer was used for mixing the solutions in the adsorption experiments. The remaining Cr (VI) in the solution phase was measured by using a UV-Visible Spectrophotometer (Shimadzu UV-1700).

The FT-IR spectra for Alg©Ka was recorded with Bruker-Platinum ATR-vertex 70 (Germany) between 550-4000 cm-1 wavenumbers at a resolution of 4 cm^{-1} using an attenuated total reflectance (ATR) accessory. The FTIR spectrum of Alg©Ka is shown in Fig. 2. The evidence for the presence of alginate comes from the appearance of two peaks at 1591 cm^{-1} due to asymmetric stretching vibration and near 1416 cm^{-1} due to asymmetric COO^- stretching vibration (Bajpai and Sharma 2004). Mannuronic and guluronic acid in the structure of alginate or in other words the polysaccharide structure represented by 796 and 679 cm^{-1} bands (Larosa et al. 2018). A broad peak around 3300-3330 cm^{-1} represents the vibrational bands of -OH and confirms the presence of -OH in the kaolin. In FTIR spectrum; bands at 3685, 3620 and 3484 cm^{-1} present vibration -OH groups in the water molecules connected to the Si-O-Al surface by a weak hydrogen bond. The asymmetric vibration band and the symmetric

vibration band of the COO^- group were observed at 1594 cm^{-1} the 1422 cm^{-1}, respectively (Li et al. 2011). Si-O vibration of Si-O-Si groups in the layer of tetrahedral was observed near 1006 cm^{-1} (Abd El-Latif et al. 2010). The characteristic sharp bands at 908 cm^{-1} can be assigned to the Al-O-H bending vibration of kaolin.

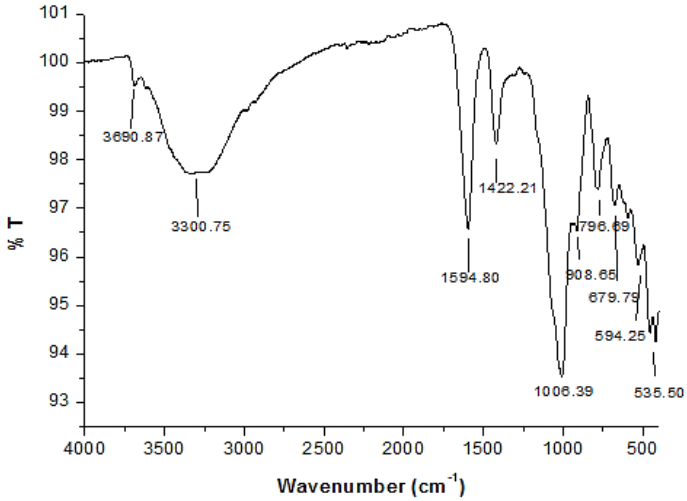

Fig. 2. FTIR spectrum of Alg©Ka

The microstructure of Alg©Ka and Cr (VI) loaded Alg©Ka (Me-Alg©Ka) was examined using scanning electron microscope (SEM, Nova Nano SEM 200, FEI Company) and given in Fig. 3a, 3b. For the analysis, the samples were covered with a gold layer and sputtered at 20 kV.

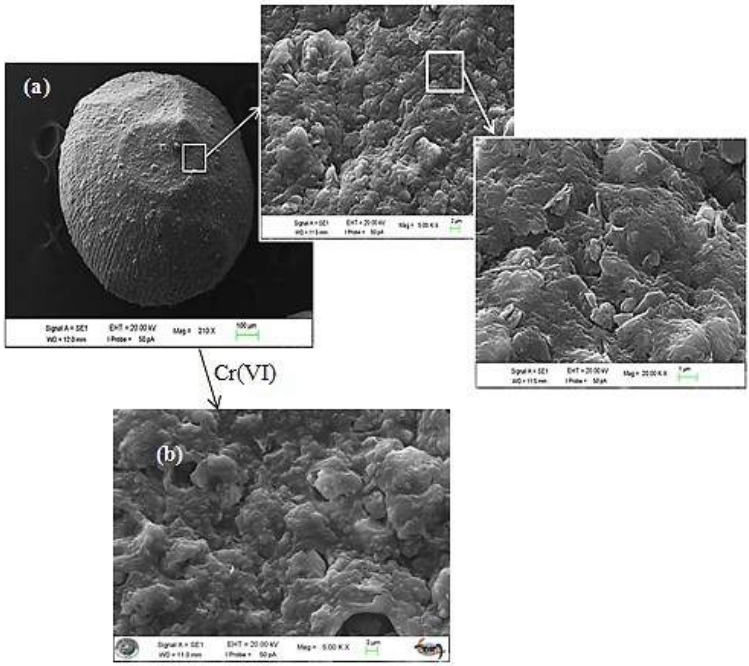

Fig. 3. SEM micrographs of Alg©Ka before adsorption **(a)** after adsorption of Cr (VI) **(b)**

3. Results and discussion

3.1. Time-dependent of Adsorption

Cr (VI) adsorption depends on the duration of the ions in contact with Alg©Ka. Adsorption capacity depending on contacting time was given in Fig. 4. Cr (VI) adsorption completed in 180 minutes and then after the extension of the period cannot affect the adsorption after the system has been reached to equilibrium.

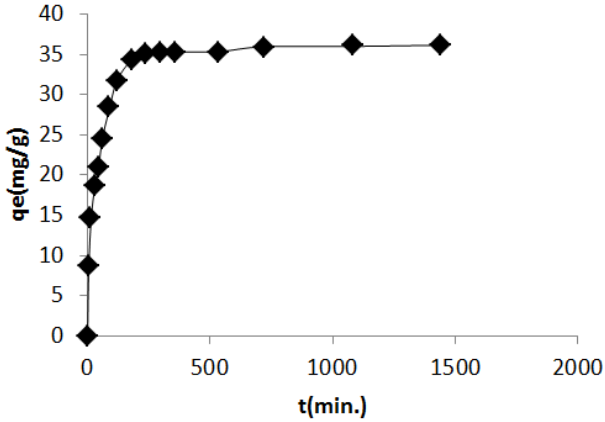

Fig. 4. Time dependence of Cr (VI) ion adsorption

3.2. Effect of initial pH

Adsorption of Cr (VI) in the aqueous solution on Alg©Ka were calculated with different pH values. There are a lot affects for binding of Cr (VI) to the adsorbent. These are electrostatic interactions, complex formation, adsorption and ion exchange mechanisms and they are effective during the adsorption process. pH of the solution influenced the adsorption as shown in Fig. 5.

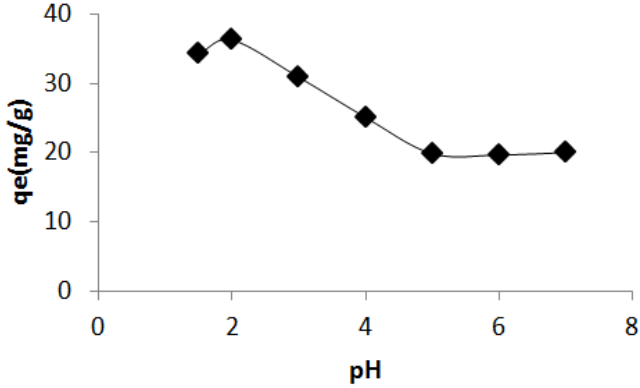

Fig. 5. pH affects on the Cr (VI) adsorption by Alg©Ka

Alg©Ka Cr (VI) adsorption was depended on the pH value and the optimum adsorption capacity value was specified by changing the initial pH of the solution. pH affects the surface charge of adsorbent and play an important role in the complexation of Cr (VI) ion with the adsorbent. Cr (VI) adsorption increased at pH value of 2. Alg©Ka can protonate with low pH values. Positively charged ions will be present on the surface of Alg©Ka in acidic medium and Cr (VI) anionic form's structure can join with complex ions formed. The following reactions can occur:

$$\text{Alg©Ka-OH}_2^+ + \text{CrO}_4^{2-} \rightarrow \text{Alg©Ka-OH}_2^+/\text{CrO}_4^{2-} \quad (1)$$

$$\text{Alg©Ka-OH}_2^+ + \text{HCrO}_4^- \rightarrow \text{Alg©Ka-OH}_2^+/\text{HCrO}_4^- \quad (2)$$

$$\text{Alg©Ka-OH}_2^+ + \text{HCrO}_4^- \rightarrow \text{Alg©Ka-HCrO}_4 + \text{H}_2\text{O} \quad (3)$$

It was found that the protonation of the surface decreases at pH value over 4. Adsorption accelerated at pH 3-4. Optimum pH value is considered as 2. Gopalakannan et al. and Karthik et al. observed the effect of pH on Cr (VI) by using aluminum oxide/alginate composite as adsorbent (Gopalakannan et al. 2016; Karthik and Meenakshi 2014). The composite protonated in the acidic environment and electrostatic interactions were created between composite surface and Cr (VI). For this reason, Adsorption becomes more in the acidic conditions and optimum pH value was found as 2.

3.3. Effect of amount of adsorbent

The amount of Cr (VI) ions adsorbed by the adsorption experiments varied between 1.0-10.0 g/L. According to the obtained data, adsorption capacities and adsorption percentage values were plotted against the variable adsorbent amount (Fig. 6). The adsorption capacity increased slightly when the amount of Alg©Ka was increased from 1 g/L to 2 g/L and decreased from 2 g/L to 4 g/L. It has been found that increasing the amount of Alg©Ka after certain value does not affect the Cr (VI) adsorption. For that reason, the amount of adsorbent was preferred as 2 g/L for experiments.

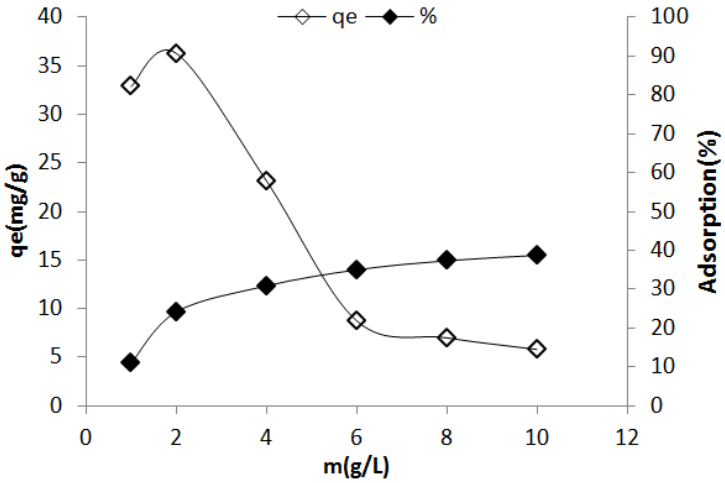

Fig. 6. The adsorption capacity of Alg©Ka for Cr (VI) and the change of adsorption percentage respect to the adsorbent dosage.

3.4. Effect of initial Cr (VI) concentration

A series of samples were prepared at different concentrations from stock Cr (VI) solution. These samples were treated with the adsorbent to complete the equilibrium. The amount of Cr (VI) adsorbed per unit mass of adsorbent (q_e) at the equilibrium state were determined by varying the initial concentrations of Cr (VI) (Fig.7.). As the initial amount of Cr (VI) ion increased, a rapid increase was observed in the adsorption, and then it remained at approximately constant values (plateau line). Alg©Ka has a limited number of active functional groups in its structure. By increasing the Cr (VI) ion concentration in the fixed adsorbent dose, the surface of the adsorbent can become saturated. Thus, different maximum adsorption values are achieved by varying concentrations of the fixed adsorbent dose and adding more Cr (VI) ion into the solution does not increase the adsorption value too much.

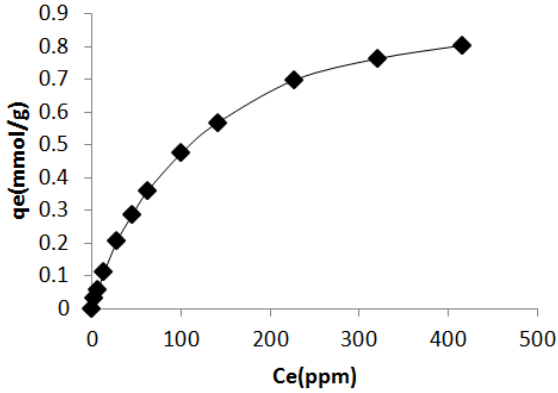

Fig. 7. Different starting Cr (VI) ion concentration for adsorption

Alg©Ka composites and Cr (VI) adsorption experiments were carried out at different starting Cr (VI) ion concentrations and adsorption capacities were calculated. When the equilibrium was reached, Cr (VI) ions adsorbed and remained in the solution phase were measured and their compatibility with Freundlich, Langmuir, Scarthard and DR adsorption isotherms were investigated (Table 1). The Freundlich equation of K_f and n values is calculated. If n value is between 1-10, the efficiency of the adsorption is high. n value calculated as 1.49 and R^2 value is 0.977. Dubinin-Radushkevich (D-R) isotherms were drawn and the adsorption energy E_{ad} value was calculated to be 9.45 kJ/mol.

These values are close to 8kJ/mol. The average adsorption energy (E_{ad}) value is in the range of 8-16 kJ/mol. The adsorption may also be associated with chemical adsorption and may be in the form of ion exchange ans complexation. The suitability of the equilibrium curve for the Langmuir isotherm was investigated. q_m and b coefficients were calculated from the Langmuir equation and are given in Table 1. As a result, the Langmuir isothermic correlation coefficient (R^2) for Cr (VI) is close to 1 (R^2; 0.99) and the R_L value is 0.285 for Langmuir isotherm. The q_m value for Langmuir isotherm was calculated to be 54.64 mg/g. The R^2 value for Scatchard isotherm for Cr (VI) adsorption was 0.99 and the maximum capacity was 54.79 mg/g. The result was supported to the Langmuir isotherm.

Table 1. Isotherm constants for Cr (VI) ion adsorption by Alg©Ka.

	Freundlich			Langmuir			Scatchard			D–R			
Metal	K_f	n	R^2	q_m	b	R^2	Q_s	K_s	R^2	X_m	K	E	R^2
Cr(VI)	0.974	1.49	0.977	54.64	0.008	0.999	54.79	0.008	0.996	1.86	0.0056	9.45	0.988

3.5. Kinetic modeling

Alg©Ka -Cr (VI) adsorption kinetics were investigated by kinetic models (Fig. 8). Pseudo-first and pseudo-second-order kinetic models were applied at different concentrations (150, 300 and 450 ppm) and given in Table 2. The regression coefficient (R^2) values of Cr (VI) adsorption was closer to 1 so the pseudo-second-order kinetic model was found to be more suitable.

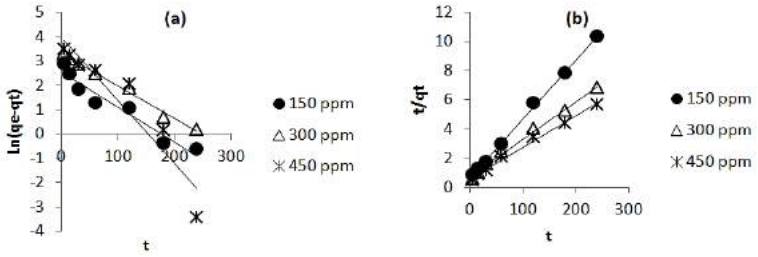

Fig. 8. Applicability of the results at different Cr (VI) concentrations a) pseudo first-order rate equations b) pseudo second-order rate equations.

Table 2. Kinetic parameters obtained at different concentrations of Cr (VI)

		Pseudo first order model			*Pseudo second order model*		
C_o(ppm)	qe_{exp}	k_1	qe_{cal}	R^2	k_2	qe_{cal}	R^2
150	23.71	0.014	12.88	0.937	0.0026	24.63	0.999
300	36.28	0.013	27.34	0.988	0.0009	38.61	0.994
450	42.28	0.026	52.33	0.893	0.0007	46.51	0.992

4. Conclusions

The mechanism of Cr (VI) adsorption on Alg©Ka was discussed. The maximum removal of Cr (VI) ion on Alg©Ka beads was at pH 2.0. The contact time to reach the equilibrium stage was recorded as 180 minutes in the experiments.The maximum monolayer adsorption capacity of Alg©Ka was 54.64 mg/g for Cr (VI). The actual Cr (VI) adsorption capacity of Alg©Ka, which had progressed in this research, was much more reported than that of kaolin and alginate. The results obtained were suited well with the Langmuir isotherm. Kinetic data showed that the dynamic tendency of Cr (VI) adsorption could be defined by the kinetic model of the pseudo-second-order.

Acknowledgements

The authors thank Selcuk University BAP Office for financial support (BAP No: 14101008).

References

1. B. Volesky, "Biosorption process simulation tools," *Hydrometallurgy* 71: 179–190, 2003.
2. C. Escudero, N. Fiol, I. Villaescusa, "Chromium sorption on grape stalks encapsulated in calcium alginate beads," *Environmental Chemistry Letters* 4: 239–242, 2006.
3. C. Larosa, M. Salerno, J. S. de Lima, R. M. Meri, M. F. da Silva, L. B. de Carvalho, A. Converti, "Characterisation of bare and tannase-loaded calcium alginate beads by microscopic, thermogravimetric, FTIR and XRD analyses," *International Journal of Biological Macromolecules*, 115: 900-906, 2018.
4. E. Pehlivan, T. Altun, "Biosorption of chromium(VI) ion from aqueous solutions using walnut, hazelnut and almond Shell," *Journal of Hazardous Materials* 30: 378–384, 2008.
5. F. Ogata, H. Tominaga, H. Yabutani, A. Taga, N. Kawasaki, "Granulation of gibbsite with inorganic binder and its ability to adsorb Mo(VI) from aqueous solution," *Toxicological and Environmental Chemistry* 94(4): 650–659, 2012.
6. G. Bonanno, J.A. Borg, V.D. Martino, "Levels of heavy metals in wetland and marine vascular plants and their biomonitoring potential: A comparative assessment," *Science of The Total Environment* 576: 796-809, 2017.
7. L. Deng, P. Yuan, D. Liu, F. Annabi-Bergaya, J. Zhou, F. Chen, Z. Liu, "Effects of microstructure of clay minerals, montmorillonite, kaolinite and halloysite, on their benzene adsorption behaviors," *Applied Clay Science* 143: 184–191, 2017.
8. M.F. Brigatti, E. Galon, B.K.G. Theng, "Structure and mineralogical of clay minerals," In F. Bergaya, B.K.G. Theng, & G. Lagaly (Eds.), *Handbooks of clay sciences*, *London: Elsevier* 2: 19–86, 2006.
9. M.M. Abd El-Latif, M.F. El-Kady, A.M. Ibrahim, M.E. Ossman, "Alginate/ Polyvinyl Alcohol - Kaolin Composite for Removal of Methylene Blue from Aqueous Solution in a Batch Stirred Tank Reactor," *Journal of American Science* 6(5): 280-292, 2010.
10. P.B. Tchounwou, C.G. Yedjou, A.K. Patlolla, D.J. Sutton, "Heavy metal toxicity and the environment," A. *Luch (Ed.), Molecular, Clinical and Environmental Toxicology, Springer Basel* 133–164, 2012.
11. R. Dong, J. Zhang, B. Zhou, J. Zhou, "Application of a novel quaternized ammonium poly(vinyl alcohol)-based hybrid anion exchange membrane for the removal of Cr (VI) from wastewater," *Water Science* and *Technology* 70: 1602–1609, 2014.
12. R. Karthik, S. Meenakshi, "Facile synthesis of cross linked-chitosan-grafted-polyaniline composite and its Cr (VI) uptake studies," *International Journal of* Biological *Macromolecules* 67: 210-219, 2014.
13. R. Mu, Z. Xu, L. Li, Y. Shao, H. Wan, S. Zheng, "On the photocatalytic properties of elongated TiO2 nanoparticles for phenol degradation and Cr (VI) reduction," *Journal of Hazardous Materials* 176: 495–502, 2010.
14. S.K. Bajpai, S. Sharma, " Investigation of swelling/degradation behaviour of alginate beads crosslinked with Ca^{2+} and Ba^{2+} ions," *Reactive and Functional Polymers*, 59 (2): 129–140, 2004.
15. Ş. Parlayıcı, A. Yar, A. Avcı, E. Pehlivan, "Removal of hexavalent chromium using polyacrylonitrile/titanium dioxide nanofiber membrane," *Desalination and Water Treatment* 57: 16177–16183, 2016.
16. T.A. Khan, S. Dahiya, E.A. Khan, "Removal of direct red 81 from aqueous solution by adsorption onto magnesium oxide-coated kaolinite: Isotherm, dynamics and thermodynamic studies," *Environmental Progress & Sustainable Energy* 36(1): 45–58, 2017.

17. T.A. Khan, R. Rahman, I. Ali, E.A. Khan, A.A. Mukhlif, "Removal of malachite green from aqueous solution using waste pea shells as low-cost adsorbent–adsorption isotherms and Dynamics," *Toxicological and Environmental Chemistry* 96: 569–578, 2014.
18. T. Altun, Ş. Parlayıcı, E. Pehlivan, "Hexavalent chromium removal using agricultural waste "rye husk"," *Desalination and Water Treatment* 57: 17748–17756, 2016.
19. T.E. Norgate, S. Jahanshahi, W.J. Rankin, "Assessing the environmental impact of metal production processes," *Journal of Cleaner Production* 15: 838–848, 2007.
20. V. Gopalakannan, S. Periyasamy, N. Viswanathan, "One pot eco-friendly synthesis of highly dispersed alumina supported alginate biocomposite for efficient chromium(VI) removal," *Journal of Water Process Engineering* 10: 113-119, 2016.
21. W. Duan, G. Chen, C. Chen, R. Sanghvi, A. Iddya, S. Walker, H. Liu, A. Ronen, D. Jassby, **"**Electrochemical removal of hexavalent chromium using electrically conducting carbon nanotube/polymer composite ultrafiltration membranes**,"** *Journal of Membrane Science* 531: 160–171, 2017.
22. X. Qu, P.J.J. Alvarez, Q. Li, "Applications of nanotechnology in water and wastewater treatment," *Water Research* 47: 3931–3946, 2013.
23. X.J. Wang, Y. Li, X.J. Lu, W.Y. Xu, W. Zhao, L.G. Wang, "Fabrication and characterization of novel polyvinylidene fluoride ultrafiltration membranes for separation of Cr (VI) from wastewater," *Adsorption Science & Technology*. 34(9–10): 526–537, 2016.
24. Y. Li, B. Xia, Q. Zhao, F. Liu, P. Zhang, Q. Du, D. Wang, D. Li, Z. Wang Y. Xia, "Removal of copper ions from aqueous solution by calcium alginate immobilized kaolin," *Journal of Environmental Sciences* 23 (3): 404-411, 2011.
25. Y. Vijaya, S.R. Popuri, V.M. Boddu, A. Krishnaiah, "Modified chitosan and calcium alginate biopolymer sorbents for removal of nickel (II) through adsorption," *Carbohydrate Polymers* 72: 261–271, 2008.

SOL-GEL TECHNOLOGY AND NOVEL APPLICATIONS OF SOL-GEL PROCESSES

Canser GÜL [1], Nilay ÇÖMEZ [2] , Hülya DURMUŞ [3]

[1] Res. Assist., Manisa Celal Bayar University, Engineering Faculty, Dept. of Metallurgical and Materials Engineering, Manisa, Turkey.
[2] Res. Assist. Dr., Manisa Celal Bayar University, Engineering Faculty, Dept. of Metallurgical and Materials Engineering, Manisa, Turkey.
[3] Assoc. Prof. Dr., Manisa Celal Bayar University, Engineering Faculty, Dept. of Metallurgical and Materials Engineering, Manisa, Turkey.

1. History of gels

Sol and gel forms have been used in history for many years in numerous sectors: from ink to clay, blood and serum to milk. In 1846, Ebelmen studied on polycondensation and hydrolysis and prepared gel for the first time for the production of silica gel. The first sol was prepared by Faraday in 1853 for the synthesis of gold in the laboratory [1]. Alumina gel was produced for the first time by Cossa in 1870 [2]. In 1932, Kistler introduced the concept of aerogel. He has reported that aerogel was formed as a result of the displacement of the liquid with the gas without disturbing the solid network. He has developed the sol-gel technology with "supercritical drying" term which means wet gel must be heated in an autoclave until it surpasses the critical temperature and pressure values. After Kistler, this definition was developed by adding the shrinkage factor of the solid network, in addition to liquid gas exchange. Consequently, the xerogel concept emerged [3].

In light of the first studies, scientists made different studies in different fields. Sol-gel and dip coatings were reported in 1939, and the first patent for the synthesis of SiO_2 and TiO_2 was obtained by Geffcken and Berger within the same year. Single oxide coatings were made by Schroeder in 1960s. Antireflection coatings were reported in 1964 and 1970s. Different multicomponent oxides were reported by Dislich, Roy and Mazdiyasni [4]. In the 1980s, many kind of research have been carried out on gel-to glass transition [5,6], shrinkage behavior of gels and avoiding cracks [7,8], solar energy applications [9], and production of fibers [10].

The sol-gel technology was discovered as early as the 1800s as mentioned above, but the studies about sol-gel process accelerated in the last two decades and the applications became widespread. Optical fibers, optical coatings, electro-optic materials, colloidal silica powders, xerogels, and aerogels, luminescence concentrators, tunable lasers, active waveguides, semiconducting devices, sunscreen formulations, chemical sensors and biosensors are fabricated by sol-gel technique. The areas such as defense, nanotechnology, environmental monitoring, and biomedical devices have potentials for new explorations of sol-gel technology [11].

2. Introduction to sol-gel process

Sol-gel is a special process based on a wet chemical production in order to form advanced materials for various applications in optics, electronics, catalysis, energy, space, medicine, sensors, architecture, etc. This process is able to shape the inorganic, organic or hybrid materials in bulk, powder, fiber, thin film, and monolith forms [12]. The sol-gel process forms an oxide network of inorganic solid materials such as glasses and ceramics by the chemical synthesis and progressive condensation reactions of precursors in prepared solutions [3,13]. It is possible to obtain high purity products and to control the composition and microstructure at the molecular level by the sol-gel process. In addition, a relatively low process temperature of sol-gel in comparison to conventional methods provides many advantages [3,12,14].

The fundamental terms of "sol" and "gel" should be well-defined for a better understanding of the process. At the beginning of the sol- gel process, the chemical compounds -in the other words "***precursors***"- are dissolved and chemically transformed in a liquid solvent. Thus a "***sol***" is formed [15]. Sol, as a liquid state phase, is composed of suspended colloidal particles in a liquid solution [3,15]. The matter that is larger than atoms or molecules but that is not observed by the naked eye, is named as "***colloid***". "***Colloidal suspension***" can be described as a mixture including one substance of microscopically dispersed insoluble particles which is suspended in another substance [16].

Sol can be cast in a mold or coated onto surfaces by several methods. In addition, it can be stored for a while before further processing. After preparing a sol, chemical transformations must be continued until a gel is generated by rigid and interconnected networks [15]. The ***gel*** is a porous structure with a three-dimensional continuous network structure supported by a liquid phase. It is formed by the process called "***gelation***" which starts with the formation of covalent bonds between the particles. Gel structure depends on the size and shape of the particles in the sol [3]. The sol- gel transition occurs at the "***gel point***" with the transition of sol to gel. At the gel point, the initial formation of a chemical or physical polymer network takes place [17].

Sol–gel processing offers a number of advantages including low-temperature processing, ease of fabrication and precise microstructural and chemical control. The sol–gel-derived film or layer not only provides a good degree of biocompatibility, but also a high specific surface area (which can be used as a carrier of adsorbed drugs) and an external surface whose rich chemistry allows easy functionalization by suitable biomolecules. Also, the thickness and pore-size distribution controlled via the withdrawal speed and sols using the sol–gel dip-coating technique [11]. The advantages of the sol-gel method over other methods are precise control of composition, low processing temperature, and better homogeneity. Other advantages of the sol-gel method in comparison with other methods are high purity, homogeneous composition, and low temperature of synthesis [14].

3. Process of sol-gel

Generally, the process of gel formation from a sol namely sol-gel process is performed by the following stages: hydrolysis; condensation and polymerization of monomers to form chains and particles; growth of these particles; agglomeration of the polymer structures; formation of networks [13].

The process is mainly based on the hydrolysis and condensation mechanisms of the precursors such as such as metal alkoxides, inorganic salts, and organic polymers. Sol-gel process and structures formed by this process are shown in **Fig.1.** Sol is the structure formed by mixing an initiator at appropriate temperatures using acid or base catalyst in a solvent. The formation of this structure is the first step of the sol-gel process. Then

hydrolysis and condensation reactions start, and an increase in viscosity with condensation reactions occurs to form a colloidal sol. The coating process can be started at the time these reactions begin or near the completion of the reactions [3,12]. After that, the sol-gel transforms to freeze gel network followed by the drying and/or heat treatment process of wet gel. In addition, the purification and stabilization of the sol and the strengthening of the gel can be performed if necessary. For some special applications, external field conditions such as strong field induction, ultrasonic assistant, microwave assistant, and magnetic field assistant can be utilized [12].

Dip coating and spin coating processes are often preferred because they are low cost and easily applicable processes [3,18]. Dip coating method consists of three steps. At first, the substrate material is dipped into the prepared solution. After that, it is retracted at a constant velocity. The last step involves drying. This method provides a good thickness control without waste and produces an adhesive thin coating. In the case of annealing at low temperature, a crack-free coating can be obtained. However, cracking of the coating may occur by virtue of rapid solidification and temperature fluctuations [19,20]. In the spin coating method, the coating material is spread by the centrifugal force arisen from the high-speed rotational motion. The higher spin rate is needed to attain a thinner film. Hence, the coating thickness can be adjusted by changing the rotation speed. Inorganic functional thin coatings are commonly produced by spin coating for the service of many fields such as molecular separation (membrane) and detection (sensing) [21].

After the coatings applied to the surfaces, the coating layer can be obtained by heating. The gelation step begins with the agglomeration of the particles in fragmentary clusters and forms cross structures. The gel often seem solid, but it is still wet. In fact, it contains solvents and various organic structures. The structure obtained by the removal of solvents from this structure is defined as ***aerogel*** [3,18]. If the gel is subjected to a drying process with evaporation, the ***dry gel*** or ***xerogel*** structure is formed. By concentrating these structures at different temperatures, glass, ceramic and porous gel structures can be obtained. After the solution is prepared, the precipitation process can be performed. Then the solution is filtered and the solvents removed by the heating. As a result of this process, the powder can be received [22].

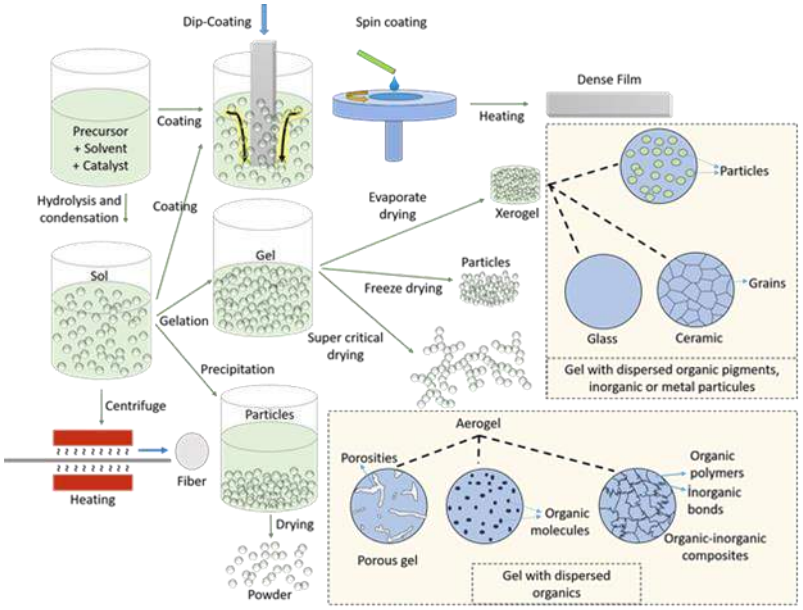

Fig. 1. Schematic of sol-gel process and structures formed by this process

A sol-gel process depends on many factors. The type of the element to be used, type of precursor, type of solvents, the temperature at which the solution will be prepared and the pH to be adjusted, composition, stabilizing agents, Drying Control Chemical Additives (DCCA), complex formers, are the main factors that determine the gelation time and structure of the solution [23,24].

The sol-gel process can be carried out under the acidic or basic conditions, and these conditions affect the properties of the resulting coating or bulk materials [25]. For example for silica gels, if the pH value is smaller than 3, cross-linked bonds occur in the sol. If the pH value between 5 and 7, cross-linked clusters become denser. If these crosslinks are more dense or porous, they may cause cracked structures or larger pore size during drying or sintering stages [26].

3.1. Precursors, solvents and catalysis

The first step of the sol-gel process is to form a sol from the precursor. Precursors can be salts, oxides, hydroxides, complexes, alkoxides, acylates or amines. Oxides are used as network modifiers Na or K are preferable. Alkoxides are most common sol-gel precursors because of their commercial availability and metal oxides coating composability [23].

All types of precursors can be used, provided they are miscible. Two main groups of metallic salts (such as chlorides, nitrates, and acetates) and metal alkoxides are mainly used as a precursor. The general formula of a metallic salt is M_mX_n where M is metal such as Ti, Si, V, Zr, Mo, Al, Zn, Ta, etc., X an anionic group, and m and n stoichiometric coefficients. For example; titanium tetrachloride, $TiCl_4$; tantalum pentachloride, $TaCl_5$; ferrous acetate, $Fe(C_2H_3O_2)_2$; ferric nitrate, $Fe(NO_3)_3$ [2,27]. As for alkoxides, their general formula is $M(OR)_n$. Here, M represents metals such as Ti, Si, V, Zr, etc., and R is typically an alkyl group (C_xH_{2x+1}). For example; titanium ethoxide, $Ti(OC_2H_5)_4$ or tantalum ethoxide $Ta(OC_2H_5)_5$ [13].

Solvents are added in the system generally to prevent liquid-liquid phase separation during the hydrolysis early stages and to control the concentration of water for the gelation kinetics. The chemistry of metal salts and metal alkoxides is different from each other. Therefore, the choice of solvent must be made according to the type of precursor. Solvents may be categorized as polar/nonpolar or protic/aprotic. Water and alcohols are protic solvents, and $C_4H_8O_2$ (dioxane), C_3H_7NO (dimethylformamide), C_4H_8O (tetrahydrofuran) are aprotic solvents [27,28]. Compared to alcohol or water, aprotic solvents are considerably more inert because they do not take part in the sol-gel process. Aprotic solvents added into the sol for increasing the strength of nucleophiles or decreasing the strength of electrophiles. As the solvent, water is used for the metal salts and the alcohols such as C_2H_5OH (ethanol), CH_3OH (methanol), C_3H_3 (propanol), C_4H_9OH (butanol) for the metal alkoxides [27].

Drying control chemical additives (DCCA), such as NH_2CHO (formamide), are used as cosolvents with alcohol for hindering crack initiation. They influence drying behavior and allow faster drying. They provide a larger and more uniform pore size in the gel, and this helps to reduce cracks [28].

Acid or base catalyst may be used as a catalyst in the process. Acid catalysts can be classified into two categories as organic acids (acetic acid, CH_3COOH) and inorganic acids (Nitric acid, HNO_3; Hydrochloric acid, HCl; Hydrofluoric acid, HF). NH_4OH (ammonium hydroxide) is generally used as the base catalyst [24].

3.2. Hydrolysis and Condensation

After the solution of the high purity precursor is prepared with the solvents and present or subsequently added water, the hydrolysis reaction begins [3]. Indeed, both the hydrolysis and condensation reactions take place synchronically when the hydrolysis starts [13]. Condensation starts while the first reactive –OH groups are formed [17]. These reactions proceed slowly and in a controlled manner when the solution has a neutral pH. If the pH value is acidic or basic, there is an increase in the rate of these reactions. Acidic or basic catalysts are used for this. Neutrality of the pH or some heating provocate gelation of the sol and provides the conversion of the prepared solution to the wet gel structure [3,29].

3.2.1. Silane based materials

Silica-based precursors (tetramethyl-orthosilicate (TMOS) and tetraethyl-orthosilicate (TEOS), aqueous solutions of silicates and silicon alkoxides, $Si(OR)_4$) are widely preferred in sol-gel processing [3,11]. The chemical reactions of the silica-based precursors rely on the condensation that involves the transformation of Si-OR- and Si-OH-containing forms to siloxane compounds (**Fig. 2**). During condensation, water or alcohol molecule is released to generate –Si–O–Si– siloxane bonds. The reaction of two –Si–OH groups constitute water as by-product whereas the interaction between –Si–OH and – Si–OR forms an alcohol molecule as a secondary product. If the number of Si-O-Si bonds is maximized and the number of silanols (Si-OH) and alkoxo (Si- OR) groups is minimized, a stable gel can be obtained [3,17].

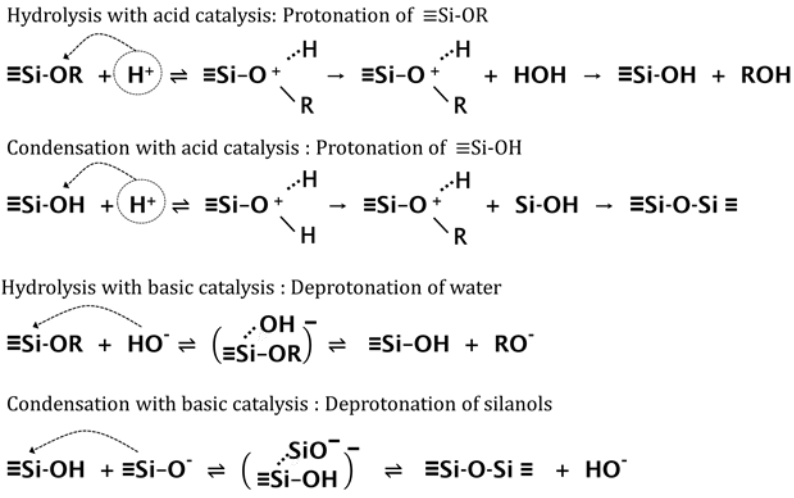

Fig. 2. Hydrolysis and condensation reactions for silanols with acidic and basic catalysis [17].

3.2.2. Metal-Oxide based materials

A macromolecular oxide network is obtained by also hydrolysis and condensation reactions.

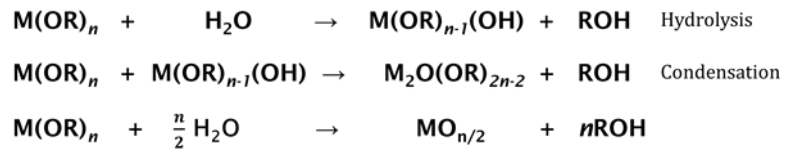

Metal alkoxides contain reactive alkoxides (–OR). In the existence of a mineral acid or a base as a catalyst during hydrolysis, alkoxide groups (–OR)

react easily with water. Metaloxane bonds (M–O–M) is formed in the condensation step after the hydrolysis reaction that involves the replacement of alkoxide groups with hydroxyl groups (–OH) [30].

3.3. Gelation

Gelation is an event that a solution suddenly loses its fluidity and becomes an elastic solid. It still contains a lot of liquid but looks glassy [26]. Sufficient polymerization performs cross-linking between the molecules and establishes the skeletal structure during gelation [31].

3.4. Aging of gels

Longtime progressing of the gelation phenomenon generated by the chemical reactions of hydrolysis and condensation is called as "aging" process. Aging does not cause a phase change. It is a critical step for microstructural evolution such as decreasing the microporosity, strengthening, stiffening and coarsening of the gel network structure [18,32-34]. The cross-linked structure of the molecules in the gel network tends to increase by the polycondensation during the aging process [31,34]. Because, the condensation reactions are not over at the gel point contrarily, they are still in progress during the aging [34]. A higher aging temperature and a longer aging time promote the cross-linking [31,34]. In brief, a dense gel structure can be obtained by the aging process. During aging, the gel that becomes cloudy transforms into the transparent xerogel by the slow evaporation of the liquid phase and shrinks up to 25% volumetrically [34].

3.5. Drying

Drying is an important stage of sol-gel in terms of the removal of excess solvent and generates an elastic or viscoelastic gel-like state [29,31]. During the drying process, capillary tension in the liquid increases due to the further evaporation. Compressive stresses of the solid stabilize this tension and induce the shrinkage of the solid [29]. Usually, two methods are used for the removal of solvents and drying steps. One of them is drying by a slow rate in a normal atmospheric condition that shrinks the gelled network. The gel dried in normal conditions is defined as "xerogel" and exhibits a volumetric reduction between five and ten times in comparison with the wet gel. During drying in normal conditions, the network is exposed to contraction deformation, and liquid in the structure moves away through the pores. Xerogel transforms into a dense glass by heat treatment at elevated temperature (viscous sintering). The other one is evaporation of the solvents at supercritical (hypercritical) conditions in the autoclave. Drying in supercritical conditions minimizes the shrinkage and forms a highly porous, low-density product called "aerogel" [3,11,15,35]. The other method "freeze-drying" involves the bypassing the triple point that applied to ultra-fine nanostructured silica gels. This method produces cracked structures or

powder-like forms [18]. In the case of freeze-drying a wet gel, cryogel can be obtained and subsequently, opaque aerogel powder can be produced [1,36].

A "monolith" forms if the minimum dimension of the gel is more than a few millimeters. Films and fibers can be formed, in case of the solvent evaporates fast during gelation. Nevertheless, controlling the shrinkage of three-dimensional network formation is difficult due to the loss of volatile by products [15].

Sintering or melting technique can be selected as a drying technique for gel-powders. For producing ultrapure gels, drying technique should be selected carefully considering the following aspects: (a) feasibility of a closed system; (b) drying period; (c) to maintain the purity in the following processing steps [35].

3.6. Sintering

The sol-gel processing ends up with sintering which involves the elimination of porous structure, removal of residual organisms and crystallization [31]. The mechanisms such as atomic diffusion, grain growth, pore transformation, viscous flow sintering, densification come into play during the sintering of coatings, powder samples or bulk ceramics. Sintering is as important as the drying step for producing high-quality coatings and, crack-free ceramics, glasses, and aerogels. Each of these mechanisms must be carried out delicately [2].

4. Applications of sol-gel technology

Sol-gel applications become more remarkable and are used in many fields. Sol-gel technology is used frequently for the production and applications of antireflective coatings with index gradation, electrical conductivity coatings, optical/infrared absorbing coatings [12,37,38], materials with improved wear, scratch or corrosion resistance in the biomaterials and automotive industry [39-42], hybrid fuel technologies and membranes to save fuel [43-45], various composites or fibers [46,47], and new technological ceramics [48].

4.1. Thin Films and Coatings

Functional coatings as a sub-class of advanced materials draw attention due to their superior chemical, optical, and mechanical properties. For instance, hard coatings are necessary for some industrial applications in order to improve scratch hardness, abrasion resistance, nano indentation hardness, and adhesion [37]. Several methods such as PVD/CVD (vapor deposition), plasma beam, electrochemical deposition, and sol–gel are employed for depositing functional coatings. Among other techniques, sol-gel coating technology steps forward owing to its advantages such as high-performance, low processing temperature and low-cost. Multi-functional (hydrophobic, abrasion and corrosion resistant, flexible, anti-bacterial and

anti-reflective etc.) coatings required for optics, energy conversion, electronics or sensing applications can be achieved by sol-gel technology [12,37].

Sol-gel coatings can be formed by inorganic and organic methods. The networks evolve in a liquid phase by the formation of colloidal suspension and gelation of the sol during the inorganic method [13]. Inorganic components enhance durability, impact strength, scratch resistance, adhesion to the metal substrates, and gloss of the coating whereas the organic components increase flexibility, density, critical thickness, and allow low-temperature curability [37,49].

Coating a sol on a substrate can be achieved by dip-coating, spin-coating, flow-coating, spray- coating, roll-coating, and electrodeposition techniques [13,50]. These deposition techniques are able to synthesize materials not only as thin films but also as monoliths, powders, and fibers. Flow- coating and spray-coating are found more applicable to the industry [50]. However, dip-coating provides some advantages in terms of fabrication such as the independence of substrate shape and highly uniform coating thickness [11].

4.1.1. Coatings for Biomedical Applications

Titanium and its alloys are biomaterials that have been used frequently in the human body for many years. For example, Nickel-Titanium (Ni-Ti) alloys have shape memory, which is often used in dental restoration wiring or stent applications. But with the effect of ions and acids found in the human body, this alloys may corrode and cause ion release [39]. Does the release of Ni ions into the body cause adverse effects? Ni described as cytotoxic (cell killing / destructing), genotoxic (DNA damaging), carcinogenicity (cancer-causing) and known to be very low biocompatibility in the human body, of course, will cause detrimental effects [40,51]. The situation for stainless steels containing Ni is not very different. Although they use in short term applications, they must remove from the body eventually because of the reverse effect of releasing Ni ions [39].

There may be similar effects for Ti6Al4V, which is the most commonly used implant material in fracture bone repair or directly in bone / hard tissue. What would you experience if Al or V is released to the body? Al element of the neurodegenerative disease, genotoxicity in the literature. V consider as carcinogenic and highly cytotoxic, genotoxic and mutagenicity. Titanium which is the main element of most biomaterial alloys has low cytotoxicity [40,41,51]. Several studies have been conducted to prevent these ion releases in titanium alloys. TiO_2 and Ag-TiO_2 sol-gel coatings were applied onto the titanium surfaces by sol-gel method in Cotolan et al. [52] study for providing corrosion resistance and reducing the bacterial adhesion. They report that coatings have a homogenous and dense structure, and provide protection for the titanium surface against the corrosive attacks in the human body.

Ion release is not the only perturbative factor for titanium and its alloys. Ti and its alloys have very high density and mechanical strength values compared to cortical bone [41]. Consider a titanium alloy for support of a damaged or broken bone. This alloy will be in contact with the surrounding tissues and bones for many years and will apply a load to them. These load bearings have been researched by many scientists, and it is thought that such materials, which have much higher mechanical strength than bone, may cause "Stress-Shielding Effect" [53]. For these reasons, the search for an alternative material to be used instead of these alloys continues.

Mg alloys have low density, close mechanical strength to cortical bone. They may hinder the stress-shielding effect in human body. Research also confirmed that they have proper biocompatibility [54]. For this reason, studies on the use of Mg alloys such as AZ91, AZ31, and ZK60 in the body are still carried out. But Mg alloys are not corrosion-resistant enough to withstand the harsh environment in the human body [55]. Most of the Mg alloys begin degradation in the human body before the healing is completed. Sol-gel coatings are also available to prevent or slow down the early degradation of Mg alloys.

Hybrid coatings which made to improve wear and corrosion resistance by sol-gel method are also attractive field nowadays. Hybrid coatings have given us the opportunity to add more than one feature to the samples at the same time. In order to improve the corrosion and wear resistance of the CoCrMo alloy and ultrahigh-molecular-weight polyethylene (UHMWPE) for biomaterial applications. Zai et al. [56] conducted studies and preferred to use the sol-gel method. They prepared solutions for the formation of MgO and ZrO_2 oxides and carried out the wear tests. Among the pairs of samples, they tested in different combinations, the performance of the pair with the best result compared to the untreated sample increased about 19.5 times. Thin hybrid coatings were obtained by the sol-gel method for the evaluation of corrosion and wear properties of low-carbon steel in the study of Claire et al. [57]. Glycidoxypropyltrimethoxysilane (GPTMS), aluminum isopropoxide (AIP) and cerium nitrate hexahydrate ($Ce(NO_3)_3.6H_2O$), polyethylene glycol (PEG), and zirconia nanoparticles were used for the sol preparation. The total thickness of the coating layer is about 10 microns at the maximum point. When the thickness of the coating is between 8-10 microns at the end of 100 cycles with 250 g load; 5 microns was observed at the end of the 1000 cycles. The study showed that the wear resistance of low carbon steels could be increased by sol-gel coating.

Zhang et al. [58] coated hydroxyapatite/phytic acid hybrid coatings by sol-gel method on AZ31 Mg alloy for improved corrosion performance of the alloy. Peres et al. [59] aim to investigate the corrosion resistance of AZ31 Mg alloy coated with TEOS-GPTMS-SiO_2 nanoparticles by sol-gel method in their study. They showed that hybrid silane coatings improved the corrosion resistance of the Mg alloy against chloride solution. Hernandes-Barrios et al. [60] also coated a silane-based hybrid layer on AZ31 Mg alloys. In their study, they applied TEOS-GPTMS hybrid coatings,and evaluated the effect of catalyst

and coating aging times on corrosion performance. As a result of the analyzes, they emphasized that the proper viscosity and pH values were reached with the effect of aging and free Si-OHs and the alloy surface could be established. Although cracks in some coatings reduce the corrosion resistance, a significant increase in corrosion performance has been observed in the overall coverage of the coatings.

Although the material for production of biomaterials is required to have wear and corrosion resistance, the most essential feature in a biomaterial is biocompatibility. In addition, it is necessary to improve or modify coating properties of medical devices such as lubricity, hydrophilicity/hydrophobicity, functionality and biocompatibility for different purposes [11]. "***Biocompatibility***" can be defined as the biomaterial used does not formation any host response. So the applied biomaterial cell death should not cause inflammation or allergic reactions and should be biologically stable. Biocompatibility may be different in different shapes depending on the material used, so different types of biomaterials can show different types of biocompatibility [61-63]. "***Bioactivity***" is the ability to form body tissue and cells upon reaction of a biomaterial with the body [11,63]. In ceramic-based biomaterials, biocompatibility is evaluated with the ***bioinertness***, which is considered as chemical stability of an implant in a human body [61,64]. ***Biotolerant*** materials are not rejected by living tissues, are covered with connective tissue and do not directly bind to the bone. Biocompatibility of metallic biomaterials is usually like that. When a metallic biomaterial is placed in the body, this tissue is formed around it. Metallic biomaterials may have some effects on the human body, but these effects are tolerable [63,65,66]. Nowadays, materials such as bone cement (polymethylmethacrylate, PMMA) and surgical austenitic stainless steel (AISI 316L) are used as biotolerant materials [63]. Coatings may have done to improve the biocompatibility of biomaterials, thus giving bioactive properties to bioinert biomaterials for accelerate tissue formation [11,67,68] or giving bioinertness to a biotolerant material has some ion release [70]. Nowadays, the bioactivity is being studied by hydroxyapatite (HA, $Ca_{10}(PO_4)_6OH_2$) which is usually obtained by the precursors Ca and P or by other coatings that promote HA formation. Bioactive layer on the surface was obtained and in-vitro studies were performed by Rojaee et al. [67], Usinskas et al. [68], and Shunzhi et al. [69]. As a result of these studies, the coating layer was found to be osteoconductive and promote apatite growth on the surface [67-69]. In-vitro tests of a produced biomaterial can be performed and HA growths can be examined. In the case of obtaining successful results from these tests, in-vivo studies can be performed within the framework of ethical rules. In-vivo studies have been conducted on rabbits and goats in the literature for coatings with different coating types and for successful results of in-vitro studies. Connections between the tissue and implant interfaces were examined, and the biocompatibility of the produced material was evaluated [63,71].

Ni-Ti alloys, which are frequently used in stent applications due to the shape memory characteristic, release ion. It is a frequently encountered

problem in the biomedical field and is tried to be prevented because of its negative effects. In order to overcome this problem Sheiko et al. [70] was made a bioinert coating with polymeric polyetheretherketone (PEEK) by using the sol-gel method on Ni-Ti alloys. As a result of the tests, they emphasized that the coated samples remained stable. They observed that there is only negligible Ni ion release, no cytotoxicity and delamination.

Coatings can be applied not only to improve biocompatibility but also to bring different properties to a biomaterial. Guo et al. [72] studied on silver containing hybrid coatings on titanium by the sol-gel method for gaining antibacterial properties of the biomaterial. They had a stronger antibacterial effect compared to uncoated samples thanks to the silver-containing coating they made and were emphasized that there was a 10% increase in the bond thickness even though there was microcracks on the surface.

Jalali et al. [73] studied antibacterial properties of Ag and TiO_2 nanoparticles embedded in TEOS-MPTMS containing sol-gel matrix. They indicated that the antibacterial properties were good in the prepared samples, the Ag^+ ion release was low even in the 21-day period, and it could be used in long-term applications. They have also emphasized that the materials used are low-cost and can be used in a wide range of applications, from medical devices to food production equipment and even cutting boards.

4.1.2. Wear and corrosion protection

Corrosion performance of aluminum and its alloys were improved with sol-gel coatings prepared different precursors against different environments such as sodium chloride [42,74,75], acetic acid, and alkaline solution [76], or Na_2SO_4 solution [77]. Different coatings were applied successfully to the surfaces by using the sol-gel method, and they were provided corrosion resistance to the alloys against different environments [74-77].

M.H. Hussin [75] coated tetraethyl-orthosilicate (TEOS) and hybrid 3-Amino(propyl)- triethoxysilane (APTES) and TEOS on the surfaces Al alloys by the sol-gel method for the improvement of corrosion properties. In this study, the corrosion resistance of the alloy has been improved against 3.5 % NaCl solution via the coatings. Similarly, Xue et al. [74] coated with the hybrid layer that includes 3-glycidoxypropyl-trimethoxysilane (GPTMS)/Zirconium (IV) n- propoxide/graphene oxide, on AA2024-T3 alloy by the sol-gel method. They applied corrosion test in 0.05 M NaCl solution for coated samples, and they observed that the films significantly increased corrosion performance and even provided 99.45% protection efficiency. Razavi et al.

Razavi et al. [42] coated sulphur, nitrogen, and carbon-doped TiO_2 layer on the copper substrate via sol-gel method. The coatings produced with the same parameters and solution were sintered at different calcination temperatures and times. After that, potentiodynamic-electrochemical corrosion test was performed on these coatings. According to the corrosion test results in NaCl, the optimum temperature and time were determined.

They clearly observed that copper increased the corrosion resistance of the non-cracked coating surfaces.

4.1.3. Optical and anti-reflection coatings

Anti-reflective films, reduce the losses of light transmitted that occur due to the reflection. These coatings have been mainly evaluated for optical applications including solar panels, show window glasses, and display panels [38]. In literature, SiO_2-TiO_2 [78], SiO_2-PEG [79], SnO_2-SiO_2 [80], Ta_2O_5-SiO_2 [81] anti-reflective multilayers have been coated by the sol-gel method. SiO_2-TiO_2 multilayer coatings gain an energy efficiency value for the colored reflection up to 2.4. This achievement seems beneficial for architectural application of colored glazed thermal solar collectors [78]. SiO_2-PEG multilayer films were reported to provide light transmittance of 96.44%. In addition, Zhu et al. [79] reported that surfaces are hydrophobic, low cost, and have a simple preparation procedure. They are also suitable for large area production. In the SnO_2-SiO_2 multilayer study, Wang et al. [80] tried different thickness values of layers as multiple layers and compared with each other. They observed some deviation in film thickness and obtained a peak transmittance of 98.2 % and 98.6 % for the SiO2/TiO2 and SiO2/SnO2/SiO2–SnO2 multilayers, respectively. In the study of Koc et al. [81] Ta_2O_5 and SiO_2 antireflective films were produced by using the spin coating method. They reported that reflectance values were less than 0.5%, at around 820 nm wavelength of these multilayer coatings.

Ouares et al. [82] synthesized Au doped ZnO sol-gel thin films onto glass substrates. The intensity of the near band edge emission increases with the Au content up to 20 at% and decreases for higher Au concentrations.

Zn_{1-x} Mg_xO:Al transparent conductive thin films were manufactured by the sol-gel method by Meng et al. [83] for using solar cells applications. Thin films were obtained with a tunable optical bandgap between 3.48 eV–3.66 eV, resistivity level of 10^{-3} Ω·cm, and low surface roughness of <10 nm.

Amri et al. [50] conducted research on high quality solar selective absorber coatings. They indicated that the sol-gel method is the promising synthesis and coating method for solar selective absorbers. They demonstrated that the optical properties and durability of the coatings applied by the sol-gel process could be adjusted by the heating temperature or the amount of precursor used. At the same time, they emphasize that the particle size, distribution, homogeneity, chemical composition, and film thickness could be adjusted by the sol-gel technique and that the sol-gel technique increases its utility for such applications because the ambient atmosphere is applicable without requiring any vacuum.

Lee et al. [84] produced magnesium-doped p-type indium nitride (InN) thin films by a relatively simple and economical spin coating method for the high-power electronics and long-wavelength light-emitting devices. This

beginning can be developed by further studies of producing low-cost InN-based semiconductors for new-generation optoelectronic devices.

4.2. Powders

It is possible to produce powders of various shapes and sizes in sizes which can be controlled by the sol-gel method. The powders to be produced are influenced from the precursor used, solvents used, from different chemicals added to the solution, pH, temperature, and each of them is a different parameter during the production process. With the sol-gel method, it is possible to obtain metallic, ceramic, polymeric or composite powders [2,4,48,85-90].

Hydroxyapatite and fluorapatite powders are widely synthesized by the sol-gel method. The fluorohydroxyapatite powder is also obtained mixing the basic materials on a molecular scale by the sol-gel technique [14]. Montazeri et al. [14] synthesized the calcium phosphate powders by the sol-gel method. The sol-gel method requires low calcination temperature for nanostructured materials. Hence, the phase change is avoided.

Another application of the sol-gel technique in powder processing is the combination of powder metallurgy and sol-gel methods. With this combination, titanium implants with porous structure can be manufactured by eliminating the defects like cracks and delaminations that are observed in the compaction step of conventional powder metallurgy process [85].

Belyaev et al. [48] synthesized by sol-gel method $ZnAl_2O_4$ ceramic powders from aluminum isopropoxide and zinc acetate for the purpose of obtaining transparent ceramics. As a result of the study, ceramic powders consist of particles with dimensions less than 5 μm then hot pressed with additive forming the liquid phase for obtaining bulk ceramic. Produced ceramics was achieved 80 % in the visible region for 1 mm thickness and 85 % at 5 μm transmittance.

The main problem in the production of nanopowders relies on the aggregation of the nanosized particles. The aggregation becomes dramatically intense. In particular, the particle size decreases to a quite small size. Dispersion of nanopowders is an essential factor for the preparation step of nanocomposite powders with uniform composition and good flowability. Surfactants such as polyvinyl pyrrolidone (PVP) and polyethylene glycol (PEG), Pluronic P123, cetyltrimethylammonium bromide (CTAB), sodium dodecyl sulfate (SDS), polyoxyethylene(23)lauryl ether (BRIJ-35) are employed in an attempt to provide dispersion and control morphology of the products. Thus, sol-gel as a powder production method ensures a practical way to produce materials with high surface areas derived from the formation of defined pore structures [12,86-90]. Dispersing the multiphase nanoparticles is also hard to achieve due to the different distinctive polarity and isoelectric points of multiphase nanoparticles that hinder the dispersion. Besides, conventional drying technology causes the re-aggregation of multiphase nanoparticles by affecting the stability of the suspension of

nanocomposite powder. The drying process can be accomplished by aqueous spray-drying to obtain spherical micron-sized nanocomposite particles [12].

Surfactants are often used for powder production in the sol-gel process for many reasons such as hindering agglomeration or controlling the morphology of the powders [88-90]. Rezaee et al. [88] conducted studies to investigate the effect of different surfactants in the production of Alumina-20 wt. % Zirconia (3 mol% Y_2O_3) nanopowders produced by the sol-gel method. In this study, they have produced nanopowders without surfactant and with different surfactants such as pluronic P123, cetyltrimethylammonium bromide (CTAB) and polyethylene glycol (PEG). The powders produced without surfactants have the highest specific surface area with 301 (m^2/g) and have a size of <10 nm but are agglomerated. CTAB, P123, and PEG have 236, 112, and 136 (m^2/g), specific surface area and powders with CTAB have 2-3 nm spherical particles. Pournajaf et al. [89] have studied the effect of surfactants on powders in their studies, and they have reached similar results. In their study, they focused on Al_2O_3-CeO_2 powder synthesis using microemulsion method and produced powder particles of approximately 20 nm size. They used anionic, cationic and nonionic surfactants in their work and achieved close results for alumina and ceria particles. Crystalline sizes approximately for nanopowders produced with anionic surfactant 17-22 nm, cationic surfactant 5-6 nm, and nonionic surfactant 8-10 nm. Specific surface areas for powders produced with anionic surfactant 120 (m^2/g), cationic surfactant 162 (m^2/g), and nonionic surfactant 134 (m^2/g).

Udduttula et al. [90] produced nanosized strontium phosphosilicate $Sr_5(PO_4)_2SiO_4$ powders for bone regeneration applications. They employed $Sr(NO_3)_2$, $NH_4H_2PO_4$ and $Si(OC_2H_5)_4$ as precursors, and CTAB as a cationic surfactant. Sol was mixed with NH_3 solution for the pH adjustment and waited for precipitation. Then they were heated and calcined. Obtained nanopowders rod-shaped and single-phased between the range of 25-70 nm have excellent apatite layer formation ability. They predicted that the powders appropriate for bone tissue engineering applications.

Najafi et al. [91] synthesized B_4C nanopowder by using the sol-gel method. They have used trimethyl borate, ethanol/distilled water, and acidic catalyst as a precursor, solvent, and catalyzer, respectively. They have studied pH adjusting and ammonium carboxylate amount of the solution. The results showed that the produced powders have 10 nm particle size which minimum ever reported particle size for B_4C with the optimum pH value and ammonium carboxylate amount.

4.3. Fibers

Glass and ceramic fibers can be produced by low-temperature sol-gel method adjusting the viscosity of the sol into an adequate viscosity range

[11,92]. Viscous sols are prepared from organic compounds such as metal alkoxides and are subjected to spinning to form fibrous precursor gels. The process follows the heat-treatment step to accomplish the conversion to glass and/or ceramic fibers [92].

The spinning of the viscous sols can be performed by the pulling-up method or centrifugal spinning. The pulling-up method allows checking the spinnability of the sol. Gel fibers are obtained by extrusion from small holes of a swiftly rotating pot in the centrifugal spinning process [92].

Roque-Ruiz et al. [46] produced dense alumina fibers from aluminum nitrate nonahydrate, $(AlNO_3).9H_2O$, polyvinyl pyrrolidone, PVP, ethanol, and deionized water by using sol-gel and electrospinning techniques. They have observed changes in diameters according to the different solutions they have prepared and have succeeded in obtaining fibers ranging in diameter from 70 to 600 nm. They observed an increase in the strength of alumina fibers when aluminum nitrates used at higher concentrations.

Liu et al. [47] produced calcium zirconate fibers by spinning for biodiesel or refractory materials. They were used poly acetylacetonato zirconium (PAZ), calcium nitrate tetrahydrate, calcium chloride, citric acid, methanol, polyvinyl alcohol (PVA), and distilled water as starting materials. Over the past several decades, the main application forms of $CaZrO_3$ were powders and its products. $CaZrO_3$ fibers were spun for the first time by Liu et al. [47]. They examined the high- temperature performances of the produced fibers using oxygen coal gas flame and indicated that the fibers had excellent thermostability.

4.4. Porous Gels

Sol-gel technology may use as scaffolds or matrices for tissue repairing and regeneration in biomedical applications [93]. Tissue engineering introduces hydroxyapatite (HA) for bone and cartilage regeneration. The existence of porosity in the HA structure is required because it allows for the development of tissue and bone around a supporting skeleton and permits the transition of nutrients. In the human body, the porosity of bone structure shows an alteration with the type and function. HA as a tailored porous bioactive and osteoconductive Si-substituted material is remarkable in terms of the improvement of bioactivity and can be produced by the sol-gel technique [11].

Silica-based systems may also use in among the matrix networks. Bio-glass is composed mainly of silica, sodium oxide, calcium oxide and phosphates [93]. Bioactive glass-ceramics also known as silica-based sol-gel bioactive glasses may use in several parts of the human body. According to available literature, sol-gel derived nanosized powders [90] or bioactive hydrogels [94] enhanced for bone regeneration applications too.

Nanosized inorganic materials draw attention in biomedical applications. In the past years, the studies accelerate for the use of nanosized inorganic

materials in bone tissue regeneration to overcome the bone loss or bone defects caused by injury or bone cancer [94-96]. Wang et al. [96], produced terbium-containing mesoporous bioactive glasses nanospheres. They investigated the formation of HA in SBF and in vitro drug release performance. They achieved superior biocompatibility, fast degradation, and controlled drug release with these nanospheres with spherical morphology.

4.5. Membranes

Due to the environmental pollution concerns and increasing tendency to fossil fuels, the alternative energy sources attract attention. Proton exchange membrane fuel cell (PEMFC) can transform chemical energy directly into electrical energy with extremely low pollution and high power density. At the same time, PEMFC prevents problems such as reduced proton conductivity due to the high temperatures, high methanol permeability and high cost in hybrid fuel cells. The sol-gel method is a proper method for improving PEMFC's [45]. In situ sol-gel method provides many advantages to the membranes such as process controllability or morphology homogeneity [43-45]. Divona et al. [43], Liang et al. [44], and Yin et al. [45] applied in their studies in-situ sol- gel method, in order to develop membranes and they obtained successful results. Similarly, Joseph et al. [97] developed mesostructured silica/Nafion and mesostructured phosphonated silica/Nafion hybrid membranes by using sol-gel method for fuel cell applications. They observed these modified Nafion composites are promising potential especially for use at high temperatures.

Membranes are also used for filtering applications, apart from fuel cell applications. The fact that if the oils in the wastewater are not filtered and remain insoluble in the water surface, they could damage the health of living creatures. For the filtering of oils and various harmful substances Gao et al. [98] studied on TiO_2 nanoparticles sol-gel coated SWCNT membranes for developing a new filtration system with high separation efficiency. They produced SWCNT/TiO_2 nanocomposite membranes with an ultrahigh separation efficiency of 99.99% and 30,000 L/m^2hbar water flux. TiO_2 has a photocatalytic property, and the final nanocomposite films have excellent self-cleaning and anti-fouling properties even during multiple cycles thanks to TiO_2.

Jiang et al. [99] also studied to improve the efficiency of oil/water separator membranes. They produced a switchable Janus membrane ($CNTs@PAN_{EN}$) by using the sol-gel method. They prepared carbon nanotube coated hydrophobic polyacrylonitrile (PAN) nanofiber membranes by using the electrospinning technique. Coatings were successfully applied to the surfaces, and interfacial compatibility between carbon nanotubes and PAN nanofibers were good. Janus membrane has ultrahigh flux with 80,000 L/m^2hbar and high separation efficiency of 99.2%.

4.6. Coatings for Textile Applications

The sol-gel technology takes place in the fabric industry at chemical finishing stage of textiles in order to bring properties such as ultraviolet protection, antibacterial, flame retardant, water repellent and self-cleaning. The sol-gel processing fulfills these properties more effectively and eco-friendly by consuming fewer chemicals [30].

Chemical finishing of fabrics by sol-gel is carried out by pad-dry-cure method consists of three steps: soaking of textile fibres by the sol, drying the fibre and curing under the proper conditions. After drying and curing steps, a polymer nanocomposite film with an approximate thickness of 10 nm is obtained on the fibre surface. Covalent bonding is formed by the reaction between the M– OH groups of precursors and the fibre surface. Consequently, the adhesion of the polymer film to the textiles is enhanced [30].

Foorginezhad and Zerafat [100] studied on sol-gel coated cotton fabrics. They were coated fabrics with the fluorine-free films generated from titania hydrosols to promote anti-adhesion and self-cleaning properties to the cotton fabrics. They characterized the coatings and tested water contact angles of surfaces. They obtained an increment of water contact angle from 0° to 134.1° with sliding angles >90° on pure fabric and achieved higher water contact angles up to ~170° and less sliding angle to <10° by polydimethylsiloxane (PDMS) addition. In brief, they produced self- cleaning, anti-adhesion, chemically resistant, and super-hydrophobic textiles through spraying.

Lin et al. [101] produced cotton fabrics and coated them with different sols to provide fabrics superhydrophobic and flame retardant properties. These fabrics are employed in different industries such as automobile interiors, indoor decorations, outdoor wear, and tents. The micro-nanostructured composite film can be successfully coated on cotton by the PDMS (hydroxyl- terminated polydimethylsiloxane)-silica and APP (ammonium polyphosphate). With a water contact angle over 160°, the coated cotton fabric exhibited superior endurance and self-cleaning ability. When the coated cotton is exposed to fire, the coating forms a dense char layer in order to extinguish the fire with the aid of the physical barrier effect of PDMS-silica and flame-retardant effect of APP.

4.7. Chemical Sensors and biosensor applications

Chemical sensors and biosensors are defined as devices that record the concentration of (bio)chemical agents continuously or reversible. Chemical sensors produced by sol-gel technology are capable of measuring the light intensity, temperature, pressure etc. such as physical sensors. Chemical sensors are expected to sense pH, oxygen, and pollutants whereas the biosensors serve for detecting cholesterol, glucose, immunoglobulins, phenytoin, and pollutants such as atrazine [102].

Glass electrodes or paper strips are often used for pH sensing nowadays. These methods sometimes cannot capture the desired accuracy or be expensive. In this case, it may be one of the more useful and cost-effective methods to use chemical sensors. For example, Pathak and Singh [103], and Pathak et al. [104] fabricated pH sensors with good stability and a wide range of pH value varied from 4 to 11 and 4 to 13 using the sol-gel method in their studies.

Biosensors are research topic for the developing a wide range of applications in clinical diagnosis, biomedical, environmental monitoring, military, industrial and food technology. Production with the sol-gel method is unique for biosensing due to its properties such as adsorption on glass surfaces or entrapment in polymer matrices based on the growing polymer chains in an inorganic oxide network [105]. Studies are focused on properties of biomolecules or the environments such as, pH value in the environment, viscosity or polarity of the environment [106,107]; structure, function, activity or dynamics of the biomolecules [108-110]. They utilized various properties of biomolecules for the entrapment. For example, Rathinamala et al. [111] produced Cadmium Sulphide/Porous Silicon (CdS/PS) electrode based biosensors for detection of glucose by using the spin coating method. Thanks to the electrochemical properties of CdS/PS, sensors have quick response time and good detection limit.

Similarly, Xu et al. [112] tried to detect propyl gallate (PG) in various things that we use in daily life. PG is generally added to protect foods containing lipids or fats against rancidness. However, an excess amount of PG is found to be harmful to human health due to its toxic effect [112,113]. Xu et al. [112] studied on the electrochemical sensor that can be determined of PG that excellent antioxidant, by modifying graphene and single-walled carbon nanotubes. The sensor they produced successfully detected PG in oils, instant noodles, and cookies.

References

1. G. Bahuguna, N. K. Mishra, P. Chaudhary, A. Kumar and R. Singh, "Thin Film Coating through Sol-Gel Technique". *Research Journal of Chemical Sciences* (C. 6), 2016.
2. A. C. Pierre, Introduction to Sol-Gel Processing, L. Klein,editor. Lyon, Springer, 1998.
3. U. Schubert, Chemistry and Fundamentals of the Sol-Gel Process, In: D. Levy and M. Zayat, editors. The Sol-Gel Handbook, Synthesis, Characterization and Applications. Vol 1. Part 1, Ch 1, pp. 3-28. Weinheim, Wiley-VCH, 2015.
4. H. Dislich, "Sol-Gel 1984- 2004 (?)," *Journal of Non-Crystalline Solids*, vol. 73, pp. 599–612. 1985. https://doi.org/10.1016/0022-3093(85)90379-5
5. P. F. James, "The gel to glass transition: Chemical and microstructural evolution," *Journal of Non-Crystalline Solids*, vol. 100(1–3), pp. 93–114, 1988. https://doi.org/10.1016/0022- 3093(88)90009-9
6. F. Orgaz-Orgaz, "Gel to glass conversion: Densification kinetics and controlling mechanisms," *Journal of Non-Crystalline Solids*, vol. *100*(1–3), pp. 115–141, 1988. https://doi.org/10.1016/0022-3093(88)90010-5
7. T. Kawaguchi, H. Hishikura and J. Iura "Shrinkage Behaviour of Silica Gels During Drying," *Journal of Non-Crystalline Solids*, vol. 100(1-3), pp. 220–225, 1988.. https://doi.org/10.1016/0022-3093(88)90021-X
8. T. Mizuno, H. Nagata and S. Manabe, "Attempts to avoid cracks during drying," *Journal of Non-Crystalline Solids*, vol. 100(1–3), pp. 236–240, 1988. https://doi.org/10.1016/0022- 3093(88)90024-5
9. R.B. Pettit and C.J. Brinker, "Use of Sol-Gel Thin Films in Solar Energy Applications," *Solar Energy Materials*, vol. 14, pp. 269–287, 1986. https://doi.org/10.1016/j.imlet.2014.08.006
10. T. Maki and S. Sakka "Preparation of alumina fibers by sol-gel method," *Journal of Non- Crystalline Solids*, vol. 100(1–3), pp. 303–308, 1988. https://doi.org/10.1016/0022- 3093(88)90037-3
11. R. Gupta, A. Kumar, "Bioactive materials for biomedical applications using sol–gel technology," *Biomedical Materials*, vol. 3(3), pp 1–15, 2008. https://doi.org/10.1088/1748- 6041/3/3/034005
12. X. Guo, Q. Zhang, X. Ding, Q. Shen, C. Wu, L. Zhang and H. Yang, "Synthesis and application of several sol–gel-derived materials via sol–gel process combining with other technologies: a review," *Journal of Sol-Gel Science and Technology*, vol. 79(2), pp. 328–358, 2016.
13. D. Wang and G. P. Bierwagen, "Sol–gel coatings on metals for corrosion protection," *Progress in organic coatings*, vol. 64(4), pp. 327–338, 2009. https://doi.org/10.1016/j.porgcoat.2008.08.010
14. N. Montazeri, R. Jahandideh and E. Biazar, "Synthesis of fluorapatite–hydroxyapatite nanoparticles and toxicity investigations," *International journal of nanomedicine*, vol. 6, pp. 197–201, 2011. https://doi.org/10.2147/IJN.S15461
15. R. B. Figueira, C. J. Silva and E. V. Pereira"Organic–inorganic hybrid sol–gel coatings for metal corrosion protection: a review of recent progress," *Journal of Coatings Technology and Research*, vol. 12(1), pp. 1–35, 2015. https://doi.org/10.1007/s11998-014-9595-6
16. "Colloid". Britannica Online Encyclopedia. Retrieved 1 February 2019.
17. P. Innocenzi, The Sol to Gel Transition, Alghero, Springer, 2016
18. A.C. Pierre, A. Rigacci, SiO2 Aerogels, In: M. Aegerter, N. Levistis M.M. Koebel, editors. Aerogels Handbook, Part 2, Ch 2, pp. 21–45, New York, Springer, 2012.
19. R. I. M. Asri, W. S. W. Harun, M. A. Hassan, S. A. C. Ghani and Z. Buyong, "A review of hydroxyapatite-based coating techniques: Sol–gel and

electrochemical depositions on biocompatible metals," *Journal of the mechanical behavior of biomedical materials*, vol. 57, pp. 95–108, 2016. https://doi.org/10.1016/j.jmbbm.2015.11.031

20. H. Kozuka, Stress Evolution and Cracking in Sol-Gel-Derived Thin Films, In: L. Klein, M Aparicio, A. Jitianu, editors. Handbook of sol-gel science and technology, Processing, Characterization and Applications Series, vol.1, Part 1, Ch 11, pp. 275–312. New York, Springer; 2018.
21. R. Nistico, D. Scalarone, G. Magnacca, "Sol-gel chemistry, templating and spin-coating deposition: A combined approach to control in a simple way the porosity of inorganic thin films/coatings," *Microporous and Mesoporous Materials*, vol. 248, pp. 18–29, 2017. https://doi.org/10.1016/j.micromeso.2017.04.017
22. R. Corriu and N. Anh, Molecular Chemistry of Sol-Gel Derived Nanomaterials. France, John Wiley & Sons, 2009.
23. H. Schmidt, "Chemistry of Material Preparation by the Sol-Gel Process," *Journal of Non- Crystalline Solids*, vol. 100(1-3), pp. 51-64, 1988. https://doi.org/10.1016/0022- 3093(88)90006-3
24. C. Sanchez, J. Livage, M. Henry and F. Babonneau, "Chemical Modification of Alkoxide Precursors," *Journal of Non-Crystalline Solids*, vol. 100(1-3), pp. 65-76, 1988. https://doi.org/10.1016/0022-3093(88)90007-5
25. K. Zheng and A. R. Boccaccini, "Sol-gel processing of bioactive glass nanoparticles: A review," *Advances in colloid and interface science*, vol. 249, pp. 363-373, 2017. https://doi.org/10.1016/j.cis.2017.03.008
26. G. W. Scherer, "Aging and Drying of Gels," *Journal of Non-Crystalline Solids*, vol. 100(1- 3), pp. 77-92, 1988. https://doi.org/10.1016/0022-3093(88)90008-7
27. M. Guglielmi, G. Carturan, "Precursors for sol-gel preparations," *Journal of Non-Crystalline Solids*, vol. 100(1-3), pp. 16-30, 1988. https://doi.org/10.1016/0022-3093(88)90004-X
28. C. J. Brinker and G. W. Scherer, Sol-Gel Science: The Physics and Chemistry of Sol-Gel Processing, New Mexico, Academic Press, 1990.
29. C. J. Brinker, A. J. Hurd, P. R. Schunk, G. C. Frye and C. S. Ashley, "Review of sol-gelthin film formation," *Journal of Non-Crystalline Solids*, vol. 147-148, pp. 424-436, 1992. https://doi.org/10.1016/S0022-3093(05)80653-2
30. W. N. W. Ismail, "Sol–gel technology for innovative fabric finishing—A Review," *Journal of Sol-Gel Science and Technology*, vol. 78(3), pp. 698-707, 2016. https://doi.org/10.1007/s10971-016-4027-y
31. W. Feng, L. Mu-Sen, L. Yu-Peng and Q. Yong-Xin, "A simple sol–gel technique for preparing hydroxyapatite nanopowders," *Materials Letters*, vol. 59(8-9), pp. 916-919, 2005. https://doi.org/10.1016/j.matlet.2004.08.041
32. D. M. Liu, T. Troczynski and W. J. Tseng, "Aging effect on the phase evolution of water- based sol–gel hydroxyapatite," *Biomaterials*, vol. 23(4), pp. 1227-1236, 2002. https://doi.org/10.1016/S0142-9612(01)00242-3
33. D. Y. Nadargi, S. S. Latthe and A. V. Rao, "Effect of post-treatment (gel aging) on the properties of methyltrimethoxysilane based silica aerogels prepared by two-step sol–gel process," *Journal of sol-gel science and technology*, vol. 49(1), pp. 53-59, 2009. https://doi.org/10.1007/s10971-008-1830-0
34. A. O. Gabriel and R. Riedel, "Preparation of Non-Oxidic Silicon Ceramics by an Anhydrous Sol–Gel Process," *A Journal of German Chemical Society, Angewandte Chemie International Edition in English*, vol. 36(4), pp. 384-386, 1997. https://doi.org/10.1002/anie.199703841
35. S.P. Mukherjee, Ultrapure glasses from sol–gel processes. In: L.C. Klein, editor. Sol–gel technology for thin films, fibres, preforms, electronics and specialty shapes, pp. 247-259. Park Ridge: N.J. Noyes; 1988.

36. T. Woignier, J. Primera, A. H. Alaoui, S. Calas-Etienne, "Mechanical behaviour of nano composite aerogels," *Journal of Sol-Gel Science and Technology*, vol. 58(2), pp. 385–393, 2011. https://doi.org/10.1007/s10971-011-2404-0
37. S. R. K. Ramachandra and R. Subasri, Sol-gel nanocomposite hard coatings, In: M. Aliofkhazraei, editor. Anti Abrasive Nanocoatings, Current and Future Applications, Part 1, Ch 5, pp. 105-136, Woodhead Publishing Limited, 2015.
38. Ö. Kesmez, E. Akarsu, H. E. Çamurlu, E. Yavuz, M. Akarsu and E. Arpaç, "Preparation and characterization of multilayer anti-reflective coatings via sol-gel process," *Ceramics International*, vol. 44(3), pp. 3183-3188, 2018. https://doi.org/10.1016/j.ceramint.2017.11.088
39. M. Z. Ibrahim, A. A. D. Sarhan, F. Yusuf and M. Hamdi, "Biomedical materials and techniques to improve the tribological, mechanical and biomedical properties of orthopedic implants – A review article. *Journal of Alloys and Compounds*, vol. 714, pp. 636–667, 2017. https://doi.org/10.1016/j.jallcom.2017.04.231
40. A. Biesiekierski, J. Wang, M. A.-.H. Gepreel and C. Wen, "A new look at biomedical Ti- based shape memory alloys," *Acta Biomaterialia*, vol. 8(5), pp. 1661–1669, 2012. https://doi.org/10.1016/J.ACTBIO.2012.01.018
41. M. Niinomi, M. Nakai and J. Hieda, "Development of new metallic alloys for biomedical applications," *Acta Biomaterialia*, vol. 8(11), pp. 3888–3903, 2012. https://doi.org/10.1016/j.actbio.2012.06.037
42. F.-S. Razavi, M. Shabani-Nooshabadi and M. Behpour, "Sol-gel synthesis, characterization and electrochemical corrosion behavior of S-N-C-doped TiO2 nano coating on copper," *Journal of Molecular Liquids*, vol. 266, pp. 99-105, 2018. https://doi.org/10.1016/j.molliq.2018.06.056
43. M. Divona, Z. Ahmed, S. Bellitto, A. Lenci, E. Traversa and S. Licoccia, "SPEEK-TiO2 nanocomposite hybrid proton conductive membranes via in situ mixed sol–gel process," *Journal of Membrane Science*, vol. 296, pp. 156-161, 2007. https://doi.org/10.1016/j.memsci.2007.03.037
44. H.-Q. Liang, Q.-Y. Wu, L.-S. Wan, X.-J. Huang and Z.-K. Xu, "Thermally induced phase separation followed by in situ sol–gel process: A novel method for PVDF/SiO2 hybrid membranes," *Journal of Membrane Science*, vol. 465, pp. 56-67, 2014. https://doi.org/10.1016/j.memsci.2014.03.068
45. Y. Yin, T. Xu, G. He, Z. Jiang and H. Wu, "Fabrication of sulfonated poly(ether ether ketone)- based hybrid proton-conducting membranes containing carboxyl or amino acid-functionalized titania by in situ sol–gel process," *Journal of Power Sources*, vol. 276, pp. 271-278, 2015. https://doi.org/10.1016/j.jpowsour.2014.11.132
46. J. H. Roque-Ruiz, N. A. Medellin-Castillo and S. Y. Reyes-Lopez, "Fabrication of α-alumina fibers by sol-gel and electrospinning of aluminum nitrate precursor solutions," *Results in Physics*, *12*, 193-204, 2019. https://doi.org/10.1016/j.rinp.2018.11.068
47. B. Liu, X. Lin, L. Zhu, X Wang, D. Xu, "Fabrication of calcium zirconate fibers by the sol– gel method," *Ceramics International*, vol. 40(8A), pp. 12525-12531, 2014. https://doi.org/10.1016/j.ceramint.2014.03.025
48. A. V. Belyaev, M. I. Lelet, N. I. Kirillova, N. M. Khamaletdinova, M. S. Boldin, A. A. Murashov, S. S. Balabanov, "Sol-gel synthesis and characterization of ZnAl2O4 powdersfor transparent ceramics," *Ceramic International*, vol. 45(4), pp. 4835-4839, 2019. https://doi.org/10.1016/j.ceramint.2018.11.179
49. T. L. Metroke, R. L. Parkhill and E. T. Knobbe "Passivation of metal alloys using sol–gel- derived materials—a review," *Progress in Organic Coatings*, vol. 41(4), pp. 233-238, 2001. https://doi.org/10.1016/S0300-9440(01)00134-5
50. A. Amri, Z. T. Jiang, T. Pryor, C. Y. Yin and S. Djordjevic, "Developments in the synthesis of flat plate solar selective absorber materials via sol–gel methods: A

review," *Renewable and Sustainable Energy Reviews*, vol. 36, pp. 316-328, 2014. http://dx.doi.org/10.1016/j.rser.2014.04.06

51. A. Maho, S. Detriche, J. Delhalle and Z. Mekhalif, "Sol-gel synthesis of tantalum oxide and phosphonic acid-modified carbon nanotubes composite coatings on titanium surfaces," *Materials Science and Engineering C*, vol. 33(5), pp. 2686–2697, 2013. https://doi.org/10.1016/j.msec.2013.02.025
52. N. Cotolan, M. Rak, M. Bele, A. Cör, L. M. Muresan and I. Milošev, "Sol-gel synthesis, characterization and properties of TiO2and Ag-TiO2coatings on titanium substrate," *Surface and Coatings Technology*, vol. 307, pp. 790–799, 2016. https://doi.org/10.1016/j.surfcoat.2016.09.082
53. A. Bandyopadhyay, F. Espana, V. K. Balla, S. Bose, Y. Ohgami and N. M. Davies, "Influence of porosity on mechanical properties and in vivo response of Ti6Al4V implants," *Acta Biomaterialia*, vol. 6, pp. 1640–1648, 2010. https://doi.org/10.1016/j.actbio.2009.11.011
54. G. Y. Liu, J. Hu, Z. K. Ding and C. Wang, "Bioactive calcium phosphate coating formed on micro-arc oxidized magnesium by chemical deposition," *Applied Surface Science*, vol. 257(6), pp. 2051–2057, 2011. https://doi.org/10.1016/j.apsusc.2010.09.050
55. F. Brusciotti, D. V. Snihirova, H. Xue, M. F. Montemor, S. V. Lamaka and M. G. S. Ferreira, "Hybrid epoxy-silane coatings for improved corrosion protection of Mg alloy," *Corrosion Science*, vol. 67, pp. 82–90, 2013. https://doi.org/10.1016/j.corsci.2012.10.013
56. W. Zai, M. H. Wong and H. C. Man, "Improving the wear and corrosion resistance of CoCrMo-UHMWPE articulating surfaces in the presence of an electrolyte," *Applied Surface Science*, vol. 464, pp. 404-411, 2019. https://doi.org/10.1016/j.apsusc.2018.09.027
57. L. Claire, G. Marie, G. Julien, S. Jean-Michel, R. Jean, M. Marie-Joëlle, … and F. Michele, "New architectured hybrid sol-gel coatings for wear and corrosion protection of low-carbon steel," *Progress in Organic Coatings*, vol. 99, pp. 337–345, 2016. https://doi.org/10.1016/J.PORGCOAT.2016.06.015
58. M. Zhang, S. Cai, S. Shen, G. Xu, Y. Li, R. Ling and X. Wu, "In-situ defect repairing in hydroxyapatite/phytic acid hybrid coatings on AZ31 magnesium alloy by hydrothermal treatment," *Journal of Alloys and Compounds*, vol. 658, pp. 649–656, 2016. https://doi.org/10.1016/j.jallcom.2015.10.282
59. R. N. Peres, E. S. F. Cardoso, M. F. Montemor, H. G. de Melo, A. V. Benedetti and P. H. Suegama, "Influence of the addition of SiO2 nanoparticles to a hybrid coating applied on an AZ31 alloy for early corrosion protection," *Surface and Coatings Technology*, vol. 303(Part B), pp. 372–384, 2016. https://doi.org/10.1016/j.surfcoat.2015.12.049
60. C. A. Hernandez-Barrios, C.A. Cuao, M.A. Jaimes, A. E. Coy, F. Viejo, "Effect of the catalyst concentration, the immersion time and the aging time on the morplogy, composition and corrosion performance of TEOS-GPTMS sol-gel coatings deposited on the AZ31 Mg alloy," *Surface & Coatings Technology*, vol. 325, pp. 257-269, 2017. https://doi.org/10.1016/j.surfcoat.2017.06.047
61. Y. Oshida, Bioscience and Bioengineering of Titanium Materials (Second Edi). Ch 6, pp. 138-168. London, Elsevier B.V., 2013.
62. M. Geetha, M., A. K. Singh, R. Asokamani and A. K. Gogia, A. K, "Ti based biomaterials , the ultimate choice for orthopaedic implants – A review," *Progress in Materials Science*, vol. 54(3), pp. 397–425, 2009. https://doi.org/10.1016/j.pmatsci.2008.06.004
63. R. B. Heimann, "Structure, properties, and biomedical performance of osteoconductive bioceramic coatings," *Surface and Coatings Technology*, vol. 233, pp. 27–38, 2013. https://doi.org/10.1016/j.surfcoat.2012.11.013

64. B. Ben-Nissan, A. H. Choi, R. Cordingley, Alumina Ceramics, In: Kokubo, T., editor. Bioceramics and their clinical applications, Part 2, Ch 10, pp. 223-242. Boca Raton, Woodhead Publishing Limited, 2008.
65. Ş. Y. Güven, "Biyouyumluluk ve Bi̇yomalzemelerİn Seçi̇mi̇," *Mühendislik ve Tasarım Dergisi*, vol. 2(3), pp. 303–311, 2014. https://doi.org/10.21923/MBTD.11616
66. M. Niinomi, "Recent metallic materials for biomedical applications," *Metallurgical and Materials Transactions A*, vol. 33(3), pp. 477–486, 2002. https://doi.org/10.1007/s11661-002- 0109-2
67. R. Rojaee, M. Fathi and K. Raeissi, "Controlling the degradation rate of AZ91 magnesium alloy via sol–gel derived nanostructured hydroxyapatite coating," *Materials Science and Engineering C*, vol. 33, pp. 3817-3825, 2013. http://dx.doi.org/10.1016/j.msec.2013.05.014
68. P. Usinskas, Z. Stankevicute, A. Beganskiene and A. Kareiva, "Sol-gel derived porous and hydrophilic calcium hydroxyapatite coating on modified titanium substrate," *Surface and Coatings Technology*, vol. 307(A), pp. 935-940, 2016. https://doi.org/10.1016/j.surfcoat.2016.10.032
69. Y. Shunzhi, L. Zhonghai, H. Liwei, Z. Yantao and F. Tao, "Biocompatible MgO Film on Titanium Substrate Prepared by Sol-gel Method," Rare Metal Materials and Engineering, vol. 47(9), pp. 2663-2667, 2018. https://doi.org/10.1016/S1875-5372(18)30206-6
70. N. Sheiko, P. Lelicheff, P. Marie, M. Schmutz, L. Jacomine and F. Perrin-Schmitt, "PEEK (polyether-ether-ketone)-coated nitinol wire: Film stability for biocompatibility applications," *Applied Surface Science*, vol. 389, pp. 651-665, 2016. https://doi.org/10.1016/j.apsusc.2016.07.159
71. X. Li, L. Wang, X. Yu, Y. Feng, C. Wang, K. Yang and D. Su, "Tantalum coating on porous Ti6Al4V scaffold using chemical vapor deposition and preliminary biological evaluation," *Materials Science and Engineering C*, vol. 33, pp. 2987-2994, 2013. http://dx.doi.org/10.1016/j.msec.2013.03.027
72. L. Guo, W. Feng, X. Liu, C. Lin, B. Li and Y. Qiang, "Sol–gel synthesis of antibacterial hybrid coatings on titanium," *Material Letters*, vol. 160, pp. 448-451, 2015. http://dx.doi.org/10.1016/j.matlet.2015.08.027
73. S. A. H. Jalali, A. R. Allafchian, S. S. Banifatemi and I. A. Tamai, "The antibacterial properties of Ag/TiO2 nanoparticles embedded in silane sol–gel matrix," *Journal of the Taiwan Institute of Chemical Engineers*, vol. 66, pp. 357-362, 2016. https://doi.org/10.1016/j.jtice.2016.06.011
74. B. Xue, M. Yu, J. Liu, J. Liu, S. Li and L. Xiong, "Corrosion protection of AA2024-T3 by sol-gel film modified with graphene oxide," *Journal of Alloys and Compounds*, vol. 725, pp. 84-95, 2017. https://doi.org/10.1016/j.jallcom.2017.05.09
75. M. H. Hussin, "Electrochemical data of single and hybrid sol-gel coating precursors for aluminum alloy corrosion protection in 3.5% NaCl," *Data in Brief*, vol. 22, pp. 971-976, 2019. https://doi.org/10.1016/j.dib.2019.01.029
76. P. Rodič, I. Milošev, M. Lekka, F. Andreatta and L. Fedrizzi, "Corrosion behaviour and chemical stability of transparent hybrid sol-gel coatings deposited on aluminium in acidic and alkaline solutions," *Progress in Organic Coatings*, vol. 124, pp. 286-295, 2018. https://doi.org/10.1016/j.porgcoat.2018.02.025
77. T. T. Thai, M.-E. Druart, Y. Paint, A. T. Trinh and M.-G. Oliver, "Influence of the sol-gel mesoporosity on the corrosion protection given by an epoxy primer applied on aluminum alloy 2024 –T3," *Progress in Organic Coatings*, vol. 121, pp. 53-63, 2018. https://doi.org/10.1016/j.porgcoat.2018.04.013
78. A. Schüler, D. Dutta, E. Chambrier, C. Roecker, G. Temmerman, P. Oelhafen and J. Scartezzini, "Sol–gel deposition and optical characterization of multilayered

SiO2/Ti1−xSixO2 coatings on solar collector glasses," *Solar Energy Materials and Solar Cells*, vol. 90(17), pp. 2894-2907, 2006. https://doi.org/10.1016/j.solmat.2006.05.00

79. Y. Zhu, L. Chen, C. Zhang and Z. Guan, "Preparation of hydrophobic antireflective SiO2coating with deposition of PDMS from water-based SiO2-PEG sol," *Applied Surface Science*, vol. 457, pp. 522-52, 2018. https://doi.org/10.1016/j.apsusc.2018.06.177
80. J. Wang, J. Ge, H. Hou, M. Wang, G. Liu, G. Qiao and Y. Wang, "Design and sol–gel preparation of SiO2/TiO2 and SiO2/SnO2/SiO2–SnO2 multilayer antireflective coatings, *Applied Surface Science*, vol. 422, pp. 970-974, 2017. https://doi.org/10.1016/j.apsusc.2017.06.133
81. K. Koc, F. Z. Tepehan and G. G. Tepehan, "Antireflecting coating from Ta2O5 and SiO2 multilayer films," *Journal of Materials Science*, vol. 40, pp. 1363 – 1366, 2005. https://doi.org/10.1007/s10853-005-0566-2
82. L. Ouarez, A. Chelouche, T. Touam, R., Mahiou, D. Djouadi and A. Potdevin, "Au-doped ZnO sol-gel thin films: An experimental investigation on physical and photoluminescence properties". *Journal of Luminescence*, vol. 203, pp. 222–229, 2018. https://doi.org/10.1016/J.JLUMIN.2018.06.049
83. L. Meng, X. Yang, H. Chai, Z. Lv and T. Yang, "Sol-gel derived Zn1-xMgxO:Al transparent conductive thin film and its application to thin film solar cells," *Thin Solid Films*, vol. 672, pp. 186–191, 2019. https://doi.org/10.1016/J.TSF.2019.01.016
84. H. S. Lee, S. S. Ng, F. K. Yam, "Sol–gel spin coating growth of magnesium-doped indium nitride thin films," *Vacuum*, vol. 155, pp. 16-22, 2018. https://doi.org/10.1016/j.vacuum.2018.05.042
85. A. A. Ribeiro, L. M. Morani, R. M. Balestra, F. M. L. Dantas, M. H. M. Rocha-Leão and M. Varella, "Study of sol-gel/powder metallurgy technique for processing titanium parts,". *In Materials Science Forum* (Vol. 727, pp. 368-373). Trans Tech Publications 2012. https://doi.org/10.4028/www.scientific.net/MSF.727-728.368
86. L. G. Possato, E. Pereire, R. G. L. Gonçalves, S. H. Pulcinelli, L. Martins and C. V. Santilli, "Controlling the porosity and crystallinity of MgO catalysts by addition of surfactant in the sol-gel synthesis," *Catalysis Today*, in press, 2018. https://doi.org/10.1016/j.cattod.2018.10.027
87. G.-Y. Huang, S.-M. Xu, L-Y. Li, X.-J. Wang, "Effect of surfactants on dispersion property and morphology of nano-sized nickel powders," *Transactions Nonferrous Metals. Soceity of China*, vol. 24, pp. 3739–3746, 2014. https://doi.org/10.1016/S1003-6326(14)63523-8
88. S. Rezaee, K. Ranjbar and A. R. Kiasat, "The effect of surfactant on the sol–gel synthesis of alumina-zirconia nanopowders," *Ceramics International*, vol. 44(16), pp. 19963–19969 https://doi.org/10.1016/j.ceramint.2018.07.263
89. R. Pournajaf, S. A. Hassanzadeh-Tabrizi and M. Ghashang, "Effect of surfactants on the synthesis of Al2O3–CeO2 nanocomposite using a reverse microemulsion method," *Ceramic International*, vol. 40(3), pp. 4933–4937, 2014. https://doi.org/10.1016/j.ceramint.2013.10.086
90. A. Udduttula, J. Li, P.-Y. Zhao, G.-C. Wang, J. V. Zhang, P.-G. Ren, "Sol-gel derived nanosized Sr5(PO4)2SiO4 powder with enhanced in vitro osteogenesis and angiogenesis for bone regeneration applications," *Ceramics International*, vol. 45(3), pp.3148–3158, 2019. https://doi.org/10.1016/J.CERAMINT.2018.10.215
91. A. Najafi, F. Golestani-Fard and H. R. Rezaire, "Sol-gel synthesis and characterization of B4C nanopowder," *Ceramics International*, vol. 44, pp. 21386–21394, 2018. https://doi.org/10.1016/j.ceramint.2018.08.196

92. K. Kamiya, Processing of Fibers. In: L. Klein, M. Aparicio, A. Jitianu, editors. Handbook of sol-gel science and technology, Processing, Characterization and Applications Series, *vol.1, Part 1, Ch 10*, pp. 257-274. New York, Springer; 2018.
93. L. Tan, X. Yu, P. Wan and K. Yang, "Biodegradable Materials for Bone Repairs: A Review," *Journal of Materials Science and Technology*, vol. 29(6), pp. 503–513, 2013. https://doi.org/10.1016/j.jmst.2013.03.002
94. X. Bai, M. Gao, S. Syed, J. Zhuang, X. Xu and X.-Q. Zhang, "Bioactive hydrogels for bone regeneration," *Bioactive Materials*, vol. 3(4), pp. 401–417, 2018. https://doi.org/10.1016/J.BIOACTMAT.2018.05.006
95. H. S. Yun, S. H. Kim, S. Lee and I. H. Song, "Synthesis of high surface area mesoporous bioactive glass nanospheres," *Materials Letters*, vol. 64 pp. 1850–1853, 2010. https://doi.org/10.1016/j.matlet.2010.04.053
96. X. Wang, Y. Zhang, C. Lin and W. Zhong, "Sol-gel derived terbium-containing mesoporous bioactive glasses nanospheres: In vitro hydroxyapatite formation and drug delivery," *Colloids and Surfaces B: Biointerfaces*, vol. 160, pp. 406–415, 2017. https://doi.org/10.1016/j.colsurfb.2017.09.051
97. J. Joseph, C.-Y. Tseng and B.J. Hwang, "Phosphonic acid-grafted mesostructured silica/Nafion hybrid membranes for fuel cell applications," *Journal of Power Sources*, vol. 196(18), pp. 7363–7371, 2011. https://doi.org/10.1016/j.jpowsour.2010.08.090
98. S. J. Gao, Z. Shi, W. B. Zhang, F. Zhang and J. Jin, "Photoinduced Superwetting Single-Walled Carbon Nanotube/TiO2 Ultrathin Network Films for Ultrafast Separation of Oil-in- Water Emulsions", *ACS Nano*, vol. 8(6), pp. 6344–6352, 2014. https://doi.org/10.1021/nn501851a
99. Y. Jiang, J. Hou, J. Xu and B. Shan, "Switchable oil/water separation with efficient and robust Janus nanofiber membranes," *Carbon*, vol. 115, pp. 477–485, 2017. https://doi.org/10.1016/j.carbon.2017.01.053
100. S. Foorginezhad and M. M. Zerafat, "Fabrication of stable fluorine-free superhydrophobic fabrics for anti-adhesion and self-cleaning properties," *Applied Surface Science*, vol. 464, pp. 458–471, 2019. https://doi.org/10.1016/j.apsusc.2018.09.058
101. D. Lin, X. Zeng, H. Li, X. Lai and T. Wu, "One-pot fabrication of superhydrophobic and flame-retardant coatings on cotton fabrics via sol-gel reaction," Journal of Colloid and Interface Science, vol. 533, pp. 198–206, 2019. https://doi.org/10.1016/j.jcis.2018.08.060
102. R. Reisfeld, "Prospects of sol–gel technology towards luminescent materials," *Optical Materials*, vol. 16(1-2), pp. 1–7, 2001. https://doi.org/10.1016/S0925-3467(00)00052-5
103. A. K. Pathak and V. K. Singh, "Fabrication and characterization of down-tapered optical fiber pH sensor using sol-gel method," *Optic*, vol. 149, pp. 288–294, 2017. https://doi.org/10.1016/j.ijleo.2017.09.051
104. A. K. Pathak, V. Bhardwaj, R. K. Gangwar, Moutusi de and V. K. Singh," Fabrication and characterization of TiO2 coated cone shaped nano-fiber pH sensor," *Optics Communication*, vol. 386, pp. 43–48, 2016. https://doi.org/10.1016/j.optcom.2016.11.021
105. R. Gupta and N. K. Chaudhury, "Entrapment of biomolecules in sol–gel matrix for applications in biosensors: Problems and future prospects," *Biosensors and Bioelectronics*, vol. 22(11), pp. 2387-2399, 2007. https://doi.org/10.1016/j.bios.2006.12.025
106. P. L. Edmiston, C. L. Wambolt, M. K. Smith and S.S. Saavedra, "Spectroscopic Characterization of Albumin and Myoglobin Entrapped in Bulk Sol-Gel Glasses," *Journal of Colloid and Interface Science*, vol. 163(2), pp. 395-406, 1994. https://doi.org/10.1006/jcis.1994.1119

107. K. K. Flora and J. D. Brennan, "Characterization of the Microenvironments of PRODAN Entrapped in Tetraethyl Orthosilicate Derived Glasses," *The Journal of Physical Chemistry B*, vol. 105(48), pp. 12003-12010, 2001. https://doi.org/10.1021/jp012598i
108. T. R. Besanger, Y. Chen, A. K. Deisingh, R. Hodgson, W. Jin, S. Mayer, M.A. Brook and
109. K. K. Flora and J. D. Brennan, "Fluorometric Detection of Ca2+ Based on an Induced Change in the Conformation of Sol–Gel Entrapped Parvalbumin,"*Analytical Chemistry*, vol. 70(21) pp. 4505-4513, 1998. https://doi.org/10.1021/ac980440x
110. G. L. G. Goring and J. D. Brennan, "Fluorescence and physical characterization of sol–gel- derived nanocomposite films suitable for the entrapment of biomolecules," *Journal of Materials Chemistry*, vol. 12(12), pp. 3400-3406, 2002. https://doi.org/10.1039/B204547H
111. I. Rathinamala, N. Jeyakumaran and N. Prithivikumaran, "Sol-gel assisted spin coated CdS/PS electrode based glucose biosensor," *Vacuum*, vol. 161, pp.291-296, https://doi.org/10.1016/j.vacuum.2018.12.045
112. G. Xu, Y. Chi, L. Li, S. Liu and X. Kan, "Imprinted propyl gallate electrochemical sensor based on graphene/single walled carbon nanotubes/sol–gel film," *Food Chemistry*, vol. 177, pp. 37-42, 2015. https://doi.org/10.1016/j.foodchem.2014.12.097
113. Y. H. Han, H. J. Moon, B. R. You and W. H. Park, "Propyl gallate inhibits the growth of calf pulmonary arterial endothelial cells via glutathione depletion," *Toxicology in Vitro*, vol. 24, pp. 1183-1189, 2010. https://doi.org/10.1016/j.tiv.2010.02.013

CATEGORIZATION OF SHORT TEXT SOCIAL MEDIA COMMENTS IN CRM SYSTEMS

Hüseyin FİDAN [1]

[1] Dr., Burdur Mehmet Akif Ersoy Üniversitesi Mühendislik Mimarlık Fakültesi Endüstri Mühendisliği Bölümü.

1. INTRODUCTION

With the opening of the Internet for social uses, the amount of data produced in electronic environment has increased extremely. Especially in 1995, the developments in web technologies that called Web 2.0 have enabled the creation of user-interactive web pages, resulting to incredible amount of data. This huge data size has attracted the attention of business and the analysis of data in the social media has become the focus of the CRM researches. As traditional statistical methods are insufficient in analysis, new approaches such as data mining, text mining and web mining have been used in CRM analysis. Machine Learning (ML) algorithms have an important place in such approaches.

Applications that developed by using past event data to obtain information about the current situation and to make predictions are defined as ML (Mitchell, 1997). The methods of ML, which are collected in three groups as supervised, unsupervised and reinforcement learning, are multidisciplinary analysis methods (Mitchell, 1997; Han, Kamber and Pei, 2012; Fidan, 2018). The ML which is preferred due to reasons such as allowing flexible uses, success in analysis of complex data and high level of performance in results has a wide usage area in data science field. However, it has some problems such as having complex algorithms, being sensitive to the amount and quality of the data, and not producing healthy results in case of insufficient data (Beleites and Salzer, 2008; Fidan, 2018).

Insufficient data is one of the major problems encountered in all analyzes. The small amount of data and the missing value in the dataset lead to unhealthy results and to failing analysis in the machine learning methods (Fidan, 2018). In order to overcome the insufficient data problem, some methods such as bagging, boosting, ensemble, mean-mode, data cleaning and value determination are used before the analysis (Han, Kamber and Pei, 2012). However, the methods have some disabilities such as deviation in results due to manipulation of data. On the other hand, Gray System Theory (GST) based methods are considered as one of the proper approaches in the literature because they provide healthier results in incomplete data analysis (Dou, Zhu and Sarkis, 2014). However, while some solutions are suggested for machine learning applications in the insufficient data environment, GST approaches are encountered rarely. Especially in short text analysis which the probability of insufficient data is quite high, classification methods that will be formed by using GST approach will make important contributions to the literature. So, the aim of the study is to develop GST based categorization algorithms which will give effective results in case of insufficient data. For this purpose, classification analysis of a small dataset that has short text was performed by algorithms which are commonly used in machine learning and the results were compared with the developed GST based classification algorithm. According to the Fscore measure, it has been determined that the improved classification algorithm has higher accuracies than other algorithms.

2. BUSINESS INTELLIGENCE

The concept of business intelligence (BI), defined as the use of information technologies to obtain information to be used for decision making, was first described by Hans Peter Luhn in his article "A Business Intelligence System" (Luhn, 1958). The first case study was carried out by Gartner Group analyst Howard Dresner in 1996 (Watson and Wixsom, 2007: 96; Ranjan, 2009: 61). BI, which is a roof concept that includes data, analysis and technology, the decision support systems associated with business activities have expanded to cover all areas of business activities (Watson and Wixsom, 2007: 96). Today, these tools are used in many areas such as finance, human resources, customer relations, business plan, business performance, competition strategies etc.

The basis of BI analysis is related to data management that contains the components such data, database and analyze (Watson and Wixom, 2007: 96). In the 1980s, analyzes have been realized by statistical methods and by using some database tools such as Query, OLAP (Online Analytical Processing), data cubes and reporting (Chen, Chiang and Storey, 2012: 1166). Data mining, which is defined as the process of obtaining confidential information from dataset, is used extensively in BI applications after 1980s (Loshin, 2003). Data mining methods, which also include statistical approaches, generally utilize machine learning techniques.

The development of user interactive systems with Web 2.0 has brought a dynamic environment for BI in terms of data collection and analysis. Especially, the huge increases in the amount of textual data have made it necessary to develop new systems for data storage and analysis. The data mining approaches will be insufficient considering the density of non-structural data such as comments, opinions, complaints, news, documents reflecting social life (Xu, et al., 2015). In this context, it is seen that analysis methods such as text mining, graph mining are the subjects of research in the data mining. One of the business activity areas in which text mining is used effectively is customer relationship management (Rygielski, Wang, and Yen, 2002).

2.1 Customer Relation Management

Customer Relationship Management (CRM) is a process of strategic management for acquiring new customers and retaining the customers in order to establish long-term profitable relationships (Ling and Yen, 2001: 82). The CRM process, which aims to understand customers, their preferences, needs and expectations and develop policies, is among the issues that is one of the most important business activities. Companies that increase customer satisfaction have a significant competitive advantage in the market (Rababah, Mohd and Ibrahim, 2011). For this reason, CRM systems are an important company strategy that enables companies of all sizes to stay in the market.

Although there are some observations based on the commercial transactions of the Mesopotamian farmers (Chakravorty, 2006: 20), the conscious studies on CRM were carried out by Robert D. Kestnbaum in the 1980s. In the approach, which is called as Direct Marketing and Database Marketing, a database was created with customer information, the data were analyzed by statistical methods and the results were used to sell the products to other consumers via e-mail (Courtheoux and Sterk, 2003). The approach of Kestnbaum, which contains data collection, analysis and implementation processes, have formed the basis of today's CRM systems. The increasing volume of data along with the widespread use of the Internet has made it difficult to establish meaningful relationships and to obtain meaningful information from intense data. With the increase in the amount of data, the lack of traditional statistical analysis led to the use of data mining methods in CRM systems after 1990s. Thus, methods such as questionnaires and complaint boxes used by companies to collect data have changed with the opportunities provided by Web 2.0 (Reinhold and Alt, 2011: 229). In the data collection process, social media applications such as Facebook, Twitter, forum, blog, e-mail provide important opportunities to the companies in the context of customer analysis.

2.2 Studies on Analysis of Customer Comments

The main topics of the CRM are the customers' evaluations which are important data for companies to develop correct strategies on commercial process and products. In this respect, customer complaints are important sources of information and are the subjects of interest to organizations in the context of information management (Tse and Wilton,

1988: 204). CRM applications, which are performed to gain customer loyalty and satisfaction, are divided into two groups as operational and analytical (He, Xu, Huang, and Deng, 2004). Operational CRM aims the automation of company processes, analytical CRM aims the analysis of customer characteristics and behavior (Ngai, Xu and Chou, 2009). After 2000 with the increasing e-commerce transactions, the customer complaint analyses have become the focus of attention in CRM researches of companies (Jutla, Craig, and Bodorik, 2001).

Data mining is one of the main methods currently used in analytical CRM applications (Berson, Smith, and Thearling, 2000; Jiang and Tuzhilin, 2006; Reinhold and Alt, 2011). Most of the studies carried out using methods such as classification, clustering, estimation and association rules are related to customer satisfaction analyzes and product or service ratings. However, it would be more realistic approach to use complaints and assessments written by the consumer rather than the scoring systems that do not fully reflect consumer opinions. In the literature, the rarity of studies carried out with customer complaints and evaluations is due to the fact that consumer complaint data are in the text type (Ngai, Xu and Chou, 2009).

The analysis of non-structural data are seen more frequently after 2000s and customer complaints analysis increased in this context. Li and Yamanishi (2001), one of the first researches on the analysis of customer comments, opinions and requests with textual data, applied rule-based text mining to consumer opinions obtained through the application of questionnaires created by open-ended questions and emphasized that the method can be used effectively in firm decision processes. Nasukawa and Nagana (2001) used the evaluation data obtained from the consumer support center instead of the survey method, identified the problems of the customers by determining the number of words in the text. In this study, it is emphasized that this method provides more healthy results than the survey method. Hu and Liu (2004), in their text mining study on the determination of the quality of electronic products in an e-commerce site, realized the clustering of consumer opinions as positive and negative. Dixit and Kr (2016) carried out the clustering analysis of consumer opinions on mobile phones from Amazon.com and demonstrated their differences in customer satisfaction. Berezina et al. (2015) stated that the hotel evaluation system could be analyzed by text mining. They have applied text mining analysis to customers' reviews on hotels from Tripadvisor and carried out consumer satisfaction categorization.

Textual data that contains a few words can be defined as short text such as social media shares, news headlines, document summaries, etc. The analysis of datasets which contain short texts is problematic process due to the inadequacies of machine learning algorithms such as clustering and classification. The article of Sahami is one of the first studies to reveal the problem arising from insufficient data in text analysis by using machine learning. The study has revealed that categorization algorithms have less performance in text data analysis (Sahami, 1996). Faguo et al. (2010) realized a comparative analysis with NB, K-nearest Neighbor (KNN) and Support Vector Machine (SVM) algorithms to present the framework of the performance problem in text categorization more clearly and they determined that the algorithms in text categorization have performances range in 60-70%. Pawar and Gawande (2012) emphasized that the decreasing performance is more critical problem for short text analysis. They have stated the no agreement in the literature and suggested further improvements for categorization algorithms of short text (Pawar and Gawande, 2012). Ni et al. (2011) developed a model, which called "Termcut", the suggesting that their analysis performance will increase by determining of core terms within the corpus. Xu et al. (2015), Deep Learning (DL) based Convolutional Neural Network (CNN) method has achieved that the performance of the results obtained from the KNN algorithm is twice as much performance. However, Majumder (2018) emphasized that DL approach has

high computational costs, long processing time and requires high dimensional dataset for analysis. The study has revealed that DL is not effective approach for short text analysis, because of the requirements of DL cannot ensure expected utility as enough as caused its cost. Another method that gives effective results in text analysis is the Fuzzy approaches (Romero et al., 2013; Kumbhar, Mali and Atique, 2017). In text categorization, it is stated that fuzzy approaches provide 7% performance increase compared to commonly used algorithms (Kumbhar, Mali and Atique, 2017). However, in another study it has been stated that the success of fuzzy methods in long texts is not seen in short texts and the feature vectors of short texts are insufficient in the producing of fuzzy rules (Khoury, Karray and Kamel, 2007). So, the study has determined that the fuzzy approaches are not suitable for short text analysis.

On the other hand, Gray Relational Analysis (GRA), which is used in numerical data analysis and which gives successful results in incomplete data, is a powerful tool for analysis. In studies related to incomplete data, it has been emphasized that the GRA approach gives successful results when the traditional methods are insufficient (Dou, Zhu and Sarkis, 2014; Fidan, 2018). Surprisingly, GRA-based analyzes cannot seen in text mining studies. Considering that the short text feature vectors have high probability of insufficient data, the use of GRA in analysis will provide positive contributions to the literature.

3. TEXT MINING

Social media contents include non-structural data such as text, image, graphics, and video. It is inevitable that the analysis of the non-structural data will be an interesting research area in the next decade (Tuzhilin, 2012). Since 85% of the data produced in commercial processes is composed of textual data, the analysis of textual data is an important issue for BI too (Tunalı and Bilgin, 2012). In the analysis of this data, the inadequacies of data mining approaches require the use of analyzes that include lingual textual operations. The first study on the analysis of textual data was carried out by Hebrail and Mersais in 1992. Researchers trying to extract key words based on Natural Language Processing (NLP) from the project descriptions recorded in the text type in the database have carried out clustering analysis of the documents by using keywords (Hebrail and Mersais, 1992). However, the conversion of textual data to structural data is first described in Feldman and Dagan's article "Text Knowledge Discovery in Textual Databases (KDT)". In the study, after the textual data in the documents were converted into structural data, the meaningful concepts were determined by using the text categorization approach of Hebrail and Marsais (Feldman and Dagan, 1995).

There are two approaches in text mining as contextual and lexical analysis (Han, Kamber and Pei, 2012). In contextual analyzes, it is aimed to determine the vocabulary and word associations according to the frequency values of the words in the text. In this approach, similarities between the texts are determined by using statistical methods such as n-gram, term frequency (TF) and term frequency-inverse document frequency (TF-IDF) (Beliga, Mestrovic and Ipsic, 2015). The lexical analyzes are carried out in order to examine the meaning of the texts in the context of NLP (Ravi and Ravi, 2015). Within the scope of lexical analysis, applications such as idea mining, opinion mining, evaluation mining and thought mining are carried out (Montoyo, Barco and Balahur, 2012). It is an interdisciplinary area because it is related to Information Retrieval (IR), NLP, name entity recognition (NER) (Han, Kamber, and Pei, 2012). In terms of analysis techniques, clustering, classification and summarizing methods are used in text mining.

Clustering: It is a categorization method that aims to group textual data with similar characteristics from non-structural data sources such as documents, news, pictures, and comments. The initial studies on clustering have been realized on document clustering

(Cutting, 1992). In order to the clustering of the documents, the textual data contained in the document should be represented numerically. This approach, which is called as Bag of Words (BoW), is based on IR and assumes that the document can be represented by the number of words in the text (Salton, 1975). According to Sebastiani (2002), in multiple documents clustering, the documents can be analyzed by using the Vector Space Model (VSM) on the basis of BoW. Cosines, Manhattan, Gini and Euclidean measures are used to determine the similarities of the documents (Turney and Pantel, 2010).

Classification: Classification is supervised machine learning technique that contains a training process to group items. In another words, it is a categorization method that involves learning process. Various machine learning algorithms are used for classification such as Decision trees, Naive-Bayes, classification and regression trees, support vector machines etc. (Han, Kamber, and Pei, 2012).

Summarization: The summarization aims to identify the meanings, words and phrases that can represent the document. The method is one of the most complex processes in terms of text mining. The summarization, which must be performed together with NLP, aims to determine the meaning of the documents that in applications such language translation, automatic response systems, text summarization (Das, 2007).

4. GRAY SYSTEM THEORY

Gray System Theory (GST) was first proposed in 1982 by J. L. Deng in his article "Control Problems of Gray System" (Deng, 1982). The method which is accepted as a new theory in case of uncertainty caused by incomplete data draws attention with its successful results (Liu and Lin, 2006). In GST, black represents the unknown information, while white is used to represent known information. The part between black and white is called insufficient information and is represented by gray (Liu, Forrest and Yang, 2012).

4.1. Gray Relational Analysis

The Gray Relational Analysis (GRA) used for classification and clustering is the determination of the relationship between the data in the gray region and extremes data. In the GRA, it is aimed to determine the most appropriate alternative according to decision criteria from the alternatives of the X decision matrix (seen in Equation2) created by the alternatives (a) and criteria (c) shown in Equation1.

First of all, normalization is applied so that the analysis is not affected by the extreme values. If the maximum value of the criterion will have a positive effect on the decision, Equation3 is applied for normalization. If the minimum value will have positive contribution, Equation4 is used. If an optimum value will have positive contribution, Equation5 is used. Thus, X^* normalization matrix shown in Equation6 is obtained. Since the classification process requires a reference, the criteria of the data to be classified (X_01,X_02 〖...X〗_0n) are added to the decision matrix as a reference series and normalization is performed. In this case, X_0 normalization matrix given in Equation7 is obtained. By applying Equation8 to the normalization matrix, the absolute difference matrix Δ is calculated shown in Equation9.

$$a = 1,2,3,\ldots.m\,,\quad c = 1,2,3,\ldots.n \tag{1}$$

$$\mathrm{X} = \begin{bmatrix} X_{11} & X_{12} & \cdots & X_{1n} \\ X_{21} & X_{22} & \cdots & X_{2n} \\ \vdots & \vdots & \cdots & \vdots \\ X_{m1} & X_{m2} & \cdots & X_{mn} \end{bmatrix} \tag{2}$$

$$X^*_{ac} = \frac{X_{ac} - minX_{ac}}{\max X_{ac} - minX_{ac}} \tag{3}$$

$$X^*_{ac} = \frac{maxX_{ac} - X_{ac}}{\max X_{ac} - minX_{ac}} \tag{4}$$

$$X^*_{ac} = \frac{|X_{ac} - X_{0c}|}{\max X_{ac} - X_{0c}} \tag{5}$$

$$\mathrm{X}^* = \begin{bmatrix} X^*_{11} & X^*_{12} & \cdots & X^*_{1n} \\ X^*_{21} & X^*_{22} & \cdots & X^*_{2n} \\ \vdots & \vdots & \cdots & \vdots \\ X^*_{m1} & X^*_{m2} & \cdots & X^*_{mn} \end{bmatrix} \tag{6}$$

$$X_0 = \begin{bmatrix} X_{01} & X_{02} & \ldots & X_{0n} \\ X_{11} & X_{12} & \cdots & X_{1n} \\ X_{21} & X_{22} & \cdots & X_{2n} \\ \vdots & \vdots & \cdots & \vdots \\ X_{m1} & X_{m2} & \cdots & X_{mn} \end{bmatrix} \tag{7}$$

$$\Delta_{jc} = \left|X^*_{ic} - X^*_{jc}\right| \tag{8}$$

$$\Delta = \begin{bmatrix} \Delta_{11} & \Delta_{12} & \cdots & \Delta_{1n} \\ \Delta_{21} & \Delta_{22} & \cdots & \Delta_{2n} \\ \vdots & \vdots & \cdots & \vdots \\ \Delta_{m1} & \Delta_{m2} & \cdots & \Delta_{mn} \end{bmatrix} \tag{9}$$

The gray relational coefficients (γ_ac) given in Equation12 are calculated using the absolute difference matrix Δ. The distinguishing coefficient ρ in this equation is used to expand and narrow the relational coefficient ranges (Hinduja and Pandey, 2017). ρ value, which is generally taken as 0,5 in the literature and does not affect the ranking of items, is in the range of [0,1] and it is selected to be close to 0 if the differentiations of correlation coefficients is high (Yıldırım, 2015). For calculating gray relational degrees δ_a, Equation13 or Equation14 is used. If each of the criteria in the decision matrix has equal importance, Equation13 is used for δ_a, otherwise Equation14 is. w_ac in Equation14 refers to the weightining coefficient of the criterion. The δ_a value indicates the relationship of the series added to the reference to all alternatives. In the classification analysis, the class of the reference is determined according to the alternative with the highest degree value.

$$\Delta_{max} = max_a max_c \Delta_{ac} \quad (10)$$

$$\Delta_{min} = min_a min_c \Delta_{ac} \quad (11)$$

$$\gamma_{ac} = \frac{\Delta_{min} + \rho\Delta_{max}}{\Delta_{ac} + \rho\Delta_{max}} \quad (12)$$

$$\delta_a = \frac{1}{n}\sum_{c=1}^{n} \gamma_{ac} \quad (13)$$

$$\delta_a = \sum_{c=1}^{n} w_{ac}\gamma_{ac} \quad (14)$$

In clustering analysis, each of the alternatives must be taken as a reference separately, as the gray correlational degrees will be determined by the similarities in the alternatives without adding external reference series. Thus, the gray relational degrees will be calculated as much as the number of alternatives in the decision matrix. An item of the alternative comparison will be taken as a reference in the next steps. So, the gray relational degree table can be formed to have different cross values. In this case, the cluster items are determined by taking the averages of the cross values with Equation15. Similarly as in the classification, two alternatives with the highest relational degrees are determined. Then, these two items are combined to identify the cluster members. This process is repeated until all alternatives are in one cluster.

$$G = [g_{ij}] = (\delta_{ij} + \delta_{ji})/2 \quad (15)$$

5. MATERIALS and METHODS

5.1 Dataset

The research dataset was obtained from www.hotelsikayet.com which publishes the comments of the users about the hotels. In the system, users are asked to comment on the hotel and to evaluate the hotel with a single sentence. The permission for the use of the data for the study has been obtained from the site in accordance with the confidentiality principles. Web mining-based software was developed with the C# programming language and data was taken in 12.02.2019 and recorded in the SqlServer 2008 database. 3432 user comments were obtained from the site. An example of a user comment is presented as raw data in Table 1.

Table 1. Consumer comments as row data

One word evaluation	Comment
Berbat	Yemekler cok vasat, hergun tavuk cikiyo, tekduze menu belirlemisler hergun ayni seyler cikiyo....mefrusat ve mobilya cok eski otelin.

In order not to affect the analysis negatively, 578 comments which have the same text were deleted from the database. In addition, the comments that have one word evaluations have been chosen for class label.

Pre-processing steps were applied to the labeled dataset, respectively. Label data and comment data have been cleared from punctuation, and then the conjunctions in the comment have been deleted. The last preprocessing that is the root finding process was

realized with Zemberek 0.16.0 Turkish NLP. The Java programming language has been used in the root-finding process because of the Zemberek library is Java-based. The label and comment data obtained after the preprocessing are given in Table 2.

Table 2. Data after preprocessing

Label	Comment
berbat	yemek tavuk menu aynı mobilya eski otel

There were 2854 records in the dataset after the preprocessing and it was observed that 103 different labels were used by the users. Because labels with few comments would reduce the learning process's success, the labels with less than 20 comments were excluded from the analysis. Thus, 7 categories were determined for classification as seen in Table 3. So, the dataset has been prepared for analysis with 1151 comments.

Table 3. Labels and number of reviews

Labels	berbat	rezalet	kötü	mükemmel	iğrenç	güzel	iyi
Number of reviews	618	253	125	66	39	30	20

5.2 Research Model

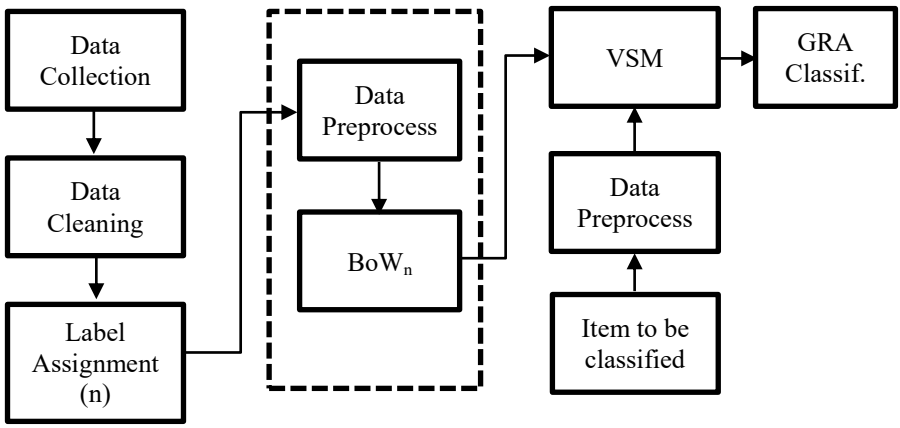

Figure 1. GRA classification model

5.3 Evaluation Methods

The performance of classification and clustering algorithms are determined by two methods of accuracy analysis, external and internal. If the analysis dataset is labelled, external accuracy measurement methods such as Purity (P), Recall (R), Fscore (F), and Accuracy-Error Ratio (Acc) are used (Nizam and Akın, 2014).

$$P = \frac{tp}{tp+fp} \qquad R = \frac{tp}{tp+fn} \tag{16}$$

$$Fscore = \frac{2.P.R}{P+R} \tag{17}$$

$$Acc = \frac{tp+tn}{N} \tag{18}$$

P represents the ratio of true positives (tp) in those grouped as positively, and R represents the ratio of tp in positive classified items (tp + fn). False negatives are denoted by fn and represent positive classified item which labelled as negative. F, which given in Equation17, is the harmonic mean of P and R values. Acc, which shows the ratio of the true classified (tp+tn) items and the total number of items (N) in the dataset, is given in Equation18. Although Acc is successful in balanced datasets, it is ineffective in unbalanced data as much as Fscore measure (Weiss and Hirsh, 2000). So, it will be appropriate choice that F is preferred. Considering that short text data is non-structural data, it will be the best choice to determine the classification accuracy rates by Fscore measure.

6. EXPERIMENTAL RESULTS

6.1 Training process results

The training process has been applied to 1151 labeled reviews and the number of words has been determined. The BoW values for each label are presented in Table 4. According to Table 4, it is seen that the hotel evaluations have the most "berbat" and "rezalet" labels, “iğrenç” and “berbat” labels have more words in average.

Table 4. Training process BoW values

Labels	Number of reviews	Number of words	Word average of labels
berbat	618	10542	17
rezalet	253	3440	13,5
kötü	125	1682	13,5
mükemmel	66	635	9,6
iğrenç	39	853	21,8
güzel	30	285	9,5
iyi	20	208	10,4
Total	**1151**	**18467**	**16**

6.2 VSM results

The VSM table should be prepared for each comment to be classified. Because each word in the comment refers to the features, VSM is created by placing each word in a column. By determining the frequency of the word within the labels, the decision matrix of GRA is obtained. The VSM table of the sample that labeled as "berbat" is presented in Table 5. Also, GRA analysis will be explained based on this selected review.

Table 5. VSM table

		Words of the review						
		yemek	tavuk	menu	aynı	mobilya	eski	otel
Labels	berbat	505	42	1	88	8	52	1035
	rezalet	223	21	1	24	3	19	519
	kötü	89	8	1	14	0	16	195
	mükemmel	58	3	0	3	1	2	80
	iğrenç	41	3	1	7	0	7	92
	güzel	16	1	0	3	0	1	34
	iyi	11	0	0	1	0	4	35

Table 5 shows the BoW values of the review. According to the table, Word of "yemek" has been mentioned 505 times in "berbat" and 223 times in "rezalet" label.

6.3 GRA results

By adding the reference series to the VSM table, the decision matrix given in Table 6 has been created. Reference series values have been determined by the maximum values from the alternative series as the highest values in the class determination will contribute positively to the decision.

Table 6. Decision matrix

	yemek	tavuk	menu	aynı	mobilya	eski	otel
	max	max	max	max	max	max	max
Reference	*505*	*42*	*1*	*88*	*8*	*52*	*1035*
berbat	505	42	1	88	8	52	1035
rezalet	223	21	1	24	3	19	519
kötü	89	8	1	14	0	16	195
mükemmel	58	3	0	3	1	2	80
iğrenç	41	3	1	7	0	7	92
güzel	16	1	0	3	0	1	34
iyi	11	0	0	1	0	4	35

Differences between the values in the decision matrix will negatively affect the GRA analysis. For this reason, the decision matrix has been normalized and results have been presented in Table 7. As the criterion of the decision, Equation4 has been used for the normalization process. The absolute difference table showing the difference between the reference series and the alternative series is calculated by using the normalization table. The table of absolute differences is presented in Table 8.

Table 7. Normalization values

	yemek	tavuk	menu	aynı	mobilya	eski	otel
Reference	1	1	1	1	1	1	1
berbat	1	1	1	1	1	1	1
rezalet	0,429	0,5	1	0,264	0,375	0,352	0,484
kötü	0,157	0,190	1	0,149	0	0,294	0,160
mükemmel	0,095	0,071	0	0,022	0,125	0,019	0,045
iğrenç	0,060	0,071	1	0,068	0	0,117	0,057
güzel	0,010	0,023	0	0,022	0	0	0
iyi	0	0	0	0	0	0,058	0,001

Table 8. Absolute differences table

	yemek	tavuk	menu	aynı	mobilya	eski	otel
Reference	0	0	0	0	0	0	0
berbat	0	0	0	0	0	0	0
rezalet	0,570	0,5	0	0,735	0,625	0,647	0,515
kötü	0,842	0,809	0	0,850	1	0,705	0,839
mükemmel	0,904	0,928	1	0,977	0,875	0,980	0,954
iğrenç	0,939	0,928	0	0,931	1	0,882	0,942
güzel	0,989	0,976	1	0,977	1	1	1
iyi	1	1	1	1	1	0,941	0,999

In order to determine the correlation coefficients between the decision matrix and the absolute difference matrix, gray relational coefficients were calculated using Equation12 and given in Table 9. Since the differences between the decision matrix values were high, the separation coefficient was determined to be close to 0 (p = 0,1).

Table 9. Gray relational coefficients

	yemek	tavuk	menu	aynı	mobilya	eski	otel
berbat	1	1	1	1	1	1	1
rezalet	0,149	0,166	1	0,119	0,137	0,133	0,162
kötü	0,106	0,109	1	0,105	0,090	0,124	0,106
mükemmel	0,099	0,097	0,090	0,092	0,102	0,092	0,094
iğrenç	0,096	0,097	1	0,096	0,090	0,101	0,095
güzel	0,091	0,092	0,090	0,092	0,090	0,090	0,090
iyi	0,090	0,090	0,090	0,090	0,090	0,096	0,090

By using the gray relational coefficients, gray relational degrees were calculated with the assumption that the words in the decision matrix have equal importance. For this reason, word weighting was not applied and Equation13 was used for calculating gray relational degrees that shown in Table 10.

Table 10. Gray relational degrees

	Gray relational degrees
berbat	**1**
rezalet	0,267
kötü	0,234
mükemmel	0,095
iğrenç	0,225
güzel	0,091
iyi	0,091

Gray relational degrees are represented by values from 0 to 1. The values close to 1 mean that the relationship is high. According to the relational degrees given in Table 10, it is seen that the highest relationship value is calculated in "berbat" label. So, the review should be in "berbat" class. The classification analysis has been performed by GRA to all reviews in the dataset and the classification values are shown in Table 11.

Table 11. GRA classification values

Class	Number of reviews	tp	fp	tn	fn
berbat	618	512	37	496	106
rezalet	253	208	24	874	45
kötü	125	112	31	995	13
mükemmel	66	61	11	1074	5
iğrenç	39	34	3	1109	5
güzel	30	27	4	1117	3
iyi	20	16	2	1129	4

6.4 Comparing results and discussion

The GRA results have been compared with the NB, SVM, and RF algorithms that commonly used in the classification of short texts. The classification analysis of the algorithms and the accuracy analysis have been realized by WEKA 3.8.3 data mining program. GRA classification algorithm and accuracy analyzes were performed by improving a software with C# programming language. The calculated P, R and F values for the accuracy analysis are presented in Table 12.

Table 12 is examined, it is seen that the RF algorithm has the highest F value in "mükemmel" labeled reviews and the SVM algorithm has the lowest F value in "iyi" labeled reviews. It is seen that the lowest algorithm for classification performance according to the average of F values is NB. However, in the classification of the comments which labeled as "iyi" and "güzel", it was observed that NB gave more successful results than SVM and RF algorithms. The results reveal the similar findings as Warnling and Bissmark (2017). So, it can be said that NB has better performance in small datasets.

Table 12: Accuracy values of classification algorithms

	NB			SVM			RF			GRA		
Class	**P**	**R**	**F**	**P**	**R**	**F**	**P**	**R**	**F**	**P**	**R**	**F**
berbat	0,738	0,573	0,645	0,839	0,964	0,897	0,885	0,797	0,838	0,932	0,828	0,877
rezalet	0,459	0,593	0,517	0,872	0,806	0,837	0,926	0,894	0,909	0,896	0,822	0,857
kötü	0,641	0,600	0,619	0,814	0,632	0,711	0,912	0,796	0,850	0,783	0,896	0,835
mükemmel	0,517	0,939	0,666	0,804	0,682	0,737	0,903	0,925	*0,913*	0,847	0,924	0,884
iğrenç	0,475	0,718	0,571	0,821	0,590	0,686	0,852	0,674	0,752	0,918	0,871	0,894
güzel	0,871	0,900	0,885	0,667	0,400	0,500	0,913	0,845	0,877	0,870	0,9	0,885
iyi	0,941	0,800	0,864	0,750	0,300	*0,428*	0,876	0,845	0,860	0,888	0,8	0,842
Average			**0,681**			**0,685**			**0,857**			**0,868**
Range			0,368			0,469			0,161			0,058

According to F values, it can be said that RF algorithm is a stable algorithm. RF has been found to be more successful than NB and SVM algorithms. This determination supports the findings of Xu et all. (2015). According to F values, GRA classification is more efficient than NB, SVM and RF classification algorithms. GRA is a stable algorithm due to the fact that the accuracy values do not vary much according to the sample numbers. In this context, the results show that GRA is a successful algorithm for short text classification. On the other hand, it is seen that the difference between the extreme values of the F values is quite low in GRA. The low range value reveals that the GRA algorithm is more homogenous in terms of results.

Some limitations such as root finding and long text classifications have been identified in the GRA process. It was observed that the data loss was high due to the careless writing of the words in user comments. The Zemberek 0.16.0 library used in the root finding process also fails to identify some roots. However, since the root finding process of all data was carried out with the same library, it was assumed that the failure would not adversely affect the analysis. On the other hand, in the classification of very long texts, it has been observed that GRA computational time has increased due to increase in VSM size. It can be problem for real time applications. So, GRA should be used for only short text classification in real time analysis.

CONCLUSION

The fact that social media comments with incomplete data are composed of short texts leads to low classification performances. The main purpose of the studies related to the subject is that the algorithms commonly used for classification are insufficient in the short text classifications. For this purpose, the literature focuses on the development of new algorithms and models. However, further studies are required on the short texts classification because of the low classification performance, the cost of the developed models and no consensus on an efficient method. On the other hand, it is seen that GRA, which is used effectively in the classification of numerical data containing missing data, is not used in text mining classifications. Since textual data have high probability of insufficient information, the social media comments that contain only a few words are problematic analysis. In this study, the gray relational based classification of the short text social media comments has been developed and applied to hotel reviews obtained from a site by web mining.

According to the results of the analysis, it was determined that the developed GRA classification algorithm gives more healthy results than the NB, SVM and RF algorithms commonly used in text classification. The average accuracy value of the GRA classification model was found 0,868. According to F accuracy values, it has been revealed that GRA algorithm is more successful in short text classification. It should be emphasized that the advantages of GRA are the algorithm is not complicated and the classification process does not require high CPU and memory capacity. It also should point that the method differs from other algorithms about no need for parameters before analysis. On the other hand, in the analysis of small dataset, there was no significant decrease in performance of GRA. Considering the results, it is revealed that GRA is a suitable algorithm for short text classification problem and it can be used for high accuracy in real time classification systems.

In the analysis process, it was observed that the data obtained from the user comments were quite irregular, the words were incomplete and inaccurate and there was no balanced data structure in terms of the number of words. These problems, especially in the analysis of social media comments, require that data cleaning and preprocessing processes be carried out meticulously. On the other hand, data loss was observed in preprocessing step. So, in short text classification analyzes, the implementation of word validation procedures in data cleaning process will be an appropriate approach to increase classification performance.

REFERENCE

1. Beleites, C. & Salzer, R. (2008). Assessing and improving the stability of chemometric models in small sample size situations. Analytical and Bioanalytical Chemistry, 390(5), 1261–1271.
2. Beliga, S., Mestrovic, A. & Ipsic, M. S. (2015). An overview of graph based keyword extraction methods and approaches. Journal of Information and Organizational Science, 39(1), 1-20.
3. Berezina, K., Bilgihan, A., Cobanoglu, C. & Okumus, F. (2015). Understanding Satisfied and Dissatisfied Hotel Customers: Text Mining of Online Hotel Reviews. Journal of Hospitality Marketing & Management, 00, 1–24.
4. Berson, A., Smith, S. & Thearling, K. (2000). Building data mining applications for CRM. McGraw-Hill.
5. Chakravorti, S. (2006). Customer Relationship Management: A Content Analysis of Issues and Best Practices. PhD Thesis, Florida International University, Miami, Florida.
6. Chen, H., Chiang, R. H. L. & Storey, V. C. (2012). Business Intelligence and Analytics: From Big Data to Big Impact. MIS Quarterly. 36(4), 1165-1188.
7. Courtheoux, R. J. & Sterk, L. G. (2003). In Memoriam: Robert D. Kestnbaum, http://maa-online.com/Articles/Kestnbaum.pdf, 02/01/2018.
8. Cutting, D., Karger, D. R., Pedersen, J. O. & Tukey, J. W. (1992). Scatter/gather: A cluster-based approach to browsing large document collections. In Proceedings of the 15th annual international ACM SIGIR conference on Research and development in information retrieval, ACM Press, 318–329.
9. Das, D. (2007). A Survey on Automatic Text Summarization Single Document Summarization. Language, 4, 1-31.
10. Deng, J. L. (1982). Control Problems of Gray System. System and Controls Letters, 1(5), 288-294.
11. Dixit, S. & Kr, S. (2016). Collaborative Analysis of Customer Feedbacks using Rapid Miner. International Journal of Computer Applications, 142(2), 29-36.
12. Dou, Y., Zhu, Q. & Sarkis, J. (2014). Evaluating green supplier development programs with grey-analytical network process-based methodology. European Journal of Operational Research, 233, 420-431.
13. Faguo, Z., Fan, Z. & Bingru, Y. (2010). Research on short text classification algorithm based on statistics and rules. In Third International Symposium on Electronic Commerce and Security, 3–79.
14. Feldman, R. & Dagan, I. (1995). Knowledge Discovery in Textual Databases (KDT). In Proceeding of KDD, 95, 112-117.
15. Fidan, H., (2018). E-ticaret Müşteri Bağlılığı Gri İlişkisel Kümeleme Analizi. AJIT-e Academic Journal of Information Technology, 9(32), 163-181.
16. Han, J., Kamber, M. & Pei, J. (2012). Data mining concepts and techniques, USA: Morgan Kaufmann Publications.
17. He, Z., Xu, X., Huang, J. Z. & Deng, S. (2004). Mining class outliers: Concepts, algorithms and applications in CRM. Expert Systems with Applications, 27, 681–697.
18. Hebrail G. & Marsais J. (1992). Experiments of Texual Data Analysis at Electricite de France. In Proceedings of IFCS- 92 of the International Federation of Classification Societies.
19. Hu, M. & Liu, B. (2004). Mining and summarizing customer reviews. In Proceedings of the ACM SIGKDD Conference on Knowledge Discovery and Data Mining (KDD), 168–177.
20. Jiang, T. & Tuzhilin, A. (2006). Segmenting customers from population to individuals: Does 1-to-1 keep your customers forever. IEEE Transactions on Knowledge and Data Engineering, 18, 1297–1311.
21. Jutla, D., Craig, J. & Bodorik, P. (2001). Enabling and Measuring Electronic Customer Relationship Management Readiness. In Proceedings of the 34th Hawaii International Conference on System Sciences, Hawaii.

22. Khoury, R., Karray, F. & Kamel, M. (2007). A fuzzy classifier for natural language text using automatically-learned fuzzy rules, International Conference on Machine Intelligence, ACIDCA-ICMI.

23. Kumbhar, P., Mali, M. & Atique, M. (2017). A genetic-fuzzy approach for automatic text categorization. IEEE 7th International Advance Computing Conference, 572-578.

24. Li, H. & Yamanishi, K. (2001). Mining from open answers in questionnaire data. KDD'01 Proceedings of the seventh ACM SIGKDD international conference on Knowledge discovery and data mining, San Francisco, California, 443-449.

25. Ling, R. & Yen, D. C. (2001). Customer relationship management: An analysis framework and implementation strategies. J. Computer Inform. Syst., 41, 82–97.

26. Liu, S., Forrest, J. & Yang, Y. (2012). A brief introduction to grey systems theory. Grey Systems: Theory and Application, 2(2), 89-104.

27. Liu, S., and Lin, Y. (2006). Grey information theory and practical applications. New York: Springer Science+Business Media.

28. Loshin, D. (2003). Business Intelligence: The Savvy Manager's Guide. Morgan Kaufmann, San Francisco, CA.

29. Luhn, H. P. (1958). A Business Intelligence System. IBM Journal of Research and Development, 2(4), 314-319.

30. Majumder, S., Balaji, N., Brey, K., Fu, W. & Menzies, T. (2018). 500+ times faster than deep learning (a case study exploring faster methods for text mining stack overflow), In Mining Software Repositories (MSR), IEEE/ACM 15th International Conference on ACM.

31. Mitchell, T. M. (1997). Machine Learning. NewYork: McGrawHill.

32. Montoyo, A., Barco, P. M. & Balahur, A. (2012). Subjectivity and Sentiment Analysis: An overview of the current state of the area and envisaged developments. Decision Support System, 53, 675-679.

33. Nasukawa, T. & Nagano, T. (2001). Text analysis and knowledge mining system. IBM Systems Journal, 40(4), 967-984.

34. Ngai, E. W. T., Xiu, L. & Chau, D. C. K. (2009). Application of data mining techniques in customer relationship management: A literature review and classification. Expert Systems with Applications, 36, 2592–2602.

35. Ni, X., Quan, X., Lu, Z., Liu, W. & Hua, B. (2011). Short text clustering by finding core terms. Knowledge and information systems, 27(3), 345-365.

36. Nizam, H. & Akın, S. S. (2014). Sosyal medyada makine öğrenmesi ile duygu analizinde dengeli ve dengesiz veri setlerinin performanslarının karşılaştırılması. XIX. Türkiye'de İnternet Konferansı.

37. Pawar, P. Y. & Gawande, S. H. (2012). A comparative study on different types of approaches to text categorization. International Journal of Machine Learning and Computing, 2(4), 423-426.

38. Rababah, K., Mohd, H. & Ibrahim, H. (2011). A Study of the Perception of the Benefits of Customer Relationship Management (CRM) System in Malaysian Private Hospitals. 2010 International Conference on Business and Economics Research IACSIT Press, Kuala Lumpur, Malaysia, 1(1), 327-330.

39. Ranjan, J. (2009). Business Intelligence: Concepts, Components, Techniques and Benefits. Journal of Theoretical and Applied Information Technology, 9(1), 60-70.

40. Ravi, K. & Ravi, R. (2015). A survey on opinion mining and sentiment analysis: Tasks, approaches and applications, Knowledge-Based Systems, 89, 14-46.

41. Reinhold O. & Alt, R. (2011). Analytical Social CRM: Concept and Tool Support. 24th Bled eConference eFuture: Creating Solutions for the Individual, Organisations and Society, Bled, Slovenia, 226-241.

42. Romero, F. P., Iranzo, P. J., Soto, A., Satler, M. F. & Casero, J. G. (2013). Classifying unlabeled short texts using a fuzzy declarative approach. Language Resources and Evaluation, 47(1), 151–178.

43. Rygielski, C., Wang, J. C. & Yen, D. C. (2002). Data mining techniques for customer relationship management. Technology in Society, 24, 483–502.

44. Sahami, M. (1996). Learning limited dependence bayesian classifiers. In KDD, 335–338.

45. Salton, G. (1975). A Vector space model for automatic indexing. Information Retrieval and Language Processing, 18(11), 613-620.

46. Sebastiani, F. (2002). Machine learning in automated text categorization. ACM Computing Surveys, 34(1), 1–47.

47. Tse, D. K. & Wilton, P. C. (1988). Models of Consumer Satisfaction Formulation: An Extension. Journal of Marketing Research, 24, 204-212.

48. Tunali, V. & Bilgin, T. T. (2012). Examining the impact of stemming on clustering Turkish texts. In Innovations in Intelligent Systems and Applications (INISTA),International Symposium. 1-4.

49. Turney, P. D. & Pantel, P. (2010). From Frequency to Meaning: Vector Space Models of Semantics. Journal of Artifical Intelligence Research, 37, 141-188.

50. Tuzhilin, A. (2012). Customer Relationship Management and Web Mining: The Next Frontier. Data Mining and Knowledge Discovery, 24(3), 584–612.

51. Warnling, O. & Bissmark, J. (2017). The Sparse Data Problem Within Classification Algorithms. Bachelor's Thesis in Computer Science. EXAMENSARBETE INOM TEKNIK,

52. Watson, H. J. & Wixom, B. H. (2007). The Current State of Business Intelligence. Computer, 40(9), 96-99.

53. Weiss, G. M. & Hirsh, H. (2000). Learning to predict extremely rare events. Proceeding of Learning from Imbalanced Data Sets, AAAI Workshop, Technical Report WS-00-05, 64-68.

54. Xu, J., Wang, P., Tian, G., Xu, B., Zhao, J., Wang, F. & Hao, H. (2015). Short text clustering via convolutional neural networks. Proceedings of NAACL-HLT, 62–69.

55. Yıldırım, B. F. (2015). Gri ilişkisel analiz, in Çok Kriterli Karar Verme Yöntemleri. B. F. Yıldırım and E. Önder, Ed., Bursa: Dora Basım Yayın, 229-236.